



PONTIFICIA UNIVERSIDAD CATOLICA DE CHILE  
UNIVERSITA DEGLI STUDI FIRENZE



# **SEISMIC FRAGILITY ASSESSMENT OF UNREINFORCED MASONRY CHURCHES OF CENTRAL CHILE**

**NURIA CHIARA PALAZZI**

Thesis submitted to Pontificia Universidad Católica de Chile and University of Florence in partial fulfillment of the requirements for the Degree of Doctor in Engineering Sciences and Doctor in Architecture

Advisors:

**JUAN CARLOS DE LA LLERA**

**LUISA ROVERO**

Santiago of Chile, October, 2019

© MMXIX, Nuria Chiara Palazzi





PONTIFICIA UNIVERSIDAD CATOLICA DE CHILE  
UNIVERSITA DEGLI STUDI FIRENZE



# **SEISMIC FRAGILITY ASSESSMENT OF UNREINFORCED MASONRY CHURCHES OF CENTRAL CHILE**

**NURIA CHIARA PALAZZI**

Members of the Committee:

**JUAN CARLOS DE LA LLERA**

**LUISA ROVERO**

**UGO TONIETTI**

**MARCO CORRADI**

**PATRICIA MARTÍNEZ**

**CRISTIÁN SANDOVAL**

Thesis submitted to Pontificia Universidad Católica de Chile and University of Florence in partial fulfillment of the requirements for the Degree of Doctor in Engineering Sciences and Doctor in Architecture.

Santiago of Chile, October, 2019





PONTIFICIA UNIVERSIDAD CATOLICA DE CHILE  
UNIVERSITA DEGLI STUDI FIRENZE



# SEISMIC FRAGILITY ASSESSMENT OF UNREINFORCED MASONRY CHURCHES OF CENTRAL CHILE

NURIA CHIARA PALAZZI

Members of the Committee:

JUAN CARLOS DE LA LLERA

LUISA ROVERO

UGO TONIETTI

MARCO CORRADI

PATRICIA MARTÍNEZ

CRISTIÁN SANDOVAL

Thesis submitted to Pontificia Universidad Católica de Chile and University of Florence in partial fulfillment of the requirements for the Degree of Doctor in Engineering Sciences and Doctor in Architecture.

Santiago of Chile, October, 2019





UNIVERSITÀ  
DEGLI STUDI  
FIRENZE



PONTIFICIA  
UNIVERSIDAD  
CATÓLICA  
DE CHILE

## **Ph.D. Thesis**

# **SEISMIC FRAGILITY ASSESSMENT OF UNREINFORCED MASONRY CHURCHES IN CENTRAL CHILE**

A dissertation presented by

Nuria Chiara PALAZZI

in partial fulfillment of the requirements for the degree of

Doctoral Program in Architecture

curriculum

Structures and Conservation of Architecture and Cultural Heritage Cycle n. XXXI

And

Doctoral Program in Engineering Sciences

curriculum

Civil Engineering

### **Supervisors**

Prof. L. Rovero  
(DIDA)

Prof. J.C. de la Llera  
(PUC)

### **Co-Supervisors**

Prof. U. Tonietti  
(DIDA)

Prof. C. Sandoval  
(PUC)

### **Reviewers**

Prof. S. Lagomarsino  
(Università di Genova)

Prof. G. De Matteis  
(Università della Campania)



*Al mio eroe, Papá, Nunzio Di Nanni.*



## **ACKNOWLEDGEMENTS**

Firstly, I wish to express deepest gratitude to my Chilean supervisor Professor Juan Carlos de la Llera, who has always taken a sincere interest in me and the future growth and development of my PhD research. He has been a fundamental reference during the last two years, from an academic, professional and personal point of view. Without his guidance, wisdom and support it would have been impossible.

I wish to thank my Italian supervisor, Professor Luisa Rovero, for her invaluable direction and sharp technical knowledge which has provided constant feedbacks and constructive critiques fundamental to this research.

I thank my co-supervisors Professors Ugo Tonietti and Cristian for providing fundamental feedbacks and employment guidance which created opportunities among professional and academic networks in the heritage conservation field.

I thank Professors Lagomarsino and De Matteis for the time spent reviewing this thesis.

This research would not have been possible without the support and assistance from Postdoctoral researcher Philomene Favier, particularly for the construction of empirical fragility curves, researcher Sebastian Castro, for improving this manuscript with his comments and, Professor Charles Fournier, for the English editing of the whole thesis text, Architect Giuseppe Berti, for the revision of the three FEM models, made with extreme speed and precision, and head of the Department of Heritage of the Ministry of Public Works Carolina Aguayo, for being available to share the documents from the archive in the department's possession.

This research was supported by the National Research Center for Integrated Natural Disaster Management CONICYT/FONDAP/15110017, and by the SIBER-RISK Regular Fondecyt project CONICYT/FONDECYT/1170836.

Thanks to my friends and colleagues at the University of Florence for the path we followed together: Sara Barducci, Daniel Pinto, Maria Teresa Miele, Sara Stefanini, and Vieri Cardinali.

Finally, I am grateful to Doctor Rafael Torres who allowed me to find myself again, and with his positive outlook he has always motivated and trusted my research.

Special thanks as well to my family and friends.



## ABSTRACT

The present thesis focuses on the seismic fragility assessment of unreinforced masonry (URM) churches in central Chile. The intrinsic value of this built heritage is due to its original features, synthesis of local and European architectural cultures. Due to the structural weaknesses of URM monuments, Chile's high seismic hazard, the absence of design standards and guidelines, and the ineffective performance of recently implemented retrofits, this built heritage is at-risk. For these reasons, the broad scope of this study is to document, for the first time, an essential part of the heritage asset of Chile, and to highlight principal vulnerabilities through a proper safety assessment framework, with the aim to promote conservation policies compatible with heritage identity and meeting new safety requirements.

Historical, typological and technological features of the selected churches, consisting of 106 churches, are outlined and consistent categories are formed. Churches of each class share stylistic and technological characteristics, but also and more importantly, the same structural weaknesses. Within this framework, two scales are adopted to investigate the seismic performance of these monuments: territorial and building.

At territorial-scale, the selected 106 churches are organized in a database that collects essential information for fragility assessment and damage forecasting (e.g. expected 2010 Maule PGA, architectural, typological, and material parameters). As a result, the main variables that control the seismic fragility of these structures were determined. The main outcome obtained downstream from this survey is related the damage suffered by the entire stock following the 2010 (8.8Mw) Maule earthquake.

The matrix of plots for the frequency distributions of the selected variables and damage level frequency diagrams enabled the identification of the following three homogeneous classes. These are: Colonial (CL), Neo-classical & Variant (NC&V) and Neo-gothic (NG). Probability Mass Functions (PMFs) and Empirical Fragility Curves (EFCs) have been obtained using validated models such as a lognormal distribution fitted by least squares, and a generalized linear model function fitted by maximum likelihood estimation.

At building-scale, three case studies representative of fragility classes are identified. These churches are: San Francisco in Santiago, San Judas in Malloa, and San Salvador in Santiago. A methodology to assess the seismic performance of these URM structures is provided, and the seismic response and risk quantified.

Finally, a new procedure is proposed to evaluate arbitrary structural retrofit interventions in view of more general ICOMOS principles. For each intervention, a conformity level in terms of alignment with conservation principles has been assessed. This methodology has been

## ABSTRACT

---

applied to evaluate the retrofit interventions proposed or implemented to reinforce the three selected case studies.

This thesis provides useful predictive tools for seismic risk reduction plans of churches, which is directly usable as a framework to be employed by stakeholders and safety related decision-makers. Moreover, the main findings can be exported to all those contexts in which European architectural revivalisms have influenced local building techniques (e.g. Central and Southern America).

# TABLES OF CONTENTS

<b>List of figures</b> .....	vii
------------------------------	-----

<b>List of tables</b> .....	xii
-----------------------------	-----

## Chapter 1

<b>INTRODUCCION</b> .....	<b>1</b>
1.1 Motivation .....	1
1.2 Seismic performance of URM churches in high seismic area.....	1
1.3 Overview on seismic fragility assessment of Chilean URM churches .....	2
1.4 Objectives of the present study.....	5
1.5 Outlines of the thesis.....	7

## Chapter 2

<b>CHILEAN BUILT HERITAGE</b> .....	<b>9</b>
2.1 Overview of URM churches in central Chile .....	9
2.2. Colonial, Neo-classical & Variant and Neo-gothic URM churches .....	17
2.2.1 Colonial churches (CL) .....	17
2.2.2 Churches with Neo-Classical style & Variants (NC&V) .....	19
2.2.3 Neo-gothic churches (NG) .....	21
2.3 Preliminary assessment of churches seismic fragility .....	23
2.4 Summary .....	27

## Chapter 3

<b>SEISMIC HAZARD OF CHILE</b> .....	<b>31</b>
3.1 Seismicity of the region .....	31
3.2 Chilean Code .....	34
3.3 Chilean seismic Code NCh433Of.2009 .....	35
3.3.1 General previsions .....	35
3.3.2 Methods of seismic analysis .....	37
3.4 Chilean Code for isolated buildings NCh 2745Of. 2013 .....	40
3.5 Summary .....	40

## Chapter 4

### SEISMIC DAMAGE AND FRAGILITY ASSESSMENT OF URM CHURCHES OF CHILE .....41

4.1 Brief review of procedures for seismic vulnerability and fragility assessment .....	41
4.2 Damage scenarios following the 2010 Maule earthquake .....	43
4.2.1 The 2010 Maule earthquake .....	43
4.2.2 Damage survey .....	45
4.2.3 Global damage index .....	52
4.3 Probability Mass Functions (PMFs) .....	55
4.4 Empirical Fragility Curves (EFCs) .....	62
4.5 Summary .....	66

## Chapter 5

### METHODOLOGICAL FRAMEWORK FOR ASSESSMENT THE SEISMIC PERFORMANCE OF SINGLE URM CHURCH .....71

5.1 Case study 1: San Tadeo Juda de Malloa, Colonial style .....	71
5.1.1 San Tadeo Juda church .....	72
5.1.1.1 Seismic history and the main interventions .....	73
5.1.2 Properties of materials .....	74
5.1.3 Assessment of crack patterns .....	81
5.1.4 Structural analysis .....	84
5.1.4.1 Linear and non-linear kinematic analysis for the out-of-plane capacity ..	
.....	85
5.1.4.2 Global response models .....	95
5.1.5 Summary .....	98
5.2 Case study 2: San Francisco de Asis, Neoclassical&Variant style .....	100
5.2.1 San Francisco church .....	101
5.2.1.1Seismic history and the main interventions .....	103
5.2.2 Properties of materials .....	105
5.2.3 Assessment of crack patterns .....	111
5.2.4 Structural analysis .....	114
5.2.4.1 Linear and non-linear kinematic analysis for the out-of-plane capacity ..	
.....	115
5.2.4.2 Global response models .....	122
5.2.5 Summary .....	124
5.3 Case study 3: Basilica del Salvador, Neo-gothic style .....	126

5.3.1	Basilica del Salvador .....	127
5.3.1.1	Seismic history and the main interventions .....	128
5.3.2	Properties of materials .....	130
5.3.3	Assessment of crack patterns .....	136
5.3.4	Structural analysis .....	140
5.3.4.1	Linear and non-linear kinematic analysis for the out-of-plane capacity... .....	141
5.3.4.2	Global response models .....	151
5.3.5	Summary .....	154

## Chapter 6

<b>SEISMIC RETROFITTING FOCUSED STRATEGIES RELATED TO CONSERVATION PRINCIPLES .....</b>	<b>155</b>
6.1 Restoration project .....	155
6.2 ICOMOS Principles and seismic retrofit project .....	157
6.3 From the diagnosis of vulnerability to conservation project .....	160
6.3.1 Stability-based techniques .....	161
6.3.1.1 Ties-rods and anchor plate, Basilica del Salvador .....	162
6.3.1.2 Ring beam &/or corner key, Malloa parish .....	166
6.3.1.3 Frenelli or Cross bracing, Basilica del Salvador .....	170
6.3.1.4 Enlargement&Buttresses, San Francisco church .....	172
6.3.2 Strength-based techniques .....	175
6.3.2.1 Unstitch-stitch .....	178
6.3.2.2 Grout injection, Basilica del Salvador .....	180
6.3.2.3 Artificial headers .....	183
6.3.2.4 Confinement or jacketing, San Francisco church .....	186
6.4 Summary .....	189

## Chapter 7

<b>CONCLUSION</b>	
7.1 Main findings .....	191
7.2 Future research .....	192

<b>References.....</b>	<b>193</b>
------------------------	------------

<b>ANNEX 1 .....</b>	<b>211</b>
<b>ANNEX 2 .....</b>	<b>211</b>
<b>ANNEX 3 .....</b>	<b>211</b>



## List of figures

**Figure 1.1** - Chilean National monuments declared by decree updated to 05 November 2018 (CMN).

**Figure 1.2** - Colonial church in the Central area of Chile: Loica church in San Pedro (RM).

**Figure 1.3** - Neoclassical church in the Central area of Chile: Santo Domingo (RM).

**Figure 1.4** - Neogothic church in the Central area of Chile: Santa Filomena parish (RM).

**Figure 2.1** -URM churches in the Metropolitan (RM) and in the Libertador General Bernardo O'Higgins (VI) Regions with indicate the seismic zoning of the RM and VI regions (according to the DE 2010, MINVU 2011): zone1 (Z1), maximum peak ground acceleration  $A_0=0.2g$ ; zone2 (Z2)  $A_0=0.3g$ ; and zone3 (Z4),  $A_0=0.4g$ . The 2010 Maule earthquake PGAs was taken by USGS Shake Maps.

**Figure 2.2** - Reinforced Concrete (RC) interventions in some churches in Santiago: a) RC slab in the narthex of San Isidro Labrador church; (c) and (d) RC ring-beam in the apse and bell tower of San Pedro's church; and (e) RC tie rods in Santa Sofía's Parish and (b) Dominicana church.

**Figure 2.3** – (a) Masonry type, categories: Stone [S], Brick [B], and Adobe [A]; (b) Architectural layout, categories: Basilica (three naves) [Bs], Latin-cross [L-c], and Single-nave [S-n]; (c) Architectural style, categories: Colonial Style [CL], Neo-Classic Style and Variants [Nc&V], and Neo-Gothic [NG]; and (d) Foot-print area (categories:  $90m^2 < A1 \leq 500m^2$ ;  $500m^2 < A2 \leq 900m^2$ ; and  $A3 > 900m^2$ ).

**Figure 2.4** - Matrix of plots for the frequency distributions of the selected variable: 2010 Maule PGA, damage levels after 2010 Maule PGA, and architectural, typological and material parameters (Masonries Type, Architectural Layout, Architectural Style, and Foot-print area).

**Figure 2.5** - Damage level frequencies and cumulative frequency distributions for the churches divided according to the Architectural Styles, normalized with respect to the total number, for three different PGA ranges according to the experienced seismic intensities suffered during 2010 Maule earthquake: (a) range  $0.16g < PGA \leq 0.28g$ ; (b) range  $0.28g < PGA \leq 0.41g$ ; (c) range  $0.41g < PGA \leq 0.53g$ . In brackets the percentage number of churches for each class.

**Figure 2.6** - Colonial church in the North area of Chile: (Antofagasta region).

**Figure 2.7** - Colonial church in Central area of Chile: Viñita church in Santiago (Metropolitan region).

**Figure 2.8** - Colonial church Central area of Chile: San Judas Tadeo in Malloa village (Libertador General Bernardo O'Higgins region).

**Figure 2.9** - Neo-classic church of Central area of Chile: Metropolitan Cathedral of Santiago (Metropolitan region).

**Figure 2.10** - Neo-classic church of Central area of Chile: Dominicana church in Santiago (RM).

**Figure 2.11** - Neo-classic church of Central area of Chile: San Ignacio church in Santiago (RM).

**Figure 2.12** - RC Neo-gothic churches located in the Central area of Chile: (a) Niño Jesus de Praga Parish (Metropolitan region), and (b) Basilica del Perpetuo Socorro Parish (Metropolitan region).

**Figure 2.13** - URM Neo-gothic church of Central area of Chile: the Basilica del Salvador.

**Figure 2.14** - URM Neo-gothic church of Central area of Chile: San Saturnino.

**Figure 2.15** – Dimensions of churches used in computation of the geometric indices.

**Figure 2.16** – The out-of-plane indexes of lateral walls, thickness-to-height  $[tw/hw]$ , of 72 URM Chilean churches are compared with the same indexes of 44 Portuguese, Spanish and Italian churches investigated in (Lourenço et al., 2013).

**Figure 2.17** - Damage levels of URM churches following 2010 Maule earthquake.

**Figure 2.18** - URM churches in the Metropolitan (RM) and in the Libertador General Bernardo O'Higgins (VI) Regions with indicate the seismic zonification of the RM and VI regions.

**Figure 3.1** - Tectonic Plates (Comte, 2010).

**Figure 3.2** - Types of interaction between the edges of tectonic plates (Comte, 2010).

**Figure 3.3** - Interaction between the Nazca, Antarctic, Scotia and South-American plates (Vigny, 2003).

**Figure 3.4** - Inclinations of Wadati & Benioff Plane (Engdahl y Villaseñor, 2003).

**Figure 3.5** - Chilean seduction zone: the four seismogenic sources (Leyton, 2010).

**Figure 3.6** - Seismic zoning of Chile of D.S.61, 2011: a) XI and XII regions; b) IV, V, VI, VII, VIII, IX, X and RM regions; and c) I, II, III regions. NCh433Of.96.

**Figure 3.7** - Soil classification adopted by ASCE 7, EC-8 and D.S.61 (Verdug & Peters, 2018).

**Figure 3.8** - Design spectrum proposed of (Nch2745Of.2013).

**Figure 4.1** - URM churches in the Metropolitan (RM) and in the Libertador General Bernardo O'Higgins (VI) Regions.

**Figure 4.2** - (a) MSK intensities map by (Astroza et al., 2010), and (b) EMS'98 intensities map by (D'Ayala & Benzoni, 2012).

**Figure 4.3** - Classification of mechanisms for religious buildings (Form A-DC 2006; source: Guidelines for Cultural Heritage 2011 G.U.).

**Figure 4.4** - Percentage of possible collapse mechanisms (relative to the total sample) and the mechanisms activated after the 2010 earthquake (compared to the possible sample).

**Figure 4.5** - (a) Out-of-plane mechanisms of the façade due to poor connections at corner: in the San Francisco de Mostazal the simple overturning involved the central part of façade, and in the San Agustín church the complete overturning of façade; (b) gable overturning effect of inadequate connection between roof structure and masonry wall of the upper part of façade, on Cathedral of Rancagua, Doñihue parish, and Codegua church; and (c) observed collapses on the haunch of the transverse arches of side aisles.

**Figure 4.6** - (a) Vertical cracks in correspondence of the windows due to the hammering roof covering; (b) deep horizontal cracks in correspondence to windows and buttresses, and total collapses of the lateral wall, due to the hammering roof and the lack of a link among the wooden trusses and the masonry walls; and (c) diagonal cracks on bell-tower walls following the Maule earthquake.

**Figure 4.7** - Assumed thresholds for indexes 1, 2, 3 and 4 as a function of PGA/g, (a) index 1, (b) index 2, (c) index 3 and (d) index 4, according to (Lourenço et al., 2013; Eurocode6; Eurocode8 and INN, 2003).

**Figure 4.8** - The in-plane indexes:  $\gamma_{1L}$ , in-plane area ratio in the longitudinal direction; and  $\gamma_{1T}$ , in-plane area ratio in the transverse direction, of 40 URM Chilean churches, compared with the same indexes of 44 Portuguese, Spanish and Italian churches investigated in (Lourenço et al., 2013). The in-plane indexes:  $\gamma_{2L}$ , area to weight ratio in the longitudinal direction;  $\gamma_{2T}$ , area to weight ratio in the transverse direction;  $\gamma_{3L}$ , base to shear ratio in the longitudinal direction; and  $\gamma_{3T}$ , base to shear ratio in the transverse direction, of 40 URM Chilean churches, compared with the same indexes of 44 Portuguese, Spanish and Italian churches investigated in (Lourenço et al., 2013).

**Figure 4.9** - Probability Mass Functions (PMFs) and Cumulative frequency distribution for the whole sample using observed data and predicted data through Binomial Distribution (BPDF), for intensities range from  $0.16g < PGA \leq 0.53g$ .

**Figure 4.10** - Probability Mass Functions (PMFs) and Cumulative frequency distribution for the whole sample using observed data and predicted data through Binomial Distribution (BPDF), for intensities range from  $0.16g < PGA \leq 0.53g$ .

**Figure 4.11** - Probability Mass Functions (PMFs) and Binomial Distribution (BPDF) for the out-of-plane behavior of the façade (M1, M2) for intensities range from  $0.16g < PGA \leq 0.53g$ .

**Figure 4.12** - Probability Mass Functions (PMFs) and Binomial Distribution (BPDF) for the in-plane behavior of the façade (M3) for intensities range from  $0.16g < PGA \leq 0.53g$ .

**Figure 4.13** - Probability Mass Functions (PMFs) and Binomial Distribution (BPDF) for the out-of-plane behavior of the lateral walls (M19) for intensities range from  $0.16g < PGA \leq 0.53g$ .

**Figure 4.14** - Probability Mass Functions (PMFs) and Binomial Distribution (BPDF) for the in-plane behavior of the lateral walls (M5, M6, M7, and M13) for intensities range from  $0.16g < PGA \leq 0.53g$ .

**Figure 4.15**- Chilean churches fragility curves for global behavior of the structures, (a) using lognormal distribution fitting by WSSE.

**Figure 4.16** - Chilean churches points of damage levels for different PGAs.

**Figure 4.17** - Chilean churches fragility curves using loglog link function, derivate from GLM distribution fitting by MLE.

**Figure 4.18**- Chilean churches fragility curves using logit link function, derivate from GLM distribution fitting by MLE.

**Figure 4.19** - Chilean churches fragility curves using probit link function, derivate from GLM distribution fitting by MLE.

**Figure 4.20** - Comparison between Chilean churches fragility curves using GLM distribution fitting by MLE and lognormal distribution fitting by WSSE.

**Figure 5.1.1** - View of the façade of the church and current plan, façade and section (Surtierra, 2011).

**Figure 5.1.2** - Exploded Axonometric of resistant structure.

**Figure 5.1.3** - (a) (b) Corner keys between rear and lateral walls.

**Figure 5.1.4** - Wooden portion walls (*tabique*) of (a) façade gable and (b) bell tower(Surtierra, 2011).

**Figure 5.1.5** - Roof system of (a) traditional timber king-post trusses with collar tie, and brick basement of foundation visible of the external lateral façade(Surtierra, 2011).

**Figure5.1.6** - Soil stratigraphy of the E3 test pit realized by (R&V Ingenieros) the April 2 and 3, 2012.

**Figure5.1.7** - Deep vertical cracks in the main façade (Surtierra, 2011).

**Figure5.1.8** - Deep vertical cracks observable in the (a) internal and (b) external elevations of side walls (Surtierra, 2011).

**Figure 5.1.9** – Failure modes of hooked scarf joints after 2010 Maule earthquake in the ring-beam.

**Figure 5.1.10** -Local collapses of Sacristy (Surtierra, 2011).

**Figure 5.1.11** – Identification of all local mechanisms in Malloa church.

**Figure 5.1.12** -  $\alpha_t$ , load multiplier which takes into account the resistive friction forces activated at the wood-masonry interfaces on orthogonal walls (Misseri, Palazzi, & Rovero, 2019).

**Figure 5.1.13** -  $\alpha_t\mu$ , the multiplier which accounting for the dry friction,  $\mu$ , and resistive mechanisms provided a good interlocking between orthogonal walls (Misseri, Palazzi, & Rovero, 2019).

**Figure 5.1.14** -  $\alpha_t\sigma_t$ , the load multiplier assumes the non-zero tensile strength,  $\sigma_t$ , is to be considered when evaluating the resistive forces opposing to the collapse mechanism (Misseri, Palazzi, & Rovero, 2019).

**Figure 5.1.15** - Capacity and demand curves of incremental kinematic analysis: (a) main Façade; (b) west lateral wall macro-element1(c) west lateral wall macro-element2; (d) west lateral wall macro-element3; (e) west lateral wall macro-element4; (f) east lateral wall macro-element1; (g) east lateral wall macro-element2; (h) east lateral wall macro-element3; (i) east lateral wall macro-element4; and (l) east lateral wall macro-element; and Acceleration Displacement Response Spectrum (ADRS) according to Nch433Of.1996.

**Figure 5.1.16** - EW Pseudo-acceleration response spectra for the February 27th 2010 Maule earthquake for the CCSP and MELP stations; elastic spectrum suggested by the

NCh433.Of1996 for seismic zone II and III, soil type E; deformed shapes of the main modes with corresponding periods and participating mass ratios in the transversal direction.

**Figure 5.1.17** - NS Pseudo-acceleration response spectra for the February 27th 2010 Maule earthquake for the CCSP and MELP stations; elastic spectrum suggested by the NCh433.Of1996 for seismic zone II and III, soil type E; deformed shapes of the main modes with corresponding periods and participating mass ratios in the longitudinal direction.

**Figure 5.2.1** - View of the façade of the church and current plan, façade and section

**Figure 5.2.2** - Concrete reinforcements of arcs (Jorquera et al., 2016).

**Figure 5.2.3** – History of San Francisco church.

**Figure 5.2.4** - Exploded Axonometric of resistant structure (Stefanini, 2016).

**Figure 5.2.5** - Laboratory Mechanical tests of stone samples from coring test samples (Jorquera et al., 2016).

**Figure 5.2.6** - Thin section of joint mortar samples (Jorquera et al., 2016).

**Figure 5.2.7** - Horizontal diaphragm placed on the central nave.

**Figure 5.2.8**– In-plane behavior of the transverse arcades.

**Figure 5.2.9** - Cracks in transverse arches (Jorquera et al., 2016).

**Figure 5.2.10** - Upper part of façade and presbytery wall.

**Figure 5.2.11** - Thrust line for the arches 1, 2, 3, 4 (Jorquera et al., 2016).

**Figure 5.2.12** - In-plane mechanism of the transverse arcade. Possible activated mechanisms: a) TA2 (current state) longitudinal wall made up of a two-leaf masonry and complete effectiveness of the anchoring of the piers; b) TA3 (current state) longitudinal walls as a monolithic masonry with complete effectiveness of the anchoring intervention on piers and c) TA5 (state before concrete reinforcements) longitudinal walls as a monolithic masonry. Horizontal and vertical virtual displacement diagram: d) TA1 (current state) longitudinal wall made up of two-leaf masonry and e) TA4 (state before concrete reinforcements) longitudinal wall made up of two-leaf masonry (Jorquera et al., 2016).

**Figure 5.1.13** - Local mechanisms of collapse in current state (Stefanini, 2016).

**Figure 5.2.14** - Horizontal bending mechanism of main façade.

**Figure 5.2.15** - Capacity and demand curves of incremental kinematic analysis: (a) north transept wall; and (b) south transept wall; and Acceleration Displacement Response Spectrum (ADRS) according to Nch2745Of.2013.

**Figure 5.2.16** - E Pseudo-acceleration response spectra for the February 27th 2010 Maule earthquake for the STL station; deformed shapes of the main modes with corresponding periods and participating mass ratios in the longitudinal direction.

**Figure 5.2.17** - N Pseudo-acceleration response spectra for the February 27th 2010 Maule earthquake for the STL station; deformed shapes of the main modes with corresponding periods and participating mass ratios in the transversal direction.

**Figure 5.3.1** - View of the Basilica and current plan, façade and section (Tandem Ltda, 2014).

**Figure 5.3.2** - Photo (a) original phase, and (b) uncertain date after 1906 (MOP).

**Figure 5.3.3** - Photo (a) west transept wall, and (b) two central nave columns, collapsed after the 1985 earthquake (Ministry of Public Works).

**Figure 5.3.4** - Photo (a) and (b): worrying crack pattern and local failures of east side aisle wall, central arch of narthex, arcades of the external gallery and columns of the central nave.

**Figure 5.3.5** - Exploded Axonometric of resistant structure.

**Figure 5.3.6** - Three points bend test of brick.

**Figure 5.3.7** - Thin sections of brick samples.

**Figure 5.3.8** - Thin sections of joint mortar samples.

**Figure 5.3.9** - Localization and soil stratigraphy of (a) excavation E1 in the west side aisle; (b) excavation E2 in the central nave; and excavation E3 in the east minor apse, (DICTUC, 2013).

**Figure 5.3.10** - Collapses of the transverse arches and arches of the longitudinal west wall.

**Figure 5.3.11** - Punching mechanism in the east aisle generate by RC beams.

**Figure 5.3.12** - Deep cracks in the lateral apses (a) and (b), and in the central apse (c).

**Figure 5.3.13** - Thrusts line of wall portion in interception of longitudinal walls 3, 2 and 1, and transverse arcade D.

**Figure 5.3.14** - Identification of local mechanisms of collapse in the current state of Basilica.

**Figure 5.3.16** - In-plane mechanism of the transverse arcade of the side aisles: (a) SAw-e (original configuration) west and east side aisles; and (b) SAw3-4 (current state) west side aisle.

**Figure 5.3.17** - In-plane mechanism of the transverse arcade of the Narthex at the current state.

**Figure 5.3.18** - Capacity and demand curves of incremental kinematic analysis of the three sub-portions of the lateral apses: (a) Ape-w1 (b) Ape-w2 and (c) Ape-w3; and Acceleration Displacement Response Spectrum (ADRS) according to Nch2745Of.2013.

**Figure 5.3.19** - Capacity and demand curves of incremental kinematic analysis, four sub-portions of the west side aisle wall: (a) SAw1 (b) SAw 2, (c) SAw 3, and (d) Saw4; and Acceleration Displacement Response Spectrum (ADRS) according to Nch2745Of.2013.

**Figure 5.3.20** - Capacity and demand curves of incremental kinematic analysis, three sub-portions of the west and east external gallery: (a) EAe-w2, (b) EAw 1, and (c) EAe1; and Acceleration Displacement Response Spectrum (ADRS) according to Nch2745Of.2013.

**Figure 5.3.21** - N Pseudo-acceleration response spectra for the February 27th 2010 Maule earthquake for the STL station; deformed shapes of the main modes with corresponding periods and participating mass ratios in the longitudinal direction.

**Figure 5.3.22** - E Pseudo-acceleration response spectra for the February 27th 2010 Maule earthquake for the STL station; deformed shapes of the main modes with corresponding periods and participating mass ratios in the transversal direction.

**Figure 6.1** - (a) Tie beams in the Kuño Tambo church, one of the prototype buildings of the SRP (image by C. Cancino, 2010); (b) exterior view of connections of tie beams in Cuzco (image by S. Lardinois, 2012). (a,b) © J. Paul Getty Trust. Reproduced by permission of J. Paul Getty Trust.

**Figure 6.2** - Deep cracks in the transverse arches of external gallery of Basilica del Salvador.

**Figure 6.3**– Retrofitting intervention for Basilica del Salvador: steel tie-rod.

**Figure 6.4** - Steel ring beam: a) connection between the wood roof element and the walls; b and c) partial strengthening of the plywood panel diaphragm and its connection with the steel ring beams (Regione Marche, 2000). (Frumento et al., 2006).

**Figure 6.5** - Retrofitting intervention for Malloa church: wooden ring-beam at lintel level.

**Figure 6.6** - Reinforced hooked scarf joint.

**Figure 6.7** - Steel cross bracing in extrados of vault (Giovanetti, 1998).

**Figure 6.8** - Retrofitting intervention for Basilica del Salvador: steel tie-rod.

**Figure 6.9** - Santo Domingo church in Santiago and Socaire church in Atacama.

**Figure 6.10** - Recommendations for buttresses design of Guidelines for earthquake resistant non-engineered construction. UNESCO (Arya et al., 2014).

**Figure 6.11** - Retrofitting intervention for San Francisco church: Brick Buttresses

**Figure 6.12** - Masonry replacement intervention. The repairs are ineffective due to the lack of compatibility between the masonry portions (Frumento et al., 2006).

**Figure 6.13** - Schematization of masonry wall (a) with a localized lesion, and (b) with an unstitch-stitch intervention (Vinci, 2012).

**Figure 6.14** - Grout injections (Source POLIMI-UNIPD).

**Figure 6.15** – Column section of Basilica del Salvador.

**Figure 6.16** – Example of Galvanized steel diatones of KERAKOLL.

**Figure 6.17** - Wall leaf connections: (a) Systematic presence of headers ( $>4-5/m^2$ ) with wall thickness similar to the stone/brick larger dimension; (b) Double leaf walls with limited number of headers ( $2-5/m^2$ ) and all thickness is larger than the brick larger dimension; and (c) No headers or less than  $2/m^2$  (Borri et al., 2015).

**Figure 6.18** - Confinement of column and pillar (Source UNIPD).

**Figure 6.19** - Worrying deep vertical crack in arch piers of central nave pillar axis F.



## List of tables

**Table 2.1** - Characterization of the six selected variables.

**Table 2.2** - Typical geometric ratios of the URM churches: width-to-length [wt/lt]; nave length-to-total length [ln/lt]; and nave width-to-total width [wn/wt] facade height-to-facade width [hf/wf] facade thickness-to-height [tf/hf]; and lateral walls thickness-to-height [tw/hw]. The data are average values for the three classes: Colonial churches (CL), Churches with Neo-classic style and Variant (NC&V), Neo-gothic churches (NG).

**Table 3.1** - Chilean Codes.

**Table 3.2** - Coefficient I of NCh433Of.96.

**Table 3.3** - Soil classification of D.S.61, 2011.

**Table 3.4** - Spectrum parameters (Nch2745Of.2013).

**Table 3.5** - Coefficient  $A_0$  and Z (Nch2745Of.2013).

**Table 4.1** - Value of MSK intensities (Astroza et al., 2010), EMS'98 intensities (D'Ayala&Benzoni, 2012), PGA and PGV (Boroschek et al., 2010 and USGS), and  $A_0$  (INN, 1996) for different sites of interest.

**Table 4.2** - Damage classification proposed by (Lagomarsino and Podestà, 2004b and De Matteis et al.2016), according to EMS-1998 scale, and description of damages.

**Table 4.3** - Masonry proprieties: \*\*INN, 2013; \*\*\*Vasconcelos& Lourenço, 2009; \*\*\*\* Magenes, 1992.

**Table 5.1.1** - Traditional timber joints in seismic areas (Parisi&Piazza, 2002).

**Table 5.1.2** - Masonry types.

**Table 5.1.3** - Young module ( $E$ ) compressive strength ( $f'_m$ ), and shear strength ( $v'$ ) of adobe masonry

**Table 5.1.4** - Soil stratigraphy of the four test pit realized by (R&V Ingenieros) the April 2 and 3, 2012.

**Table 5.1.5** - Results of Linear Kinematic Analysis of current state: ID macro-elements; Mechanism types (CM-O, Compound overturning; S-O, simple overturning; DL-O, double leaf overturning; C-O corner overturning); Participating Mass  $M^*$ , Kinematic multiplier of loads

$\alpha_0$  ( $\alpha_t$ , load multiplier which takes into account the resistive friction forces activated at the wood-masonry interfaces on orthogonal walls;  $\alpha_{t-\mu}$ , the multiplier which accounting for the dry friction,  $\mu$ , resistive mechanisms provided a good interlocking between orthogonal walls; and  $\alpha_{t-\sigma_t}$ , the load multiplier assumes the non-zero tensile strength,  $\sigma_t$ , is to be considered when evaluating the resistive forces opposing to the collapse mechanism); Mechanism Activation Acceleration  $a_0^*$ , equation (2) for the Demand Acceleration at ground level , equation (3) for the Demand Acceleration at elevated level.

**Table 5.1.6** - Mechanical proprieties of materials.

**Table 5.2.1** - Masonry types

**Table 5.2.2** - Principal mineralogical composition, clay minerals composition of the earthen materials, calcimetry and grain sizes, of the mortar samples.

**Table 5.2.3** - Young module ( $E$ ) compressive strength ( $f'm$ ), and shear strength ( $v'$ ) of M01, M02 and M03.

**Table 5.2.4** - Results of Linear Kinematic Analysis current state: ID of analyzed macro-element; Mechanism types; Participating Mass  $M^*$ , Kinematic multiplier  $\alpha_0$ , Mechanism Activation Acceleration  $a_0^*$ , Da1 Demand Acceleration at ground level,, and Da2 the Demand Acceleration at elevated level.

**Table 5.2.5** - Results of Linear Kinematic Analysis before the RC interventions: ID of analyzed macro-element; Mechanism types; Participating Mass  $M^*$  [kN], Kinematic multiplier  $\alpha_0$ , Mechanism Activation Acceleration  $a_0^*$  [m/s<sup>2</sup>], Da1 Demand Acceleration at ground level [m/s<sup>2</sup>], and Da2 the Demand Acceleration at elevated level [m/s<sup>2</sup>].

**Table 5.3.1** - Results of Linear Kinematic Analysis before the RC interventions: Kinematic multiplier  $\alpha_0$ , Participating Mass  $M^*$ , Mechanism Activation Acceleration  $a_0^*$ , equation (2) for the Demand Acceleration at ground level , equation (3) for the Demand Acceleration at elevated level.

**Table 5.3.2** - Results of Linear Kinematic Analysis of current state: Kinematic multiplier  $\alpha_0$ , Participating Mass  $M^*$ , Mechanism Activation Acceleration  $a_0^*$ , equation (2) for the Demand Acceleration at ground level , equation (3) for the Demand Acceleration at elevated level.

**Table 5.3.3** - Mechanical proprieties of materials.

**Table 6.1**- Steps of conservation project (Giaretton et al., 2016).

**Table 6.2-** ICOMOS principle ID, judgement category (JC), conservation's principle score( $\rho_k$ ) given to each JC, and description for each conservation principles of performance levels.

**Table 6.3** - Conservation intervention conformity level to ICOMOS principles.

**Table 6.4** - Stability-bases techniques.

**Table 6.5** - TR, check of respect: total (R), partial (PR), or absence (A) of ICOMOS principles and individuation of material device considering the architectural style.

**Table.6.6** - Effectiveness of steel TR in terms of acceleration for Basilica del Salvador.

**Table 6.7** - RB, check of the respect: total (R), partial (PR), or absence (A) of ICOMOS principles and individuation of material device considering the architectural style.

**Table 6.8** - Effectiveness of wooden RB in terms of acceleration for Malloa parish.

**Table 6.9** - CB, check of respect: total (R), partial (PR), or absence (A) of ICOMOS principles and individuation of material device considering the architectural style.

**Table 6.10-** FR, check of respect: total (R), partial (PR), or absence (A) of ICOMOS principles and individuation of material device considering the architectural style.

**Table 6.11** - Effectiveness of CB in terms of acceleration for Basilica del Salvador.

**Table 6.12-** EB, check of respect: total (R), partial (PR), or absence (A) of ICOMOS principles and individuation of material device considering the architectural style.

**Table 6.13** - Effectiveness of BT in terms of acceleration for San Francisco church.

**Table 6.14** - Strength-bases techniques.

**Table 6.15** - US, check of respect: total (R), partial (PR), or absence (A) of ICOMOS principles and individuation of material device considering the architectural style.

**Table 6.16** – GI, check of respect: total (R), partial (PR), or absence (A) of ICOMOS principles and individuation of material device considering the architectural style.

**Table 6.17** - Correction coefficients are in accordance with the masonry type (NTC, 2018, C8A.2).

**Table 6.18** - Effectiveness of AH in terms of Masonry quality index for Malloa Parish.

**Table 6.19**– AH, check of respect: total (R), partial (PR), or absence (A) of ICOMOS principles and individuation of material device considering the architectural style.

**Table 6.20** - Effectiveness of AH in terms of Masonry quality index for Malloa Parish.

**Table 6.21**- CN, check of respect: total (R), partial (PR), or absence (A) of ICOMOS principle and individuation of material device considering the architectural style.

**Table 6.22** - Effectiveness of CF in terms of design axial force  $N_{Rmc,d}$  and axial capacity of the FRP strengthened member,  $N_{sd}$ , for San Francisco church.

# Chapter 1

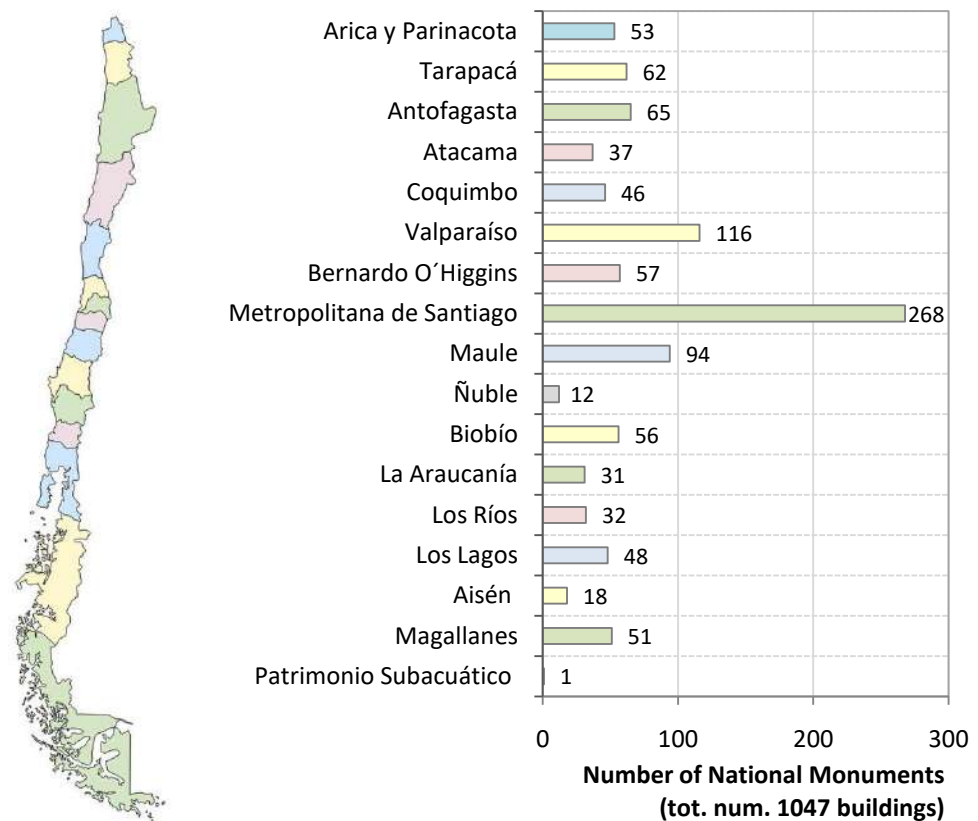
## INTRODUCTION

### 1.1 Motivation

The study of the Chilean unreinforced masonry (URM) built heritage is a topic of scientific interest because it is characterized by distinct features and uniqueness (Carta Roma, 1931; Carta Venecia, 1964; Carta Cracovia, 2000). This heritage is a convergence between different construction cultures: local and Inca traditional earthquake resistant practices, and European construction techniques expressed by Colonial architecture, and the revivalisms such as Neo-Baroque, Neo-Classic, Neo-Renaissance and Neo-Gothic.

### 1.2 Seismic performance of URM churches in high seismic area

The Central region of Chile holds the highest number of historic buildings deemed National Monuments (CMN, Law No. 17.288, Fig.1.1).



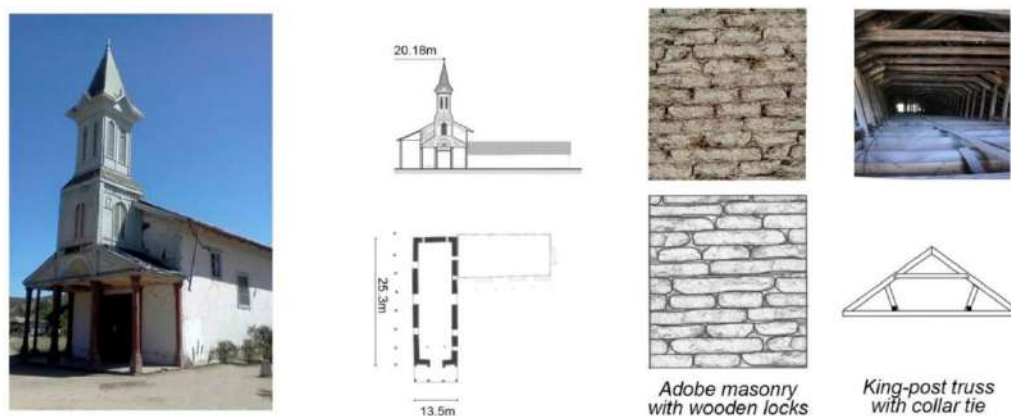
*Figure 1.1—Chilean National monuments declared by decree updated to 05 November 2018 (CMN).*

A significant portion of this architectural Heritage consists of unreinforced masonry (URM) churches and is particularly vulnerable to earthquake ground motions. Severe earthquakes have shown to be very damaging as evidenced by field data obtained from post-earthquake reconnaissance work (Nelsen, 2010; EERI, 2001; Decanini et al., 2012; and D'Ayala&Benzoni, 2012).

The specific seismic vulnerability of URM churches results from their intrinsic structural weaknesses (D'Ayala, 1999, 2000; Brandonisio et al. 2013; Lourenço et al. 2013) characterized by: the big size of the buildings, complex shapes, great height to width ratio, non-box-like behaviour, horizontal thrusting of structures from vaulted ceilings and timber roofs, heterogeneous materials with low tensile strength, past structural and non-structural modifications, and the environmental effects that have deteriorated the physical and chemical properties of structural materials, among other causes.

### 1.3 Overview on seismic fragility assessment of Chilean URM churches

The Chilean religious buildings are characterized by marked architectural features, due to the merge of the European Architecture characteristics with the Chilean constructive culture during Spanish domination (1536–1818). In the local Chilean constructive culture, the influence derived from the Inca domination (1470-1530) was strong, as well as the awareness of seismic hazard affected the structural solutions (Fig. 1.2).

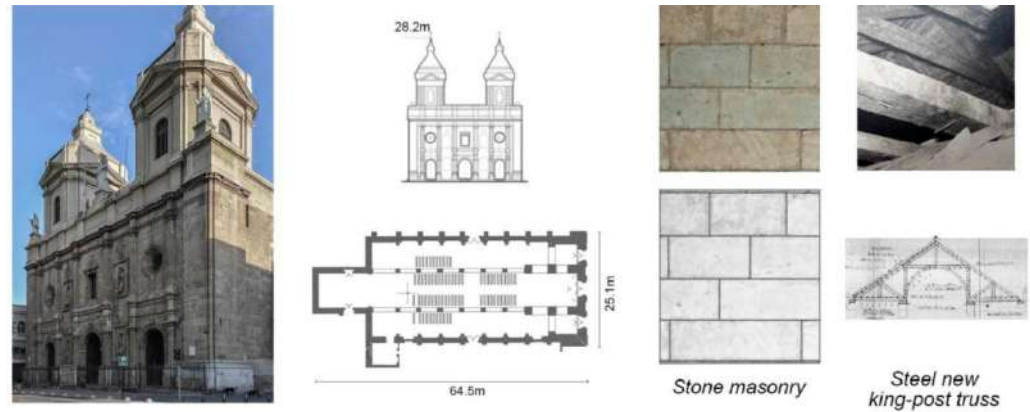


**Figure 1.2** - Colonial church in the Central area of Chile: Loica church in San Pedro (RM).

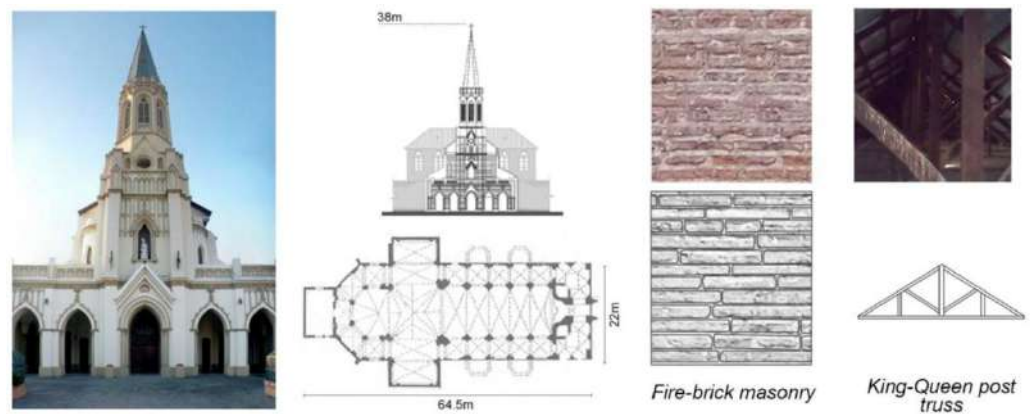
Conversely, the constructive culture introduced by the Spanish was unaware of seismic aspects and characterized by the European architectural revivalisms, i.e. the Neo-Baroque, Neo-Classical (Fig. 1.3), Neo-Renaissance and Neo-Gothic (Fig. 1.4).

The convergence of different construction cultures produced a considerable variety of buildings with different characteristics, as well as hybrid buildings with different materials and construction techniques. In particular, the use of cyclopean stone masonry, the cob technique (mix of earth, straw and water) and the *quincha* technique (timber structure with earth and straw) (Cancino et al., 2009; Cancino, 2010; Fonseca&D'Ayala, 2012; Terrealva&Vicente, 2013; Varum et al., 2014) all derive from an indigenous architecture. Moreover, the use of

adobe masonry (earthen blocks) derives from the Inca culture; and the use of brick masonry derives from the European building culture.



**Figure 1.3** - Neoclassical church in the Central area of Chile: Santo Domingo (RM).



**Figure 1.4** - Neogothic church in the Central area of Chile: Santa Filomena parish (RM).

Furthermore, Chilean seismicity is well recognized in the world. It is an active subduction zone characterized by the convergence between the Nazca and the South America plates. In particular, the Chilean central valley is one of the most seismically active zone of the world, with earthquake of moment magnitude  $M_w \geq 8$  occurring approximately every ten years (Udías et al., 2012).

The absence of seismic vulnerability studies at territorial scale and the lack of standards oriented to the protection and valorization of historical structures is in its own right a vulnerability factor. In fact, the current requirements for Adobe Structures, NCh3332. c.2012 (INN, 2013), is the only standard aimed to preserve existing buildings and provides only general criteria for the strengthening of adobe constructions covering 43% of the historic churches

It became apparent that many retrofit and repair techniques implemented following prior Chilean earthquakes resulted in ineffective performance during the Mw 8.8 2010 megathrust

earthquake in central Chile (Decanini et al., 2012; D'Ayala et al., 2012). In particular, the seismic behavior of unreinforced masonry (URM) monuments highlighted the need to implement new protective and safety strategies according to the International Council on Monuments and Sites (ICOMOS) principles<sup>1</sup> laid out Venice, Charter, 1964(Venice, 1964).

Therefore, the problem statement to characterize the Chilean Built Heritage is due to the: (1) intrinsic structural weaknesses of URM buildings (D'Ayala, 1999; Lourenço et al. 2013); (2) Chile's high seismic hazard; (3) absence of design standards and guidelines; and (4) the ineffective performance of implemented retrofits (Valdebenito et al., 2011; D'Ayala et al., 2012).

Recent studies at single-building scale have been carried out to assess seismic vulnerability of Chilean historical buildings: the Torreón los Canelos, in Valdivia (Sanchez, 2013); the colonial churches of Laonzana in Tarapacá and Chiu Chiu in Antofagasta (Díaz, 2016); two centennial masonry Palaces, Luis Cousiño and Subercaseaux in Valparaíso, exploiting a simplified method to assess seismic performance (Sturm, 2008, Saragoni et al., 2009); churches La Matriz, San Francisco del Barón, and Las Hermanas de la Divina Providencia in Valparaíso (Indirli, et al., 2011); and, the following four important church case studies in Santiago, San Francisco, the most ancient monument (Jorquera et al. 2017a, and Jorquera et al. 2017b), the Santiago Cathedral, a Neo-classic structure in stone masonry (Torres et al., 2017, 2018); the

---

<sup>1</sup>ICOMOS CHARTER-PRINCIPLES FOR THE ANALYSIS, CONSERVATION AND STRUCTURAL RESTORATION OF ARCHITECTURAL HERITAGE (2003), ICOMOS 14th General Assembly in Victoria Falls, Zimbabwe, in 2003

1.1 Conservation, reinforcement and restoration of architectural heritage requires a multidisciplinary approach.

1.2 Value and authenticity of architectural heritage cannot be based on fixed criteria because the respect due to all cultures also requires that its physical heritage be considered within the cultural context to which it belongs.

1.3 The value of architectural heritage is not only in its appearance, but also in the integrity of all its components as a unique product of the specific building technology of its time. In particular the removal of the inner structures maintaining only the façades does not fit the conservation criteria.

1.4 When any change of use or function is proposed, all the conservation requirements and safety conditions have to be carefully taken into account.

1.5 Restoration of the structure in Architecture Heritage is not an end in itself but a means to an end, which is the building as a whole.

1.6 The peculiarity of heritage structures, with their complex history, requires the organization of studies and proposals in precise steps that are similar to those used in medicine. Anamnesis, diagnosis, therapy and controls, corresponding respectively to the searches for significant data and information, individuation of the causes of damage and decay, choice of the remedial measures and control of the efficiency of the interventions. In order to achieve cost effectiveness and minimal impact on architectural heritage using funds available in a rational way; it is usually necessary that the study repeats these steps in an iterative process.

1.7 No action should be undertaken without having ascertained the achievable benefit and harm to the architectural heritage, except in cases where urgent safeguard measures are necessary to avoid the imminent collapse of the structures (e.g. after seismic damages); those urgent measures, however, should when possible avoid modifying the fabric in an irreversible way.

Basilica del Salvador, large neo-gothic church (Rendel et al., 2014, Palazzi et al., 2018a), and the Pereira Palace (Sandoval et al., 2017). In addition a set of older buildings, located in the historic colonial center of Santiago (Jorquera et al. 2016) and in the Central region of Chile (Palazzi et al., 2018b, 2019) was analyzed considering their geometrical features to explain the longevity and dynamic structural performance across time.

The results of this research would represent a first Chilean study at territorial scale of the seismic fragility of URM heritage buildings, and will show the potential impact of future earthquakes on this heritage. It will also help develop predictive tools for seismic risk reduction plans, which would be directly usable as a framework employed by stakeholders and safety related decision-makers.

This study contributes to reduce the knowledge gap previously identified by providing a specific methodology to assess the seismic performance of URM structures and apply it to specific case studies.

## 1.4 Objectives

Even today, structural safety requirements are often in conflict with conservation requirements based on the well-known criteria of authenticity, minimum intervention, chemical and physical compatibility, non-obtrusiveness, reversibility and controllability (Venice, 1964).

Thus, seismic hazard mitigation of Built Heritage is still a complex task. In particular in a high seismicity context, it is very difficult to conjugate the needs of structural retrofitting while preserving heritage value. In fact, the impact of an intervention of consolidation on a historical building could be significant in terms of loss or alteration of the original material and structural features. Indeed, the application of restoration criteria may encounter significant or even insurmountable difficulties in practice.

The *seismic restoration* must comply with two goals: the necessities of safety and conservation. “The conjugation of an only verb “restore” it is not such if it does not preserve, and does not preserve unless it ensures” (Giuffré). Thus, the main question of this research is connected to help resolve the tension between safety and conservation needs.

The thesis is focused on the assessment of the seismic fragility of URM Built Heritage located in the central Chile, both at the macro and single-building scales, based on comprehensive and multidisciplinary research and validated international methodologies adapted to the specific features of Chilean architecture.

The general research question is: How can seismic risk of URM Built Heritage be mitigated in a highly seismic region, while protecting its value in accordance with ICOMOS principles?

General hypothesis: A new method, Intervention Quality Index (IQI) method, based on an index that quantifies the conformity of consolidation intervention to ICOMOS conservation

principles, would allow for the performance of design intervention to be taken into account in terms of both safety and conservation. It will assess the restoration intervention quality considering: (i) current state of conservation of the monument; (ii) seismic intensity; and (iii) the level of compliance given by the conservation's principle score.

From the general question, two specific questions arise:

- a) What are the critical variables that control the seismic fragility of these structures?
- b) Despite the heterogeneity of this Built Heritage, is it possible to identify homogenous fragility classes?

The specific hypotheses are:

- a) We state that four main variables determine the seismic fragility: (a) masonry type (Stone, Brick, Adobe); (b) architectural layout (Basilica, Single Nave, Latin Cross); (c) architectural style (Colonial Style, Neo-classic Style & Variants, Neo-gothic Style); and (d) foot-print area ( $90\text{m}^2 < A1 \leq 500\text{m}^2$ ;  $500\text{m}^2 < A2 \leq 900\text{m}^2$ ; and  $A3 > 900\text{m}^2$ ).
- b) The architectural style exerts a first-order role on fragility; and allows classifying the URM churches into three groups of somewhat homogeneous fragility classes (*Colonial, Neo-classical & Variant and Neo-gothic*).

General Aim:

To assess the seismic fragility of URM Built Heritage located in the central region of Chile, both at the macro-scale and single-building-scale, based on a comprehensive and multidisciplinary research using validated international methodologies, which should be adapted to the specific features of Chilean architecture.

At macro-scale, the specific objectives are:

- To determine the main variables controlling the seismic fragility.
- To identify somewhat homogeneous fragility classes.
- To quantify the seismic fragility of URM churches using validated models.

At single building scale:

- To provide a methodology to assess the seismic performance of a single URM structure.
- To quantify the seismic response and risk through case studies representative of fragility classes.
- To provide an index that quantifies the conformity of retrofit interventions to ICOMOS principles.

## 1.5 Outlines of the thesis

The rest of the thesis manuscript is organized into five main chapters. Chapter 2, focused on macro-scale, is dedicated to database construction. In order to systematize the assessment of the seismic fragility of Chilean URM churches belonging to different geographic areas, and to extrapolate probabilistic models for damage, an extensive survey of the Chilean Historical Heritage is needed. This survey motivated the archival nature of this Chapter which reports the results of an comprehensive analysis to build a complete database of the architectural, constructive, and structural characteristics of a representative number of URM churches (106, total number of analyzed buildings). The database includes damage observed, after the February 27, 2010 (Mw 8.8) Maule earthquake. Afterwards, main variables determining the seismic fragility of URM churches are presented, and the homogeneous fragility groups (Colonial [CL], Neoclassical & variants [NC&V], and Neo-gothic [NG]) and related cases studies for each group are identified. Chapter 3 introduces to the seismic hazard of Chile, briefly presenting the physical phenomena that determine the occurrence of Chilean earthquakes and the predictions of the Chilean seismic code. Chapter 4, focused on macro-scale, tackles the prediction of future damage of Chilean URM churches using probabilistic tools, Probability Mass Functions (PMFs) and Empirical Fragility Curves (EFCs), taking into account global and local behaviors of the structures. Chapter 5 is focused on the earthquake performance of single-buildings, and provides a methodology for structural analysis of local and global seismic behaviors of three case studies representative of homogeneous fragility groups identified in Chapter 2: San Tadeo de Malloa [CL], San Francisco in Santiago [NC&V], and Basilica del Salvador in Santiago [NG] churches. The safety assessment of the monuments is carried out based on a multi-disciplinary approach. Main fields comprise historical research, in situ surveys, crack pattern analysis, physical and mechanical characterization of materials and multi-level structural analyses. In Chapter 6 strengthening solutions are proposed for improving the seismic performance of Chilean URM churches which take into account the unique architectural, structural and constructive features of this Heritage proposing a method to evaluate the accordance with the ICOMOS Principles. The criteria used in the consolidation and repair interventions for the three cases studies representative of each fragility class, will be the basis for general guidelines for post-earthquake retrofit programmes of URM churches belonging to the same architectural style. Finally, in Chapter 7 the main findings are collected rimandando la discussione dei risultati alle conclusioni di ogni capitolo.

Due to the “thesis by publications” format, this thesis is a fusion of published, accepted, or submitted manuscripts for publication in international journal and/or conferences on structural engineering and architectural heritage. Each manuscript is presented in form of Chapter.



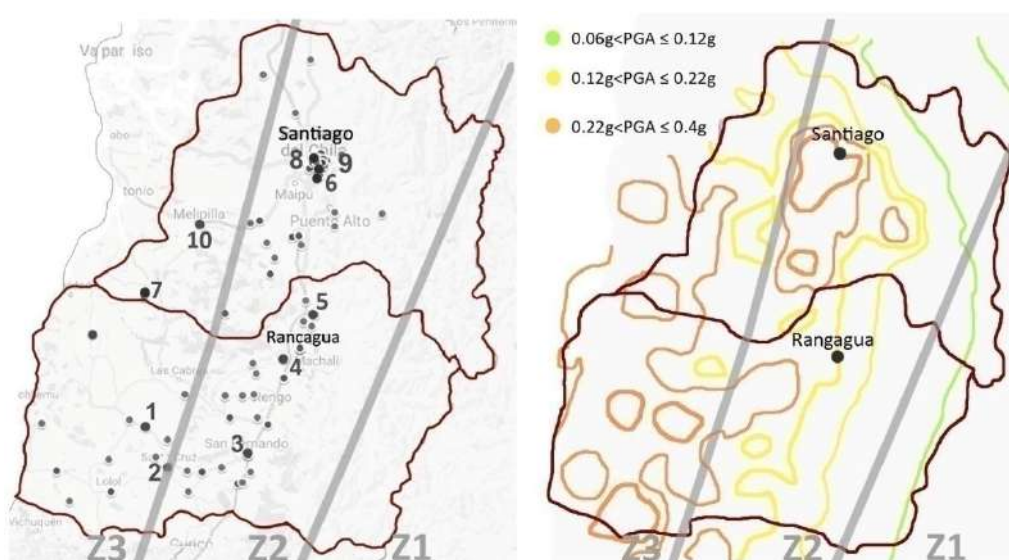
# Chapter 2

## CHILEAN BUILT HERITAGE

### 2.1 Overview, URM churches in central Chile

Most Chilean National Monuments (LY.17 288) are located along the Central Valley of the country (longitudinal N-S depression). A large portion of this Built Heritage is composed of URM churches and, therefore, suffered significant losses after the 2010 Maule earthquake. This group of churches belongs to the Archdiocese of Santiago, the dioceses of Melipilla and San Bernardo, and an Opus Dei personal prelature.

Fig.2.1 shows the geographical distribution of the 106 URM churches analyzed in this study, situated in the Metropolitan and the Libertador General Bernardo O'Higgins Regions. The seismic zoning of Chile that considers three macro-zones with maximum peak ground accelerations of 0.2g (Z1), 0.3g (Z2), and 0.4g (Z3), respectively, it is also distinguished. Additionally, a map of PGA values registered in the study area during the 2010 Maule earthquake is shown.



**Figure 2.1** -URM churches in the Metropolitan (RM) and in the Libertador General Bernardo O'Higgins (VI) Regions with indicate the seismic zoning of the RM and VI regions (according to the DE 2010, MINVU 2011): zone1 (Z1), maximum peak ground acceleration  $A_0=0.2g$ ; zone2 (Z2)  $A_0=0.3g$ ; and zone3 (Z3),  $A_0=0.4g$ . The 2010 Maule earthquake PGAs was taken by USGS ShakeMaps.

This Built Architectural Heritage exhibits very original characteristics and successful strategies must be deployed to protect it against seismic risk.

The first churches, built in the central area of Chile during the Spanish colonial period (1536-1818), are characterized by a synthesis of local, Inca, and the Spanish construction cultures that led to a new architectural style: the so called *Colonial Style*. Subsequently, in the transition

period between Colonial and Modern Times, religious buildings are better characterized by the hybridization of *Colonial Architecture* with several of the *European Architectural Revivalisms*, i.e *Neo-Baroque*, *Neo-Classic*, *Neo-Renaissance* and *Neo-gothic* styles.



**Figure 2.2** - Reinforced Concrete (RC) interventions in some churches in Santiago: a) RC slab in the narthex of San Isidro Labrador church; (c) and (d) RC ring-beam in the apse and bell tower of San Pedro's church; and (e) RC tie rods in Santa Sofia's Parish and (b) Dominicana church.

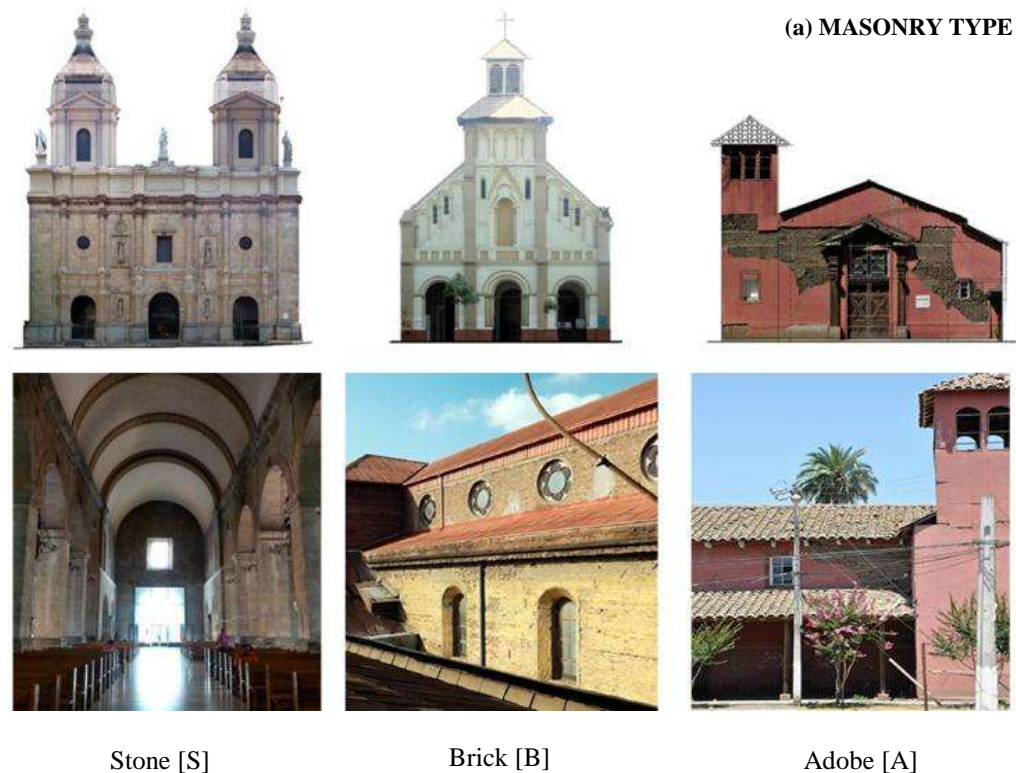
Significant changes and stratifications have taken place in these churches due to reconstruction processes and restorations after earthquakes.

From the beginning of the Spanish colonial period, seventeen seismic events with moment magnitudes  $M_w$  between 7 and 9.5 have occurred in the central Chile (Astroza et al. 2012; Chilean National Seismological Center), such as the 1647 Santiago earthquake ( $M_w 8.5$ ) and

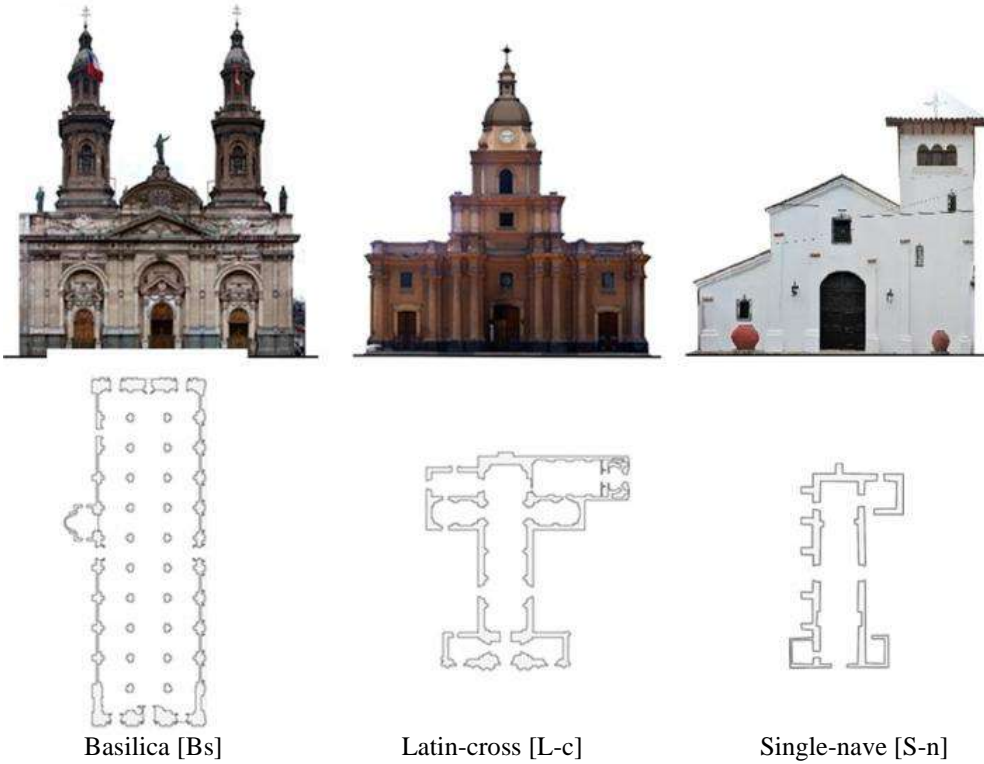
the 1730 Valparaíso earthquake (Mw8.7). These seismic events completely destroyed Santiago and caused severe damage from La Serena to Chillán (Montessus de Ballore 1912, and Cisternas, 2012). After the Valparaíso 1906 (Mw8.2) and Algarrobo 1985 (Mw8.0) seismic events, many churches were strengthened using Reinforced Concrete (RC) ring beams and slabs, aiming to ensure a *box-behavior* of the entire structure (Figures 2.2a, b, and c). For the Basilica (three-nave) churches, the RC tie-beams were introduced to improve the in-plane response of the aisles (Figures 2.2d and e).

The RC structural strengthening retrofits resulted in increased mass and stiffness of the masonry construction and consequently changes in seismic response, often with undesirable outcomes, such as crushing, hammering, and torsion effects (Borri et al., 2009; Modena et al., 2011; Lagomarsino, 2012; Ciber et al., 2015). In particular, the RC structural strengthening interventions were inadequate and harmful for adobe structures, given their very low mechanical parameters (Varum et al., 2014).

In order to archive a more comprehensive investigation of the intrinsic weaknesses of the studied buildings, typological, geometrical, and material features were analyzed in detail. In particular, the following parameters recurrent in the literature (and the related categories), are considered, as shown in Table 1.1 and illustrated in Fig. 2.3: (a) Masonry type (categories: Stone [S], Brick [B], and Adobe [A]); (b) Architectural layout (categories: Basilica (three naves) [Bs], Latin-cross [L-c], and Single-nave [S-n]); (c) Architectural style (categories: Colonial Style [CL], Neo-Classic Style and Variants [NC&V], and Neo-Gothic [NG]); (d) Foot-print area (categories:  $90\text{m}^2 < A1 \leq 500\text{m}^2$ ;  $500\text{m}^2 < A2 \leq 900\text{m}^2$ ; and  $A3 > 900\text{m}^2$ ).



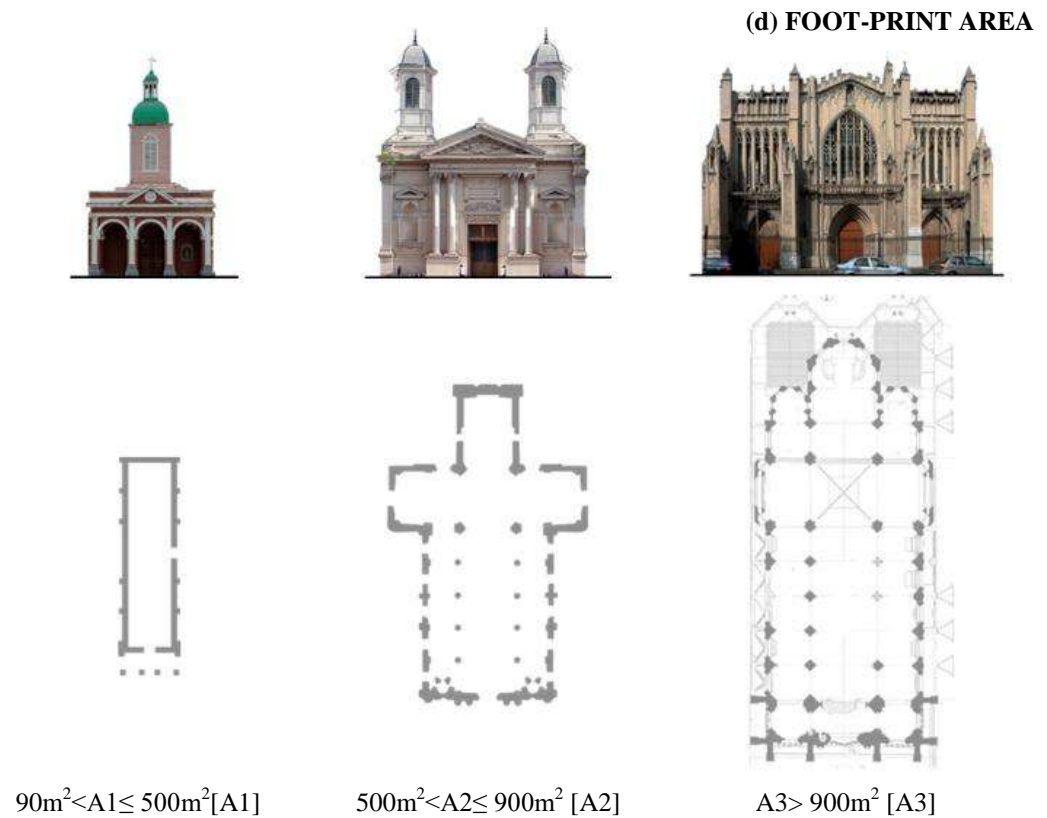
**Figure 2.3-** (a) Masonry type, categories: Stone [S], Brick [B], and Adobe [A].

**(b) ARCHITECTURAL LAYOUT**

**Figure 2.3- (b)** Architectural layout, categories: Basilica (three naves) [Bs], Latin-cross [L-c], and Single-nave [S-n].

**(c) ARCHITECTURAL STYLE**

**Figure 2.3- (c)** Architectural style, categories: Colonial Style [CL], Neo-Classic Style and Variants [Nc&V], and Neo-Gothic [NG].



**Figure 2.3–** (d) Foot-print area (categories:  $90\text{m}^2 < A1 \leq 500\text{m}^2$ ;  $500\text{m}^2 < A2 \leq 900\text{m}^2$ ; and  $A3 > 900\text{m}^2$ ).

Moreover, the database includes the 2010 Maule PGA [g] values and the damage levels recorded after the 2010 Maule earthquake, observations from numerous direct in-situ inspections and damage data from technical reports of Ministry of Public Work (MOP), Council of National Monument (CMN) , and Chilean Episcopal Conference (CECh).

**Table 2.1** - Characterization of the six selected variables

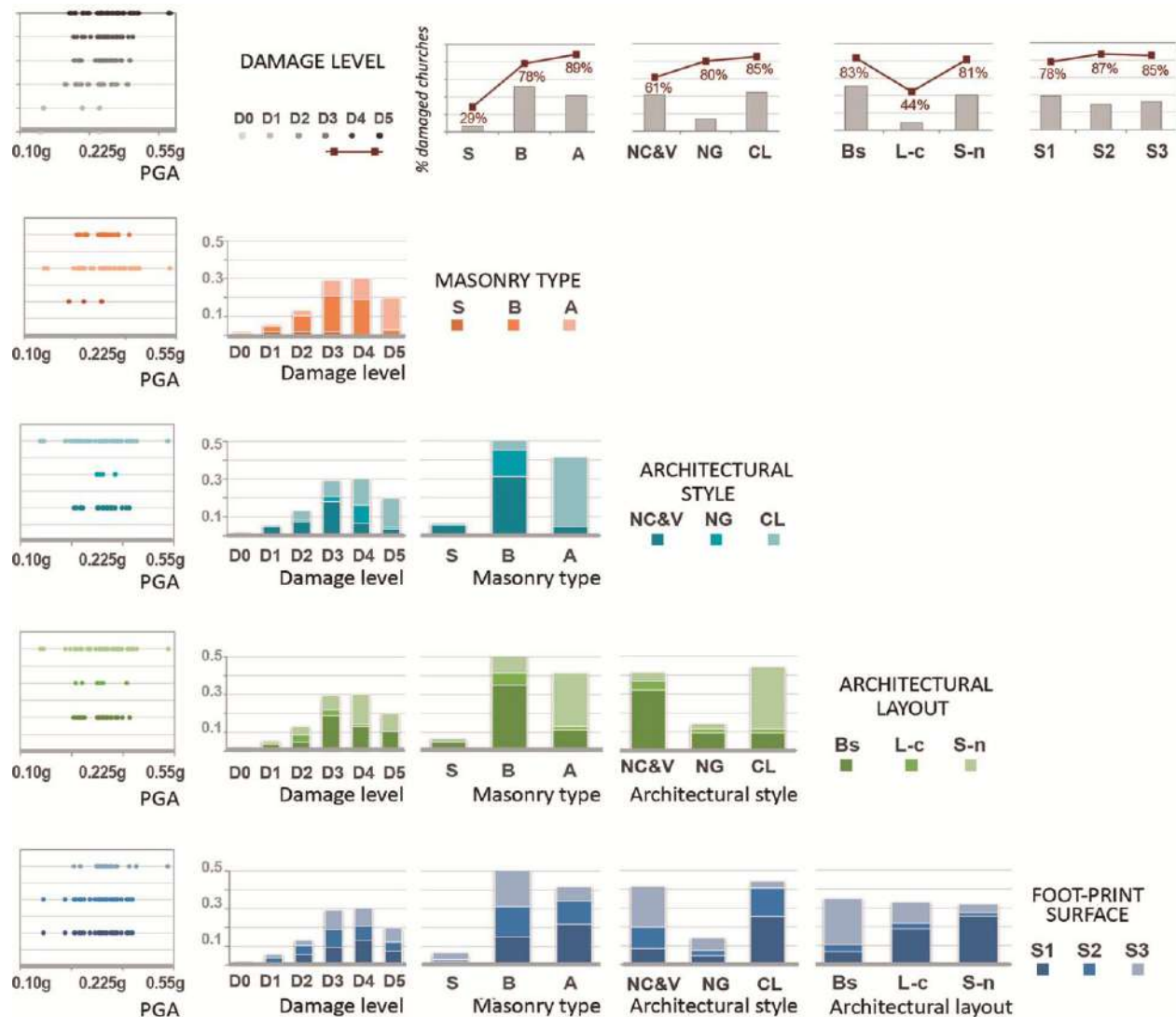
Variables	Description	Type	Range of values
PGA	2010 Maule PGA	Numerical continuous	[0.159g - 0.531g]
Dk	Damage Level	Numerical discrete	[0; 1; 2; 3; 4; 5]
M	Masonry Type	Categorical nominal	Stone, Brick, Adobe
St	Architectural Style	Categorical nominal	Colonial Style, Neo-classic Style & Variants, Neo-gothic Style
L	Architectural Layout	Categorical nominal	Basilica, Single Nave, Latin Cross
S	Foot-print Area	Categorical nominal	$90\text{m}^2 < S1 \leq 500\text{m}^2$ ; $500\text{m}^2 < S2 \leq 900\text{m}^2$ ; and $S3 > 900\text{m}^2$

A global damage index was calculated for each church applying the second-level of the macro-seismic method proposed in (Lagomarsino et al. 2004; Lagomarsino and Podestà, 2004a). This

method has been exhaustively explained in the following Chapter 3, paragraphs 3.2.2 Damage survey, and 3.2.3 Damage indexes.

Briefly, the macro-seismic method used studies the possibility of the formation of varying possible failure mechanisms and, at the end of the analysis through predefined correlations, provides a global damage index for the structure. The Italian practice (G.U. no.55, 7/03/2006 and DPCM, 2011), due to extensive experience with earthquakes and masonry structures, has gathered an abacus of 28 possible failure mechanisms for church typology.

Since the values of the global damage index are real numbers, a transformation of the indices into a discrete variable was carried out to obtain a measurable level of damage in relation to the European Macro seismic Scale (Grunthal, 1998). Thus, each damage index was correlated to a damage level ranging between 0 and 5. As suggested previously (Lagomarsino and Podestà, 2004b; Marotta et al., 2015; and De Matteis et al. 2016), damage classification is done in five levels according to the EMS-1998 scale.



**Figure 2.4-** Matrix of plots for the frequency distributions of the selected variable: 2010 Maule PGA, damage levels after 2010 Maule PGA, and architectural, typological and material parameters (Masonries Type, Architectural Style, Architectural Layout, and Foot-print area).

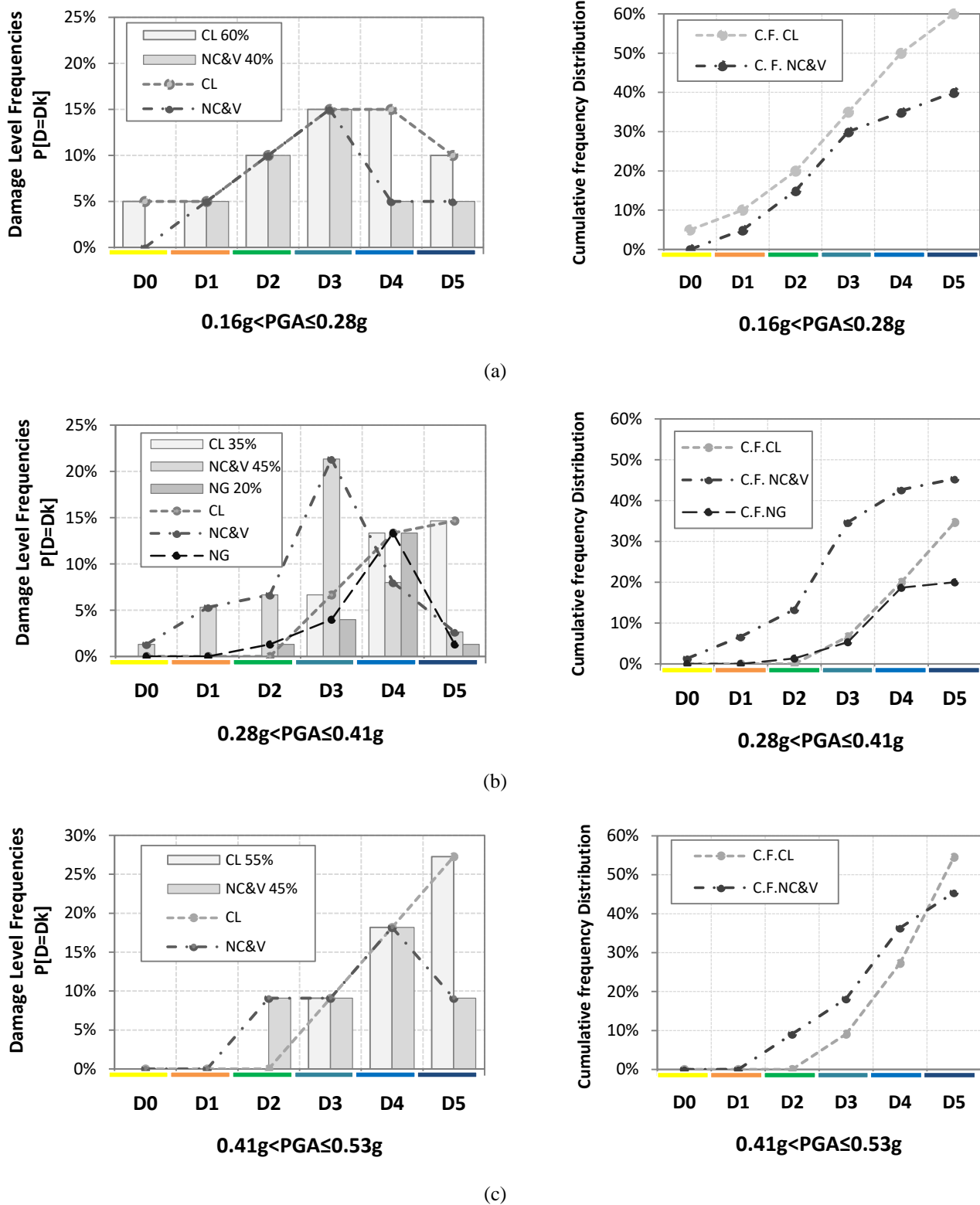
The frequency distribution of Damage Level after the 2010 Maule earthquake and of selected parameters in the studied buildings is summarized in the pie-charts of Fig.2.4. From these diagrams it is possible to observe that half of the stock is constructed with brick and adobe masonry. In fact, only seven churches, mainly concentrated in the City of Santiago, are built with stone masonry. The three-nave Basilica (28% with transept) and the single-nave layouts represent the most common plan-wise arrangement, as opposed to the Latin-cross layout which corresponds to just 9% of the sample. Foot-print area, ranging from 90 to 500m<sup>2</sup>, 500 to 900m<sup>2</sup>, and 900m<sup>2</sup> or greater, is almost evenly distributed in the churches considered.

In Fig.2.4, a matrix of histogram plots the reciprocal frequency distributions of the selected variables described in Table 1.2. This matrix allowed detection a close correlation and interdependency between the construction, architectural, and typological features of the building. It can be observed, for example, that CL churches have predominantly a single-nave layout and are mainly built with adobe. NC&V and NG churches have Basilica layout and are usually built with bricks. Regarding the foot-print area, the CL churches have a smaller surface than the NC&V ones and NG.

Considering similar PGA levels for each class, it is apparent that during the Maule earthquake, adobe churches had the highest damage level followed by CL and the single-nave churches. Conversely, brick churches with Basilica layout and NC&V style demonstrated a lower damage level. Moreover, churches with NG style have suffered higher damage than NC&V churches, despite their stone or brick construction. Such observations are also confirmed by the diagrams of Fig.2.5 which show damage level frequencies reported for the churches classified according to the architectural styles, and averaged according to their total number, and three ranges of seismic intensity during the 2010 Maule earthquake corresponding to: a) moderate level of PGA, range  $0.16g < PGA \leq 0.28g$ ; b) high level of PGA, range  $0.28g < PGA \leq 0.41g$ ; and c) very high level of PGA, range  $0.41g < PGA \leq 0.53g$ . In the diagrams of damage level frequencies presents in Fig.2.5 (a) and (c), the NG churches are not present because they are all located in the Santiago, where the PGA registered was between  $0.28g < PGA \leq 0.41g$ .

From the diagrams of Fig.2.5, it is observed that for the CL style and for higher PGA values (Fig.2.5b,c), the most frequent damage level is D5, while for lower PGA (Fig.2.5a) they are D3 and D4. The most frequent damage level for the NC&V style and lower PGA (Fig.2.5a, b) is D3 while for larger PGA (Fig.2.5c) is still D4. All NG churches are in the mid-range of PGA, and the most frequent damage level is D4.

Both, the matrix of plots and the damage level frequency diagrams, enable the identification of the following three homogeneous classes based on architectonic style, typological-constructive features, and damage levels suffered during the 2010 Maule earthquake. Next, the architectonic and constructive features of each of these groups of churches are analyzed.



**Figure 2.5** - Damage level frequencies and cumulative frequency distributions for the churches divided according to the Architectural Styles, normalized with respect to the total number, for three different PGA ranges according to the experienced seismic intensities suffered during 2010 Maule earthquake: (a) range  $0.16g < PGA \leq 0.28g$ ; (b) range  $0.28g < PGA \leq 0.41g$ ; (c) range  $0.41g < PGA \leq 0.53g$ . In brackets the percentage number of churches for each class.

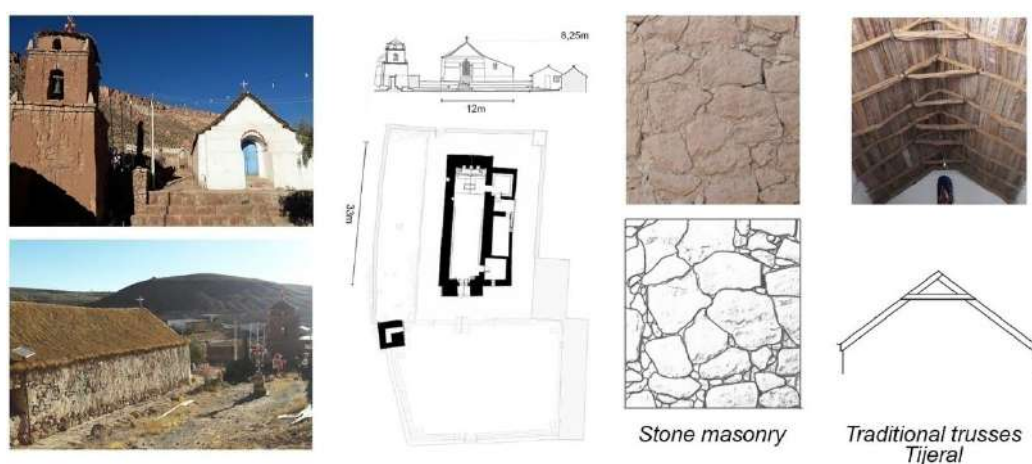
## 2.2 Colonial, Neo-classical and Neo-gothic URM churches

### 2.2.1 Colonial churches (CL)

The first religious Chilean architecture was built in the north and central area of the country during the Hispanic Viceroyalty (1536-1810). These *Colonial* religious buildings are an architectural paradigm, defined by a simple and austere design characterized by a single-nave with an elongated layout, sloping timber roof, with a *par* and *nudillo* traditional trusses (*tijeral*), a plain ceiling, buttresses in same case, and an adobe or wooden bell-tower.

These churches are the result of the combination of different constructive techniques, using the available materials in the different climatic zones of the country, and inherited from different building traditions. In particular, the stone rubble masonry -calcareous stone composed of calcium carbonate and magnesium- and the timber roof -wood of *Queñoa*, *Polylepisrugulosa*- were already employed by Pre-Hispanic indigenous populations (Benavides, 1988). Also, the adobe masonry already existed during the Inca Empire (1470-1530) (Stehberg, 1995).

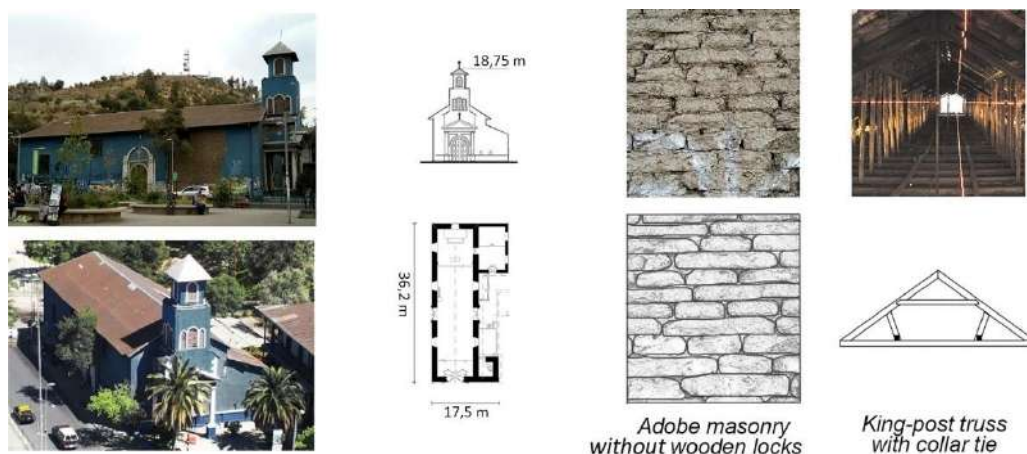
Significant example of this original typology includes the Northern Andean churches of the Cordillera (Fig.2.6 Caspana church). The churches of the Chilean central area generally date back to the 17<sup>th</sup> century and represent a particular constructive variant of the Andean Colonial typology, due to the different climatic context.



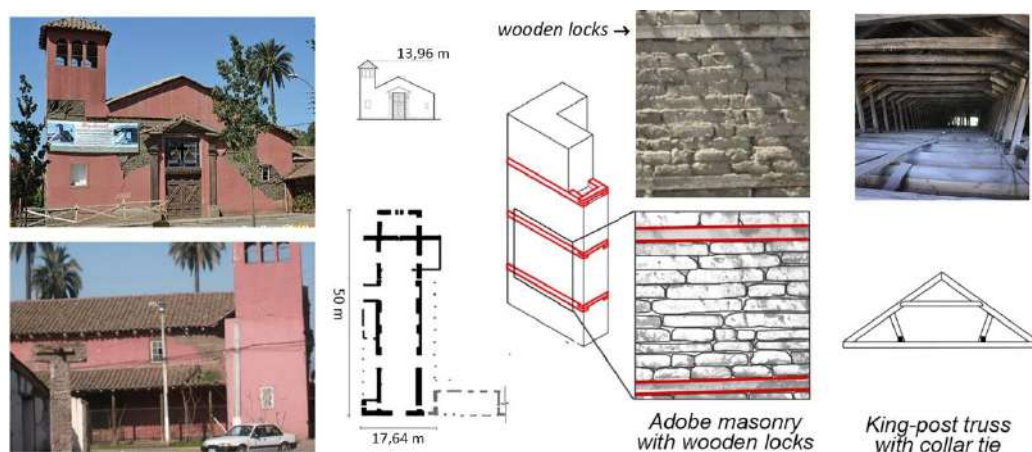
**Figure 2.6** - Colonial church in the North area of Chile: (Antofagasta region).

Indeed, the Central Valley, unlike the Norte Grande and Norte Chico, is rich in wood, and so the architectures have wooden macro-elements, such as porches and bell towers located above a prothyrum set on four slender columns (Fig.2.7 Viñita church).

The churches of this central area are often characterized by mixed masonries, supported by a stone or brick basement of average size of height 90-100cm and depth 60cm, and wooden elements placed inside the wall as internal reinforcement (Fig.2.8 San Judas Tadeo church).



**Figure 2.7** - Colonial church in Central area of Chile: Viñita church in Santiago (Metropolitan region)



**Figure 2.8**- Colonial church Central area of Chile: San Judas Tadeo in Malloa village (Libertador General Bernardo O'Higgins region).

The basement prevents erosion and excessive moisture. On top of the basement, the adobe wall is made of 30x60x10cm earthen blocks, this leading to thicknesses of 60, 90 or 120 cm.

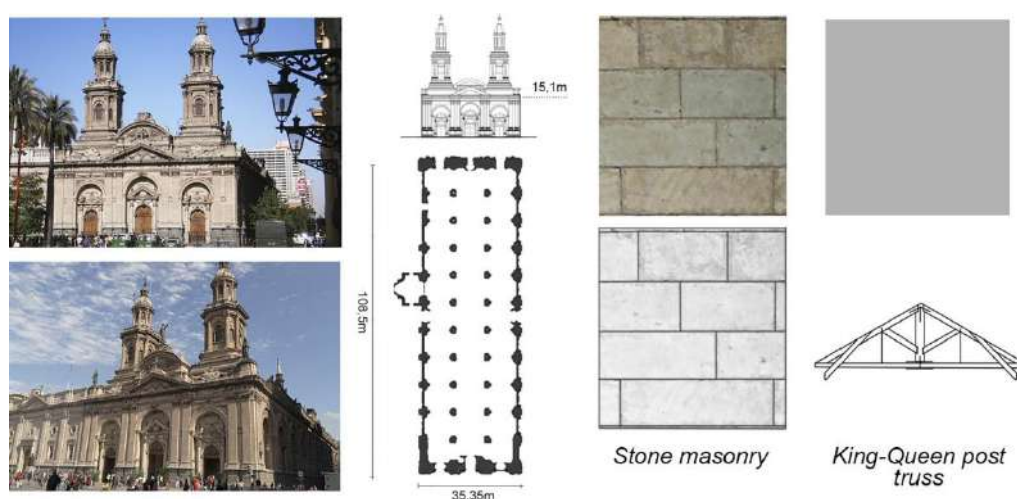
The longitudinal-transverse wooden locks within the masonry impede the separation of walls into different leaves, allowing the vertical load to be distributed along the entire width of the walls (Ortega et al., 2017).

This common traditional earthquake-resistant technique improves the monolithic response of the wall and structural integrity under horizontal actions (Ortega et al., 2018). In this way the wooden elements allow the horizontal in-plane action to work over the entire wall thickness, generating a greater capacity of deformation to the masonry structures.

In general, the structural weaknesses of CL churches are characterized by the lack of tie rods, the absence of adequate interaction between roof structure and longitudinal walls, and a thrusting wooden roof. The absence of effective seismic retrofitting technique is the most critical factor of adobe structure (Dowling, 2004), given the low tensile strength of adobe blocks (INN, 2013). A total of 47 churches were studied in the central zone, considering the Metropolitan and the Libertador General Bernardo O'Higgins regions.

### 2.2.2 Churches with Neo-Classic style & Variants (NC&V)

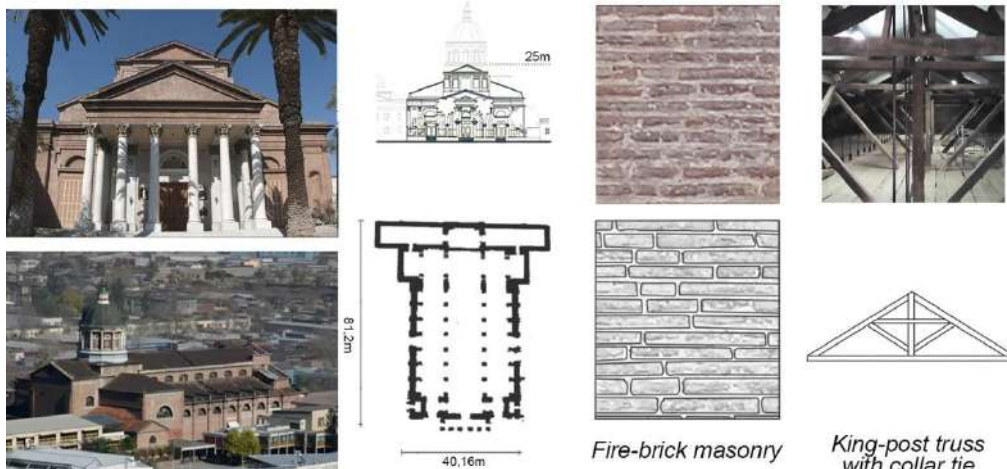
In the last decade of the 18th century, the Italian architect Joaquin Toesca introduced the Neo-classical style in Chile which revolutionized the national architecture (Cáceres, 2007). At the end of the 17<sup>th</sup> century, numerous colonial representative buildings, including many religious constructions, were demolished, such as the Cathedral of Santiago (1747-1913) (Huneus, 1968 and Iglesias & Porte, 1955), to introduce the new Neo-classical forms. After the defeat of the Spanish colonial rule in 1810, the establishment of a Republic (1831) led to economic liberalism and free flowing technological and cultural exchange with other European countries and the United States, thus encouraging new building technologies and architectural languages. This new political condition revolutionized Chilean architecture, producing the hybridization between the European revivalisms (Neo-Baroque, Neo-classical, Neo-Romanesque and Neo-Renaissance styles) and the local construction tradition. The structures of this period, named Republican Buildings became the expression of the transition period between the Colonial and Modern Times. *In this period churches were designed with greater freedom and audacity, becoming more slender and greater in size, radically changing the image of the Chilean cities* (Bahamondez et al. 2012). After the colonial style, these churches were characterized by a more refined and complex morphology such as a Basilica or Latin-cross layouts, consisting of the following *macro-elements*: a central nave, two side aisles (in some case crossed by a transept), an apse, two bell towers, a sloping roof, and false vaults. Despite a wide variety of ornamental and decorative devices, these churches present the same structural and constructive layout.



**Figure 2.9**– Neo-classic church of Central area of Chile: Metropolitan Cathedral of Santiago (Metropolitan region).

During the 1647 and 1730 earthquakes, all churches located in the Santiago were destroyed, except the Colonial San Francisco's church (1572), the oldest building in the city (De Ramón, 2000; Jorquera et al., 2017a, b). The only churches rebuilt of stone masonries were the

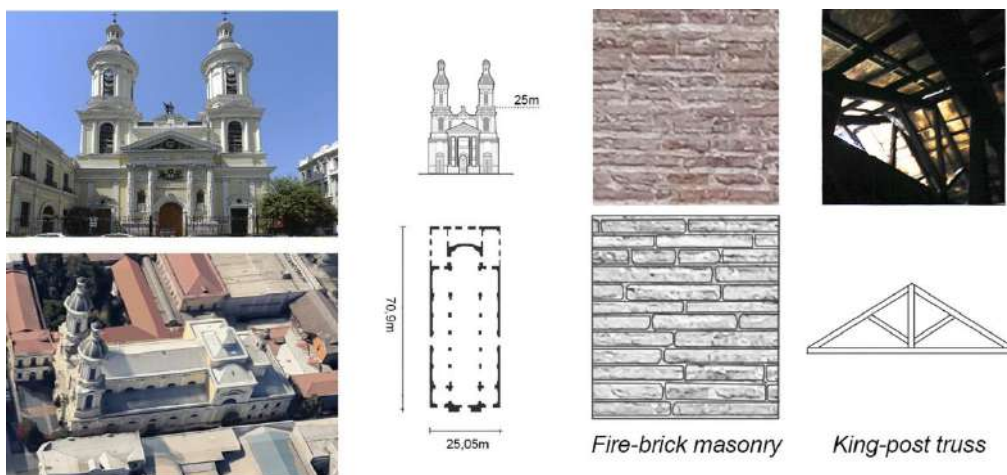
Metropolitan Cathedral of Santiago (1748, Fig.2.9), El Sagrado (1863), Santo Domingo (1747) and La Merced (1736), in *Neoclassical* style.



**Figure 2.10**– Neo-classic church of Central area of Chile: Dominicana church in Santiago (RM).

The stone walls of these churches have common features i.e. a square cut stone elements 100x50x50cm -generally, *Biotite Andesite* and *Clinopyroxene Basaltic Andesite* rocks-, staggering of vertical joints, and good quality mortar that provides friction resistance and high resistance to in-plane response. It has also the presence of transverse blocks that cross the wall thickness, ensuring a monolithic behavior of the wall, and horizontal layers of the blocks that produce a good distribution of vertical loads.

Most of these churches, which were also built in brick masonry, consist of two (rarely three) heads with brick element sizes of about 40x22x7cm and 20x12x5cm, lime or earth mortar, and a stone or brick basements of depth about 60 cm to prevent basal wall erosion. These churches have the same architectural layout of the Neo-classical stone churches.



**Figure 2.11** – Neo-classic church of Central area of Chile: San Ignacio church in Santiago (RM).

Distinguished examples are the Recoleta Dominicana in Fig.2.10, which has a resemblance to the *San Paolo Fuori le Mura* church in Rome (Cazanova, 1998), and the San Ignacio church,

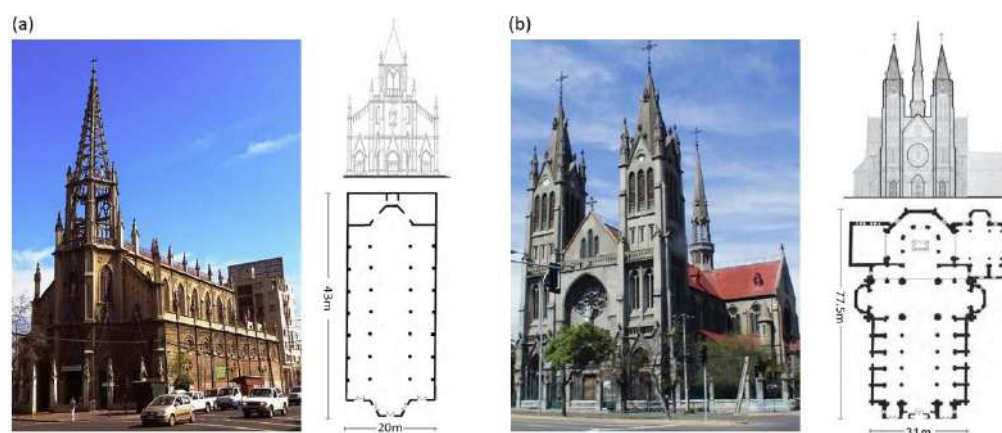
both located in Santiago and designed by the architect Eusebio Chielli, one of the leading representatives of the neo-classical modernism, Fig.2.11.

During 2010 Maule earthquake, low damage levels were observed in the Neo-classical churches. The lower vulnerability of these buildings can be related to symmetric and rectangular Basilica plans with three naves, massive lateral walls, facades characterized by good quality masonry, light timber roof, and bell tower structures with the absence of a dome. Moreover, constant maintenance works have led to a good preservation. Including the Metropolitan and the Libertador General Bernardo O'Higgins Regions, a total stock of forty-four NC&V churches were analyzed.

### 2.2.3 Neo-gothic churches (NG)

The first manifestations of Gothic reminiscence occurred in Chile almost 100 years later than those seen in Europe. In fact, the construction of Neo-gothic ecclesiastic buildings was constant from the 19<sup>th</sup> century and the first three decades of the 20<sup>th</sup> century, when the President José Manuel Balmaceda called on European architects, as Emilio Doyère and Eugène Joannon, to complete a vast plan of constructions.

The Chilean Neo-gothic churches (NG) represent overlap with the German Brick-Gothic, *Backsteingotik*, in a highly seismic context. Generally, these huge brick structures present a Basilica plan composed by three slender aisles, where the central nave is higher than the lateral aisles, in some case crossed by a transept. The central nave and the side aisles are covered by lightweight rib vaults, with a roof structure constituted by timber or steel trusses and galvanized iron plates. The presence of slender buttresses, large windows and rose-windows, a slender bell-tower (rarely two), and the absence of flying-buttresses -mostly destroyed after severe earthquakes- characterize the shape of these buildings.

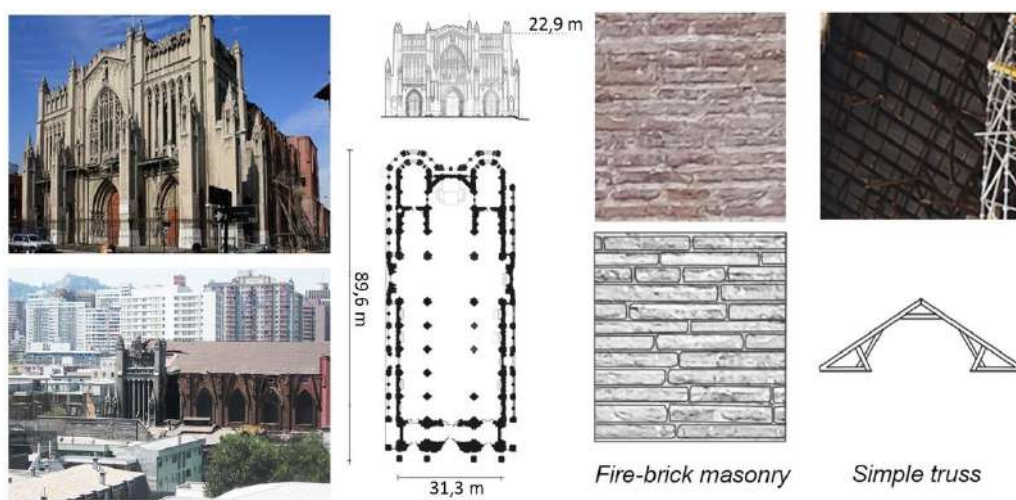


**Figure 2.12** – RC Neo-gothic churches located in the Central area of Chile: (a) Niño Jesus de Praga Parish (Metropolitan region), and (b) Basilica del Perpetuo Socorro Parish (Metropolitan region).

From the beginning of the 20<sup>th</sup> century, reinforced concrete and steel structures began to be adopted in the construction of the Neo-gothic churches. Examples of this architectural style

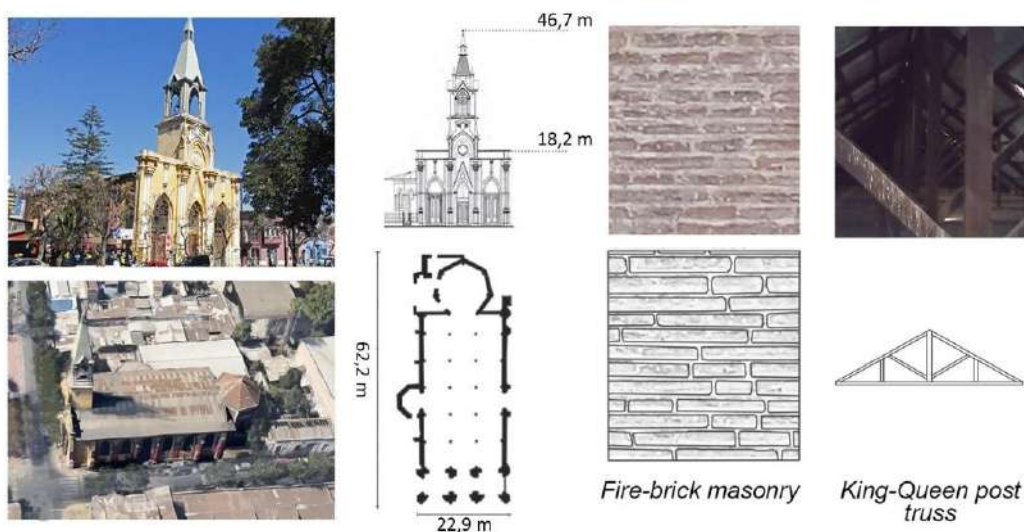
and material in Santiago are the Basilica del Perpetuo Socorro (1906-1919) Fig.2.12a, and the Niño Jesus of Prague Parish (1916-1920) Fig.2.12b, in Santiago.

On the other hand, the constructive features of the URM Neo-gothic churches led to high seismic vulnerability because the geometrical canons produced inadequate geometrical ratios of the structural elements. In addition to their high vertical and horizontal slenderness, the lack of structural elements necessary to guarantee a *box-like behavior*, using chains and tie-rods, and the absence of flying buttresses, make these churches very vulnerable (Fig.2.13, Basilica del Salvador).



**Figure 2.13** – URM Neo-gothic church of Central area of Chile: the Basilica del Salvador.

The churches of San Saturnino (Fig. 2.14), Santísimo Sacramento, Santa Filomena, and San Pedro, in Santiago, present an additional vulnerability associated with the presence of a bell tower located on the narthex. It should be noted that the towers, although slender, can contribute to the lateral rigidity, while they can cause tensional effects.



**Figure 2.14** – URM Neo-gothic church of Central area of Chile: San Saturnino.

After the March 3, 1985 earthquake, all of these churches were heavily damaged, and many of the bell-towers collapsed and had to be rebuilt with mixed structures of bricks, steel, and RC. In the analyzed Regions, fifteen Neo-gothic churches of brick URM were studied.

### 2.3 Preliminary qualitative assessment of seismic fragility of churches

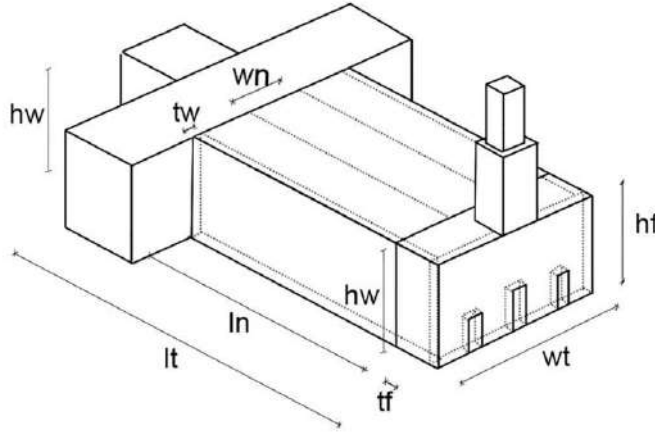
A preliminary qualitative assessment of the seismic capacity of the URM churches of central Chile was carried out by surveying some geometrical indices, defined mostly by geometric ratios between building dimensions. These indices allow to define of a so-called earthquake-resistant architectural morphology, since building dimensions are involved in the activation of local mechanisms induced by seismic actions, or somewhat associated with the global seismic resistance of the buildings. This procedure is based on a simplified approach that permits easy estimation of the vulnerability of a large number of buildings. The vulnerability is assessed by comparing the geometrical data and taking into account a local seismic hazard intensity measure of the Maule earthquake, i.e. PGA values. The average values ( $\mu_x$ ) of selected indices and the corresponding standard deviation ( $\sigma_x$ ), summarized in Table 2.2 and indicated separately for Colonial (CL), Neo-Classic (NC&V) and Neo-gothic (NG) churches, are: (i) the width-to-length ratio [wt/lt] of the church, (ii) the nave length-to-total length [ln/lt], (iii) the nave width-to-total width [wn/wt], (iv) the façade clear height-to-width aspect ratio [hf/wt], (v) the façade thickness-to-height [tf/hf], and (vi) the lateral wall thickness-to-height [tw/hw] ratio.

**Table.2.2** -Typical geometric ratios of the URM churches: width-to-length [wt/lt]; nave length-to-total length [ln/lt]; and nave width-to-total width [wn/wt] facade height-to-facade width [hf/wf] facade thickness-to-height [tf/hf]; and lateral walls thickness-to-height [tw/hw]. The data are average values for the three classes: Colonial churches (CL), Churches with Neo-classic style and Variant (NC&V), Neo-gothic churches (NG).

ID	wt/lt ( $\mu_{wt/lt}$ )	ln/lt ( $\mu_{ln/lt}$ )	wn/wt ( $\mu_{wn/wt}$ )	hf/wt ( $\mu_{hf/wt}$ )	tf/hf ( $\mu_{tf/hf}$ )	tw/hw( $\mu_{tw/hw}$ )
<b>CL</b> ( $\sigma_x$ )	0.38 (0.107)	1.0 (0.121)	1.0 (0.248)	1.0 (0.187)	0.111 (0.024)	0.125 (0.039)
<b>NC&amp;V</b> ( $\sigma_x$ )	0.45 (0.085)	0.7 (0.152)	0.5 (0.223)	0.7 (0.327)	0.1 (0.019)	0.12 (0.025)
<b>NG</b> ( $\sigma_x$ )	0.38 (0.091)	0.7 (0.222)	0.6 (0.21)	1.9 (0.602)	0.095 (0.016)	0.07 (0.025)
Thresholds	0.5*	-	-	2**	0.111*** or 0.145***	0.111*** or 0.145***

\*(Cruz, 1995; Elnashai & Di Sarno, 2008); \*\* (Eurocode 8); \*\*\* (Eurocode 6; Eurocode 8; and ACI-530-99/ASCE 5-99); \*\*\*\* (INN, 2013)

In Fig.2.15 a schematic representation of churches with the dimensions used in computation of the geometric indices reported in Table 2.2 is presented.



**Figure 2.15** -Dimensions of churches used in computation of the geometric indices

The  $[wt/lt]$ ,  $[ln/lt]$  and  $[wn/wt]$  indices are recurrent in the literature (Arnold, 1982; Lourenço & Roque, 2006; Lourenço et al., 2013; Jorquera et al., 2017b) and are codified in some international Codes such as the European Standards of *Design of masonry structures* (Eurocode 6, 2006) and *Design of structures for earthquake resistance* (Eurocode 8, 2004), the Chilean *Standard for the Structural Intervention of Earthen Historical Buildings* (INN, 2013), and the *American Building Code Requirements for Masonry Structures* (ACI-530-99/ASCE 5-99). In Table 2.2, the code thresholds are reported in agreement with (Cruz, 1995; Elnashai & Di Sarno, 2008; Lourenço et al., 2013; INN, 2013; Eurocode 6; and Eurocode 8).

The CL and NG buildings present a width that is on average 0.38 times greater than its length, while the NC&V buildings approximately 0.45 times greater. These geometrical proportions determine an unsatisfactory seismic response of lateral walls according to Cruz (1995) and Elnashai & Di Sarno (2008), where a minimum ratio threshold  $wt/lt=0.5$  is proposed in the definition of a structural configuration for effective earthquake resistance. The shape of the plan has been identified as a fundamental parameter in the control of the seismic performance of buildings (Mezzi, 2003). In fact, elongated plans are disadvantageous causing not uniform displacements and leading to tensional effects (Grases, 1987). After the 2010 Maule earthquake, in about 75% of churches with  $wt/lt < 0.5$ , the local failures related to out-of-plane mechanisms of lateral walls have been observed.

The nave length-to-total length  $[ln/lt]$  and nave width-to-total width  $[wn/wt]$  ratios reflect the simplicity of the CL layout often characterized by a single nave, (i.e.,  $\mu_{ln/lt}=1.0$  and  $\sigma_{ln/lt}=0.121$ ; and  $\mu_{wn/wt}=1.0$  and  $\sigma_{wn/wt}=0.248$ ). While, a greater layout complexity due to the presence of narthex and apse ( $\mu_{ln/lt}=0.7$  and  $\sigma_{ln/lt}=0.152$ ), and side aisles ( $\mu_{wn/wt}=0.5$  and  $\sigma_{wn/wt}=0.223$ ) in the

NC&V and NG (i.e.,  $\mu_{ln/lt}=0.7$ ,  $\sigma_{ln/lt}=0.222$ , and  $\mu_{wn/wt}=0.6$ ,  $\sigma_{wn/wt}=0.21$ ) architectures is highlighted.

Regarding the facade index clear height-to-width ratio [hf/wt], all groups fulfill the requirement proposed elsewhere (Cruz, 1995 and Eurocode 8), which imposes a maximum clear height twice the width of the wall height for masonry walls subjected to vertical loading, so as to give appropriate stability and robustness. Despite the fulfillment of this demand, NG churches show a safety limit condition due to the presence of a bell-tower in the façade (present in 93% of the NG buildings) that determines a predominance of verticality ( $\mu_{hf/wt}=1.9$ , and  $\sigma_{hf/wt}=0.6023$ ).

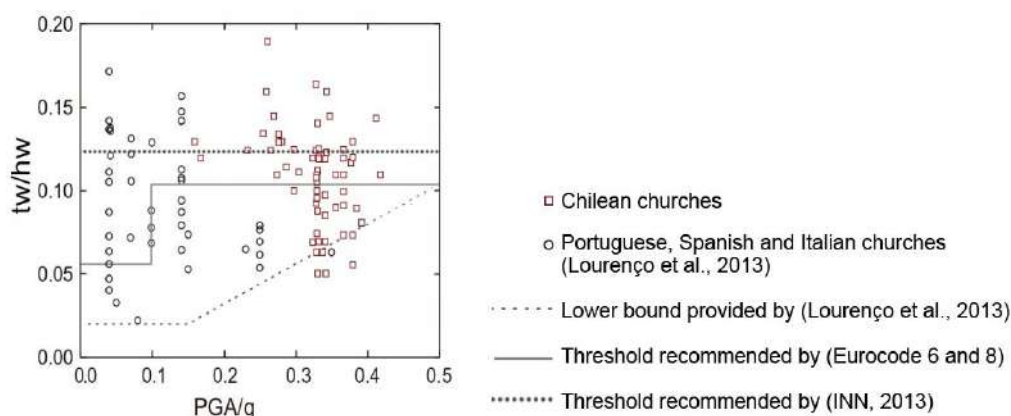
The out-of-plane indices (Lourenço et al., 2013) stiffness-to-height of façade [tf/hf] and stiffness-to-height of lateral walls [tw/hw] are computed only for 72 churches with known wall thickness. According to codes (Eurocode 6 and Eurocode 8; and ACI-530-99/ASCE 5-99), in order to prevent the out-of-plane bending collapse, the height of macro-element must be greater than or equal 0.111 times the thickness in the case of URM buildings located in high ( $0.25g < PGA \leq 0.5g$ ) and moderate ( $0.1g < PGA \leq 0.25g$ ) seismic zones.

The Chilean Code NCh3332, Standard for the Structural Intervention of Earthen Historical Buildings (INN, 2013), defines for adobe structures a limit ratio  $t/h \geq 0.125$ . Regarding the CL churches, it is interesting to note that in about 62% of the analyzed buildings, while the side walls satisfy the NCh3332 requirement ( $\mu_{tw/hw}=0.125$  and  $\sigma_{tw/hw}=0.0386$ ), the façade wall is slenderer due to the presence of a tympanum ( $\mu_{tf/hf}=0.111$ , and  $\sigma_{tf/hf}=0.024$ ).

In Fig.2.16, the indices (tw/hw) of 72 Chilean churches are compared with the indices of 44 monuments from Italy, Portugal, and Spain (Lourenço et al., 2013), with normalized PGA [ag/g]. In this diagram, the thresholds proposed in codes (INN, 2013; Eurocode 6; and Eurocode 8) are also reported. The stock of Chilean churches, always localized in high seismicity areas, doesn't satisfy the Eurocode's requirements in the 36.1% of the cases, while, the European stock shows deficient performance to out-of-plane behavior in the 18.1% of the sample for low seismicity areas, and 29.5% for moderate seismicity zones. Furthermore, the tw/hw indices increase continuously with the PGA for the Portuguese, Spanish and Italian churches, while the out-of-plane indices of lateral walls of Chilean stock are independent of the seismicity.

As mentioned above, the Chilean constructive culture before the Spanish colonization was aware of seismic risk and traditional seismic resistant practices were implemented, as squat structures with one-floor, and regular and simple geometries.

Conversely, anti-seismic construction techniques were not used in architectures characterized by European architectural revivalisms, where builders of Spanish origin demonstrated to be insufficient awareness of Chilean seismicity. As a result, traditional seismic practices were forgotten and disappeared in subsequent construction techniques.



**Figure 2.16** -The out-of-plane indexes of lateral walls, thickness-to-height [ $t_w/h_w$ ], of 72 URM Chilean churches are compared with the same indexes of 44 Portuguese, Spanish and Italian churches investigated in (Lourenço et al., 2013).

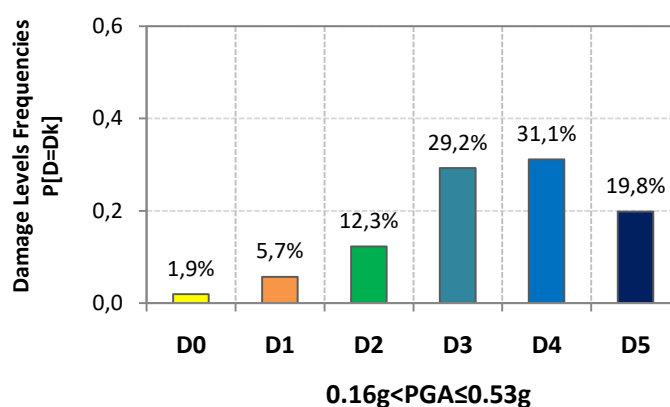
It can be noted that the activation of the overturning and the bending out-of-plane mechanism of the façade top, during the 2010 seismic event, is present in the 70% of the analyzed cases. The absence of ties, the presence of a significant distance between the transverse walls and the presence of wide openings represent critical components for these mechanisms. As observed elsewhere (D'Ayala and Speranza 2003, Lagomarsino and Podestà 2004a, b), façade mechanisms were frequent occurred in Italian churches. A common retrofit strategy to improve the seismic response of façade macro-elements in Chilean buildings has been the reconstruction of the upper part of façade (gable) with wooden partition walls (*tabique*). Despite this retrofitting with wood-elements, increasing heterogeneity, good links between the wooden partition walls and the beams of the roof constrain the structure, providing a *box-behavior*. Furthermore, it also reduces the height of URM façade macro-element and, consequently, the destabilizing moment. The effectiveness of this type of retrofitting was evaluated in Chapter 5.2 where the assessment of seismic performance of *San Francisco* church (in Santiago) was carried out. Particularly, in this church after the collapse of the upper part of presbytery façade, the gable was replaced with a wooden structure linked to the roof elements: the comparative analysis between the current state and the state before the collapse shows a significant improvement of the seismic behavior, confirmed by the good response of the macro-element following the 2010 Maule earthquake.

The thickness-to-height ratio of NG macro-elements reveals the large seismic vulnerability of these structures due to the slenderness of the façade and lateral walls, which do not meet the Standard requirements in 87% of the analyzed stock ( $\mu_{t_w/h_w}=0.07$ , and  $\sigma_{t_w/h_w}=0.012$ ; and  $\mu_{t_f/h_f}=0.025$ ,  $\sigma_{t_f/h_f}=0.016$ ), as confirmed elsewhere (De Matteis, 2007, De Matteis, 2010) also for Gothic buildings in the Mediterranean area where seismic risk is much lower. In contrast, 75% of the NC&V churches present satisfactory thickness-to-height ratios of façade and lateral walls according to the requirements of International Masonry Codes (Eurocode 6, Eurocode 8, and ACI-530-99/ASCE 5-99) with  $\mu_{t_w/h_w}=0.12$  and  $\sigma_{t_w/h_w}=0.025$ , and  $\mu_{t_f/h_f}=0.10$  and  $\sigma_{t_f/h_f}=0.019$ .

## 2.4 Summary

This archival Chapter is a preliminary study of the seismic fragility of URM Chilean churches and offers a complete overview of their architectural, structural, and constructive characteristics.

The 2010 Maule Earthquake was a large megathrust event that rupture almost 550 km of the interface between the Nazca and South American plate in a bilateral longitudinal mode, causing severe ground motions that proved once again the inadequate structural response of URM churches in highly seismic areas. About 20% of these heritage buildings were demolished due to major structural damage, and almost 60% were classified with moderate structural damage levels (Fig. 2.17).



**Figure 2.17** - Damage levels of URM churches following 2010 Maule earthquake

A total of 106 buildings were analyzed using the following descriptive parameters: masonry type, architectural layout, architectural style and foot-print area. Among the analyzed parameters employed, the architectural style was added as an original to those usually assumed in the literature. The damage level observed after the Maule earthquake was determined for each building.

These analyses have led to the identification of three groups of buildings defined according to architectural style that present rather homogeneous characteristic. The classes connected to the architectural style are: Colonial, CL, Neoclassical and Variant, NC&V, and Neo-gothic NG (Fig. 2.18).

As a relevant outcome, it is found that the parameter “architectural style” is more representative than others in sorting the stock of churches in homogeneous groups under the constructive point of view, and in relation with the observed damage levels (first objective of this research at macro-scale, section 1.4). This result is highlighted through the crossed comparison among the frequency distributions of the selected variables, Figure 2.4.

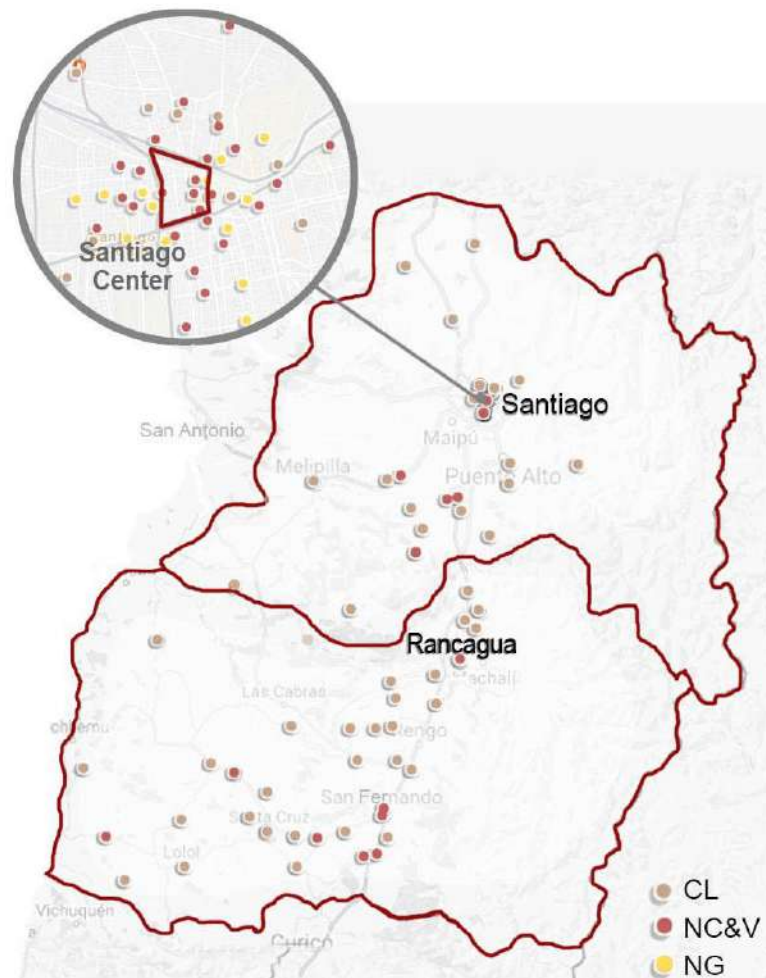
Further results obtained from these preliminary analyses lead to the following observations and conclusions:

- All churches are located in high intensities seismic areas - zones II and III according to the classification of the Chilean code NCh433Of96 - with peak ground acceleration (PGA) ranging between 0.3g and 0.4g.
- The architectural style groups also correspond to different time periods: Colonial (1536-1810), Neoclassical (last decade of 18th century) and Neo-gothic (since the 19th century and the first three decades of the 20th century).
- The most recurrent architectural layouts are the three-nave Basilica layout (51%) and single-nave layout (41%). Furthermore, Neo-gothic and Neo-classic churches have a more complex plan layout than colonial churches.
- A total of 52% of the churches were built with brick masonry, 42% of adobe and/or *quincha*, and the remaining 7% with stone masonry.
- The roof structure of colonial churches is usually made with trusses. The use of wood and metal trusses is common in Neo-classical and Neo-gothic churches, while rare is the use of earthquake reinforcements such as ties-rod and ring-beam. Cross and barrel vaults are always false vaults consist of mats of reeds tied with thread and anchored to wooden ribs with square nails (*camorcanna* or *incannicciato*).

In addition to this, a set of geometric indices, representative of the volumetric layout of the churches is defined to carry out, a preliminary assessment of seismic vulnerability of the three groups of architectural style. A quantitative analysis of geometrical indices confirmed that these groups, CL, NC&V and NG, as representative of seismic fragility classes (second objective of this research at macro-scale, section 1.4). Further and specific considerations can be drawn:

- Longitudinal walls of the Neo-gothic and Colonial churches exhibit high vulnerability due to low masonry quality, absence of earthquake-resistant devices, lack of bonds and absence of adequate connections with roof structure and nave walls. Severe damage and collapse in longitudinal walls were observed in 75% of churches during the 2010 Maule earthquake, attributed to an elongated building plan, with plan length-to-width aspect ratio of 0.38.
- The façade of the Neo-gothic churches shows predominant verticality ( $\mu_{hf/wt}=1.9$ ) and a limit safety condition, while the same macro-element in the Neo-classical and Colonial churches fulfills the provision of the Eurocode8 (i.e. facade height-to-facade width  $\leq 2$ ) with a largely horizontal development ( $\mu_{hf/wt}=0.7$  and 1, respectively).
- The slenderness of the facades of Colonial churches (mostly built in adobe), does not meet in the 61.9% of the cases the requirements of the Chilean Code for Intervention of Historic Adobe Structures, with facade thickness-to-height  $\geq 0.145$ .

- With regards to the out-of-plane behavior, of both, the facade and lateral walls, the Neoclassical churches satisfy 77.8% of the cases the threshold imposed by Eurocode8 for high seismicity, i.e. facade thickness-to-height  $\geq 0.111$ , while the Neo-gothic churches do not verify this provision in 73.4% of the cases.



**Figure 2.18** - URM churches in the Metropolitan (RM) and in the Libertador General Bernardo O'Higgins (VI) Regions with indicate the seismic zonification of the RM and VI regions.

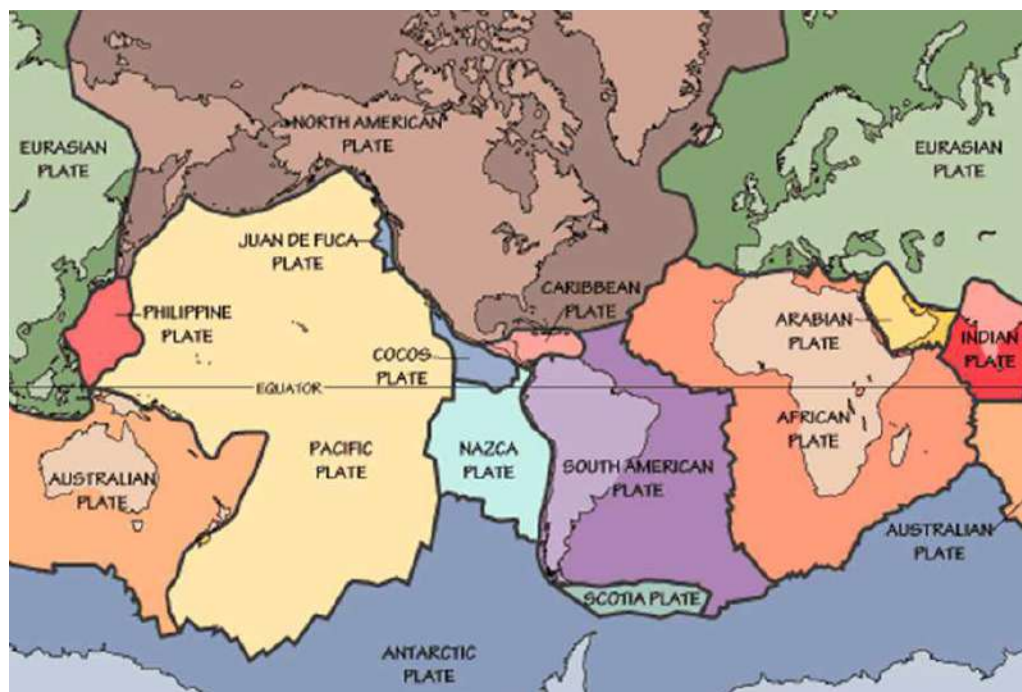


# Chapter 3

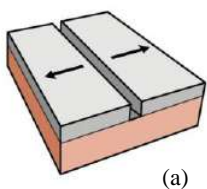
## SEISMIC HAZARD OF CHILE

### 3.1 Seismicity of the region

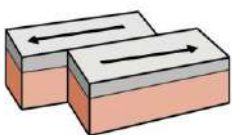
According to plate tectonics theory, which explains the occurrence of most earthquakes, the surface of the earth is composed of large moving plates (lithosphere). They displace over more ductile, dense and higher temperature layers (asthenosphere) due to convection currents. The high degree of ductility of the asthenosphere allows Tectonic Plates to displace at average speeds of 1 to 13 cm/year and interact with each other (Fig.3.1, Comte, 2010). This movement is responsible for the formation of the crust, volcanism, minerals and most earthquakes.



*Figure 3.1 - Tectonic Plates (Comte, 2010).*



(a)



(b)

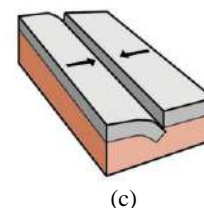
The main types of interaction between edges of tectonic plates are the following (Fig.3.2):

a) Divergent boundaries (Fig.3.2a): Corresponds to the separation or parallel separation between two plates. It can occur between two continental plates (in-land) forming new seas and lakes and creating over the years new micro-plates, or between two oceanic plates (under the sea), which favor the intrusion of magma.

b) Transform boundaries (Fig.3.2b): It occurs when two plates move parallel to each other in opposite directions, producing friction and accumulating energy when locked. An example of this type of interaction is the San Andreas Fault in California.

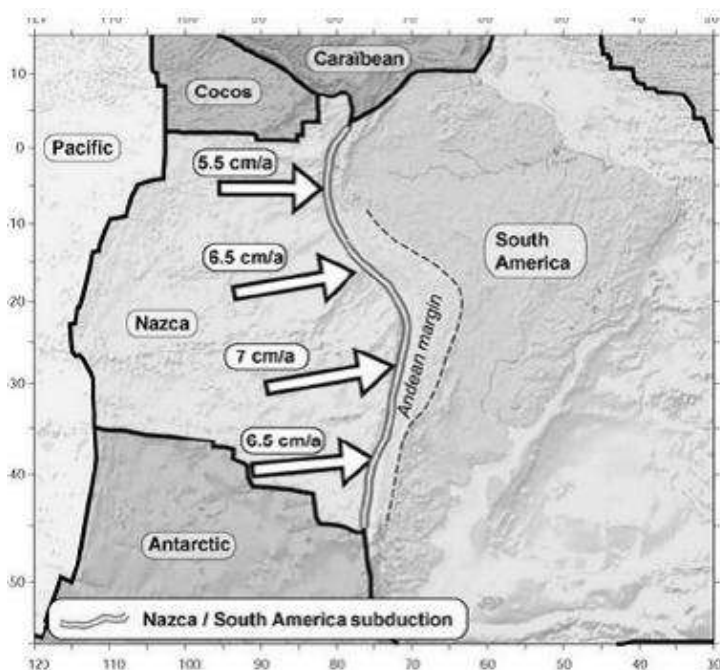
c) Convergent boundaries (Fig.3.2c): It occurs when two or more plates collide:

- If the convergence is between an oceanic and a continental plate, the first sinks under the second by a phenomenon called subduction. Consequence of this interaction is an ocean trench on the ocean side and a volcanic mountain range parallel to the trench on the continental side, usually forming a volcanic arch (Mariana Trench, 10,915m).
- If the convergence is two oceanic lithospheres, one of the two subduct under the other generating this time an insular archipelago, consisting of volcanic islands (Peruvian-Chilean Trench, 8,693m).
- When two continental plates directly collide, a subduction, or a battle can take place, from which a mountain range will arise (examples are the European Alps and Himalayas). In very rare cases, one clod rises above the other causing the phenomenon of obduction, a process opposite to subduction, so that scraps of crust are pushed upwards instead of sinking downwards, and overflow the contact margin.



**Figure 3.2** - Types of interaction between the edges of tectonic plates (Comte, 2010).

Chile is one of the most seismically active countries in the world. This high activity is a product of the interaction between the Nazca, Antarctic, Scotia and South-American plates. The Nazca plate (oceanic plate) is subducting beneath the South-American plate (continental plate). The Nazca plate moves east ward with a convergence velocity ranging from 5.5 to 7 cm/yr (Khazaradze and Klotz 2003; Leyton, Ruiz, and Sepúlveda 2009). The South-American plate moves to west ward with a convergence velocity of about 3 cm/yr, generating a convergence rate of a estimated 8 to 10 cm / yr (Silva, 2008).



**Figure 3.3**- Interaction between the Nazca, Antarctic, and South-American plates (Vigny, 2003).

This subduction phenomenon is defined by the *Wadati & Benioff Plane*, which corresponds to the geometrical space of subduction zone, where earthquake hypocenters occur. The *Wadati*

&Benioff Plane has an inclination between 10° to 30° toward the east, defining three main segmentation zones of the Nazca plate in Chile (Barazangi and Isacks, 1976).

- i) Segment 1: Zone between the 15°S and 27°S latitudes where the Nazca plate descends under the South American continent at an angle of about 25° to 30°;
- ii) Segment 2: Zone between the 26° S and 33° S latitudes, where the Nazca plate bent under the South-American continent and descends under Argentina with an angle of only about 10° of inclination; and
- iii) Segment 3: Zone from 33° S where the Nazca plate descends under the South American continent at an angle of about 30°.

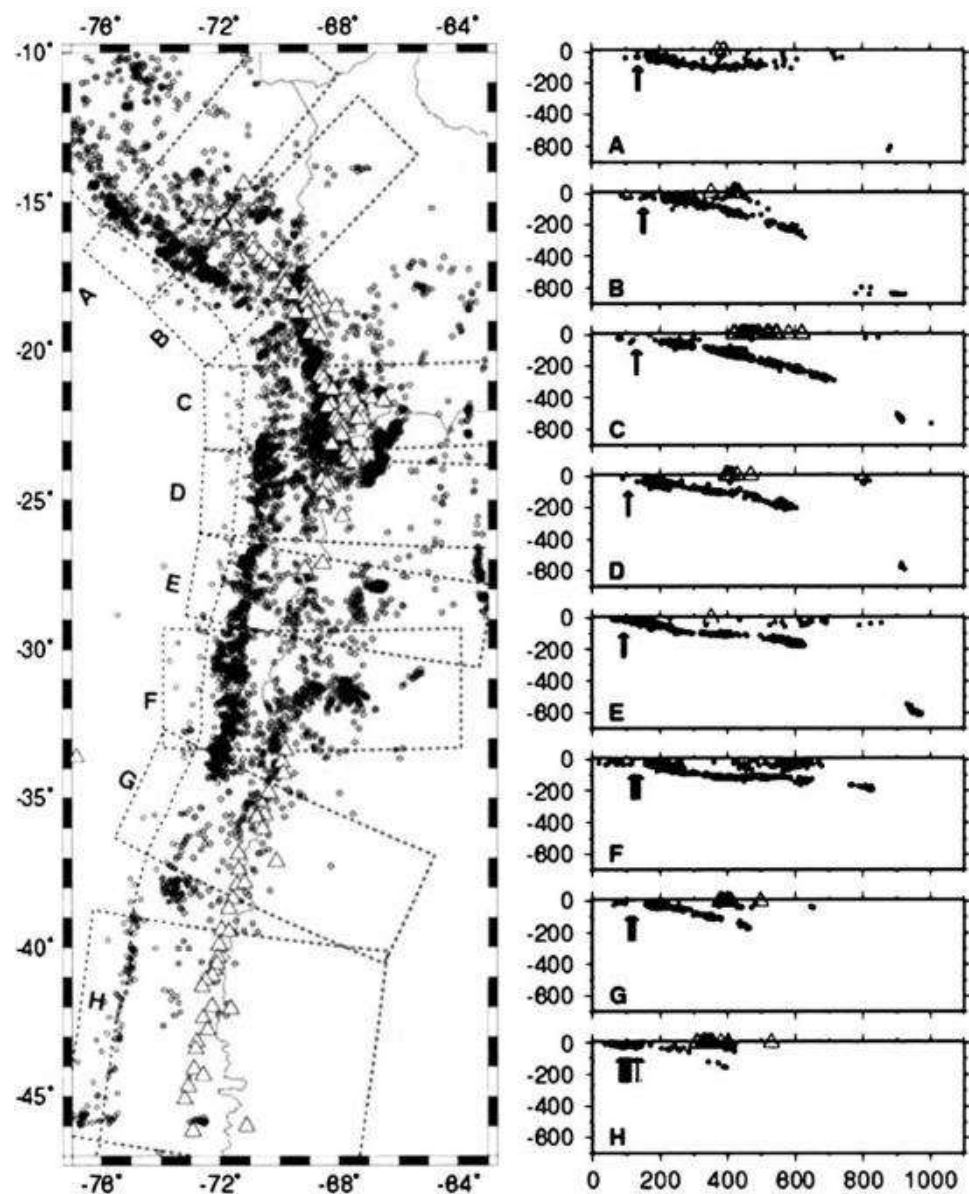


Figure 3.4- Inclinations of Wadati & Benioff Plane ( Engdahl y Villaseñor, 2003).

The earthquakes in the Chilean subduction zone are due to the continuous displacements of the plates, which generate stresses due to interpolate friction and locking. Thus, the shear stresses

increase until the sliding limit is reached. Sliding occurs and the two plates go back to an intermediate state but without stresses. As shown elsewhere (Leyton, 2010), four seismogenic sources are distinguishable:

- a) Inter-plate earthquakes: at the contact surface between the South-American and Nazca plates, extending from an approximate depth of 50 km to of 60 km;
- b) Intra-plate earthquakes: at the contact surface between the South-American and Nazca plates, extending from a depth of 50 km to 200 km;
- c) Cortical earthquakes: within the South-American plate mainly in the pre-cordillera and cordillera zones at a depth shallower than 30km.
- d) Outer-rise earthquakes: produced by a bending of the Nazca plate before to subduction.

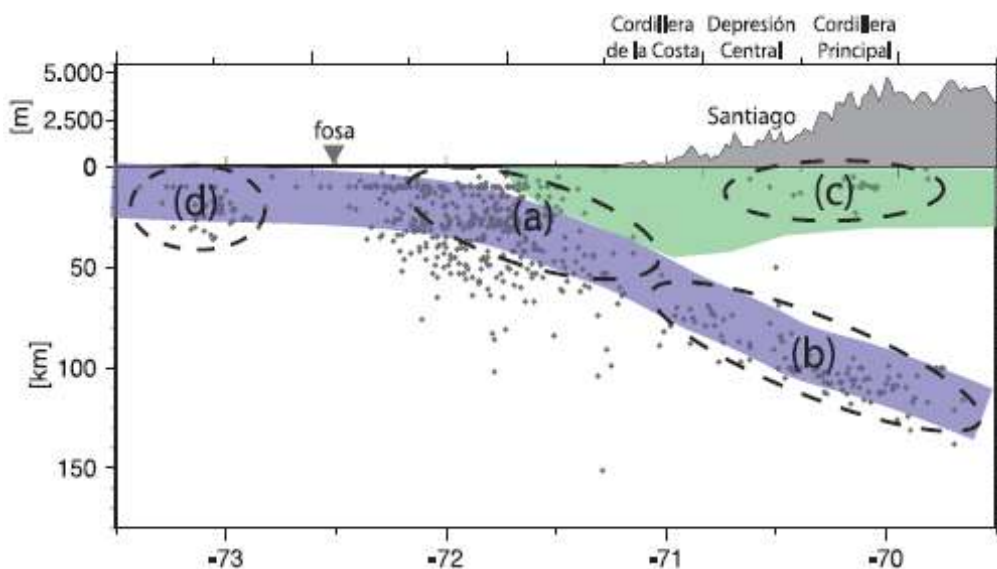


Figure 3.5 - Chilean subduction zone: the four seismogenic sources (Leyton, 2010).

The main discussions on this issue (Barrientos 2007; Scholz 2002) all agree on the presence of two seismogenic sources that generate both shallow and deep rupture ground motions. Shallow thrust fault events are related to interplate activity with epicenters located near the coastline and with depths ranging between 15 and 50 Km. Intra-slab events are located instead at depths greater than 50 Km (Kausel and Campos 1992).

### 3.2 Chilean Codes

Chilean codes are classified into three groups as shown in Table 3.1: a) Codes to define loads and actions; b) Codes devoted to earthquake resisting-design; and c) Codes dealing with material behavior.

**Table 3.1** –Chilean Codes

	Number	Name	Date	Status
a) Load actions	NCh431	Snow	1977	Applicable
	NCh432	Wind	1971	Applicable(*)
	NCh1537	Dead/Live Loads	1986	Applicable(*)
b) Seismic analysis and design	NCh433	Buildings	2009	Applicable
	NCh2369	Industrial structures	2003	Applicable
	NCh2745	Base isolation	2003	Applicable
c) Material/Design	NCh427	Steel	1977	Applicable
	NCh430	Reinforced Concrete	2008	Applicable
	NCh1198	Wood	2006	Applicable
	NCh1928	Reinforced masonry	2003	Applicable
	NCh2123	Confined masonry	2003	Applicable
	NCh3332	Earth masonry	2012	Applicable
	-	Unreinforced masonry	2017	Under review

(\*) Modifications are being studied

### 3.3 Chilean seismic Code, NCh433Of.2009

#### 3.3.1 General previsions

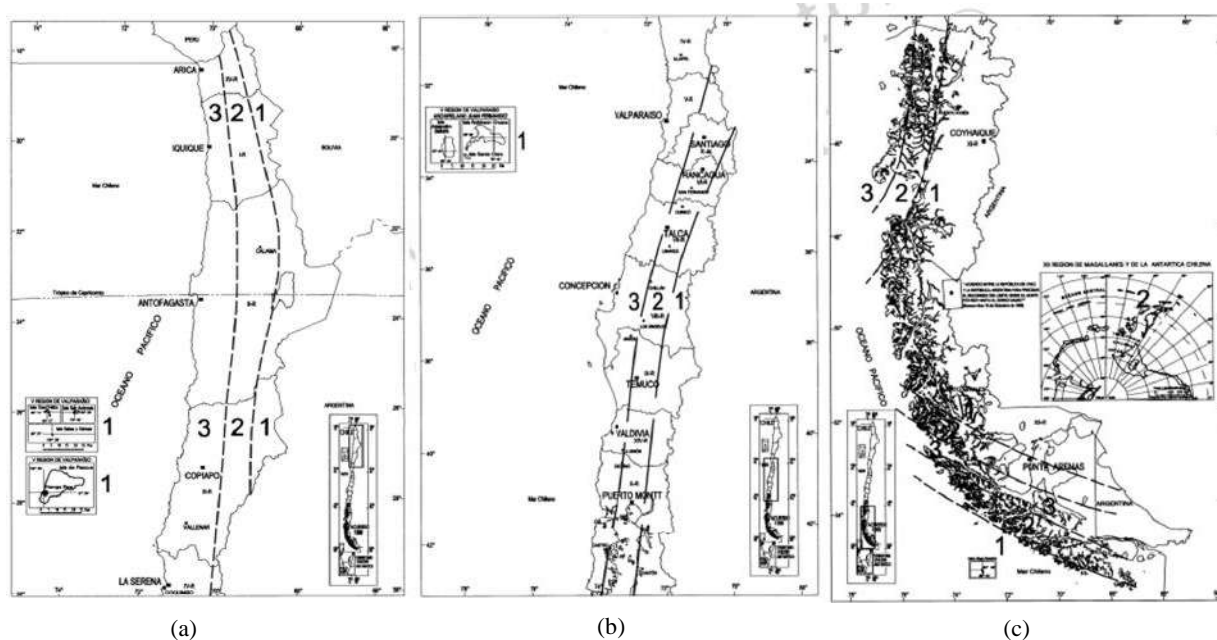
Seismic codes allow estimation of forces and displacements, and are used in combination with International Codes (IBC, 2015; ASCE 7, 2010; Eurocode, 2004) to specify design standards for each structural type and material.

The main design philosophy of NCh433Of.2009 (INN, 1996) is that:

- Structures resist without damage moderate seismic intensities;
- Limited damage is acceptable to non-structural elements under medium seismic intensity;
- Avoid collapse for earthquakes with exceptionally severe intensity.

The NCh433Of.2009 divides the national territory into three seismic zones from the mountain range to the coast (Fig.3.6). Indeed, Zone1 corresponds to the Cordillera area and has a peak ground effective acceleration,  $A_0$ , defined equal to 0.1g; Zone2, which corresponds to the

central valley of the country, and has a peak effective acceleration of  $A_0=0.2g$ . Finally, Zone3, which corresponds to the coast and has  $A_0=0.3g$ .



**Figure 3.6** - NCh433Of.96 Seismic zoning of Chile of D.S.61, 2011: a) XI and XII regions; b) IV, V, VI, VII, VIII, IX, X and RM regions; and c) I, II, III regions.

Buildings are classified into four categories according to their importance and use i.e., A- public buildings which use is important in the case of catastrophic events; B- Public buildings with large people assembly; C – Private buildings or public buildings not falling in the other categories; and D – Isolated structures. The coefficient  $I$  is associated with building categories according to Table3.2.

**Table 3.2** - Coefficient  $I$  of NCh433Of.96

Building categories	$I$
<b>A</b>	1.2
<b>B</b>	1.2
<b>C</b>	1.0
<b>D</b>	0.6

The soil profiles are classified into six categories, A being the stiffer and F being the softer, according to (D.S.61, 2011) Table3.3. The soil classification focuses on the stiffness parameter at low deformations of the upper strata, corresponding to the time-averaged shear-wave velocity 30m on the top ( $V_{s30}$ ), defined by:

$$V_{s30} = \frac{\sum_{i=1}^n h_i}{\sum_{i=1}^n \frac{h_i}{V_{s-i}}} \quad (3.1)$$

Where  $V_{s-i}$  is the shear-wave velocity of strata  $i$  in [m/s];  $h_i$  is the thickness of  $i$ -th strata [m];  $n$  is the number of the strata on the top 30 m of the ground.

**Table 3.3 – Soil classification of D.S.61, 2011**

	Soil type	Vs30 (m/s)	RQD	$\epsilon_{qu}$ (MPa)	(N1)	Su (MPa)
<b>A</b>	Rock, cemented soil	$\geq 900$	$\geq 50\%$ ( $\epsilon_{qu} \leq 2\%$ )	$\geq 10$ ( $\epsilon_{qu} \leq 2\%$ )		
<b>B</b>	Soft rock, very dense soil	$\geq 500$		$\geq 0.4$ ( $\epsilon_{qu} \leq 2\%$ )	$\geq 50$	
<b>C</b>	Dense or firm soil	$\geq 350$		$\geq 0.3$ ( $\epsilon_{qu} \leq 2\%$ )	$\geq 40$	
<b>D</b>	Medium dense or firm soil	$\geq 180$			$\geq 30$	$\geq 0.05$
<b>E</b>	Soil of medium consistency	$< 180$			$\geq 20$	$< 0.05$
<b>F</b>	Soils require a special dynamic analysis	*	*	*	*	*

where RQD is the Rock Quality Designation, according to ASTM D 6032;  $qu$  is the compressive strength of soil;  $\epsilon_{qu}$  is the unitary deformation developed when maximum compressive strength is reached; N1 is the standard penetration index normalized by a confining pressure of 0.1 MPa (applicable only to soils that classify as sands); and Su is the tensile strength of the un-drained condition of the soil.

As observed elsewhere (Verdugo and Peters, 2018) the ASCE7, Eurocode8 and DS61 use similar values of  $V_{s30}$  as limits for each soil type, except for soil type C.

### 3.3.2 Methods of seismic analysis

The NCh433Of.96 establishes two methods of seismic analysis: (a) Equivalent Static; and (b) Modal Spectral analysis.

- a) The Equivalent Static analysis can only be used if the structures comply with the following limitations:
  - All buildings in C and D categories located in t seismic Zone1;
  - The structure does not exceed more than 5 stories or 20m in height;

- Structures with 6 to 15 stories with base shear equal to the one determined as indicated in Eq. (3.2), but not less than the one obtained with the modal spectral analysis; and story shear and overturning moments that do not differ in more than 10% with respect to those obtained through a Modal Spectral analysis;
- All structures for which modal analyses are performed.

The base shear is computed by:

$$Q_0 = C I P \quad (3.2)$$

where  $C$  is the seismic coefficient equal to  $C = (A_0 c^{-gR}) \cdot (T'/T^*)^n$ ;  $I$  is the building category;  $P$  is the total weight of the structure above the base level;  $c$ ,  $n$ ,  $T'$  are parameters relative to the foundation soil type according to Table 3.3(D.S.61, 2011);  $A_0$  is the peak ground acceleration, that is determined according to seismic zoning;  $R$  is the response modification factor; and  $T^*$  is the mode period with the highest equivalent translational mass in the analyzed direction.

*Table 3.3- Parameters that depend on the soil type(D.S.61, 2011).*

Soil type	$S$	$T_0$	$T'$	$n$	$p$
<b>A</b>	0.9	0.15	0.2	1.0	2.0
<b>B</b>	1.0	0.3	0.35	1.33	1.5
<b>C</b>	1.05	0.4	0.45	1.4	1.6
<b>D</b>	1.2	0.75	0.85	1.8	1.0
<b>E</b>	1.3	1.2	1.35	1.8	1.0
<b>F</b>	*	*	*	*	*

- b) The design spectrum proposed by NCh433Of.96 is given by:

$$Sa = (IA_0 \alpha)^{-R^*} \quad (3.3)$$

where  $R^*$  is the spectral reduction factor that is a function of the periods of the structure and the soil; and  $\alpha$  is the dynamic amplification function equal to  $\alpha = [1 + 4.5 (T_n / T_0)^p] / [1 + (T_n / T_0)^3]$ , where  $T_n$  is the vibration period of the  $n$ -th mode of the structure and,  $T_0$  and  $p$  are parameters that depend on the soil type evaluated according to Table 3.3(D.S.61, 2011).

The reduction factor  $R^*$  is given by:

$$R^* = 1 + \frac{T^*}{0.1T_0 + \frac{T^*}{R_0}} \quad (3.4)$$

Where  $T^*$  is the modal period with the highest equivalent translational mass in the analyzed direction; and  $R_0$  is the modification factor according to the structural type and behavior.

Parameter  $R^*$  reflects the characteristics of energy absorption and dissipation of the structure. Code NCh433Of.96 does not specifically indicate values of  $R^*$  for URM structures, the type of structures analyzed in this work. Thus, the Chilean seismic code does not provide the possibility of verifying the seismic behavior of existing non-confined-masonry buildings. However, the Chilean Standard NCh3332.Of.2013 for the Structural Intervention of Earthen Historical Buildings (Instituto Nacional de Normalización –INN, 2013) provides general criteria for interventions intended to result in strengthening.

For this reason, it was decided to address the gap in this standard using the behavior factor,  $q$ , proposed in the Eurocode,8, and the Italian Code NTC2008 (MIT, 2008), Circ.617/2009 (MIT, 2009). For unreinforced masonry, according to EN 1998-1, the behavior factor recommended is 1.5 (elastic behavior).

The modal superposition of the maximum modal values must be carried out through:

$$S = \sqrt{\sum_i \sum_j \rho_{ij} S_i S_j} \quad (3.5)$$

where  $\rho_{ij}$  is the cross correlation modal coefficient. Response  $S$  must be determined by Complete Quadratic Combination, CQC; where  $S_i$  is the corresponding response of the  $i$ -th mode; and  $S_j$  the corresponding response of the  $j$ -th mode.

### 3.3 Chilean Code for seismically isolated buildings NCh 2745Of.2013

To improve the estimation of seismic demand, another Code could be used. Indeed, the Nch2745Of.2013 (INN 2013) for seismically isolated structures proposes a Newmark & Hall design spectrum whose generic definition is presented in Fig.3.7. This spectrum was developed for the design of seismically isolated structures, but it can be adopted for any other building types such as the historical structures analyzed in this work.

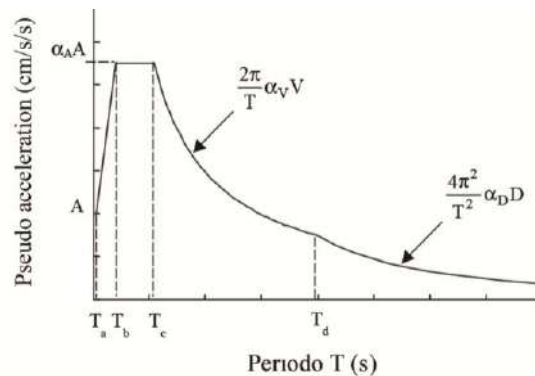


Figure 3.7 - Design spectrum proposed of (Nch2745Of.2013).

Numerical values for the parameters of this spectrum are presented in Table 3.4.  $\alpha_A A$  is the stretch of the curve with a constant pseudo-acceleration ( $S_a$ );  $[2\pi/T]\alpha_V V$  is the stretch of the curve with a constant pseudo-velocity; and  $[(4\pi^2)/T]\alpha_D D$  is the stretch of the curve with a constant pseudo-displacement.

$$\begin{aligned} S_a &= \alpha_A A & T_b &\leq T_c \\ S_a &= [2\pi/T]\alpha_V V & T_c &\leq T_d \\ S_a &= [(4\pi^2)/T]\alpha_D D & T &\geq T_d \end{aligned}$$

**Table 3.4** – Spectrum parameters (Nch2745Of.2013).

Soil	$T_a'$ [s]	$T_b'$ [s]	$T_c'$ [s]	$T_d'$ [s]	$T_e'$ [s]	$T_f'$ [s]	$\alpha_A A$ [cm/s <sup>2</sup> ]	$\alpha_V V$ [cm/s <sup>2</sup> ]	$\alpha_D D$ [cm]
<b>I</b>	0.03	0.11	0.29	2.51	10	33	1085	50	20
<b>II</b>	0.03	0.2	0.54	2.0	10	33	1100	94	30
<b>III</b>	0.03	0.375	0.68	1.58	10	33	1212	131	33

**Table 3.5** - Coefficient  $A_0$  and  $Z$  (Nch2745Of.2013).

Seismic zone	$A_0$	$Z$
<b>1</b>	0.2g	3/4
<b>2</b>	0.3g	1
<b>3</b>	0.4g	5/4

### 3.4 Summary

This section contains a brief account on the seismic hazard used for building design in Chile. The high level of Chilean seismicity is a product of interaction between the Nazca, Antarctic, Scotia and South-American plates. Most significant earthquakes occur because the Nazca plate subducts beneath the South-American plate. As a consequence of this, four different seismogenic sources are distinguishable: inter-plate, intra-plate, cortical, and outer-rise earthquakes.

To determine seismic demand, two different codes can be used: the design code NCh433Of.2009 for conventional structures, and the Nch2745Of.2013 for base isolated systems. These two codes define a different level of hazard, being NCh2745 a step 0.19 above the one for conventional structures for the same return period  $T_r = 475$  years earthquake. With regard to the seismic design procedures, two possible analysis methods are proposed: (a) Equivalent Static, and (b) Modal Spectral Analyses.

# Chapter 4

## SEISMIC DAMAGE AND FRAGILITY ASSESSMENT OF URM CHURCHES OF CHILE

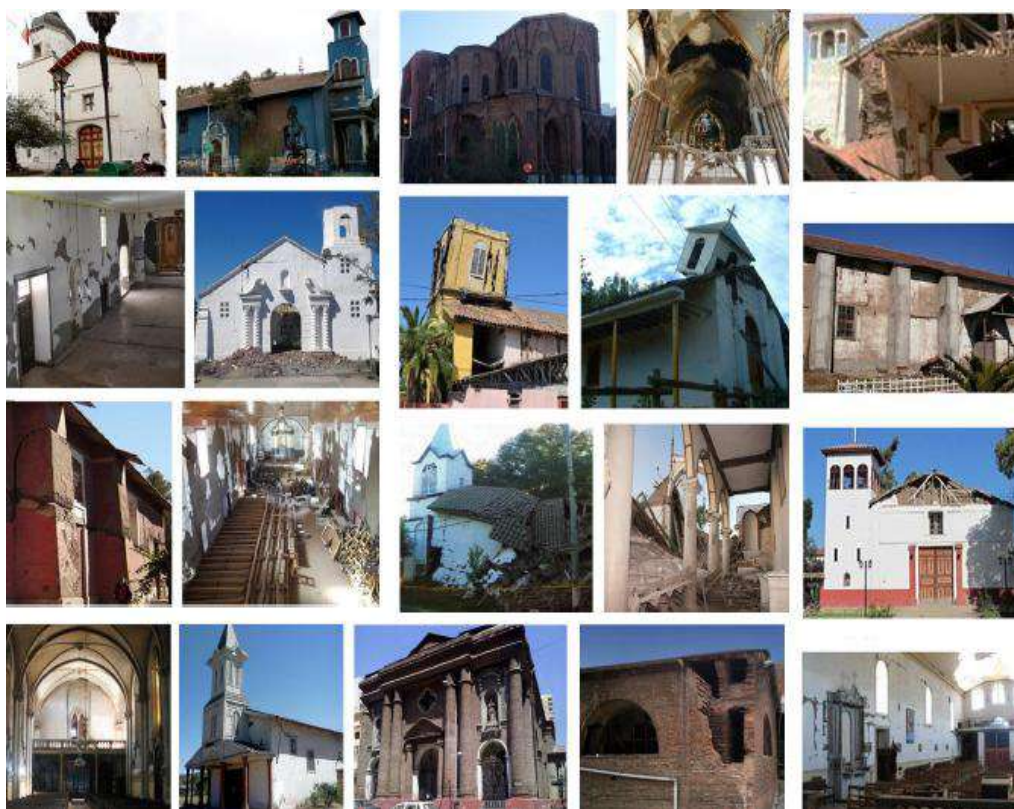
### 4.1 Brief review of procedures for seismic vulnerability and fragility assessment

Past earthquake surveying activities after the 2010 Maule earthquake (Mw 8.8), highlighted that Chilean Built Heritage underwent extensive structural damage in particular, in URM churches (D'Ayala, 1999; Lagomarsino & Podestà, 2004; Sorrentino et al., 2014; D'Ayala & Benzoni, 2012; Brandonisio, 2013; Fonseca & D'Ayala, 2012; De Matteis et al. 2016; Marotta et al., 2017). Safeguarding strategies for this heritage not only need studies using detailed analyses of a single church (Indirli, et al., 2011; Rendel et al., 2014; Jorquera et al. 2016; Sandoval et al., 2017; Torres et al., 2017), but also studies at urban and territorial level. In fact, urban and/or territorial analyses of the seismic vulnerability and fragility of the Built Heritage lead to action plans for risk mitigation by identifying a list of priorities and procedures suitable for seismic emergency management (Braga et al., 2015; Bergami and Nuti 2013; Staniscia, 2017).

For almost twenty years, significant research has made contributions to the assessment of the seismic vulnerability at a large geographical scale, as summarized elsewhere (Calvi et al., 2006). The first predictions in this field were based on the observation of post-earthquake scenarios, through Probability Mass Functions (PMFs), also called Damage Probability Matrices (DPMs), (Whitman et al., 1973; Braga et al., 1982), which express in a discrete form the probability of being in a given damage level  $D_k$ , conditioned to a ground motion intensity  $IM$ , i.e.  $P(D_k = j | IM)$ . Afterwards, vulnerability and fragility functions, which describe in a continuous form the probability of being in a given damage state conditioned to a specific seismic hazard intensity, have been proposed (Orsini, 1999; Singhal & Kiremidjian, 2004; Rota et al., 2006; Martinelli et al., 2008; Rossetto et al., 2013). A large number of procedures for seismic vulnerability and fragility assessment can be found and three classes of methods are usually distinguished: (a) empirical (e.g. Colombi et al., 2008; Rota et al., 2006); (b) expert judgment based (e.g. Lagomarsino & Giovinazzi 2006); and (c) analytically based on mechanical models (e.g. Bernardini et al. 1990; Kircher et al., 1997; Glaister and Pinho 2003; Restrepo and Magenes 2004). A fourth category, called hybrid, is sometimes considered when a combination of the three previous methods is used, e.g., analytical and empirical in (Singhal et al., 1998), and expert judgment based and empirical in (Jaiswal et al., 2011).

The Chilean territory is characterized by an Architectural Heritage with unique constructive and typological features, and despite the high seismic hazard, seismic fragility assessments of monumental buildings at territorial level are not reported in the literature. The MARVASTO project (Indirli, 2006; and MARVASTO, 2007) is the only research focused on the evaluation of the seismic vulnerability in the urban area of Valparaíso, composed by a sample of monuments located in the UNESCO site (i.e., Cerro Cordillera).

Consequently, this chapter presents the seismic damage and fragility assessment for 106 URM churches (Fig. 4.1), located in the central Valley of Chile, after the 2010 Maule earthquake. During the post-seismic survey activities an abacus developed by Italian practice (DPCM, 2011) was used for each *church* typology.



**Figure 4.1** - URM churches in the Metropolitan (RM) and in the Libertador General Bernardo O'Higgins (VI) Regions.

The macro-seismic method (Lagomarsino & Podestà, 2004c) for estimating the damage index, *id*, for each church considered was implemented. Index *id* considers the possibility of generation of 28 possible failure mechanisms and, at the end of the analysis, throughout predefined correlations, provides a global damage index for the structure. The Italian practice (G.U. no.55, 7/03/2006 and DPCM, 2011) due to a large experience with earthquakes and masonry structures, has gathered an abacus of 28 possible failure mechanisms for church typology.

After the post-seismic survey for the Maule earthquake, only 22 mechanisms were observed, due to the specific features of Chilean churches.

Since the values of the damage index are defined in the field with real numbers, a transformation is needed into discrete variables, which represent a measurable level of damage consistent with the European Macro-seismic Scale (Grunthal, 1998).

Given the data collected for the 106 churches, an empirical approach based on a probabilistic analysis of the earthquake failures was carried out. Probability Mass Functions (PMFs), for global and local behaviors (De Matteis, Criber and Brando, 2016; Marotta et al., 2016), and Empirical Fragility Curves for damage level (EFCs) are proposed for the Chilean URM churches.

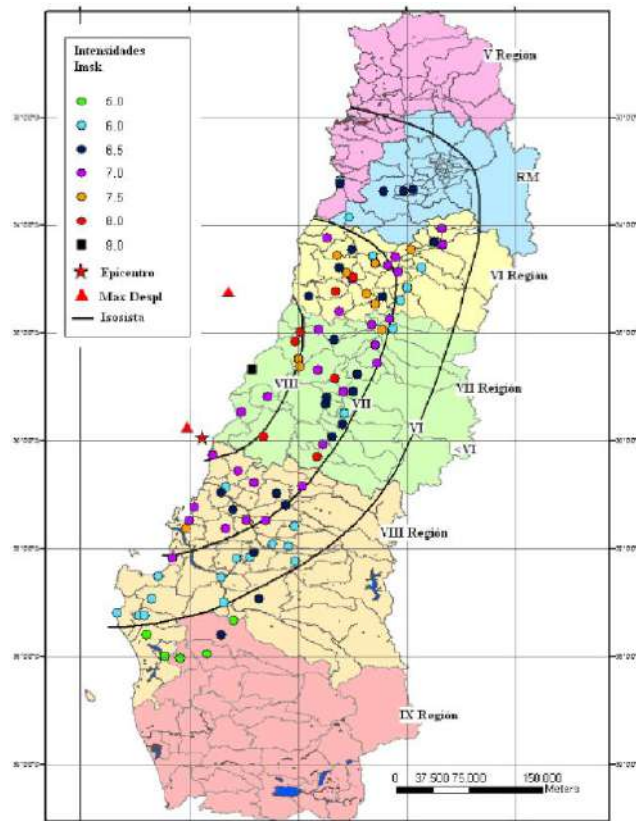
## **4.2 Damage scenarios following the 2010 Maule earthquake**

### **4.2.1 The 2010 Maule earthquake**

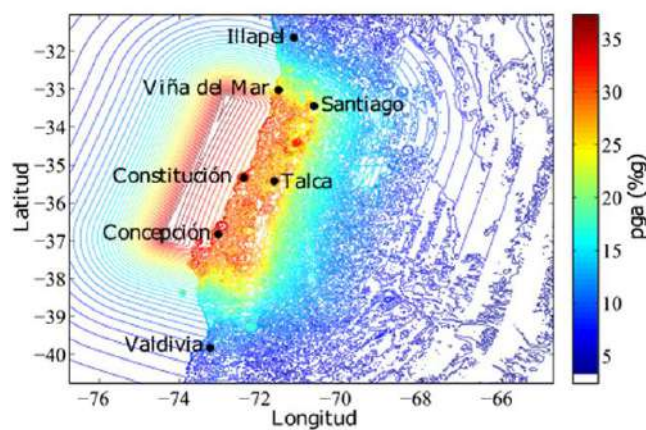
On February 27, 2010 at 3.34 am, the Maule earthquake ( $M_w=8.8$ ) struck the central region of Chile. This seismic event generated perhaps one of the most extensive ground shaking ever measured with peak horizontal and vertical ground accelerations well over 0.6g. The Maule megathrust earthquake with epicenter at 35.846°S 72.719°W (USGS) was produced by the interplate subductions phenomena at the convergence zone between the Nazca and South American plates. The tsunami triggered by the earthquake, left several coastal towns either devastated or heavily damaged in the south and central area of the country. An average of 12 million people was impacted by the earthquake and tsunami, leading to 524 deaths (INE, 2002). The built Heritage suffered significant losses and substantial damage, comprising an estimated of 290 million dollars in repair costs (Conferencia Episcopal de Chile, 2010). The adobe and brick unreinforced masonry buildings built before 1940 were the most affected. In particular, heavy structural damage was observed as shaking occurred, in alluvial and fluvial soils.

For the V, RM, VII, VIII, IX regions, researchers (Astroza et al. 2010) developed the Macro-seismic Medvedev-Sponheuer-Karnik Scale Intensities map of Maule earthquake (Fig.4.2a). In (D'Ayala & Benzoni, 2012), the European Macro-seismic Scale (EMS-98) intensity map was proposed for the cities of Santiago and Valparaíso, the O'Higgins region, and the cities of Curicó and Talca in the Maule region, according to the seismic damage classification used by the Chilean authority. The PGAs were recorded by the stations of the National Seismological Network and by the RENADIC of the Faculty of Civil Engineering at the University of Chile (Boroschek et al., 2010a, 2010b, 2012 and Decanini et al., 2012). Due to the low number of records at the vicinity of the investigated churches (i.e., distance less than 2 km), and because of their high concentration in the city of Santiago, which does not allow a sufficiently large intensity range of measurement levels, the PGAs were taken from the USGS Shake Maps for 0.3s, 1.0s and 3.0s were used in this research (Fig. 4.2b), as suggested by GEM

guidelines (Rossetto et al., 2013). A summary of the values of MSK, EMS'98, PGA, PGV and A0 (maximum ground acceleration at T=0 for different seismic zones according NCh433, INN, 1996) values are presented in Table 4.1 for the different sites of interest.



(a)



(b)

**Figure 4.2**—(a) MSK intensities map by (Astroza et al., 2010), and (b) EMS'98 intensities map by (D'Ayala&Benzoni, 2012)

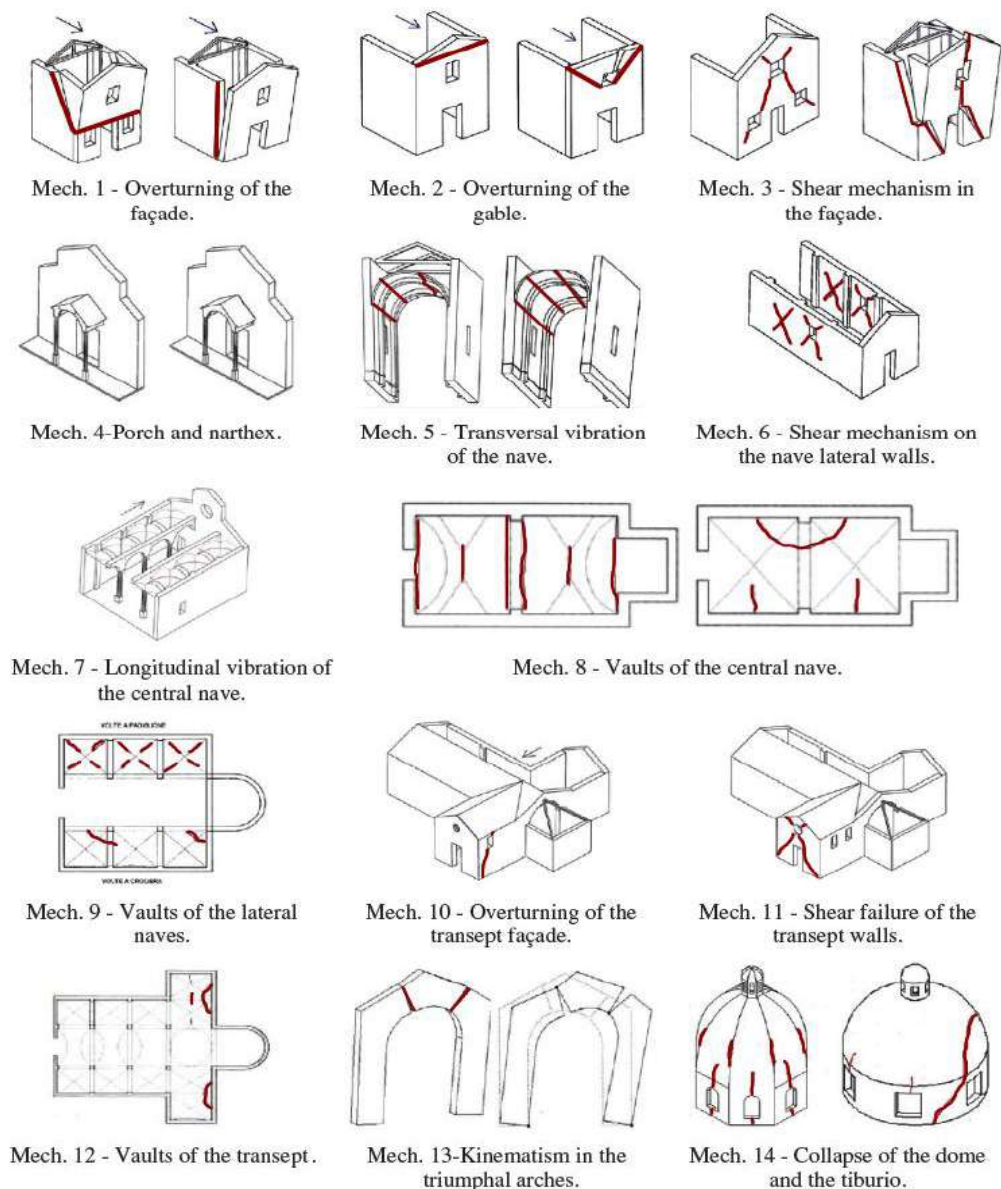
**Table 4.1.** Value of MSK intensities (Astroza et al., 2010), EMS'98 intensities (D'Ayala&Benzoni, 2012), PGA and PGV (Boroschek et al., 2010 and USGS), and  $A_0$  (INN, 1996) for different sites of interest.

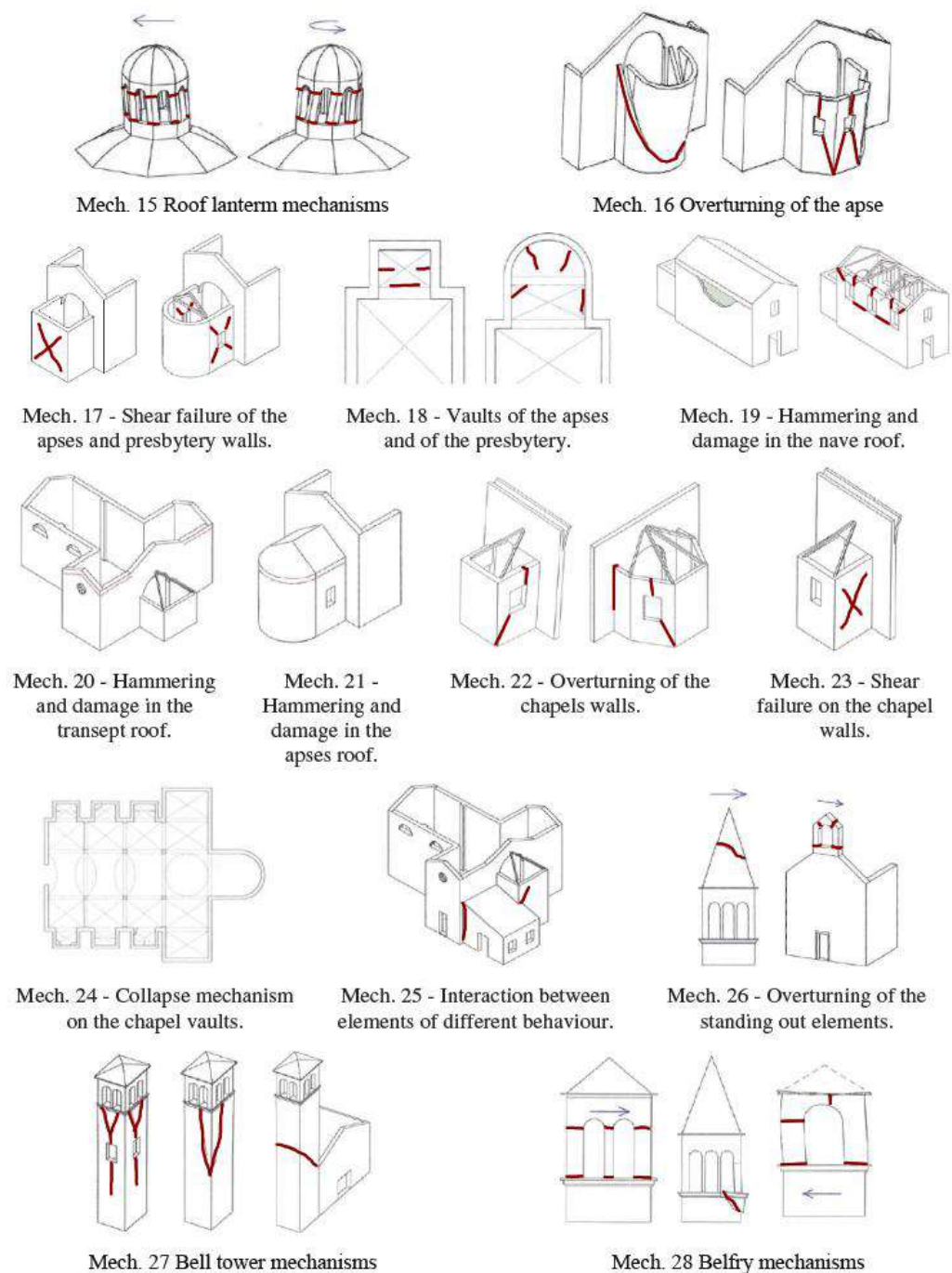
City/Town	Lat °.mil; Lon °.mil	Epicenter Distance (km)	MSK	EMS'98	PGA (g)	PGV (g)	Seismic Zone $A_0$ (g)
Melipilla	-33.687; -71.214	284	6.5	-	0.343	0.279	III-0.4
Talagante	-33.77622; -70.98867	297	6.5	-	0.28	0.251	II-0.3
Santiago Centro	-33.3404; -70.6428	330	6.5	7	0.218-0.309	0.182	II-0.3
Santiago, Providencia	-33.4314; -70.6093	330	6.5	7	0.139-0.104	0.08	II-0.3
Codegua	-34.0370; -70.6729	280	6.0	-	0.274	0.249	II-0.3
Rancagua	-34.166667; -70.75	264	6.5	-	0.257	0.249	II-0.3
Rengo	-34.4024; -70.8674	238	7	-	0.248	0.225	II-0.3
Requínoa	-34.2884; -70.8158	250	6	-	0.302	0.166	II-0.3
Doñihue	-34.2290; -70.9579	247	7.5	-	0.354	0.343	II-0.3
San Vicente Tagua Tagua	-34.3917; -71.0848	222	7	-	0.326	0.384	II-0.3
Peralillo	-34.4773; -71.4873	196	8	9	0.137-0.304	0.079	III-0.4
Pumanque	-34.6027; -71.6553	175	8	8.5	0.44	0.37	III-0.4
Lolol	-34.7284; -71.6458	165	7	8	0.382	0.223	III-0.4

#### 4.2.2 Damage survey

The seismic performance of the URM churches depends on several parameters, among which the prevalent are: the quality of masonry and the connection between orthogonal walls, the irregularity of the in-plane and elevation arrangement, the presence of discontinuities in the structural system, the implementation of inadequate interventions, and the absence of a rigid diaphragm. Nevertheless, in post seismic scenarios, the damage assessments presented by numerous authors (Augusti et al., 2002; Lagomarsino et al. 2003; Sousa 2003; Irizarry et al. 2004; Lagomarsino&Podestà 2004a; 2004b; 2004c; Lagomarsino et al. 2004; Lagomarsino 2012) have highlighted that the structural response of churches exhibit recurrent patterns. In fact, the seismic action selects the most vulnerable building portions, called macro-elements, which present an autonomous behavior relative to the global response of the structure (Giuffrè 1991; Da Porto et al., 2010; Lagomarsino & Podestà, 2004).

Hence, post-seismic scenario of Chilean churches after the 2010 Maule earthquake have been analyzed according to feasible dominant behaviors of macro-elements of the church is architectural typology, say façade, narthex, bell-tower, lateral walls, transversal walls, colonnade, transept, apse, and chapels, using the catalogue of mechanisms developed elsewhere (Doglioni, 1994). Following Giuffrè, 1989, the crack pattern was analyzed using the three fundamental damage phenomena associated with well-known mechanisms: the *zero mode* (disaggregation of masonry wall); the *first mode* (the out-of-plane behavior, OOP): mechanisms Mech.01, 02, 10, 14, 15, 16, 19, 22, 26 and 27 ; and the *second mode* (the in-plane behavior, IP) mechanisms Mech.03, 04, 05, 06, 07, 11, 13, 17, 23, 25, and 28. Shown in Fig.4.4 are percentages of the faction of possible and activated mechanisms in the sample of churches considered. Possible mechanisms are defined as the potential collapse modes that could be activated in the churches due to the presence of a macro-element associated to that type of mechanism.





**Figure 4.3** -Classification of mechanisms for religious buildings (Form A-DC 2006; source: *Guidelines for Cultural Heritage 2011 G.U., Lagomarsino et al., 2004*).

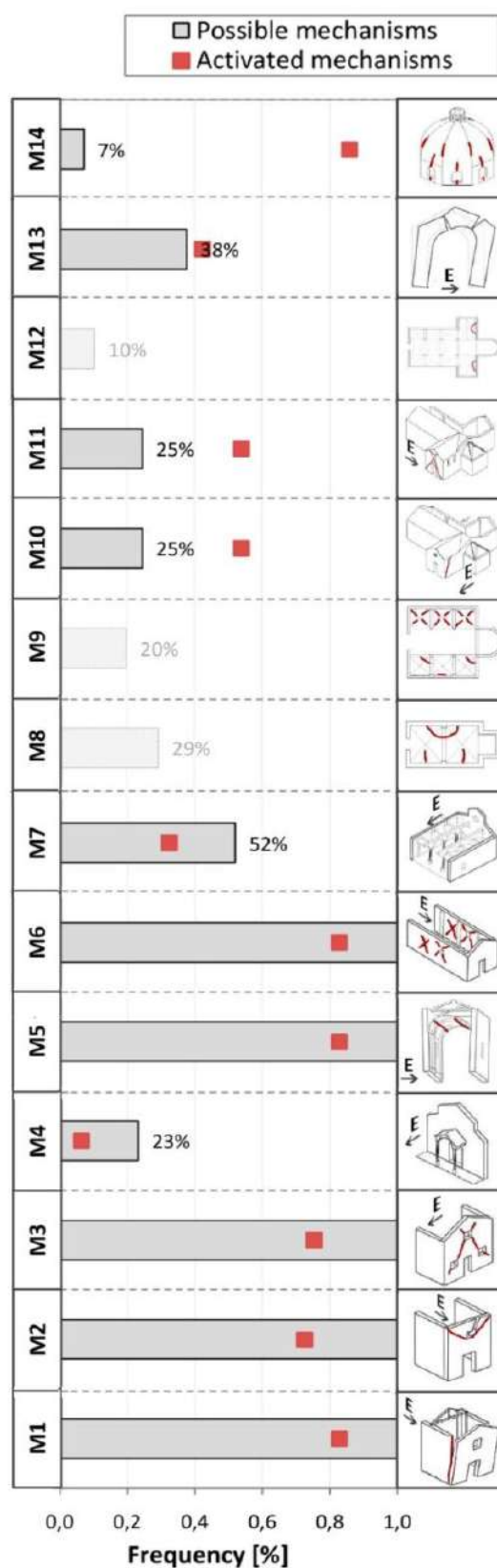
In particular, due to specific structural features of the Chilean churches, the 28 analyzed collapse mechanisms were assessed using the Italian form post-earthquake survey (PCM-DPC MiBAC, 2006). Results led to 22 mechanisms, Fig. 4.4 (a) and (b) observed in the survey.

The presence of each macro-element (façade, triumphal arch, bell tower, etc.) is sufficient to make possible the activation of associated collapse mechanisms. Thus, in Fig. 4.4 the percentages of the potential failure modes that could be activated in the churches, i.e. possible mechanism [PM] even if they are not associated with damage, are shown together with a ratio

between the numbers of churches where the mechanisms were actually activated following the 2010 earthquake (effective mechanisms, EM), and the number of the possible mechanisms. The PM parameter highlights the specific features of Chilean URM churches with respect to the European religious buildings. Some mechanisms are absent, such as the damage involving the main nave (mechanism 8) and the side aisles (mechanism 9) vaults, due to the presence in churches of false vaults made of timber ribs clad in cane (present in about the 25% of the total stock) or *tijerales*. The mechanisms 1, 2 and 3, which analyze the in-plane and the out-of-plane behavior of the facade, and mechanisms 5 and 6, which respectively evaluate the transversal response of the central nave (and of the aisles, if present), and the in-plane response of the longitudinal walls, show that a systematic activation and the involved macro-elements, facade and central nave, are always present.

In all the bell towers, in-plane and out-of-plane damage was observed (mechanism 27 and 28), and the considered macro-element is present in almost all of the analyzed churches. The apse overturning causes frequent damage and through the interaction between the side walls and the roof structure (mechanism 16 and 19).

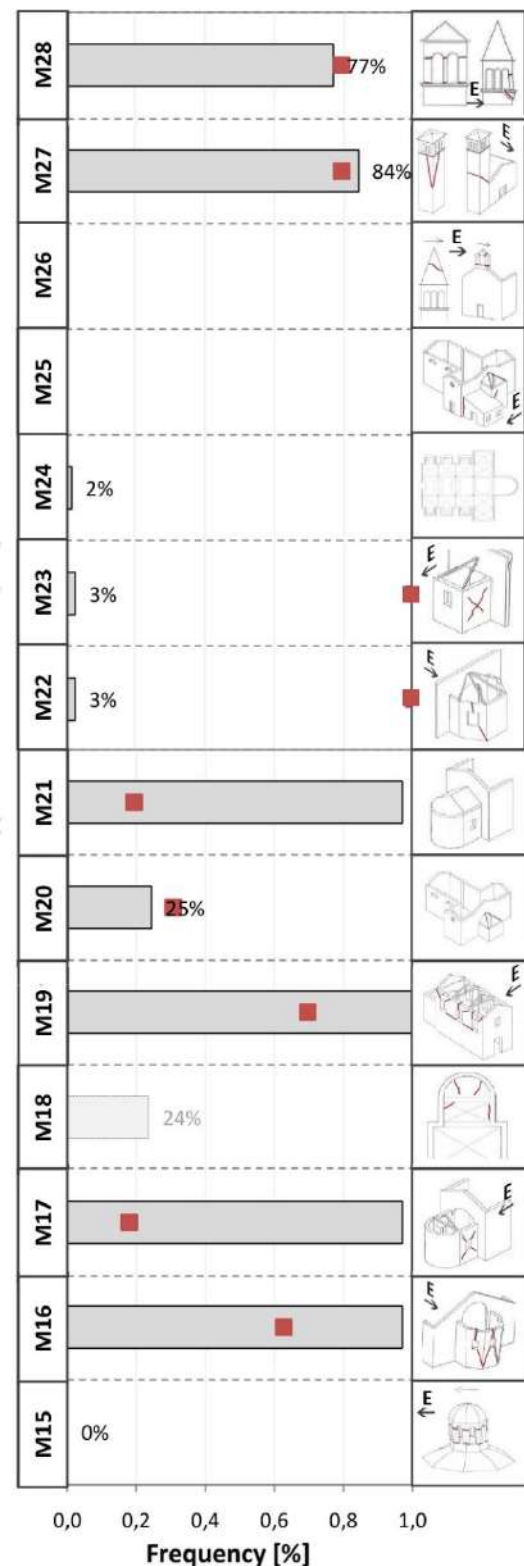
In the aftermath of the Maule earthquake, the most common mechanism observed in the churches was the activation of a simple overturning of the façade. This mechanism was typically evidenced by



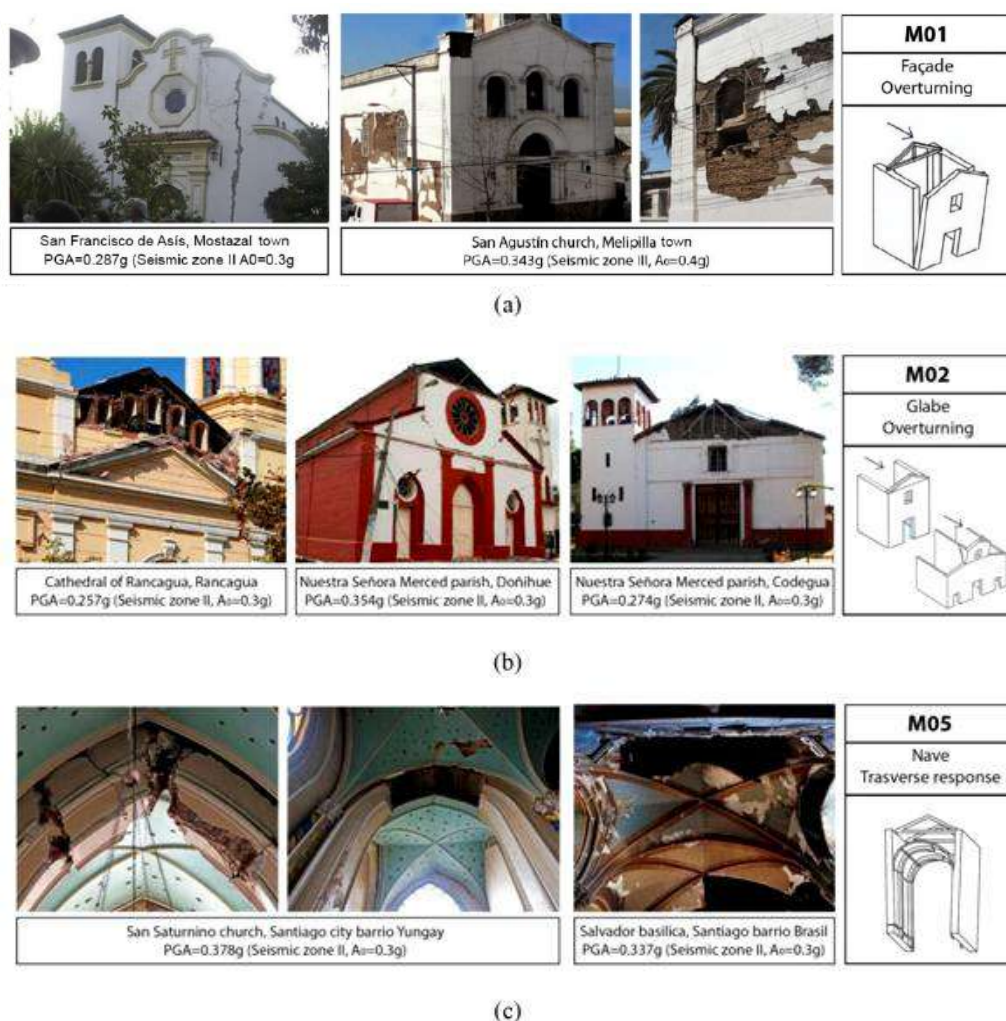
**Figure 4.4** -(a) Percentage of possible collapse mechanisms (relative to the total sample) and the mechanisms activated after the 2010 earthquake (compared to the possible sample).

vertical cracks at the wall corners and in the haunch of the transverse arches of the narthex. The failure pattern, which is usually due to poor connections between horizontal diaphragms and walls, varies according to the geometry of the façade.

A typical out-of-plane mechanism of the central part of façade was observed in the San Francisco de Mostazal's church (PGA=0.287g) in the municipality of Rancagua built in 1858. Deep vertical cracks were observed due to the lack of connection between the façade, the longitudinal nave walls, and the bell-tower (Fig. 4.5a). In the San Agustín's church (PGA=0.343g), located in the town of Melipilla and built in 1744, triggering of the first mode mechanism of the façade was detected. Different materials in the façade (brick masonry) and the side walls (adobe) were a critical link between structural elements. Maule's shaking produced detachment of the entire façade with 7m wide and 1.5m height extension (Fig.4.5a) and the collapsed stucco, (Lira&Arévalo, 2010). The presence of good quality connections between the façade and lateral walls of the side aisles limited the collapse of the façade macro-element at the upper part (i.e. gable). In several Colonial churches, the collapse of tympanums was observed. Its reconstruction with wooden elements and brick (*tabiquería*), and the lack of a good connection between the roof and façade represent an important discontinuity and weakness to present an overturning of the wall.



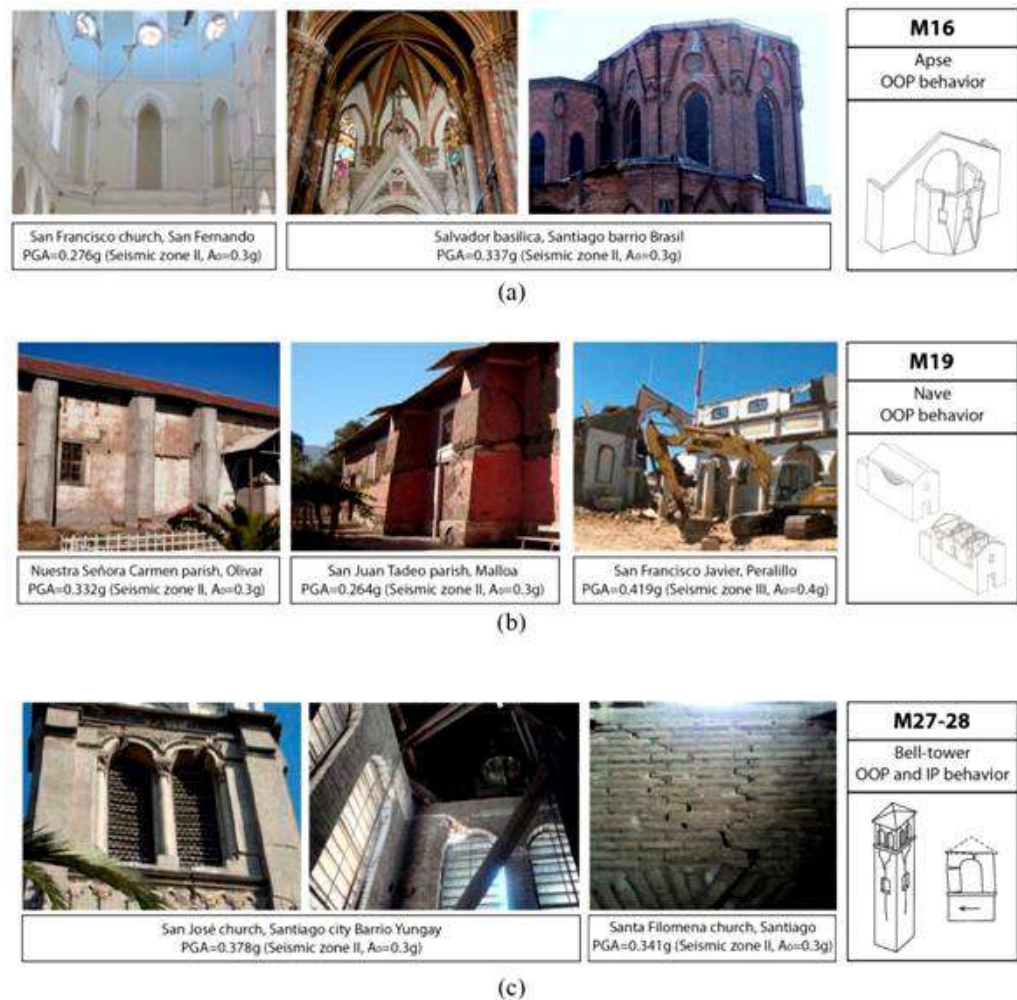
**Figure 4.4 -(b)**Percentage of possible collapse mechanisms (relative to the total sample) and the mechanisms activated after the 2010 earthquake (compared to the possible sample).



**Figure 4.5 -** (a) Out-of-plane mechanisms of the façade due to poor connections at the corners: in the San Francisco de Mostazal the simple overturning involved the central part of façade, and in the San Agustín church the complete façade; (b) gable overturning effect of inadequate connection between roof structure and masonry wall of the upper part of façade on Cathedral of Rancagua, Doñihue's parish, and Codegua's church; and (c) observed collapses on the haunch of the transverse arches of side aisles

Such is the case for Rancagua's Cathedral (PGA=0.257g), Nuestra Señora de la Merced parish in Doñihue (PGA=0.354g), and Nuestra Señora de la Merced church in Codegua (PGA=0.274g), which presented collapse of the façade's gable (Fig. 4.5b). Moreover, the San Saturnino church (PGA=0.378g) and the Salvador basilica (PGA=0.337g) are both Neo-gothic structures, which were designed by the architect Teodoro Burchard at the end of 19<sup>th</sup> century. Both have shown dangerous cracking with partial and total collapse of the transverse arches and lateral walls at the base of columns as a consequence of the in-plane response of the central nave and the side aisle arcades (Fig. 4.5c). The activation of apse overturning was also frequently observed in Neo-gothic and Revivalist churches (Fig. 4.6a), such as the San Francisco's church (PGA=0.276g) in the city of San Fernando built by Jesuit missionaries in 1744 and declared a National Monument in 1984 and the Salvador basilica. Walls of the side aisles show wide openings in the proximity of the wall ends, the hammering roof, and the lack of linkages among wooden trusses and masonry walls triggered first mode mechanisms with

deep horizontal cracks and partial collapse in parishes Nuestra Señora del Carmen in Olivar, in San Juan Tadeo in Malloa (PGA=0.264g) and in San Francisco Javier of Peralillo (PGA=0.419g), which west nave completely collapsed (Fig.4.6b).



**Figure 4.6-** (a)Vertical cracks in windows due to the hammering roof covering; (b) deep horizontal cracks windows and buttresses, and total collapse of the lateral wall due to the hammering roof and connection between the wooden trusses and the masonry walls; and (c)diagonal cracks on bell-tower walls.

Other typical localized failures were diagonal cracks and total collapse of bell-gables. Diagonal cracks were produced as a result of shear failure on walls, usually at the bell-tower of Neo-gothic churches such as the Santísimo Sacramento (PGA=0.378g) and San José churches (PGA=0.341g) in Santiago, (Fig. 4.6c). Total collapse of bell-gables was due to out-of-plane behavior, which is recurrent in Colonial churches.

Parishes San Andrés in Ciruelos, San Nicodemo in Coinco (PGA=0.352g), Nuestra Señora del Rosario in Guacarhue, and San Andrés in Pichilemu (PGA=0.531g), are some examples of CL churches that underwent total bell-tower collapse.

### 4.2.3 Damage indices

Herein, the macro-seismic method (Lagomarsino et al., 2004) for estimating a damage index,  $id$ , was implemented in each church. This damage index considers the possibility of generating various possible failure mechanisms (28 mechanisms) by using a standardized mean of the weighted level of damage detected for each possible mechanism computed by the following equation:

$$id = \frac{1}{5} \cdot \sum_{k=1}^{m=28} \left( \frac{\rho_k}{\rho} \right) \cdot d_k = \frac{1}{5} \cdot \sum_{k=1}^{m=28} \hat{\rho}_k \cdot d_k \quad (4.1)$$

Where  $\hat{\rho}_k$  the normalized is weighted score concerning the influence of each mechanism on the global behavior of the structure, and ranges between 0 and 1; and  $d_k$  is the damage score that considers the  $k$ -th mechanism and ranges from 0 to 5.


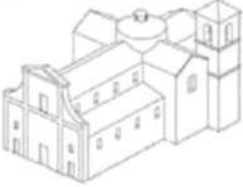

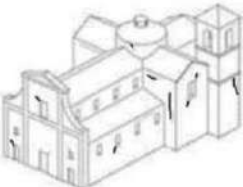

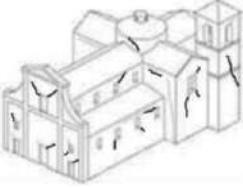

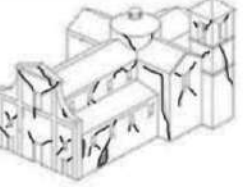

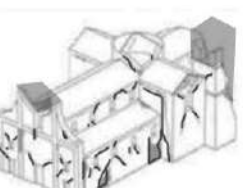

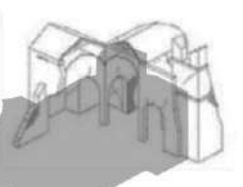
The mechanisms considered for the Chilean URM churches are  $m = 22$ , and exclude mechanisms of macro-elements not present in Chilean URM churches (Fig.4.3).

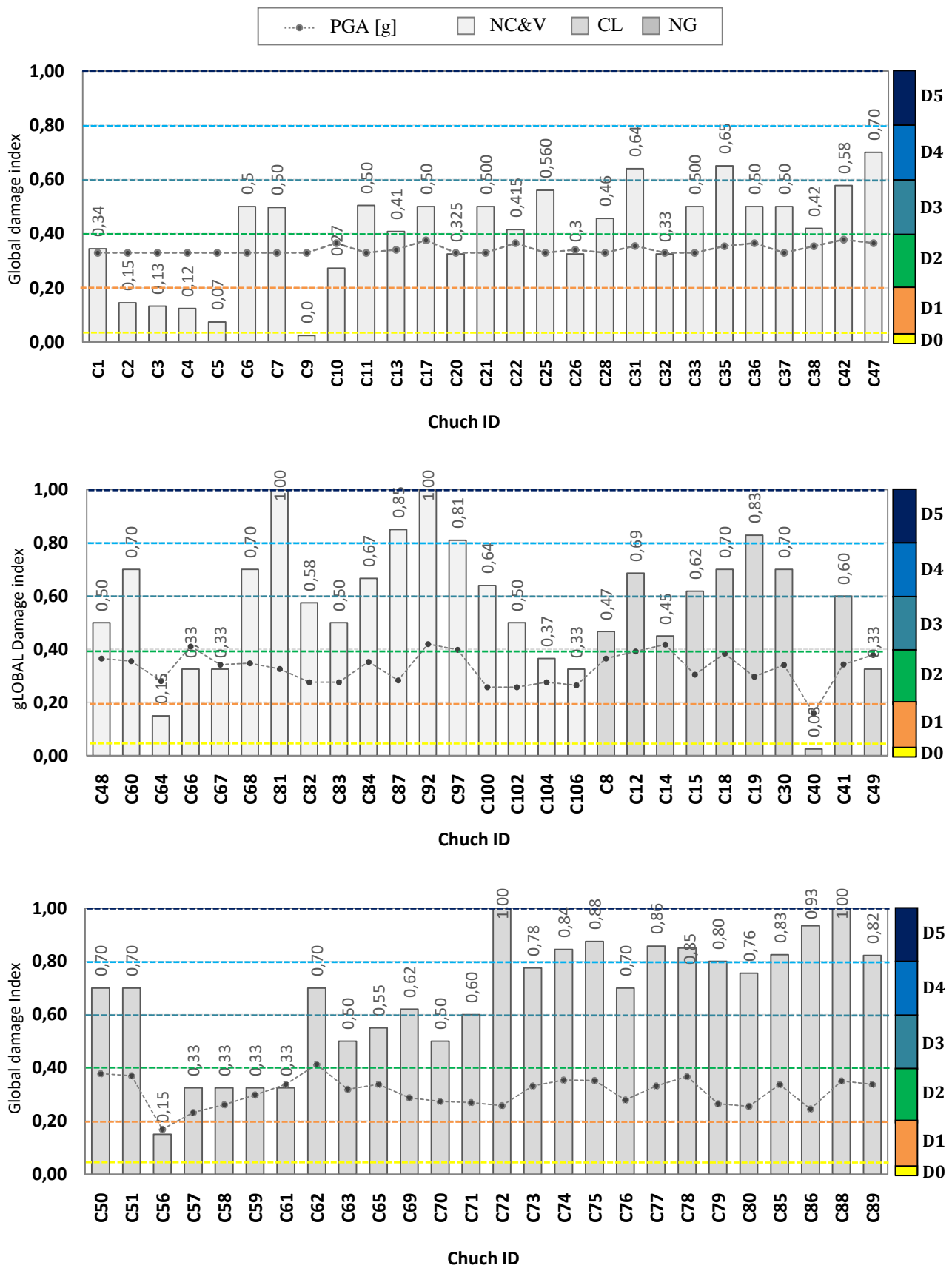
Since the values of the damage index are defined during the field inspection using real numbers, a transformation of the indices into discrete variables is carried out to obtain a measurable level of damage comparable to the European Macro-seismic Scale (Grunthal, 1998). Thus, each damage index associated with a  $D_k$  damage level was considered as suggested elsewhere (Lagomarsino and Podestà, 2004b and De Matteis et al.2016), by classifying the damage in six levels according to the EMS-1998 scale (Table 4.2).

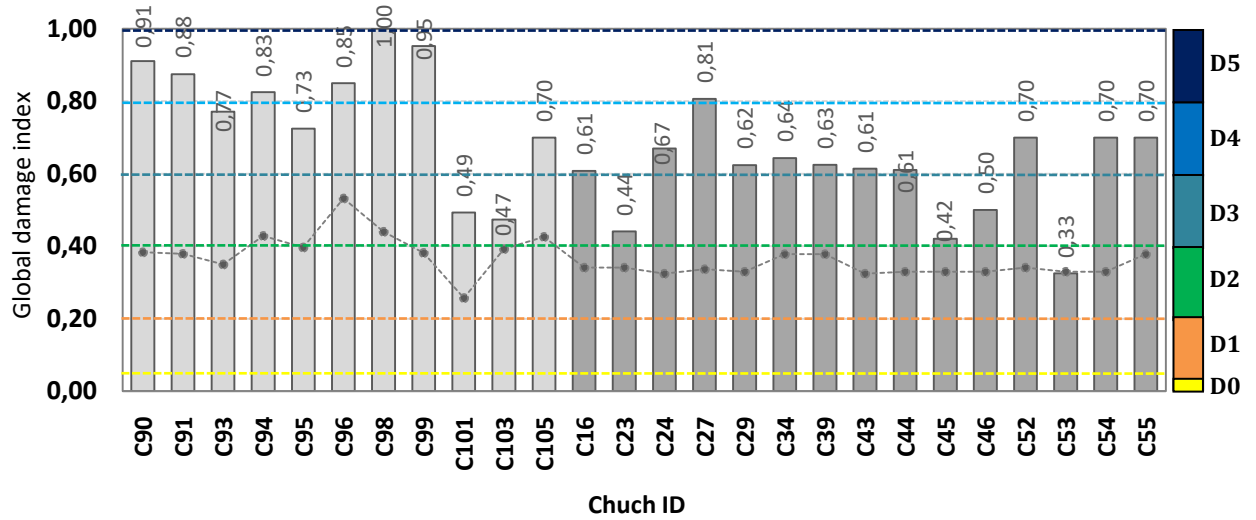
The results obtained by the damage index method, show better correlation in stone masonry churches (7 in totals) rather than brick and adobe structures. Indeed, during the Maule earthquake, CL and NG churches were the most damaged structures. Several of CL religious buildings, of which 57.4% were located in the both region 6<sup>th</sup> region (Libertador General Bernardo O'Higgins), underwent heavy structural damage. Extensive and deep cracks were observed activating local failure modes of different macro-elements, and in some case, total or near total collapse (66% of global damage levels in Colonial churches reached  $D_4$ - $D_5$ ).

The NG buildings located in the city of Santiago at 325 kilometers from the epicenter exhibited activation of failures of numerous macro-elements and a prevalent damage level  $D_k$  in 66.6% of the cases. Compared to the previously analyzed buildings, the NC&V churches have shown a better structural response, with moderate structural and non-structural damage, 75% of the cases. The stone churches are focused on a more limited range of PGA (range between 0.25g to 0.3g).

**Table 4.2** - Damage classification proposed by (Lagomarsino and Podestà, 2004b and De Matteis et al.2016), according to EMS-1998 scale, and description of damages.

Damage level, $D_k$ (Grunthal, 1998)		Damege index, $i_d$ (Lagomarsino et al. 2004)	Description of damage (De Matteis et al.2016)
<b>D<sub>0</sub></b> 		$i_d \geq 0.05$	Absence of damage or light damage involving one/two mechanisms
<b>D<sub>1</sub></b> 		$0.05 < i_d \leq 0.25$	Absence of structural damage and negligible to slight non-structural damage. Few cracks in very few parts of the macro-element, falling to small pieces of plaster only, falling of loose stones from upper parts
<b>D<sub>2</sub></b> 		$0.25 < i_d \leq 0.4$	Failures of the limited entity as slight structural damage and moderate non-structural damage. Many cracks with falling of fairly large pieces of plaster
<b>D<sub>3</sub></b> 		$0.4 < i_d \leq 0.6$	Moderate structural damage and heavy no-structural damage. Activation of the first out-of-plane mechanisms, severe and extensive pattern cracks
<b>D<sub>4</sub></b> 		$0.6 < i_d \leq 0.8$	Heavy structural damage and hefty no-structural damage. Triggering of several OOP mechanisms
<b>D<sub>5</sub></b> 		$i_d > 0.8$	Heavy damage. Total or near total collapse of the macro-elements





**Figure 4.7** - Damage levels according to Table 2 (Grunthal, 1998) and global damage index (Lagomarsino et al. 2004; Lagomarsino and Podestà, 2004b) for the 106 URM churches of Central Chile affected by the 2010 Maule earthquake.

### 4.3 Probability Mass Functions (PMFs)

Probability Mass Functions (PMFs) of seismic damage level (Whitman et al., 1973; De Natale et al., 1987; Dolce et al., 2003; Di Pasquale et al., 2005) were derived from the empirical data of the 106 URM churches described above for intensities ranging from  $0.16g < PGA \leq 0.28g$ ,  $0.28g < PGA \leq 0.41g$  and  $0.41g < PGA \leq 0.53g$ . The limits on these brackets are based only on the clustering of the information and the existence of significant differences on the states of damage. The PMF expresses the probability of getting a damage level  $k$  due to a ground motion of intensity measure  $IM$ , and is expressed mathematically as  $P(D_k = j | IM)$ . These PMFs are shown in (Fig. 4.10), and considered the damage levels derived from Equation (4.1). The results fit well a binomial probability density function, BPDF (Braga et al. 1982; Matteis et al., 2016, and De Matteis & Zizi, 2019), given by Equations (4.2) and (4.3).

$$pk = \frac{5!}{k!(5-k)!} \left( \frac{\mu D}{5} \right)^k \left( 1 - \frac{\mu D}{5} \right)^{5-k} \quad (4.2)$$

where  $\mu D$  is the average of the observed damage level obtained through the ratio between the number of buildings  $D_{k,i}$  that reached a damage level  $k$  at a given intensity  $IM = IM_i$ , and the total numbers of the observed buildings  $N_i$  at a given intensity  $IM = IM_i$ ; and  $pk$  is the probability of having a damage level  $k$  ( $k = 1, 2, 3, 4, 5$ ).

$$\mu D = \frac{\sum_{i=1}^n D_{k,i}}{N_j} \quad (4.3)$$

The only presence of a macro-element (façade, triumphal arch, bell tower, etc.) is sufficient to make the activation of an associated collapse mechanism (event) possible. Thus, each potential failure mode that could be activated in a church, i.e. a possible mechanism [PM] even if it is

not present, has a probability that is computed as the ratio between the number of churches for which the mechanism activated following the 2010 earthquake (EM) and the total number of possible mechanisms. PMFs for the out-of-plane and in-plane behaviors of the façade (M1, M2, and M3), and of the nave (M19, M5, M6, and M13), were evaluated (Figs.4.11, 12, 13, and 14). The mean damage is computed according to Equation (4.4), as suggested elsewhere (Matteis et al., 2016) and applied by previous authors (Marotta et al. 2016, Marotta et al. 2017, De Matteis & Zizi, 2019) in the study of New Zealand URM churches.

$$\mu d = \frac{\sum_{i=1}^n d_{k,i}}{N_j} \quad (4.4)$$

where  $\mu d$  is the average of the observed damage level for damage mechanisms obtained through the ratio between  $d_{k,i}$  the number of macro-elements (i.e. Façade and lateral walls) of the buildings that reached a damage level  $k$  at a given intensity,  $IM = IM_j$  and  $N_j$  the total numbers of observed macro-elements at a given intensity,  $IM_j$ .

To estimate the probability that the set of observed data is represented by the BPDF function, the chi-squared test of goodness of fit has been carried out. The variable  $\chi^2$  is the weighted sum of squared error between the measured variable and its theoretical value, each error is weighed by the measurement of the standard deviation. Given  $N$  independent random variables ( $x_i$ ) with mean values ( $m_i$ ), and variance ( $\sigma^2$ ), the  $\chi^2$  is defined as:

$$\chi^2_{calc} = \sum_{i=1}^k \frac{(x_i - m_i)^2}{\sigma_i} = \sum_{i=1}^k \frac{x_i^2}{m_i} - n \quad (4.5)$$

$\chi^2_{calc}$  distribution depends on a single parameter the degrees of freedom,  $dof = k - 1$ . The critical value of the theoretical distribution of  $\chi^2$  for 4 degrees of freedom with significance possible level,  $\alpha$ , equal to 0.05,  $\chi^2_{crit, 4gdl, \alpha=0.05}$ , is equal to 9.49.

Considering the PMFs of church global behaviors (Fig.4.10) at intensity range from  $0.16g < PGA \leq 0.28g$ , the  $\chi^2_{calc}$  is equal to 2.72; at intensity range from  $0.28g < PGA \leq 0.41g$ ,  $\chi^2_{calc} = 4.72$ ; and at intensity range from  $0.41g < PGA \leq 0.53g$ ,  $\chi^2_{calc} = 0.61$ .

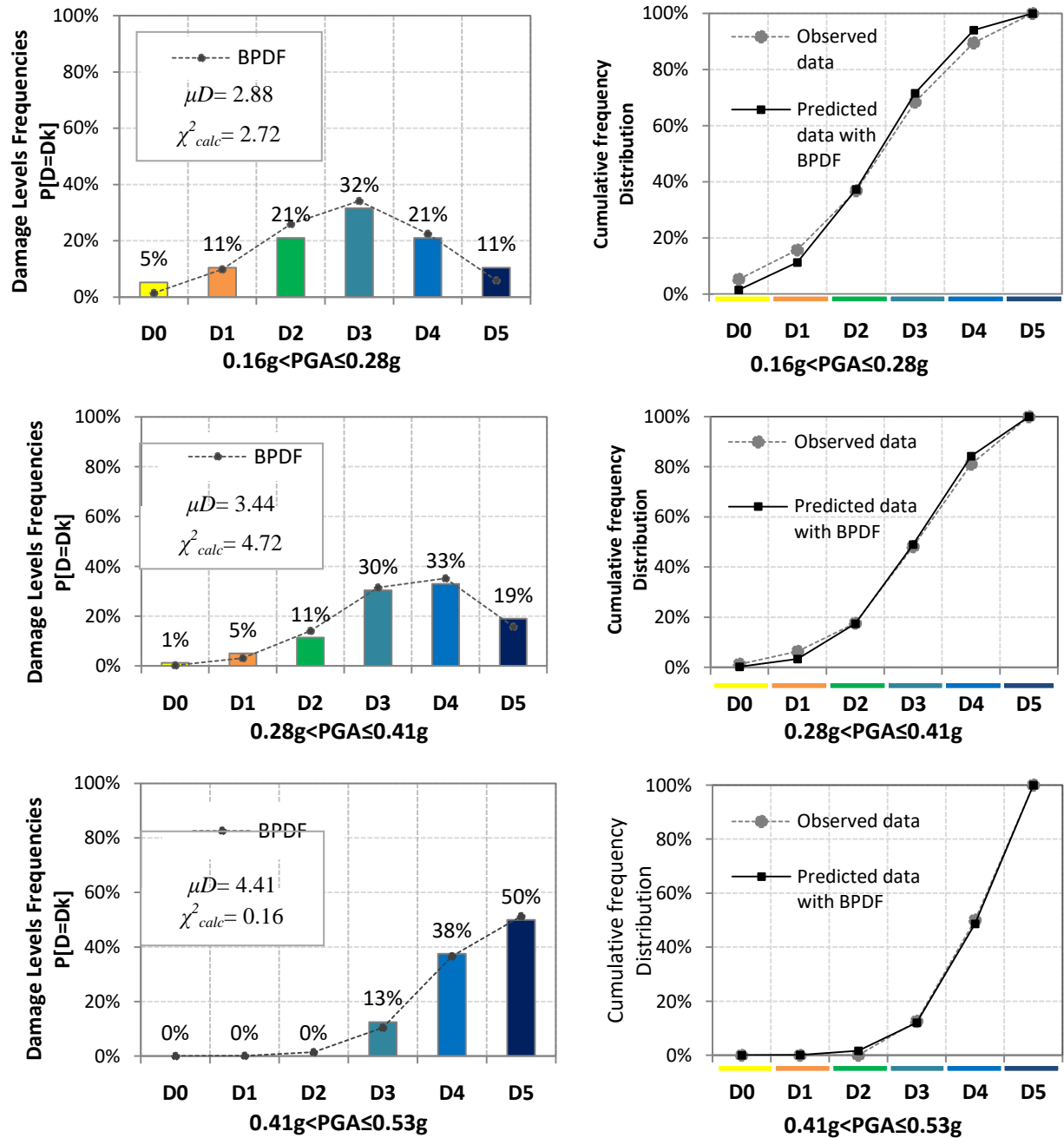
In these cases, a good agreement can be observed between the BPDF and the empirical distributions.

As concerning the PMFs for OOP behavior of façade macro-element (Fig.4.11): at intensity range from  $0.16g < PGA \leq 0.28g$ , the  $\chi^2_{calc}$  is equal to 4.18; at intensity range from  $0.28g < PGA \leq 0.41g$ ,  $\chi^2_{calc} = 8.13$ ; and at intensity range from  $0.41g < PGA \leq 0.53g$ ,  $\chi^2_{calc} = 1.23$ . For IN behavior of façade macro-element (Fig.4.12): at intensity range from  $0.16g < PGA \leq 0.28g$ , the  $\chi^2_{calc}$  is equal to 2.81; at intensity range from  $0.28g < PGA \leq 0.41g$ ,  $\chi^2_{calc} = 15.57$ ; and at intensity range from  $0.41g < PGA \leq 0.53g$ ,  $\chi^2_{calc} = 0.55$ .

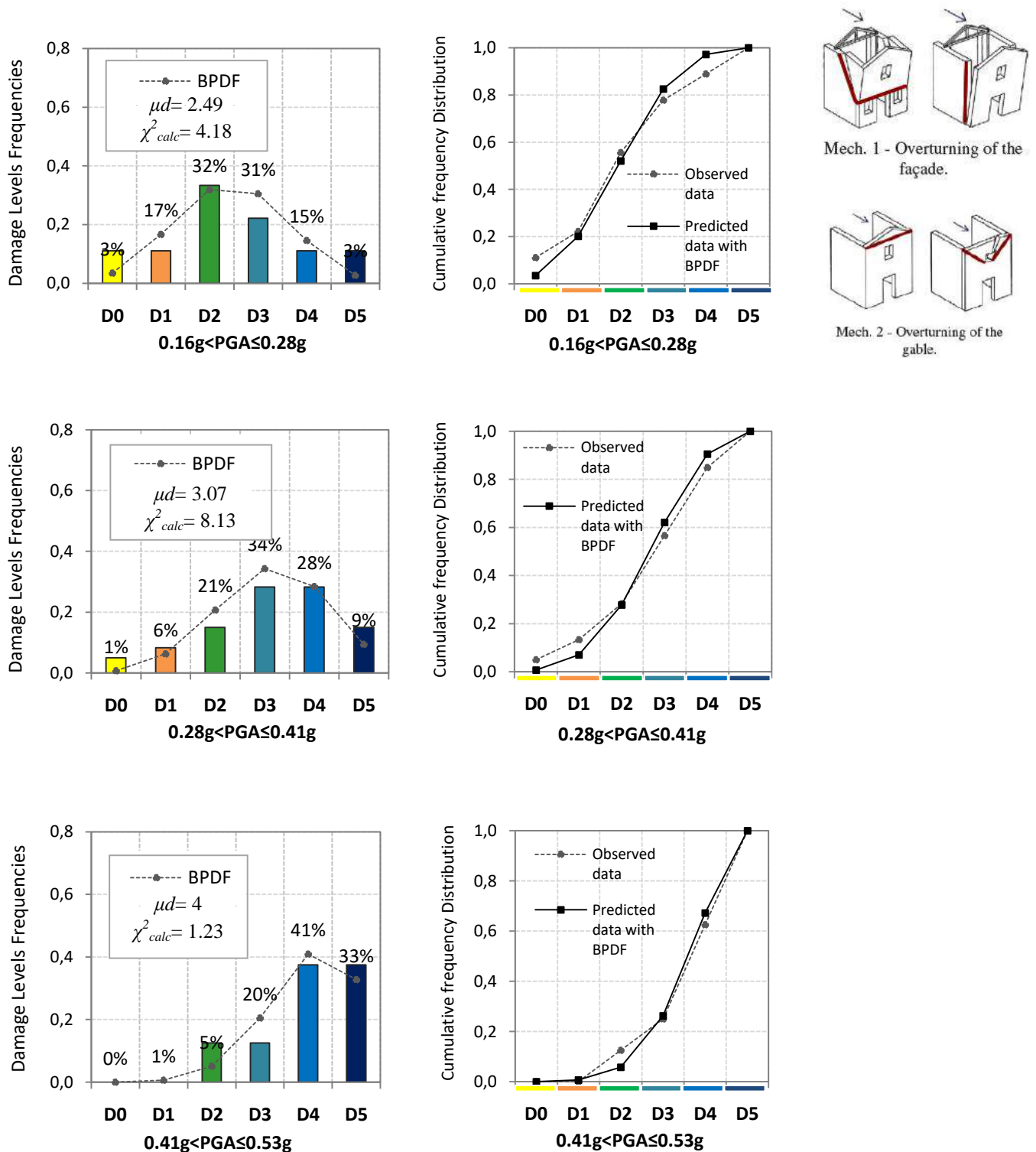
As concerning the PMFs for OOP behavior of lateral wall macro-element (Fig.4.13): at intensity range from  $0.16g < PGA \leq 0.28g$ , the  $\chi^2_{calc}$  is equal to 4.71; at intensity range from  $0.28g < PGA \leq 0.41g$ ,  $\chi^2_{calc} = 3.7$ ; and at intensity range from  $0.41g < PGA \leq 0.53g$ ,  $\chi^2_{calc} = 1.4$ . For

IN behavior of façade macro-element (Fig.4.14): at intensity range from  $0.16g < PGA \leq 0.28g$ , the  $\chi^2_{calc}$  is equal to 6.5; at intensity range from  $0.28g < PGA \leq 0.41g$ ,  $\chi^2_{calc} = 16.38$ ; and at intensity range from  $0.41g < PGA \leq 0.53g$ ,  $\chi^2_{calc} = 1.2$ .

Again, a good agreement can be observed between the BPDF and the empirical distributions, with the exception of IN behavior of façade and lateral walls at intensity range from  $0.28g < PGA \leq 0.41g$ .



**Figure 4.10.** Probability Mass Functions (PMFs) and Cumulative Frequency Distribution (CFDs) for the whole sample using observed data and predicted data through Binomial Distribution (BPDF) for ground motion intensities in the range from  $0.16g < PGA \leq 0.53g$ .



**Figure 4.11** - Probability Mass Functions (PMFs) and Binomial Distribution (BPDF) for the out-of-plane behavior of the façade (M1, M2) for intensities ranging from  $0.16g < PGA \leq 0.53g$ .

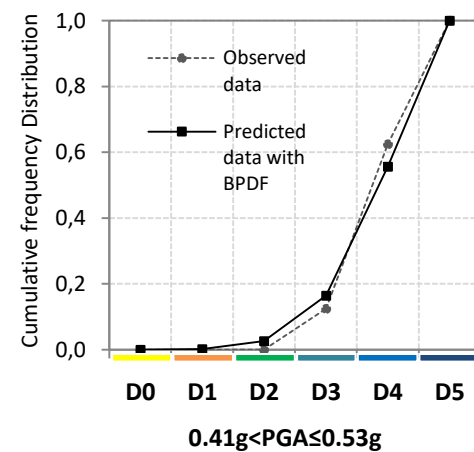
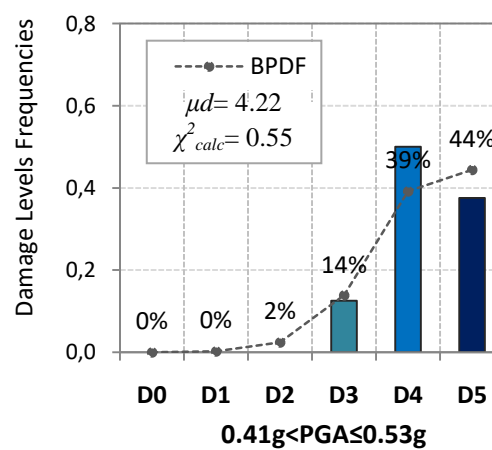
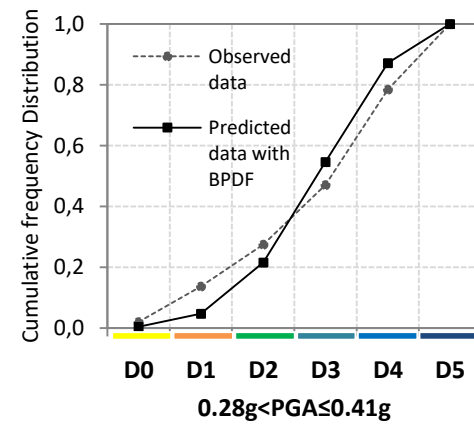
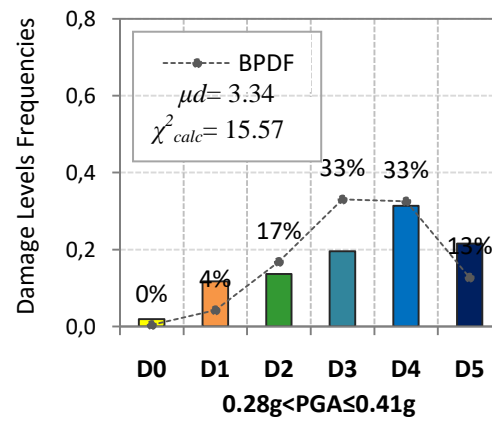
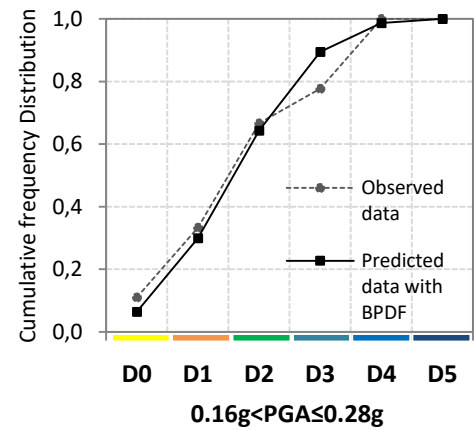
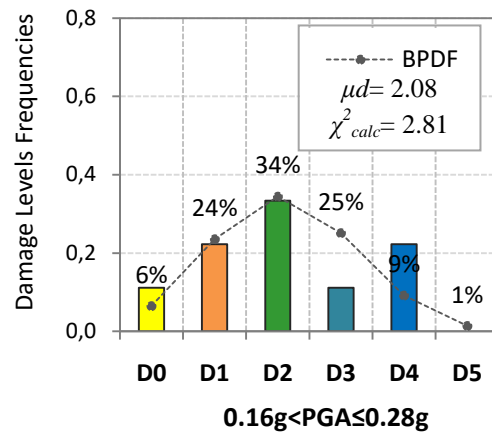
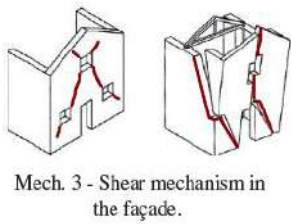
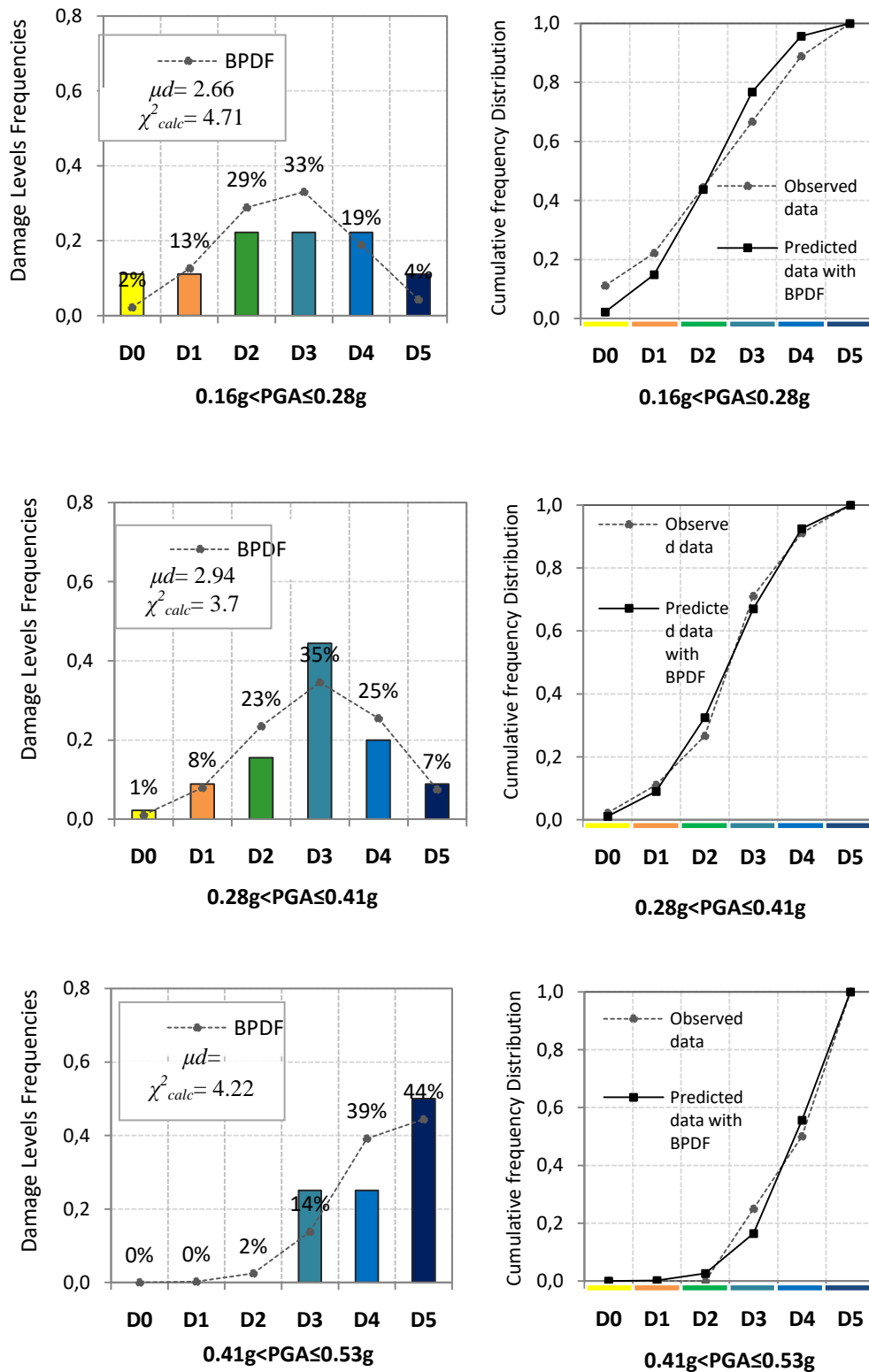
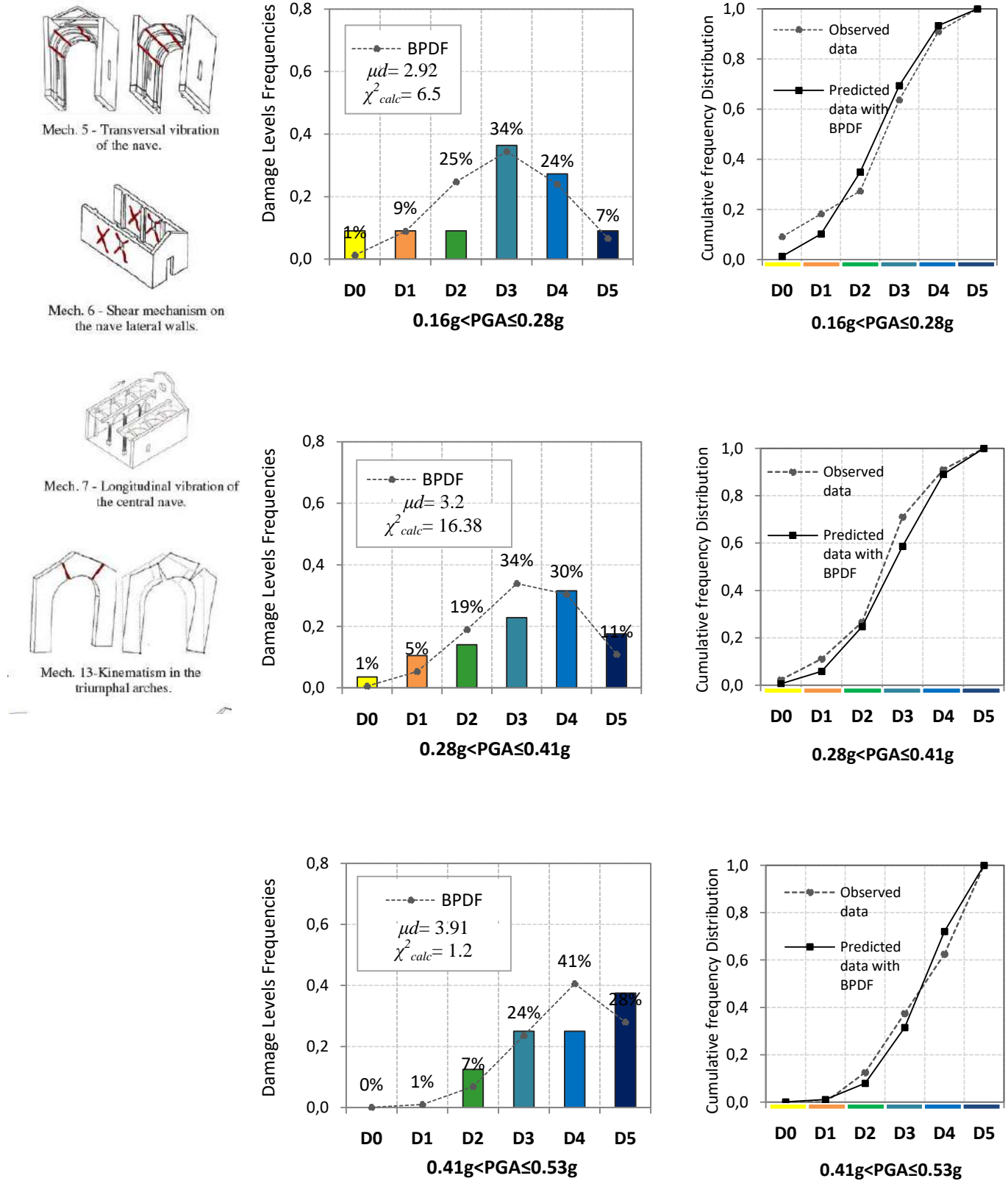


Figure 4.12 - Probability Mass Functions (PMFs) and Binomial Distribution (BPDF) for the in-plane behavior of the façade (M3) for intensities ranging from 0.16g < PGA ≤ 0.53g.



**Figure 4.13 - Probability Mass Functions (PMFs) and Binomial Distribution (BPDF) for the out-of-plane behavior of the lateral walls (M19) for intensities ranging from  $0.16g < PGA \leq 0.53g$ .**



**Figure 4.14 - Probability Mass Functions (PMFs) and Binomial Distribution (BPDF) for the in-plane behavior of the lateral walls (M5, M6, M7, and M13) for intensities ranging from 0.16g < PGA ≤ 0.53g.**

#### 4.4 Empirical Fragility Curves (EFCs)

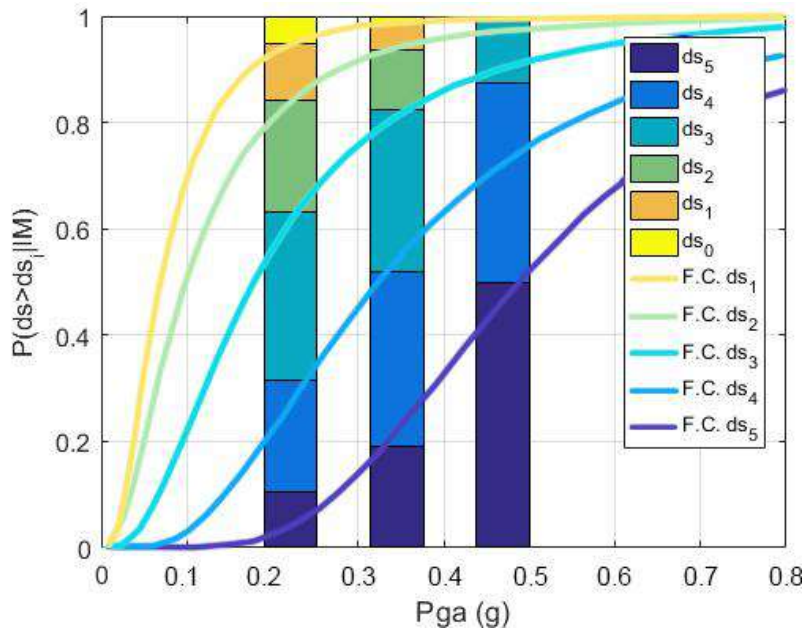
In this research, empirical fragility curves based on the observed database of URM churches will be derived as a function of PGA using different statistical models proposed elsewhere Lalléman et al., 2015. First, we use a lognormal cumulative distribution (CDF) fit obtained by minimizing the weighted sum of the squared errors (SSE), between the CDF:

$$P(C/IM = IM_i) = \varphi\left(\frac{\ln(IM_i) - \mu}{\beta}\right) \quad (4.5)$$

where  $\varphi$  is the standard cumulative normal distribution function;  $\mu$  and  $\beta$  are the sample mean and the standard deviation, computed such that the weighted sum of squared errors between the probabilities predicted by the fragility function and the ones observed from the data is minimum. Parameters  $\mu$  and  $\beta$  are estimated by Equation 4.6, as follows:

$$\mu, \beta = \arg \min_{\mu, \beta} \sum_{i=1} N_i \left( \frac{n_i}{N_i} - \varphi\left(\frac{\ln(IM_i) - \mu}{\beta}\right) \right)^2 \quad (4.6)$$

Where  $\frac{n_i}{N_i}$  is the ratio between the number of buildings that reached a damage level  $i$  at a given intensity,  $IM = IM_i$  and  $N_i$  is the total number of observed building sat that intensity  $IM = IM_i$ . The given fragility curves for the SSE-based lognormal model are shown in (Fig.4.15).



**Figure 4.15-** Chilean churches fragility curves for global behavior of the structures, (a) using lognormal distribution fitting by SSE.

Other models used for regression avables are the generalized linear models (GLMs), which are defined by three components (i) a conditional probability distribution of the exponential

family; (ii) a linear predictor; and (iii) a link function that relates the linear predictor with the response (Rossetto et al., 2013, Fig.4.16). These models may be written by the linear form (Lallemant et al., 2015):

$$g(\mu) = \alpha + \beta_1 X_1 + \beta_2 X_2 + \dots + \beta_n X_n = \eta \quad (4.7)$$

where  $\mu$  is the expected response of given predictor variables  $X_1, X_2, \dots, X_n$ , and  $\eta$  is the linear predictor related to the expected response through function  $g$ .

In developing fragility curves, Eq.(4.7) is reduced to a single explicative variable say the logarithm of IM, and two linear coefficients, the intercept  $\alpha$  and the slope  $\beta$ . The value of  $\mu$  is the probability of exceedence once of a particular damage state threshold ( $DS > ds$ ), conditioned to the value of IM, i.e.:

$$\mu = P(DS \geq ds | IM) = g^{-1}(\alpha + \beta \log(IM)) \quad (4.8)$$

The process of fitting a GLM then involves to find the coefficients that maximize the likelihood function (MLE) based on the assumption of a conditional distribution of the exponential family.

Different formulations of lognormal distribution fitting by MLE are also proposed. The loglog (Fig.4.17), logit (Fig.4.18) and probit (Fig.4.19) links functions are used for fitting fragility curves.

Lognormal GLM CD-based curve fit by maximum likelihood estimation, probit GLM and log(IM) provide a good representation of earthquake damage fragility but constrain the shape of FCs.

The Fragility curves obtained from a lognormal distribution fit by SSE, and from a GLM distribution fit by a MLE, are presented in Fig.4.20. The shapes and values of the resulting curves are very similar at low and medium PGAs, although the GLM distribution fit using a by MLE has a sharper increase at low IMs and a sharper asymptotic behaviour at high IMs.

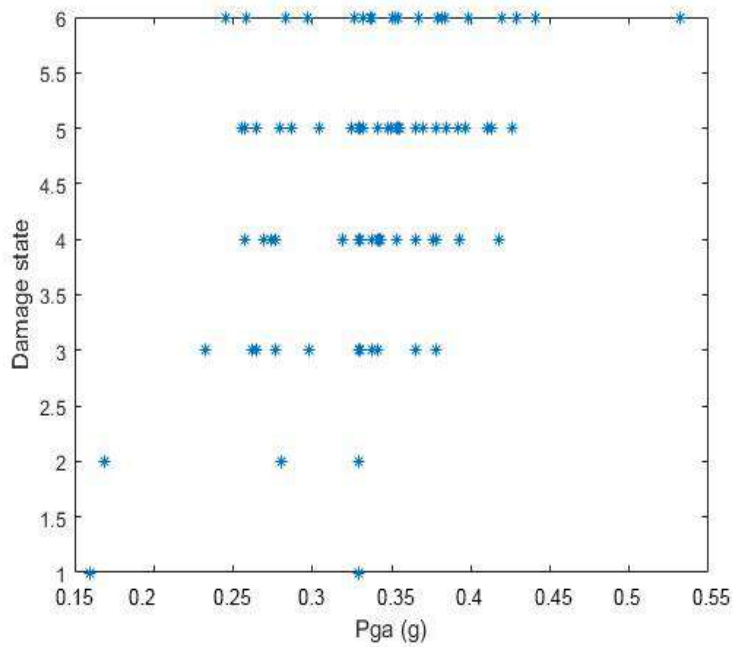


Figure 4.16 - Chilean churches points of damage levels for different PGAs

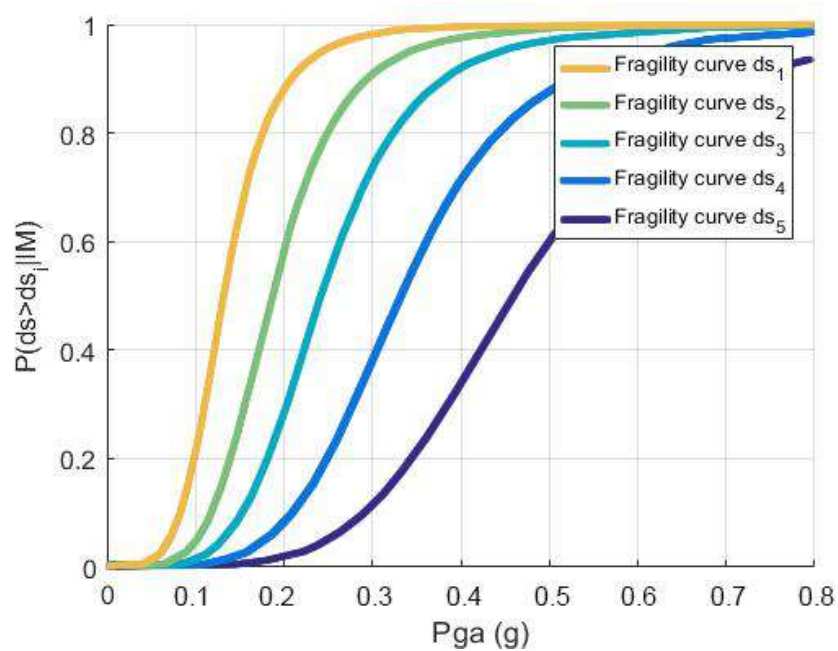
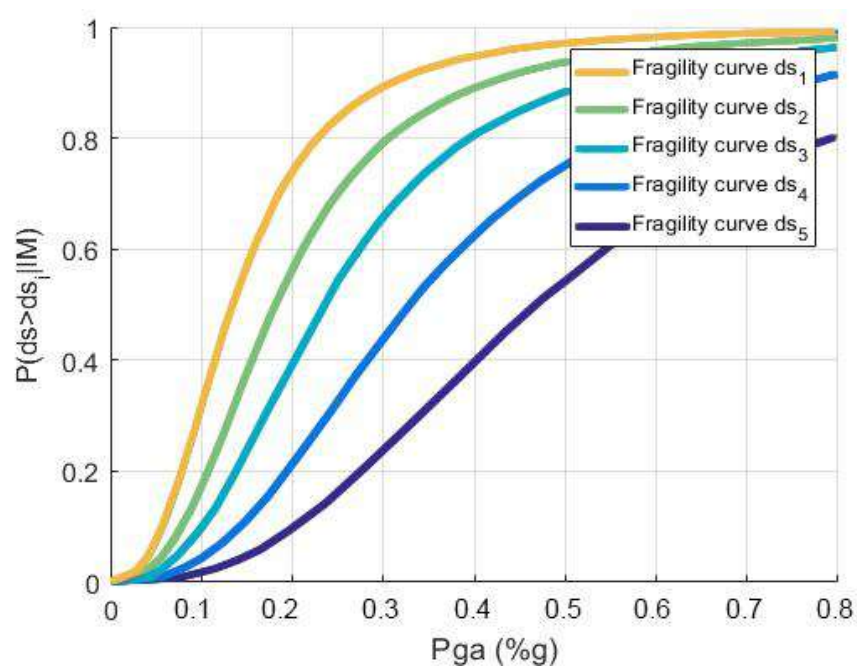
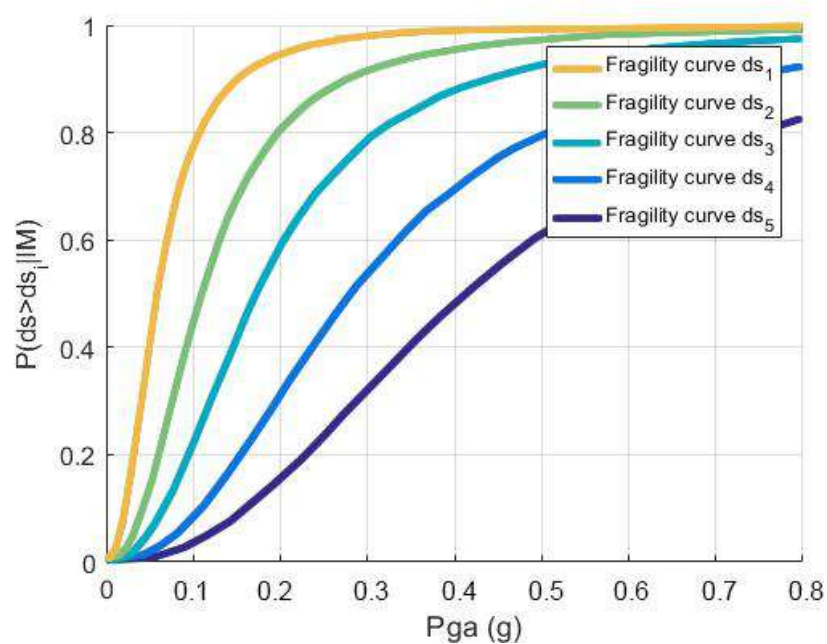


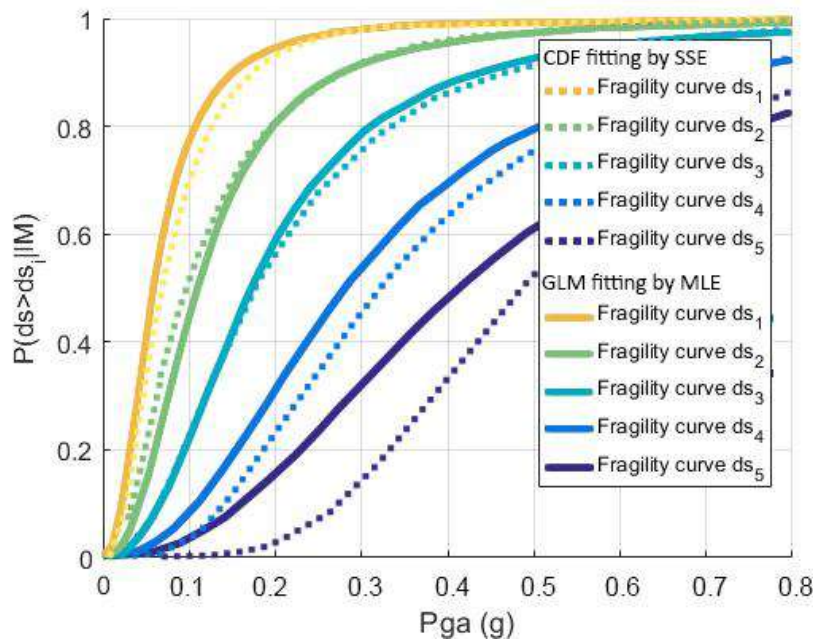
Figure 4.17 - Chilean churches fragility curves using loglog link function, derivate from GLM distribution fitting by MLE.



**Figure 4.18-** Chilean churches fragility curves using logit link function, derivate from GLM distribution fitting by MLE.



**Figure 4.19 -** Chilean churches fragility curves using probit link function, derivate from GLM distribution fitting by MLE.



**Figure 4.20** –Comparison between Chilean churches fragility curves using GLM distribution fitting by MLE and lognormal distribution fitting by WSSE.

## 4.5 Summary

This Chapter presents a macro-scale statistical analysis based on in-situ inspections of the structural damage underwent by 106 URM Chilean churches during the 2010 Maule earthquake.

The macro-seismic method (Lagomarsino et al., 2004) for estimating the global damage index,  $id$ , was implemented for each church following the 2010 Maule earthquake. Six of the twenty-eight mechanisms, usually employed in the literature for churches (PCM-DPC MiBAC, 2006), were not activated in any church mainly due to the absence of vaults and isolated elements standing in the structural masonry. Indeed, these elements are realized in timber or with similar light materials, e.g. *incannicciato*.

Some mechanisms were activated in around 80% of cases; those mechanisms involved in-plane and out-of-plane mechanisms of the façade, side aisle walls and bell tower.

Qualitative and quantitative post-seismic scenario has been reported by use of macro-element approach in function of PGA, Probability Mass Functions and Fragility Curves.

A statistical analysis, which correlates the global damage levels to the recorded PGA, was carried out. Empirical PMFs were computed and a binomial distribution was fit to the data. PMFs are defined both for global damage indices and for those damage mechanisms of single macro-elements that most frequently activated during Maule earthquake.

Finally, the fragility curves have been obtained using lognormal distribution fitting by weighted sum of squared error (SSE), and generalized linear model (GLM) fitting by maximum likelihood estimation (MLE).

Results of PMFs show a good agreement between the predicted damage by models and the observational data. This is consistent with what it was observed in the Umbro-Marches churches (Lagomarsino & Podesta, 2004a,b, and c) and of the L'Aquila basin (De Matteis et al, 2016).

Furthermore, for mechanisms that activate more frequently, say in-plane and out-of-plane behaviors involving the façade (M1 and M2 activated in 4/5 of the total sample) and the sidewalls (M19 activated in 3.5 / 5), specific PMFs were quantified. For the PMFs of the out-of-plane behavior (M19) of the nave macro-element (Fig.4.13) the following observations are obtained:

- at high intensity,  $0.41g < PGA \leq 0.53g$ , the probability of total or partial collapse ( $D_k = D_5$ ) of at least 2/3<sup>ths</sup> of the mechanisms is  $P[D_k = D_5] = 50\%$ ;
- at intermediate intensity,  $0.28g < PGA \leq 0.41g$ , the probability of activation of severe mechanisms with severe structural damage is  $P[D_k = D_3] = 45\%$ ;
- at low intensity,  $0.16g < PGA \leq 0.28g$ , the probability of light damage in several cases with the activation of one or two mechanisms is  $P[D_k = D_2] = 22\%$ .

For the PMFs of the in-plane behavior of the same macro-element (M5, M6, M7, and M13)(Fig.4.14) the following observations can be obtained:

- at high intensity, the probability of reaching a damage level  $D_5$  is  $P[D_k = D_5] = 38\%$ ;
- at intermediate intensity, the probability of activation of several mechanisms that include the collapse of some macro-elements is  $P[D_k = D_4] = 33\%$ ;
- at low intensity, the probability of severe damage is  $P[D_k = D_3] = 44\%$ .

Unlike the side walls, the façade macro-element shows greater vulnerability in the in-plane rather than in the out-of-plane behavior (Fig.4.12):

- at high intensity, the probability of reaching a level of severe damage with collapse of 2 or more macro-elements is  $P[D_k \geq D_4] = 88\%$ ;
- at intermediate intensity, the probability of detecting substantial to heavy damage is  $P[D_k = D_3] = 28\%$ ;
- at low intensity, the probability of observing light damage in several mechanisms is  $P[D_k = D_2] = 38\%$ .

Moreover, FCs were obtained using two methods, a generalized linear model (GLM) fit using maximum likelihood estimation (MLE), and a lognormal distribution fit by minimizing a weighted sum of the squared error (SSE). The resulting curves are very similar at low and medium PGAs, though the GLM curves have shaper increase at low PGAs and shaper asymptotic behavior at high PGAs. These results suggest strategies for choosing improve

interventions, Furthermore, potential future post-seismic scenarios for URM churches could be contrasted with the proposed PMFs and FCs.

Despite the heterogeneity of churches presented elsewhere Chapter 2, the whole sample (106 churches) was used to obtain PMFs and FCs and hence, limitation of this research lies in the use of this heterogeneous database, coming from architectural, constructive, and geometric features.

Despite of this, it was possible to define seismic fragilities for a historical “church” architectural typology. Further investigations are necessary to obtain specific fragility functions for each architectural style. Currently this is not possible because data limitations that impede such goal. Empirical data of damage caused by low, medium and high earthquake intensities must be systematically recorded. Survey activities may be realized using the methodology proposed herein with the aim to collect a sufficient number of observations. In fact, as shown elsewhere (Rossetto et al., 2014) the quality of PMFs and FCs strongly depends on the quality and quantity of observations within the empirical database. A high quality database should derive from a large sample say  $\geq 100$  buildings (representative of total population) for each building class.

Regardless of these limitations, this research a first important attempt toward systematically defining the seismic fragility of these buildings.

## Chapter 5

### METHODOLOGICAL FRAMEWORK FOR ASSESSMENT THE SEISMIC PERFORMANCE OF SINGLE URM CHURCH

The empirical fragility curves for URM churches of central Valley, developed in Chapter 4, are a fundamental tool for assess future post-seismic scenarios in terms of damage and loss for structures similar to those studied in this research. Damage scenario investigations serve ultimately as prioritization tools for single-building retrofitting interventions, which should meet specific guidelines. At the moment, no such recommendations or standards for intervention on URM building (similar to those provided in some other areas, ACI-530-99/ASCE5-99; Eurocode 6, 2006; MIT, 2009) are provided.

To fill this gap and considering also the high seismic hazard of the area and the specific features of the building culture, an investigation focused on the assessment of the seismic performance of single-buildings representative of each fragility class, as defined in the Chapter 4, seemed worth considering.

Three representative case studies are identified, taking into account the typological, geometrical, and material variables analyzed in Chapter 2: Masonry type (categories: Stone [S], Brick [B], and Adobe [A]); (b) Architectural layout (categories: Basilica (three naves) [Bs], Latin-cross [L-c], and Single-nave [S-n]); (c) Architectural style (categories: Colonial Style [CL], Neo-Classical Style and Variants [NC&V], and Neo-Gothic [NG]); (d) Foot-print area (categories:  $90\text{m}^2 < A1 \leq 500\text{m}^2$ ;  $500\text{m}^2 < A2 \leq 900\text{m}^2$ ; and  $A3 > 900\text{m}^2$ ); and the geometrical indices for each fragility class (CL, NC&V, and NG).

The case studies located in the Metropolitan and the Libertador Bernardo O'Higgins regions are:

- Case study1, San Juda Tadeo of Malloa parish representative of the colonial style [CL], is characterized by adobe masonry [A], Single-nave [S-N], and a foot-print area  $90\text{m}^2 < A1 \leq 500\text{m}^2$ ;
- Case study2 San Francisco de Asis church representative of neo-classical and variant style [NC&V]. It is characterized by stone-brick masonry [S-B], three naves [Bs], and a foot-print area  $A3 > 900\text{m}^2$ ;
- And Case study3 Basilica del Salvador representative of neo-gothic style [NG], and characterized by brick masonry [B], three naves [Bs], and a foot-print area  $A3 > 900\text{m}^2$ .

The first fundamental step to understand the seismic behavior of a historic URM structure is to conduct a comprehensive study through a multi-disciplinary approach that is capable of

providing and integrating knowledge from different fields. Multi-disciplinary research is particularly essential in the case of URM churches, which were modified, expanded and reconstructed over the centuries, often, using different construction techniques and materials. The result of this transformation process is a complex structure characterized by a high degree of uncertainty.

Direct observation of cultural heritage buildings 'post-earthquakes scenarios (Giuffrè 1991; Giuffrè and Carocci, 1993; Doglioni, 1994; Carocci, 2001) has shown that the seismic motion selects the most vulnerable masonry portion (macro-elements), triggering the activation of local failures related to the loss of equilibrium (Augusti, Ciampoli, and Zanobi 2001; D'Ayala and Speranza 2003), rather than to states of stress exceeding the materials ultimate capacity. These macro-elements demonstrate autonomous structural behavior with respect to the global response of the building (Mele, de Luca, and Giordano 2003; Lourenco 2005; Lourenco et al. 2007; Mallardo et al. 2008; Roca, Cervera, and Gariup 2010).

An effective approach to describe such a behavior consists in the application of limit analysis to the macro-block configuration (rigid blocks) of masonry structure subjected to overturning. The limit analysis procedures, formulated by (Heyman, 1966), have been proposed in several studies on masonry buildings, as in (Bernardini, 1988; 1990; Giuffrè, 1997; Brun, 1999; D'Ayala, 1999; de Felice and Giannini, 2001; D'Ayala and Speranza, 2003; Casapulla and D'Ayala, 2006; Casarin and Modena, 2008; Casolo and Sanjust, 2009; Lagomarsino and Resemini, 2009; De Matteis and Mazzolani, 2010).

The assessment of safety condition through limit kinematic analysis, LKA, allows for the definition of the collapse-load factor ( $\alpha_0$ , ratio between equivalent inertial forces and vertical loads involved in the mechanism), characterized by the limit equilibrium condition.

Furthermore, the combination of the incremental kinematic analysis, IKA, and the Capacity Spectrum (the Capacity Curve plotted in terms of spectral acceleration and displacement), describes the evolution of the horizontal-loads multiplier,  $\alpha$ , when increasing the displacement of a control point in the kinematic chain, until the annulment of the horizontal seismic force (Freeman, 1978; Freeman, 1998; Fajfar, 1999; Fajfar, 2000; Doherty et al. 2002). Thus, through a graphical representation, this method determines how the Capacity Curve changes and as the mechanism evolves (Doherty et al., 2000; Restrepo and Magenes, 2004; D'Ayala, 2005; Lagomarsino, 2006). In addition to the local analysis, the linear dynamic analysis (LDA) allows a control of the global behavior of the building.

Other different methods are commonly used tools to evaluate the seismic performance of URM structures (Nonlinear static i.e. pushover, response spectrum, FEM nonlinear dynamic in the time-domain analyses, among the other), but they are not included in the objectives of this thesis.

**CL Style**

### **5.1 Case study 1: San Tadeo Juda de Malloa**

This section of Chapter 5 focuses on the seismic behavior assessment of the Juda Tadeo parish (Malloa, Chile), an iconic example of the Colonial architecture of Chilean Central Valley. This small unreinforced adobe church is a single-nave building consisting of the nave, the bell-tower located in façade, and additional units (sacristy, chapel and two services areas) built during different historical periods.

Despite the severe damage state after the 2010 Maule earthquake, the parish showed remarkable resilience due to the implementation of traditional seismic retrofitting techniques for earthen buildings. In fact, the use of wooden bond beams, corner keys and wooden gable has proved an effective solution against strong earthquakes.

For these reasons the study of San Juda Tadeo is relevant; it is a representative case in Chile of anti-seismic constructive techniques in the 17<sup>th</sup> century colonial architecture.

With the aim to assess the seismic behavior of the monument, a complete study of the parish has been carried out using a multi-level approach comprising historical research, such as in situ surveys, crack pattern analysis, physical and mechanical characterization of materials, and local and global structural analyses. An integrated use of different structural analyses with different complexity levels is proposed: (1) as concerning numeric modal identification analysis, by finite element method, linear dynamic analysis has been carried out; with respect to the local analyses by damage mechanisms, (2) linear and incremental kinematic analyses have been proposed.

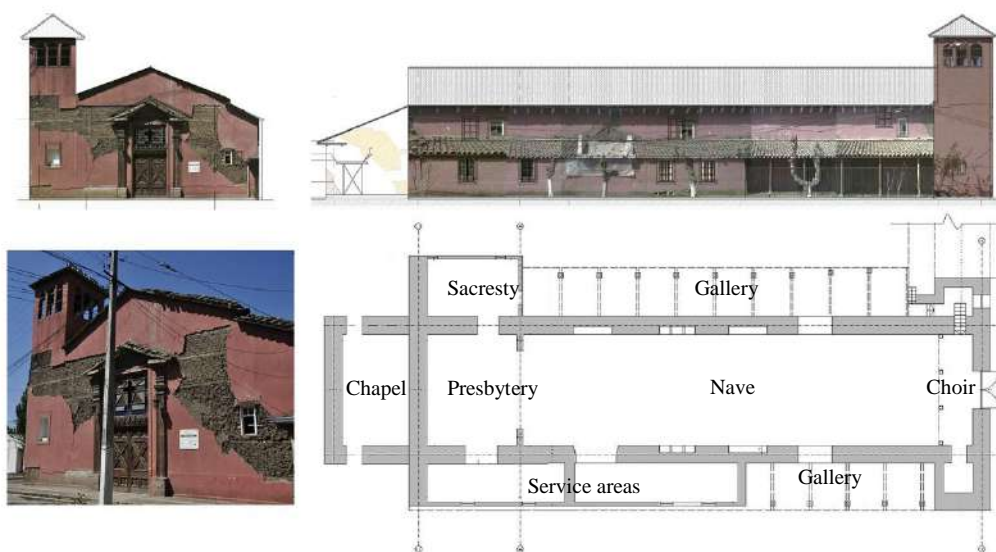
### 5.1.1 San Judas Tadeo de Malloa parish

San Judas Tadeo is the parish of the community of Malloa (-34.442247, -70.943377), a rural village of 12,000 inhabitants located in Cachapoal Province, Libertador General Bernardo O'Higgins region (VI), at 113 km south of Santiago.

The first parish was erected in 1635 and was completely destroyed by the May 13, 1647 (Ms~8) Santiago earthquake (Arias Arquitectos & Fercovic, 2011). The current parish was founded in 1845 under the avocation of San Juan Batista, but years later the devotion to San Judas Tadeo prompted a name change. The fervor of the community for this saint, known as the employer of the difficult causes, arose in 1887. During this year an epidemic of cholera broke out in the zone. While the parish priest was in Italy, he went to his intercession and got a painting with his image to take to the parish of Malloa. The tragedy touched the citizenry and settled in the collective memory of the village. Thus, the San Judas Tadeo church became a significant religious and civil Landmark of Malloa. It was declared Historic Conservation Zones (ZCH) according to Art. 60 of the General Urban Planning and Buildings Law; and Historical Monument according to Law N°17.288 of National Monuments (CMN, 2011).

San Judas Tadeo de Malloa was constructed following the typical architectural, constructive and structural features of Colonial style of the Chilean central valley (Chapter 2.2.1). The morphology of the structure consists of an austere rectangular plane of a single-nave, and additional units built later, during different historical periods.

The plane is 45.1m long in the longitudinal direction, 9.9m wide in the transversal direction, with a maximum roof height of 9.92m, accommodating 5,00 people.



*Figure 5.1.1 - View of the façade of the church and current plan, façade and section (Surtierra, 2011)*

The church has an area of 815.84 m<sup>2</sup>, and it features a central rectangular space oriented north-east south-west, a sacristy adjacent to the western wall, and two additional service areas located

respectively on the northern and eastern walls. The main nave is divided in three different sectors: a choir loft, a nave and a presbytery (Fig. 5.1.1).

The parish has undergone several modifications over the time consequently different construction techniques and materials are distinguishable.

#### **5.1.1.1 Construction phases and main interventions**

Malloa village is located in the territory of an indigenous village which motivated the installation of Franciscan convent which back to 1635 and was dedicated to San Antonio, one of the oldest in the VI region. As mentioned previously, the first temple was completely destroyed by the 1647 earthquake and a new Parish was erected in 1662, under the invocation of San Antonio de Papua. The first records date back to 1824. The current building was founded on the 17<sup>th</sup> November, 1845, although there is no documentation indicating which parts of the 1662 temple were reused.

After the 1928 Talca earthquake (7.6Mw), the complex suffered from considerable damage, and in the same year it was restored (Arias Arquitectos & Fercovic, 2011).

Despite the lack of historical information about the parish, during direct surveying activities carried out by the author, it was possible to recognize the original structure and the main subsequent construction phases. In fact, through the detection of construction techniques corresponding to specific historical periods and the survey of structural discontinuities, three main construction phases have been identified.

The first period corresponds to the original block composed by the main nave (choir loft, nave and presbytery) and the base of the bell tower at the side of the facade (dated back 1662-1824).

The second construction phase corresponds to the parish enlargement with northern and eastern service areas attached to the main block. These areas were built with *adobillo*, a system originated in the Valparaíso region in the middle of 19<sup>th</sup> century (Correia et al., 2014).

Finally, during the third construction phase (undated) a chapel and a sacristy were erected with adobe masonry walls, simply juxtaposed to the rear and west walls, respectively.

The actual configuration of the Parish is the result of seismic consolidation interventions and reconstructions during the past centuries characterized by different building techniques and materials, which present different structural behaviors. Probably after the 1985 Valparaíso earthquake (Mw8.0), the parish suffered considerable damage in the façade and bell tower, which were then reconstructed by wooden portion walls and reinforced through timber ring beam.

After the 2010 earthquake (Mw 8.8) Maule earthquake, the church incurred in significant damages due to severe crack pattern that induced separation among the walls. Structural

damage amplified due to rising damp and local deformation. In 2016, Arias Arquitectos carried out a wide conservation project that addressed the whole parish (Arias Arquitectos & Fercovic, 2011).

### 5.1.2 Architectural elements and properties of materials

The parish has undergone several modifications over the time. Consequently, different construction techniques and materials are observable. According to the historical analysis, three traditional constructive systems of masonry wall were recognizable: 4-wythe English bonds with the insertion of timber elements (W01), *adobillo* which is a mixed wooden-earth technique where a thin timber frame interlocks a single-wythe shiner bond (W02); and stacked 2-wythe masonry with header bond (W03), see Fig. 5.1.2 and Table5.1.2.

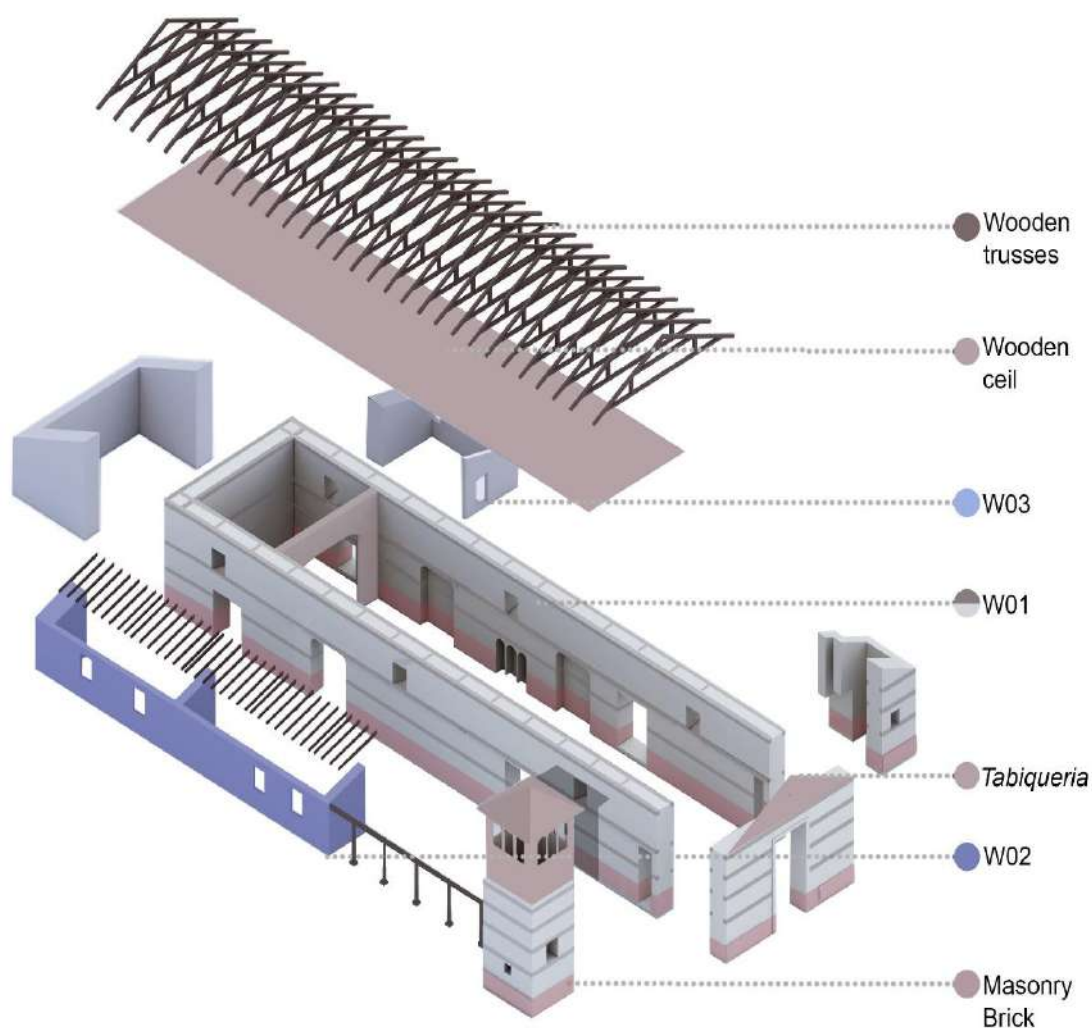
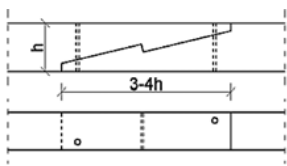
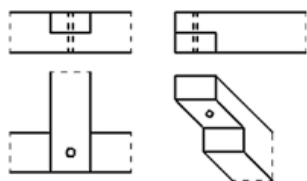


Figure 5.1.2 - Exploded Axonometric of resistant structure

The central nave walls (W01) are adobe masonry with the insertion of timber elements within the thickness, which are traditional seismic resistant technique of the local colonial culture (Fig. 5.1.2). These timber reinforcements are composed of horizontal and transversal elements. The wooden horizontal-elements run around the walls of the central nave and the base of bell tower, and transversal-elements across the full whole thickness. The horizontal elements have a section of 10x20cm located about every 1.8-2.7m, while the wooden transversal about 5x10cm every 2.25m. Despite this, traditional construction practice exploits the excellent mechanical proprieties of wood, improving the out-of-plane bending capacity and in-plane shear resistance of adobe walls. The woodworking joints are the main seismic weakness of this system when subjected to the seismic motion. In San Tadeo parish there are two types of joints (Table 5.1.1).


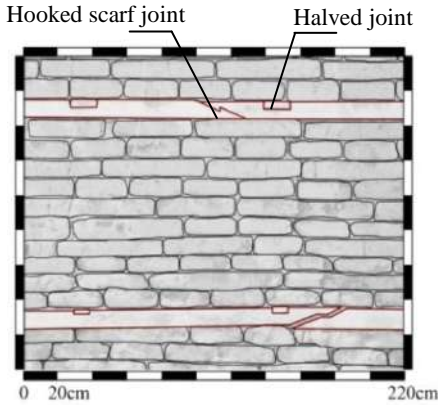
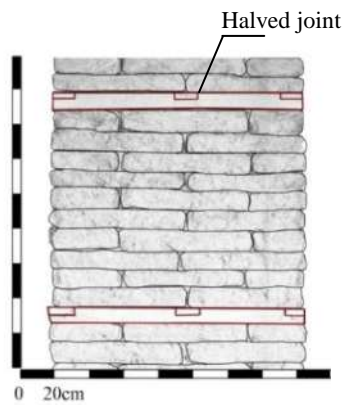
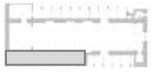
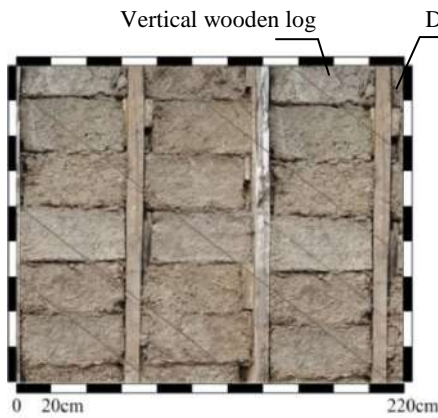

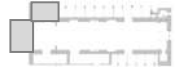
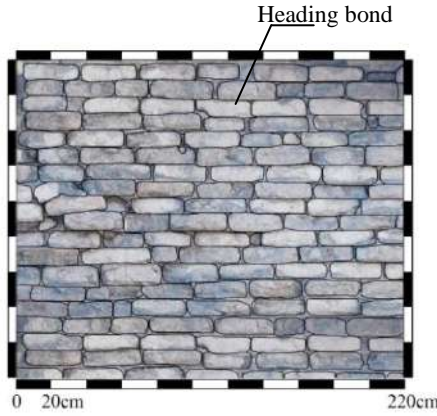

**Table 5.1.1** - Traditional timber joints in seismic areas (Parisi&Piazza, 2002).

Type of joint	Joint	Description
Hooked scarf joint		This joint offers greater tensile and compressive strength, but the link most depends on mechanical fastening to keep the joint closed
Halved joints		Four angled corners, for ground beams on a supporting masonry wall; pegging is essential; does not transfer tension

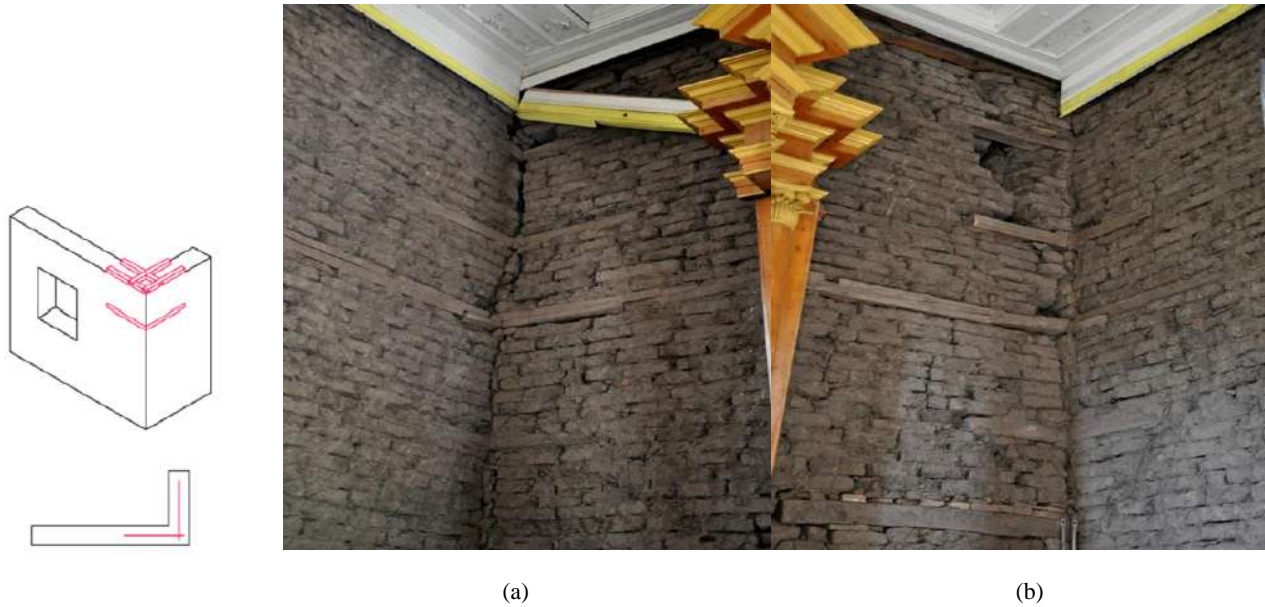
The hooked scarf joint, used to connect the wooden horizontal elements, is a traditional method of joining two members end-to-end (Table 5.1.1). This technique offers remarkable capacity in the longitudinal direction because it extends resistive area of the joint, thus maximum allowed force heightens, but the link mostly depends on the mechanical fastener employed to keep the joint closed. The halved joints, another traditional link, are used to join two orthogonal members by removing material from each at the point of insertion so that they overlap (Table 5.1.1). The amount of material removed is equal to half of the width, so the connections are weak and prone to splitting. Following the 2010 Maule earthquake, the failure of the joint interlocking between wooden elements it is observed, in particular for the hooked scarf joint. The link failures are shown by the slippage between the wooden elements in a horizontal direction, determining the propagation of vertical and diagonal cracks along the entire height of the wall.

The W01 walls of central nave (thickness 1.45m) are made of 4-wythe earthen wall, of adobe brick with dimensions 35x60x15cm, bond by an earth mortar. The wall-to-wall connections of central nave, despite the absence of bond, consist of using wooden corner keys (Table 5.1.2).

Table 5.1.2 – Masonry types

<b>[W01]_4-wythe English bond with the insertion of timber elements</b>		
		
(a) W01 elevation	(b) W01 section	
<b>[W02]_Adobillo wall mixed wood-earth system of a single-leaf</b>		
		
(c) W02 elevation	(d) W02 section	
<b>[W03]_Stacked 2-wythe masonry with header bond</b>		
		
(e) W03 elevation	(f) W03 section	

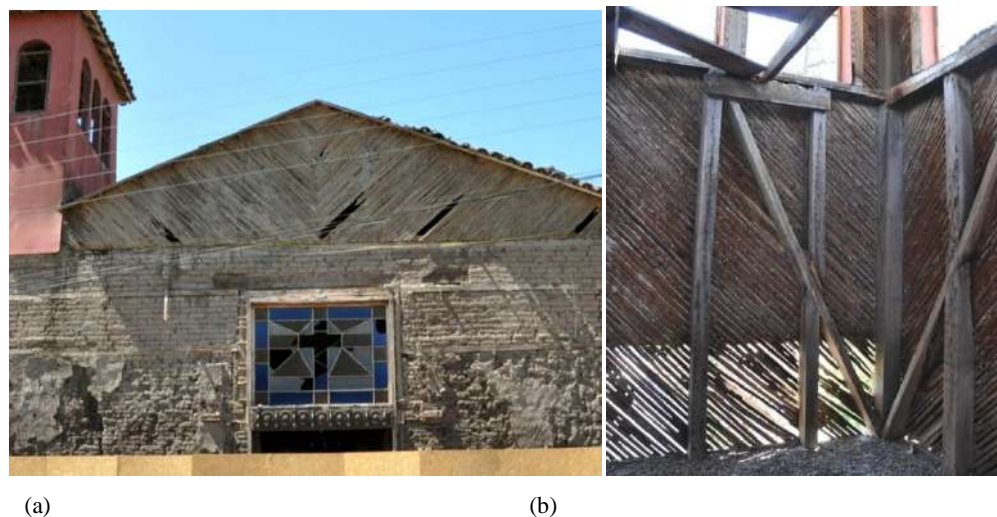
This traditional strengthening solution induces walls working together even when the bonds between perpendicular walls crack during an earthquake (Ortega et al., 2017), as can be seen in the 2010 post-earthquake photos of the rear wall of central nave (Fig.5.1.3 a-b).



**Figure 5.1.3** – (a) (b) Corner keys between rear and lateral walls.

The upper part of façade (the gable) and bell tower are built by wooden portion wall well bound to the beam of roof (Fig. 5.1.4), and settled on a timber ring-beam. This traditional constructive system, already described in Chapter 2.3.1, constrains the structure and reduces the height of façade and bell tower macro-elements and their destabilizing moment.

The main nave is covered by plain ceiling constituted by timber elements. The light roof system is supported by traditional timber king-post trusses with collar tie (Fig. 5.1.5a), covered by ceramic tiles. The foundation is composed of a 72cm high brick basement (Fig. 5.1.5b), and a 60cm stone masonry wall.



**Figure 5.1.4** - Wooden portion walls (tabique) of (a) façade gable and (b) bell tower.



**Figure 5.1.5** – Roof system of (a) traditional timber king-post trusses with collar tie, and brick basement of foundation visible of the external lateral façade (Surtierra, 2011).

The slender walls of two service areas located on lateral northern wall of central nave are made of *adobillo*, another traditional mixed wood-earth single-leaf wall (W02, Table 5.1.2). *Adobillo* walls are composed: by vertical wooden logs (10x10cm) every 75cm, horizontal wooden twigs (10x30cm), adobe blocks (60x30x10cm) of shiner course, and interior and exterior earth plaster with diagonal steel wires.

In general, this constructive system, originated in Valparaíso, uses a particular shaped earth blocks having two 1'x1' notches in the headers of block, that allow to fix the *adobillo* to wooden logs. However, these efficient links between earthen blocks and wooden elements are absent in the *adobillo* walls of San Tadeo Parish. Nevertheless, the presence of diagonal steel wires prevents the overturning of blocks. The *adobillo* walls of Malloa parish are the result of traditional local anti-seismic techniques and modern materials introduced in 19<sup>th</sup> century.

Finally, the masonries of chapel and sacristy, adjacent to the presbytery walls, were built with adobe masonry W03, block dimensions of 35x70x15cm. The W03 is double-leaf masonry without blocks crossing the whole thickness which generated a transversal locking, the *diatones*. Consequently, the wall is composed into sections simply positioned one next to the other, very vulnerable to the out-of-plane seismic actions. Furthermore, this adobe masonry is characterized by heading bond pattern resulting lower shear strength than a monolithic panel and an inadequate seismic behavior (Borri et al., 2015).

In order to define the mechanical proprieties of adobe blocks, the values suggested by three main universities (PUCP, Aveiro and Los Andes) that deal with the study of earthen buildings in the world, compared with Chilean Standard (INN, 2013) for adobe structures have been used. The Young's modulus  $E$ , compressive strength  $f'm$ , and shear strength  $v'$  of adobe masonry are shown in Table 5.1.3. The data is expressed through the average values ( $\mu x$ ) and standard deviation ( $\sigma x$ ) of mechanical proprieties.

**Table 5.1.3** - Young module ( $E$ ) compressive strength ( $f'_m$ ), and shear strength ( $v'$ ) of adobe masonry.

ID	NCh3332of12 [MPa]	Aveiro* [MPa]	PUCP** [MPa]	Los Andes*** [MPa]	M.Q.I**** [MPa]
$\mu E$ ( $\sigma_E$ )	200 ( - )	189.4 (77.0)	174.0 (10.6)	117.0 ( - )	166 ( - )
$\mu f'_m$ ( $\sigma_{f'_m}$ )	0.6 ( - )	1.13 ( 0.32 )	0.84 ( 0.04 )	- ( - )	1.2 ( - )
$\mu v'$ ( $\sigma_{v'}$ )	0.025 ( - )	0.11 (0.222)	0.07 (0.04)	0.031 ( - )	0.025 ( - )

\*Varum et al., 2006; \*\*Vargas et al., 1984; 2005, San Bartolome and Pehovaz 2004; Blondet et al., 2006); \*\*\*Yyamin et al., 2005;\*\*\*\*M.Q.I. Method, Borri et al. 2015

The data of Table 5.1.3 has been integrated through the results obtained by the method of Masonry Quality Index (M.Q.I.) (Borri et al. 2015) which is useful to estimate the mechanical features of masonry when it is not possible to carry out in situ Flat-jack tests. The mechanical parameters of adobe masonry with lime mortar were assessed: Young modulus ( $E_{medium} = 166\text{MPa}$ ), compressive strength ( $f'_{m,medium} = 1.2\text{MPa}$ ), and shear strength ( $v'_{o,medium} = 0.025\text{MPa}$ ), in agreement with Chilean Standard and the international literature.

In regards to the brick masonry basement with earth mortar lime compressive strength equal to  $1.0\text{MPa}$  ( $f_{m,min}$ ), Young modulus equal to  $600\text{MPa}$  ( $E_{min}$ ) and shear strength equal to  $0.025\text{MPa}$  ( $v'_{o,min}$ ), have been assumed according to the requirements of the Chilean preliminary Code of Intervención Estructural en Construcciones de Valor Patrimonial - Construcciones Históricas (INN, 2013).

The drying shrinkage process affects the shear strength of adobe; it induces micro-cracking in the adobe masonry in two phases. The absorption by adobe blocks is the first phase, during which most of micro-cracks develop. The water evaporation corresponds to the second phase (Neumann Vargas et al., 1986).

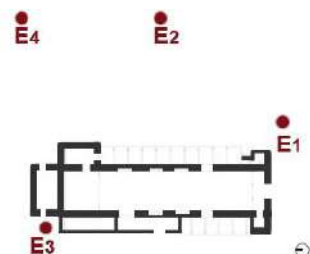
The wooden tresses of the roof structures consist of oak elements (*Nothofagus oblique*), Fig. 5.1.5, with density ( $\gamma = 624\text{kg/m}^3$ ), compressive strength ( $f'_{m,medium} = 46.65\text{MPa}$ ), and shear strength ( $v'_{o,medium} = 6.08\text{MPa}$ ).

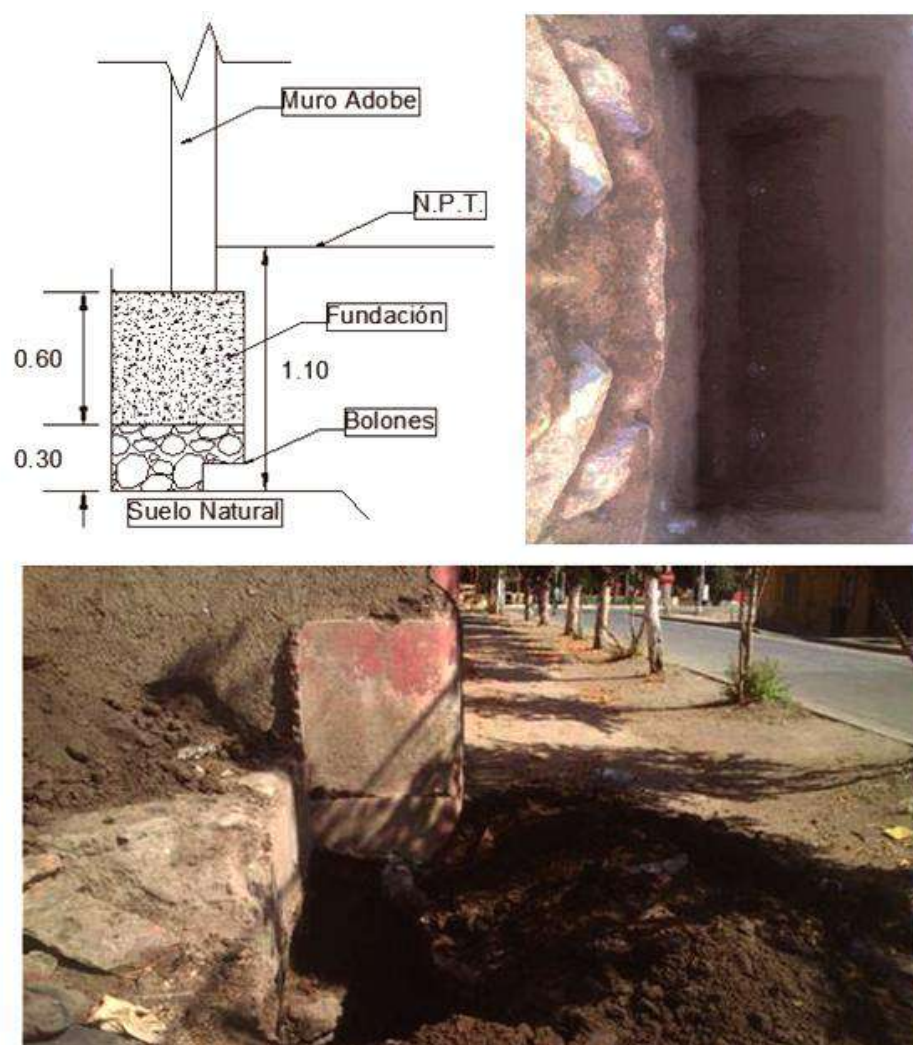
Finally, with the aim of characterize the soil mechanics and the foundation type, four excavations (Fig. 5.1.6) located near the west wall of the north chapel [E1], the south area of parish house [E2], the north area of parish house [E3], and the inner courtyard [E4], with a depth of 3m, 2.6m, 3m, and 3m, were carried out by (R&V Ingenieros, 2012). Based on the Chilean Code NCH433of 96 (INN, 1996) and D.S.61, 2011 (MINVU, 2011) the soil, having medium dense soil,  $V_{s30} = 332\text{ ms}^{-1}$ , and shear strength non-drained minor of  $0.05\text{MPa}$ , was classified as soil type D, with soil coefficient  $S=1$ . The foundation profundity measure was

about 2.90m. The embedding of the foundation, measured in the gravel was 25cm, consisting of quarry blocks of different shapes and dimensions (about 8"), and sand filling part of the gaps between blocks. The stratigraphy of excavations is shown in Table5.1.4.

**Table5.1.4** – Soil stratigraphy of the four test pit realized by (R&V Ingenieros) the April 2 and 3, 2012.

Test pit	Horizon n°	Depth range	Thickness	Description
<b>E1</b>	1	0.0 0.8	0.8	Filling, composed of clay of medium plasticity and low humidity. Soil of medium consistence.
	2	0.8 3.0	2.2	Low plasticity slime and medium humidity. Soil of homogeneous structure, medium porosity and soft consistency, with approximately 20% of sand and 5 to 10% of gravel. Have rootlets in low content. Do not observe expansive characteristics.
<b>E2</b>	1	0.0 1.1	1.1	Filling, composed of clay of medium plasticity and low humidity. Soil of medium consistence.
	2	1.1 2.6	1.5	Low plasticity slime and medium humidity. Soil of homogeneous structure, medium porosity and consistency between medium to soft, with approximately 10% to 15% of sand and 5 to 10% of gravel. Have rootlets in low content. Do not cracking and does not observe expansive characteristics.
<b>E3</b>	1	0.0 1.0	1.0	Filling, composed of clay of medium plasticity and low humidity. The 10cm higher correspond to granular material. It presents bolones until 0.40m of depth.
	2	1.0 3.0	2.0	Low medium plasticity slime and humidity. Soil of homogeneous structure, medium porosity and consistency between medium to soft, with approximately 20% of sand and 5 to 10% of gravel. Have rootlets in low content. Do not cracking and does not observe expansive characteristics.
<b>E4</b>	1	0.0 0.8	0.8	Filling, composed of clay of medium plasticity and low humidity. Soil of medium consistence.
	2	0.8 3.0	2.2	Low plasticity slime and medium-low humidity. Soil of homogeneous structure, medium porosity and consistency between medium to soft, with approximately 20% of sand and 5 to 10% of gravel. Have rootlets in low content. Do not cracking and does not observe expansive characteristics.





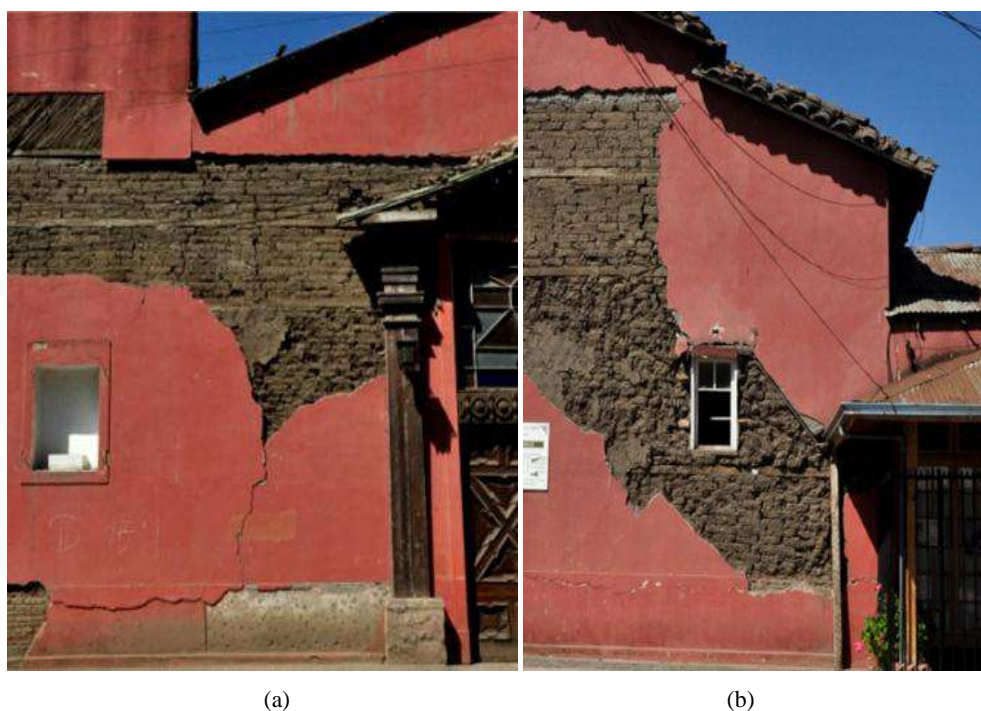
**Figure 5.1.6**– Soil stratigraphy of the E3 test pit realized by (R&V Ingenieros) the April 2 and 3, 2012.

### 5.1.3 Assessment of crack patterns

The San Juan Tadeo parish has suffered severe damage after the 2010 Maule earthquake. In particular, different seismic behaviors depending on construction techniques were observed in the main block (W01 masonry type), the service areas (W02 masonry type), and the sacristy and rear chapel (W03 masonry type).

The main block of Malloa parish consists of heavy and thick walls ( $H/t_f=6.8$ ), wooden beam bonds within the thickness and corner keys. Despite this, traditional anti-seismic system keeps the walls working together (*box-behavior*), in the main façade, the failure of joints, which used to attach (kink) end-to-end two horizontal members, aided the propagation of deep vertical cracks. The compound overturning of the thick façade ( $H/t_f=5.2$ ) is highlighted by vertical cracks passing through the wall thickness (Fig. 5.1.7a-b) and the disconnections between the façade and longitudinal side walls, internally observable (Fig. 5.1.8). Furthermore, the presence

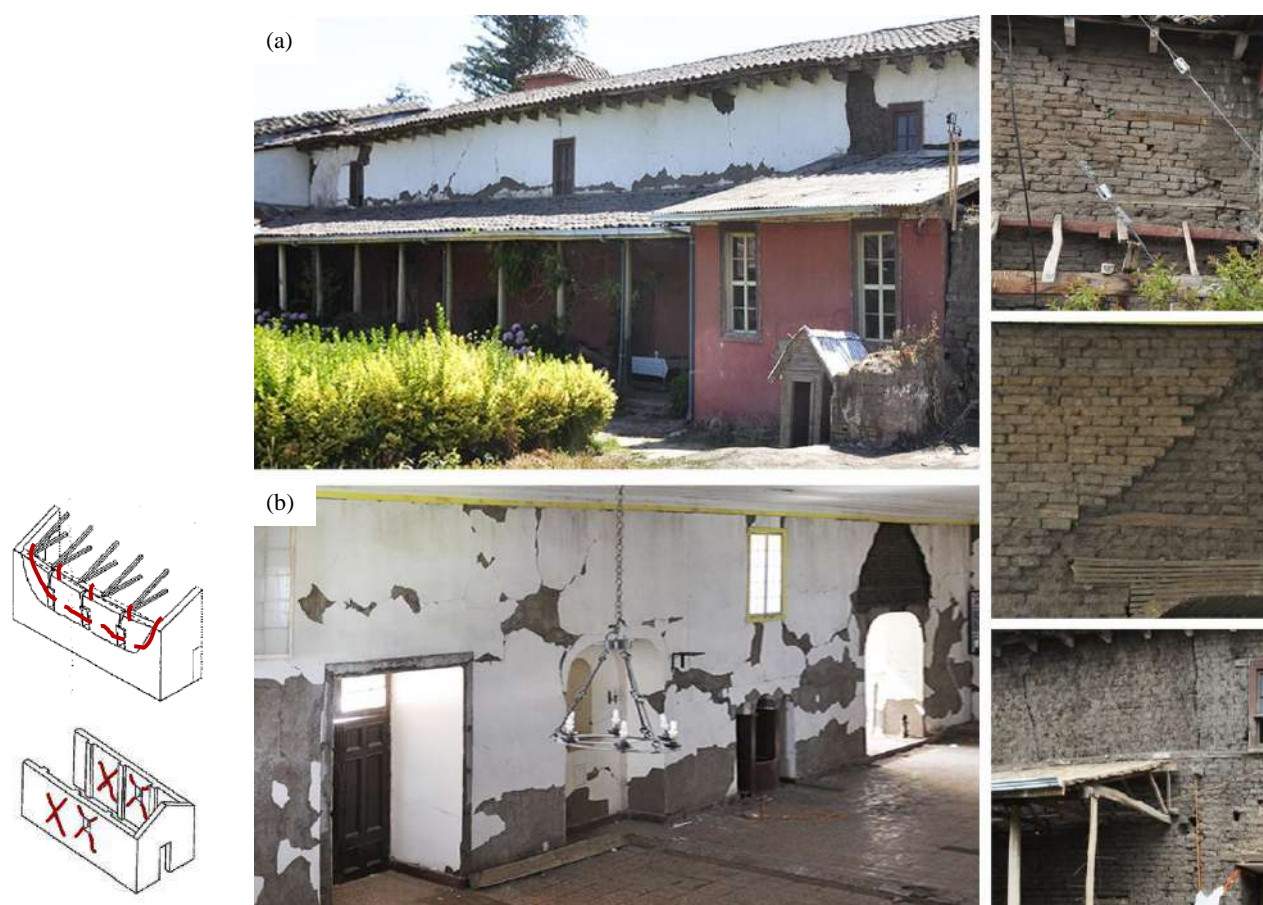
of timber corner keys provides reinforcement, improving the post-elastic behavior of the walls. Thus, a part of the longitudinal side walls and the façade continue to work together (Fig. 5.1.7). The diagonal cracks observed in the longitudinal walls highlight the activation of an overturning mechanism that involved the façade and triangular portions (two side wings) of the longitudinal walls around a horizontal hinge, located at 72cm above the ground level. The shape of façade macro-element depends on several factors, mainly: the length and number of corner keys, the masonry-wood friction, and the distance between openings and wall-corner.



**Figure 5.1.7** – Deep vertical cracks in the main façade (Surtierra, 2011).

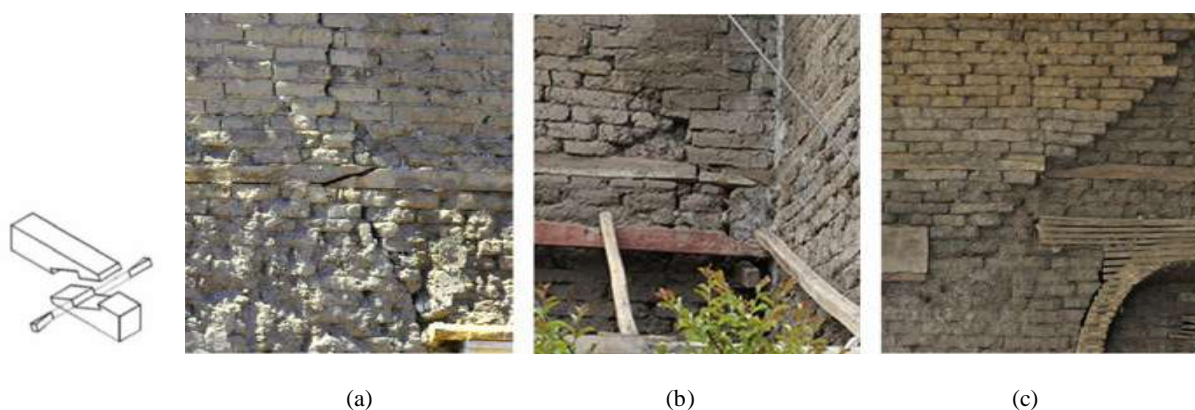
Significant vertical cracks are also visible in the upper part of longitudinal side walls of the nave, mainly near the openings of windows and doors. This crack pattern, observable in the internal (Fig. 5.1.8a) and external (Fig. 5.1.8b) elevations of side walls, suggests the activation of out-of-plane failure mechanisms, triggered by horizontal flexure of the wall, and involving the upper part of the discretized longitudinal walls between the openings (Fig. 5.1.8). The rotation towards the outside occurs around a horizontal hinge defined by the crack in correspondence of the wooden horizontal reinforcements of the W01, located at 4.6m above ground level.

Diagonal shear cracks caused by the seismic action along the in-plane direction of the wall nave were observed near the openings, in correspondence with the spandrels.



**Figure 5.1.8** – Deep vertical cracks observable in the (a) internal and (b) external elevations of side walls (Surtierra, 2011).

The influence of the carpentry links (Fig. 5.1.9) on the global seismic behavior of the structure is often neglected. Nevertheless, as demonstrated by the activation of the local failures in the façade and side walls of the parish, it is essential to analyze these particular behaviors in order to reach an understanding.



**Figure 5.1.9** - Failure modes of hooked scarf joints after 2010 Maule earthquake in the ring-beam.

Concerning the presbytery wall, the level of connections obtained through the corner keys at different heights is sufficient to generate restraint with the longitudinal walls. Nevertheless,

localized vertical crushing in the corner occurs due to the absence of masonry bonds (Fig.5.1.3). The fracture lines are in correspondence of longitudinal wall planes.

With respect to the chapel, several local collapses involving the external leaf of the two-leaf adobe masonry (W03) were observed. Two double-leaf-wall overturning mechanisms were triggered, determining the collapse of the external leaf, with trapezoidal shape in the upper part of the wall. The low quality of W03 masonry, the absence of good bond, and the presence of big openings close to the wall corner affected failure shape. Furthermore, the collapse of the corner of sacristy was observed (Fig.5.1.10).



**Figure 5.1.10** - Local collapses of Sacristy (Surtierra, 2011).

The timber consolidation interventions of bell-tower cell and façade gable avoided local collapses and significant damage, guaranteeing ductility and allowing oscillation without loss of equilibrium. These traditional strengthening techniques showed high efficacy in avoiding complete loss and collapses after the several earthquakes that have hit the church.

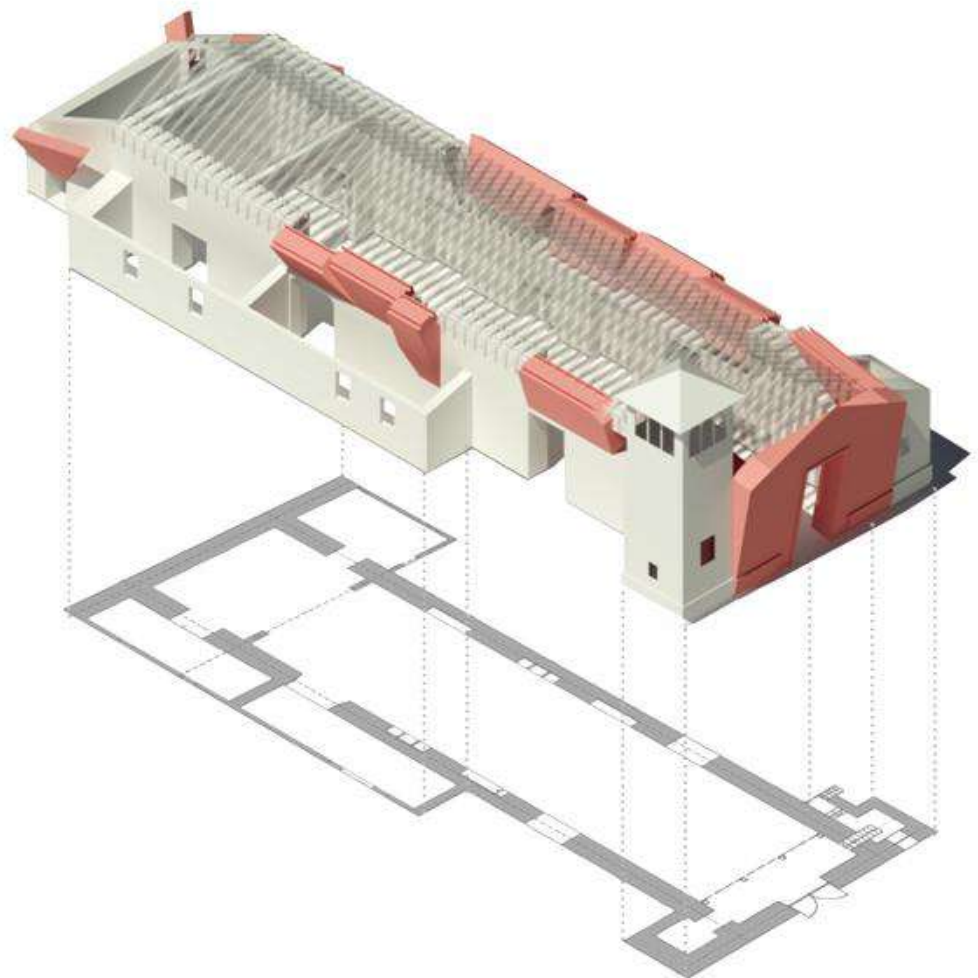
#### 5.1.4 Structural analysis

As introduced in the Chapter 3.3.2 the seismic Chilean Code, NCh433 (INN 1996), does not provide requirements for the assessment of the seismic behavior of URM structures. Furthermore, the Standard for the Structural Intervention of Earthen Historical Buildings, NCh3332 (INN 2013), provides generic criteria for the consolidation and restoration of the adobe constructions. Thus, in order to determine the structural safety of the Parish, multi-level analyses that embrace local and global behavior have been employed, and the main collapse modes have been analyzed according to the prevision of the Italian Code NTC2008 (MIT 2008), Circ.617/2009 (MIT 2009) and the Guidelines of Cultural Heritage (G.U. no.55, 7/03/2006), combined with Chilean Codes.

The results described in previous Sections (5.1.1, 5.1.2 and 5.1.3) suggest that the analyses should be focused on the recurring failure modes of the observed macro-elements, which have exhibited significant damage during the past seismic events. With the aim of assessing the vulnerability of identified macro-elements, considering the out-of-plane behavior, linear (LKA) and incremental (IKA) kinematic analyses were conducted. Moreover, a control on the global response of the building has also been carried out to define preferential displacement shapes. The global response of San Tadeo church has been addressed through linear Dynamic Analyses of a 3D FE model with the commercial code STRAUS7.



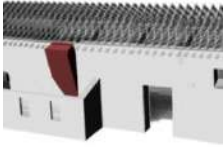
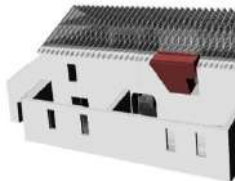
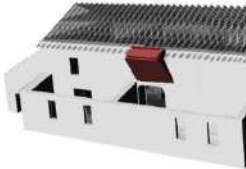

#### **5.1.4.1 Linear and non-linear kinematic analysis**



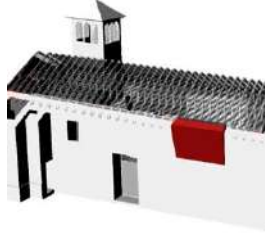
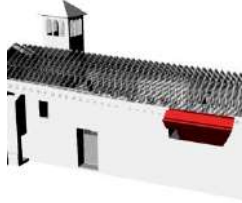
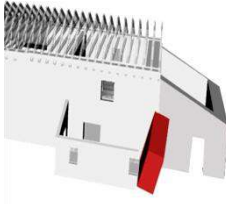

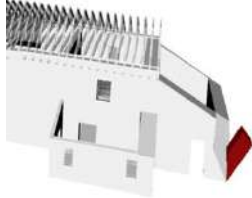
Firstly, the layout of the mechanisms that are most likely to be activated in the Parish has been defined for the current state and the identified mechanisms are shown in (Fig.5.1.11). The results of LKA (Kinematic multiplier  $\alpha_0$ , Participating Mass  $M^*$ , Mechanism Activation Acceleration  $a_0^*$ , the Demand Acceleration at ground and elevated levels) are shown in Table 5.1.5.



*Figure 5.1.11 – Identification of all local mechanisms in Malloa church.*

**Table 5.1.5** - Results of Linear Kinematic Analysis of current state: ID macro-elements; Mechanism types (CM-O, Compound overturning; S-O, simple overturning; DL-O, double leaf overturning; C-O corner overturning); Participating Mass  $M^*$ , Kinematic multiplier of loads  $\alpha_0$  ( $\alpha_\mu$ , load multiplier which takes into account the resistive friction forces activated at the wood-masonry interfaces on orthogonal walls;  $\alpha_{t-\mu}$ , the multiplier which accounting for the dry friction,  $\mu$ , resistive mechanisms provided a good interlocking between orthogonal walls; and  $\alpha_{t-\sigma\tau}$ , the load multiplier assumes the non-zero tensile strength,  $\sigma\tau$ , is to be considered when evaluating the resistive forces opposing to the collapse mechanism); Mechanism Activation Acceleration  $a_0^*$ , equation (5.2) for the Demand Acceleration at ground level  $Dag$ , equation (5.3) for the Demand Acceleration at elevated level,  $Dal$ .

ID	Mech-Type	State Current	$M^*$ [kN]	$\alpha_0$	$a_0^*$ [m/s <sup>2</sup> ]	$Dag$ [m/s <sup>2</sup> ]	$Dal$ [m/s <sup>2</sup> ]
Fa	CM-O		2286	$\alpha_i=0.263$	1.92	5.3	-
				$\alpha_t=0.334$	2.78		
				$\alpha_{t-\mu}=0.71$	5.27		
				$\alpha_{t-\sigma\tau}=1.06$	8.8		
LW1w	S-O		328	$\alpha_i=0.397$	3.46	5.3	4.14
				$\alpha_t=0.687$	5.98		
LW2w	S-O		239	$\alpha_i=0.212$	1.995	5.3	4.39
				$\alpha_t=0.653$	4.87		
LW3w	S-O		201	$\alpha_i=0.362$	3.12	5.3	4.14
				$\alpha_t=0.653$	5.97		
LW4w	S-O		212	$\alpha_i=0.445$	4.25	5.3	4.14
				$\alpha_t=0.693$	6.61		
LW5w	DL-O		134	$\alpha_i=0.183$	1.34	5.3	3.06

<b>LW1e</b>	S-O		235	$\alpha_i = 0.378$ $\alpha_t = 0.663$	3.25 5.7	5.3	4.14
<b>LW2e</b>	S-O		312	$\alpha_i = 0.411$ $\alpha_t = 0.758$	3.7 6.83	5.3	4.14
<b>LW3e</b>	S-O		262	$\alpha_i = 0.384$ $\alpha_t = 0.738$	3.39 6.52	5.3	4.14
<b>LW4e</b>	S-O		268	$\alpha_i = 0.367$ $\alpha_t = 0.599$	4.01 6.56	5.3	4.14
<b>LW5e</b>	S-O		397	$\alpha_i = 0.334$	2.92	5.3	-
<b>LW6e</b>	DL-O		95.6	$\alpha_i = 0.099$	0.722	5.3	3.28
<b>LW7e</b>	C-O		47.4	$\alpha_i = 0.242$	1.756	5.3	-

The parish damage can be interpreted as the activation of the out-of-plane collapse mechanisms that involved: (i) the walls of main building, and (ii) the wall of the sacresty and chapel.

- (i) Concerning the main building, all detected out-of-plane mechanisms are simple overturning of rigid sub-blocks that activated on the west and east lateral walls around a cylinder hinge placed 4.6m off the ground level, LWe1, LWe2, LWe3, LWe4, LWe5, and LWw1, LWw2, LWw3, LWw4, LWw5.

Also a compound mechanism of façade, FA, which involves the triangular portions of side walls, has been detected. The cylinder hinge was placed at the ground level. All mechanisms are shown in Fig.5.1.11.

- (ii) Only in the case of the sacresty walls the triggered mechanisms involved the external leaf of masonry, which collapsed, these mechanisms are labelled LWw5 LWe6 and LWe7. The overturning of the external shell of a masonry is one of the weakest mechanism since the stabilizing action of the weight can be reduced up to 4 times if compared to a monolithic block.

After the identification of the layout of the failure modes and the forces involved in the mechanisms, the kinematic multiplier of the horizontal equivalent forces producing the activation of the mechanisms,  $\alpha_0$ , has been determined. Consequently, the  $\alpha_0$  has been converted into acceleration capacity  $a_0^*$ , according to the codified procedure (MIT, 2009; POLIMI, 2010; Sorrentino et al., 2017) based on the hypotheses of the absence of tensile strength of masonry; the absence of sliding between the interconnected rigid blocks; and the unlimited compressive strength of masonry.

$$\alpha_0 \left( \sum_{i=1}^n P_i \cdot \delta_{xi} \right) = \sum_{i=1}^n P_i \cdot \delta_{yi} \quad a_0^* = \frac{a_0 \sum_{i=1}^{n+m} P_i}{M \cdot FC} \quad M_{eff} = \frac{(\sum_{i=1}^n P_i \cdot \delta_{xi})^2}{g \cdot (\sum_{i=1}^n P_i \cdot \delta_{xi}^2)} \quad (5.1)$$

where:  $\alpha_0$  is the kinematic multiplier;  $P_i$  is the  $i$ -th load;  $\delta_{xi}$  is the virtual horizontal displacement of the gravity center of the  $i$ -th load  $P_i$ ;  $\delta_{yi}$  is the virtual vertical displacement of the gravity centers of the  $i$ -th load  $P_i$ ;  $M_{eff}$  is the participating mass;  $a_0^*$  is the acceleration capacity; and  $FC=1.35$  is a confidence factor-related to the knowledge level of the building.

For a more realistic simulation, the limited state due to masonry crushing for compressive stress ( $f_m=1.2\text{MPa}$ ) has been considered assuming the slippage of the cylinder hinge,  $t = 0.05 \sum_{i=1}^n W_i (f_d l)^{-1}$ , which depends on  $i$ -th self-weight,  $W_i$ , the width of the wall,  $l$ , and the design compressive strength,  $f_d = f_m (FC \gamma_M)^{-1}$ .

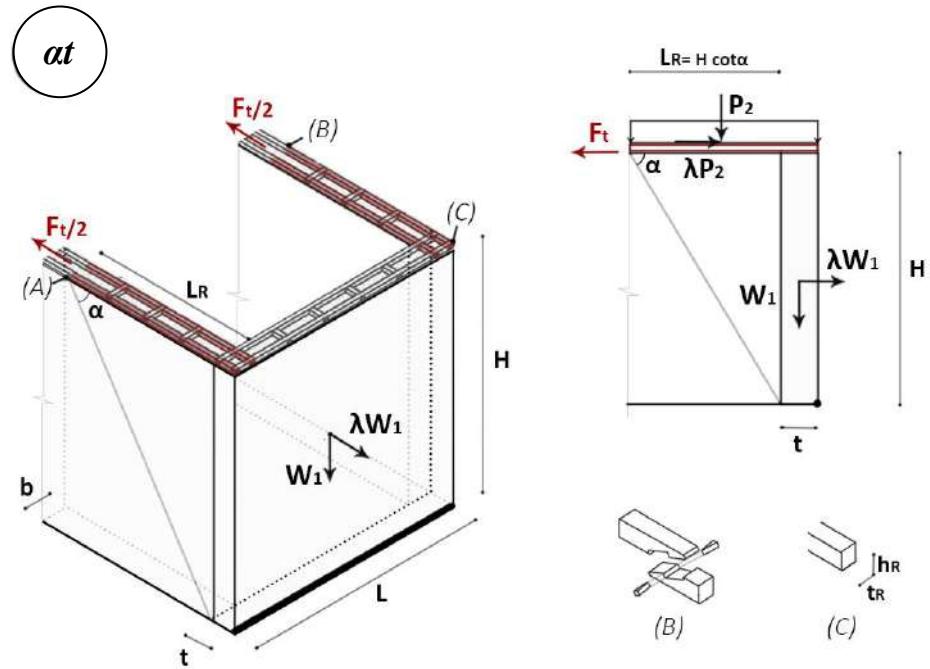
The safety conditions require that the structural capacity ( $\alpha_0^*$ ) must be equal or greater than the seismic demand  $Dag[\text{m/s}^2]$ , calculated according to the NCh433 Chilean Code (for soil type E, as shown in Chapter 3.3). When the masonry macro-element is placed at the ground level it imposes  $a_0^* \geq a_g(P_{VR}) S q^{-1} = 5.3 \text{ ms}^{-2}$  (equation 5.2). Thus,  $Dag$  depends on  $a_g(P_{VR})$ , the peak ground acceleration with an exceeding probability of 10% in 50 years;  $S$ , the sub-soil factor (here assumed equal to 1); and  $q$ , the behavior factor to account for energy dissipation capacity of the unreinforced masonry structure, equal to 1.5 according to (Eurocode8, 2004). In the case

of the macro-elements placed higher than ground level, a further check must impose  $\alpha_0^* \geq S_e(T_1)\Psi(Z)\gamma$  (equation 5.3), due to the input demand amplified by the effect of height  $Dal[m/s^2]$ . It is in dependence on the design spectrum acceleration,  $S_e(T_1)$ , with respect to the first vibration period of the macro-block  $T_1$ , being  $T_1 = 0.09 H^{3/4}$  (characterizing the adobe buildings, Tarque, 2008). Finally  $\psi(z)=Z/H$  is a function depending on the height from the foundation of the centroid of the weight forces applied on the rigid bodies,  $Z$ , on the total height of the building from the foundation,  $H$ , and on  $\gamma=3N/(2N+1)$ , which corresponds to a modal participation coefficient, depending on  $N$  number of floors.

According to (Misseri, Palazzi, & Rovero, 2019), when the anchoring system of the corner keys of the ring beam is not present or ineffective, and a good interlocking at orthogonal walls cannot be ensured, then, overturning of the façade can occur if the resistive friction forces activated at the wood-masonry interfaces on orthogonal walls, here labeled  $F_t$ , are exceeded. The restraining forces at timber masonry interface depend on the dimensions of the restraining device equal to  $F_t = 4 \mu p t_R l_R$ , where  $\mu$  is the friction coefficient, and  $t_R$  and  $l_R$  are respectively the length and the thickness of the restraining element, as represented in (Fig.5.1.12). Then, if the slab rests on longitudinal walls, the multiplier of loads can be expressed through the following Equation:

$$\alpha_t = \frac{2 P_2 \frac{l_R+t}{2} + W_1 \frac{t}{2} + F_t H}{2 P_2 H + W_1 \frac{H}{2}} \quad (5.4)$$

where  $P_2$  is the weight of the slab,  $W_1$  is the weight of façade macro-element,  $t$  and  $H$  are the thickness and height of the façade macro-element.

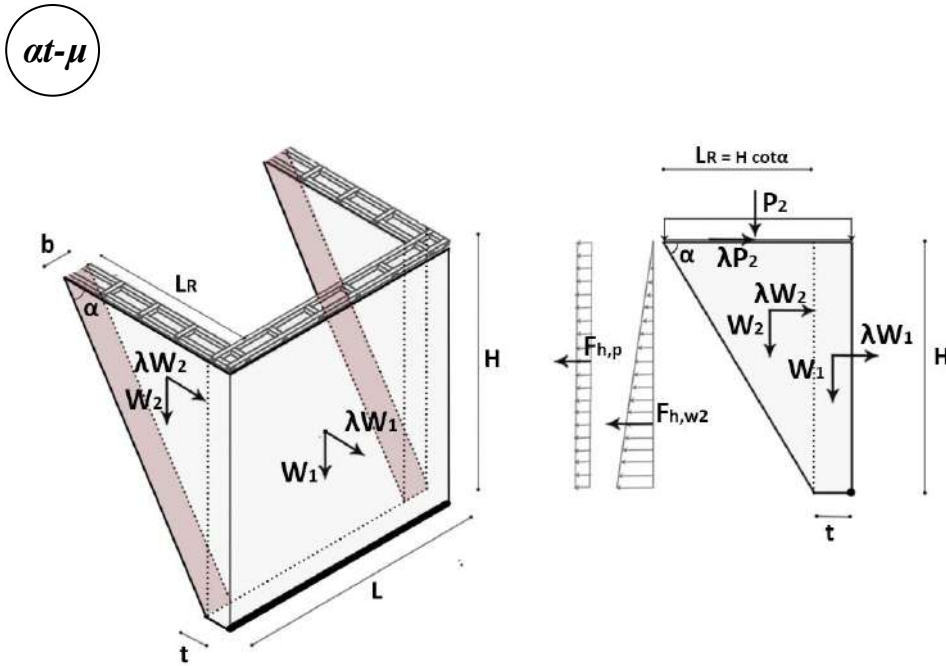


**Figure 5.1.12-**  $\alpha_p$  load multiplier which takes into account the resistive friction forces activated at the wood-masonry interfaces on orthogonal walls (Misseri, Palazzi, & Rovero, 2019).

On the contrary, if the anchoring system of the ring beam or corner key is effective, an OOP mechanism is activated for the façade and portions of transverse walls overturn together with it (Fig.5.1.13, Misseri, Palazzi, & Rovero, 2019). For the case at hand, the slope of the fracture will depend on the length of the timber element,  $l_R$ . Accounting for the dry friction resistive mechanisms, provided a good interlocking between orthogonal walls, the multiplier is:

$$\alpha_{t-\mu} = \frac{2 P_2 \frac{l_R+t}{2} + W_1 \frac{t}{2} + W_2 \left( \frac{H \cot \alpha}{3} + t \right) + F_{h,w} \frac{H}{2} + F_{h,p} \frac{H}{2}}{2 P_2 H + W_1 \frac{H}{2} + W_2 \frac{H}{2}} \quad (5.5)$$

where  $\alpha$  is the angle between the diagonal crack of lateral walls,  $L_R$  is the length of the timber element,  $F_{h,w2}$  is the horizontal force offered by dry friction and due to self-weight depends on the compression found at each block interface equal to  $F_{h,w2} = \frac{H(H \tan \theta + t)}{2} \gamma b \mu$ , and  $F_{h,p}$  is the contribution offered by dry friction due to overburden loads equal to  $F_{h,p} = p H \tan \theta b \mu$ .



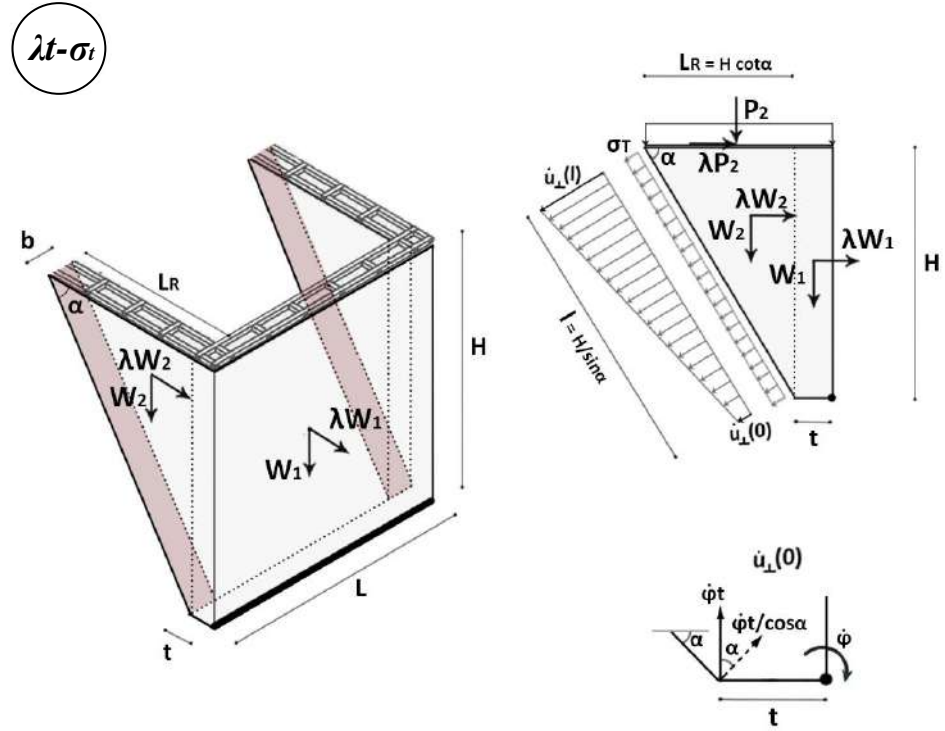
**Figure 5.1.13** -  $\alpha_{t-\mu}$ , the multiplier which accounting for the dry friction,  $\mu$ , resistive mechanisms provided a good interlocking between orthogonal walls (Misseri, Palazzi, & Rovero, 2019).

Finally, if the non-zero tensile strength is considered (Fig.5.1.14, Misseri, Palazzi, & Rovero, 2019) when evaluating the resistive forces opposing to the collapse mechanism, the load multiplier assumes the following form:

$$\alpha_{t-\sigma} = \frac{2 P_2 \frac{l_R+t_T}{2} + W_1 \frac{t_T}{2} + W_2 \left( \frac{H \cot \alpha}{3} + t_T \right) + \frac{D_P}{d\phi}}{2 P_2 H + W_1 \frac{H}{2} + W_2 \frac{H}{2}} \quad (5.6)$$

The rate of the displacement orthogonal to the fracture is  $d\dot{u}_\perp = d\dot{\phi} (x + t \cos \alpha)$

$$D_p = b \int_0^{\frac{H}{\sin \alpha}} \sigma_t \, d\dot{u}_\perp dx = \sigma_t b \, d\phi \left( \frac{H^2}{2 \sin^2 \beta} + H t \cot \alpha \right) \quad (5.7)$$



**Figure 5.1.14-**  $\alpha_{t-\sigma_t}$ , the load multiplier assumes the non-zero tensile strength,  $\sigma_t$ , is to be considered when evaluating the resistive forces opposing to the collapse mechanism (Misseri, Palazzi, & Rovero, 2019).

In order to obtain a more accurate assessment of the expected seismic response in relation to the analyzed local mechanisms, the tests have been also conducted through incremental kinematic analysis, IKA, in terms of pushover curve (Sorrentino et al., 2017). The capacity curve has been obtained assessing the decrease of the minimum kinematic multiplier,  $\alpha_0$ , (between the  $\alpha_p$ ,  $\alpha_{t-\mu}$  and  $\alpha_{t-\sigma_t}$ , load multipliers) estimated applying the Virtual Work Theorem through the Equation (5.8) and the increase of the displacement  $d_k$  of a control point for any varied configurations of the kinematic chain representatives of the mechanism's evolution. From the unchanged initial configuration, a succession of finished displacements has been applied, and the multiplier associated with each varied configuration has been obtained. Then, once transformed the real system into an equivalent SDOF system, the control displacement  $d_k$  is converted in the equivalent spectral displacement  $d_0^*$ :

$$d_0^* = d_{k,0} \frac{\sum_{j=1}^{n+m} P_i \delta_{x,i}^2}{\delta_{x,k} \sum_{j=1}^{n+m} P_i \delta_{x,i}^2} \quad (5.8)$$

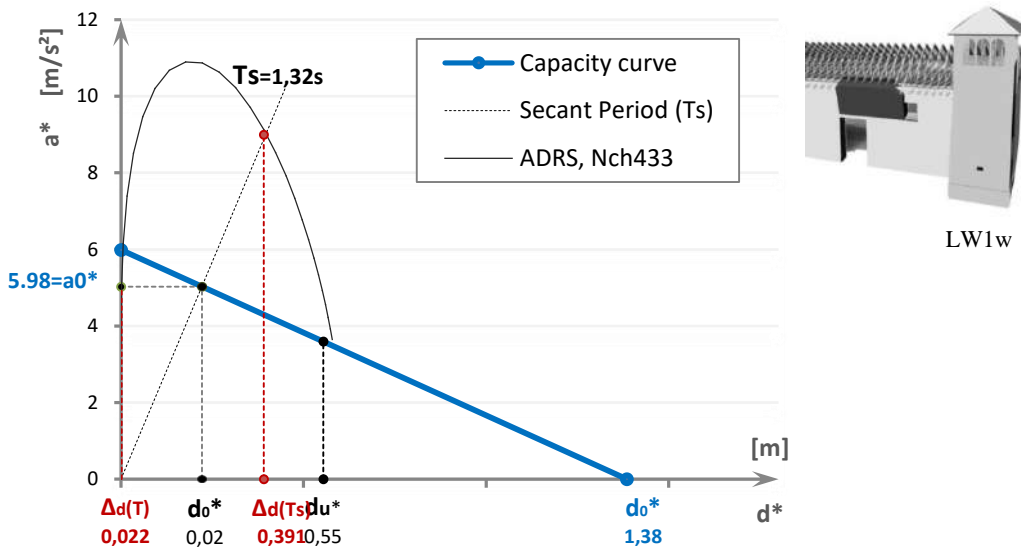
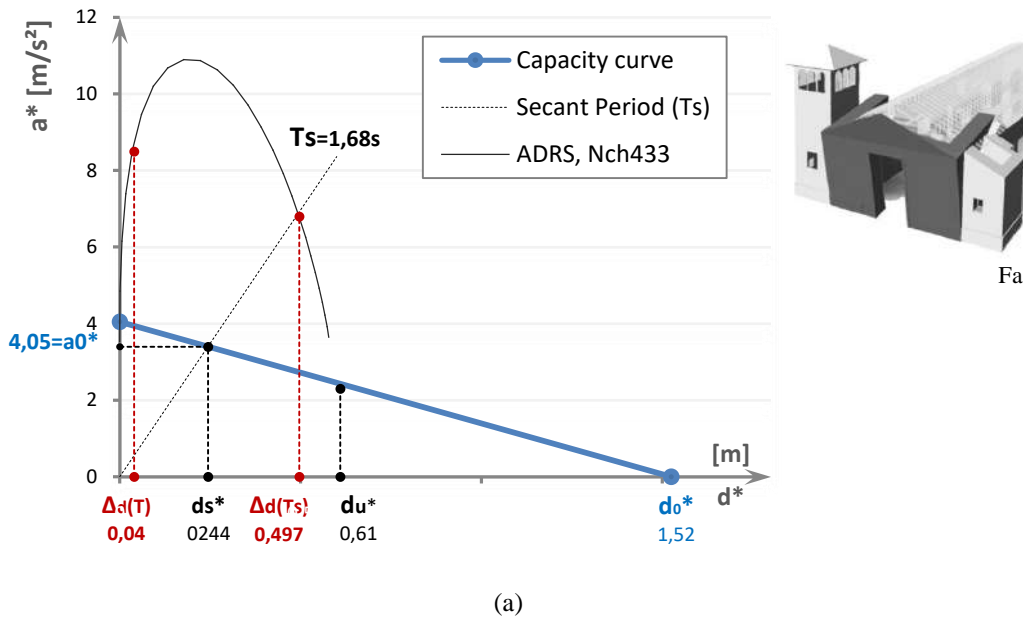
where  $d_{k,0}$  is the horizontal displacement of the control point at collapse which depends on the finite rotation value  $\theta_{k,0}$  that leads a macro-block to collapse and  $d_{k,0} = H_{cp} / \sin(\theta_{k,0})$ ;  $P_i$  is the  $i$ -th weight force,  $\delta_{x,k}$  and  $\delta_{x,i}$  are the horizontal virtual displacement of the control point and the  $i$ -th force respectively. The safety condition is a displacement demand,  $\Delta_d$ , lower than the ultimate displacement capacity,  $d_u^*$ , equal to the minimum between 40% of the mechanism

instability displacement and the displacement corresponding to local instability in the structural elements ( $d_u^* = 0,4 d_0^*$ ). The safety condition involves the following checks:

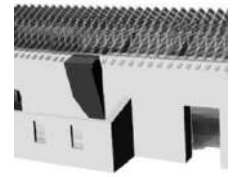
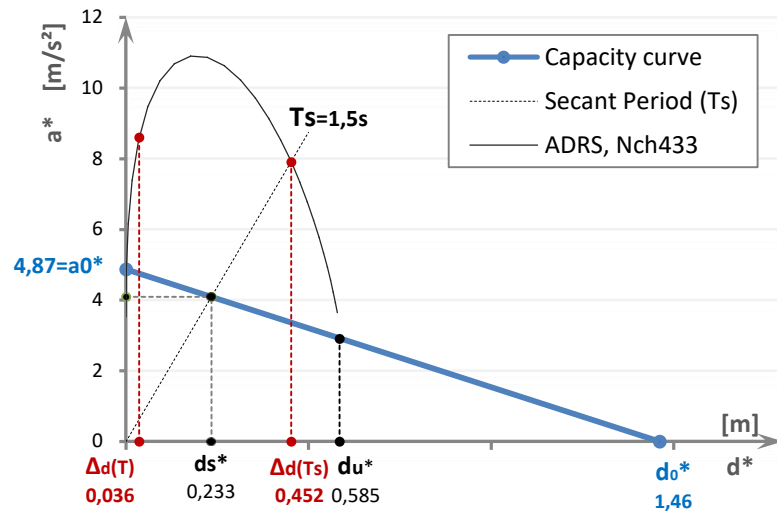
$$d_u^* \geq \max \left\{ S_{De}(T_s); S_{De}(T_s) \psi \gamma \frac{\left(\frac{T_s}{T_1}\right)^2}{\sqrt{\left(1 - \frac{T_s}{T_1}\right)^2 + 0.02 \frac{T_s}{T_1}}} \right\} \quad (5.9)$$

where  $T_s = 2\pi (d_s^*/a_s^*)^{0.5}$ ;  $d_s^* = 0,4 d_u^*$  and  $a_s^* = a_0^* (1 - d_s^*/d_0^*)$

From the comparison between the displacement Capacity and Demand (equation 5.9) of each mechanisms analyzed, the checks are satisfied (Fig.5.1.15). The Capacity Spectrum highlights the great capacity in terms of displacement of the all squat macro-elements, far from collapse. The damage scenario is in concord with the crack pattern annotated during the surveying.

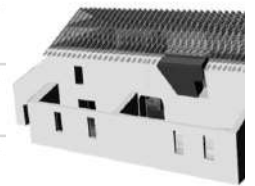
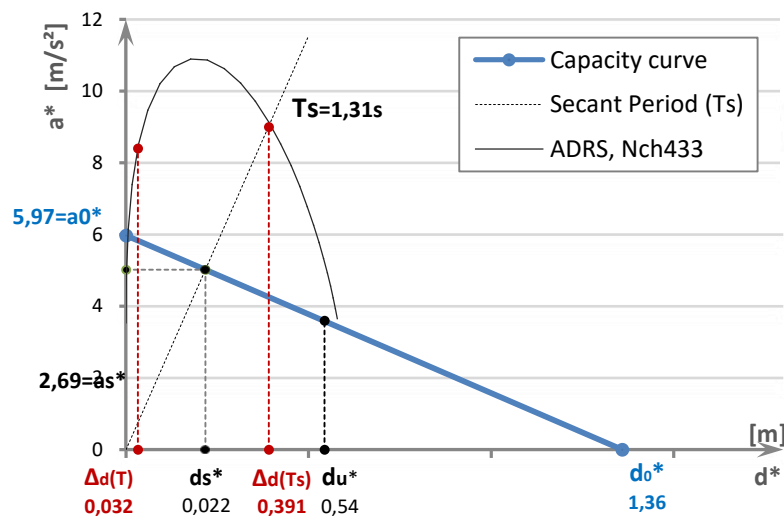


(b)



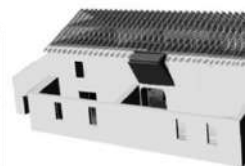
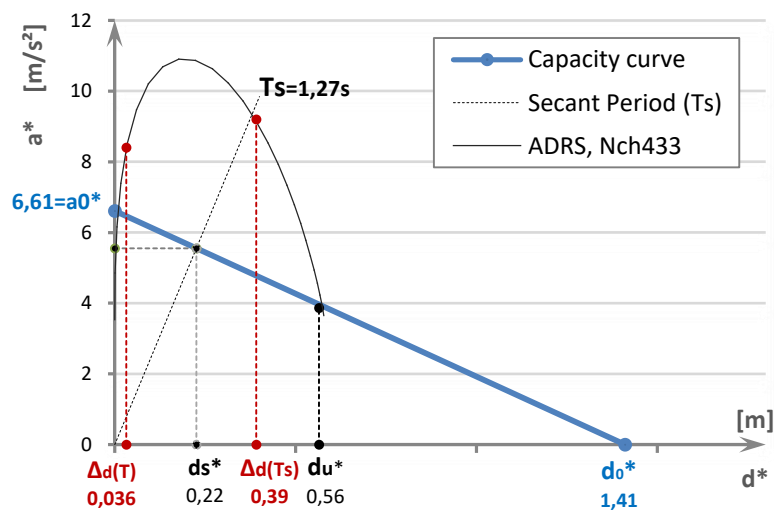
LW2w

(c)



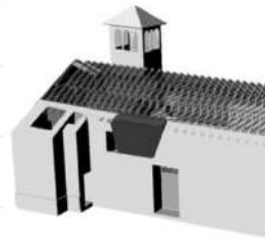
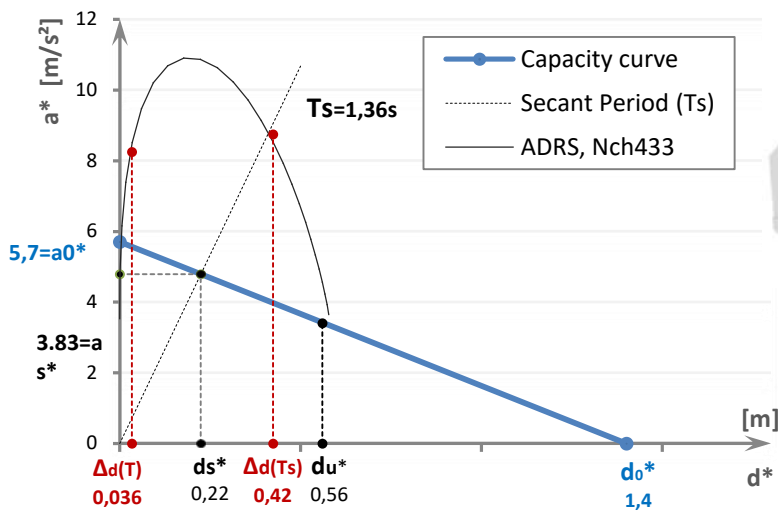
LW3w

(d)



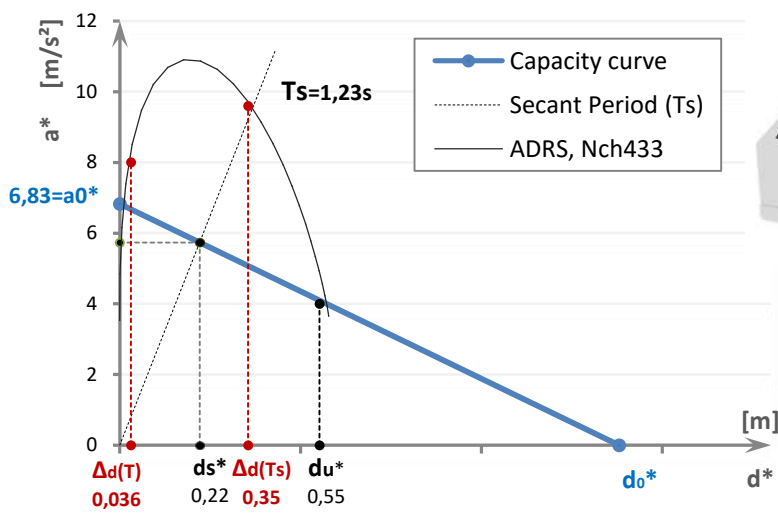
LW4w

(e)



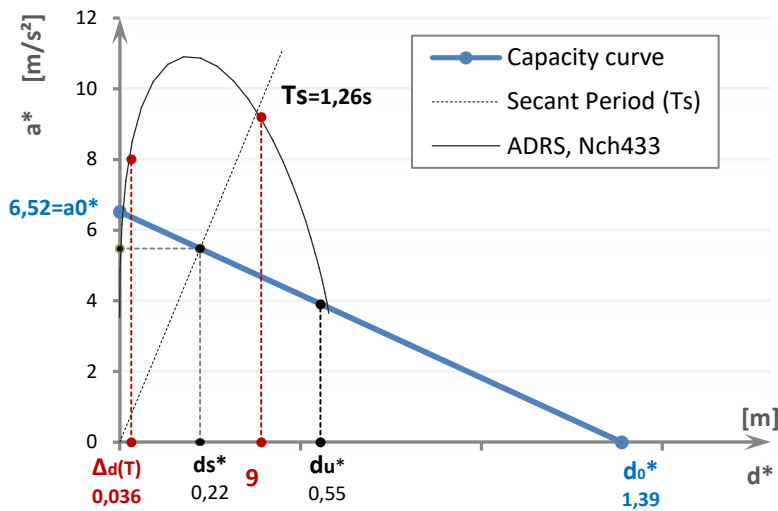
LW1e

(f)



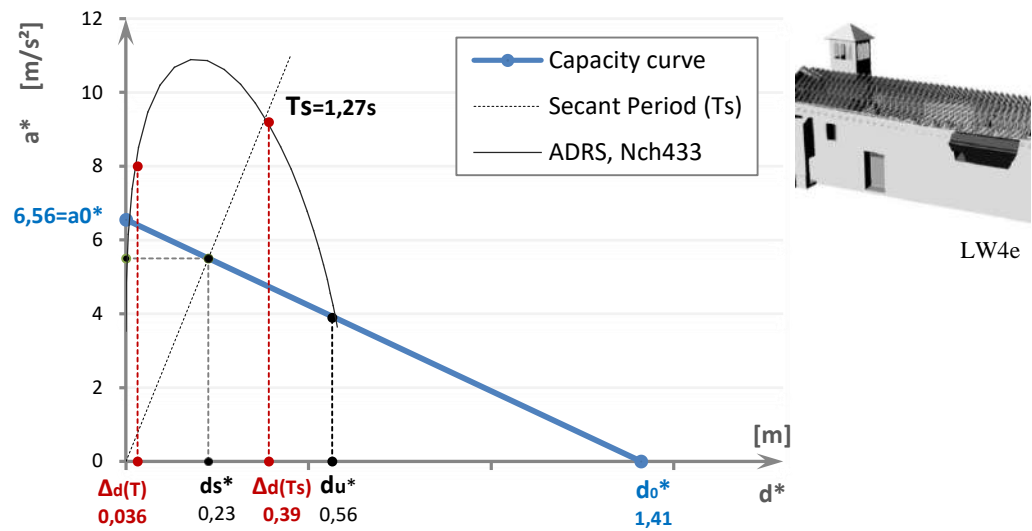
LW2e

(g)

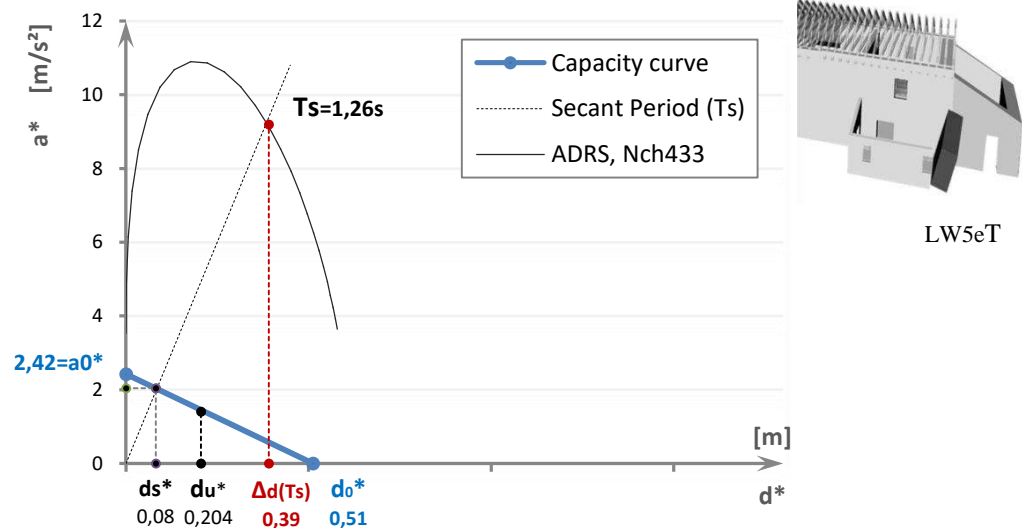


LW3e

(h)



(i)



(l)

**Figure 5.1.15** - Capacity and demand curves of incremental kinematic analysis: (a) main Façade; (b) west lateral wall macro-element1; (c) west lateral wall macro-element2; (d) west lateral wall macro-element3; (e) west lateral wall macro-element4; (f) east lateral wall macro-element1; (g) east lateral wall macro-element2; (h) east lateral wall macro-element3; (i) east lateral wall macro-element4; and (l) east lateral wall macro-element; and Acceleration Displacement Response Spectrum (ADRS) according to Nch433Of.1996

### 5.1.4.2 Global response models

In addition to local analysis, 3D linear dynamic analysis (LDA) has been carried out using the commercial computer software Straus 7 (Strand 2004). An accurate numerical model, consisting of 3,646 brick elements for the masonry walls, 2,358 beams for wooden elements of trusses and masonry reinforces, and 5,962 nodes, was created. According to Section 5.1.3, the

FEM model of the Malloa parish was obtained assuming the mechanical properties indicated in (Table 5.1.6).

**Table 5.1.6 - Mechanical proprieties of materials**

Element	Young modulus [MPa]	Poisson modulus [-]	Specific weight [kN/m <sup>3</sup> ]
Adobe bricks	166	0.25	16
Wooden beams	14,400	0.12	62

Modal dynamic analysis was carried out using the elastic spectrum suggested by the NCh433.Of1996 (INN, 1996), and the design inelastic spectrum is plotted considering a reduction factor  $R=1.5$ , with takes into account the dissipative capacity of the structure, as indicated in Chapter3.3.

In order to identify the modal shapes of main vibration modes, and to calculate the effective participating Mass ( $M_{eff}$ ) and the corresponding periods ( $T$ ), an Eigen frequency analysis was carried out. In Fig.5.1.16 modal participating mass, in the longitudinal and transverse directions, of the first 150 modes are plotted as a function of the vibration period. The results of Eigen frequency analysis are compared with the pseudo-acceleration response spectra for the main shock of February 27<sup>th</sup> 2010 Maule earthquake elaborated by (Liberatore, Sorrentino & Liberatore, 2012), and Chilean code values. The Malloa parish is located between the two considered stations, CCSP and MELP. NS direction corresponds to the longitudinal direction of church, and EW to the transversal direction.

Considering the NS pseudo-acceleration response spectra, all modes with participating mass larger than 5% have a period within 0.145-0.377s, except the first mode with a period equal to 0,703. Both period intervals correspond to a relevant spectral demand ( $S_a$ ), Fig. 5.1.17.

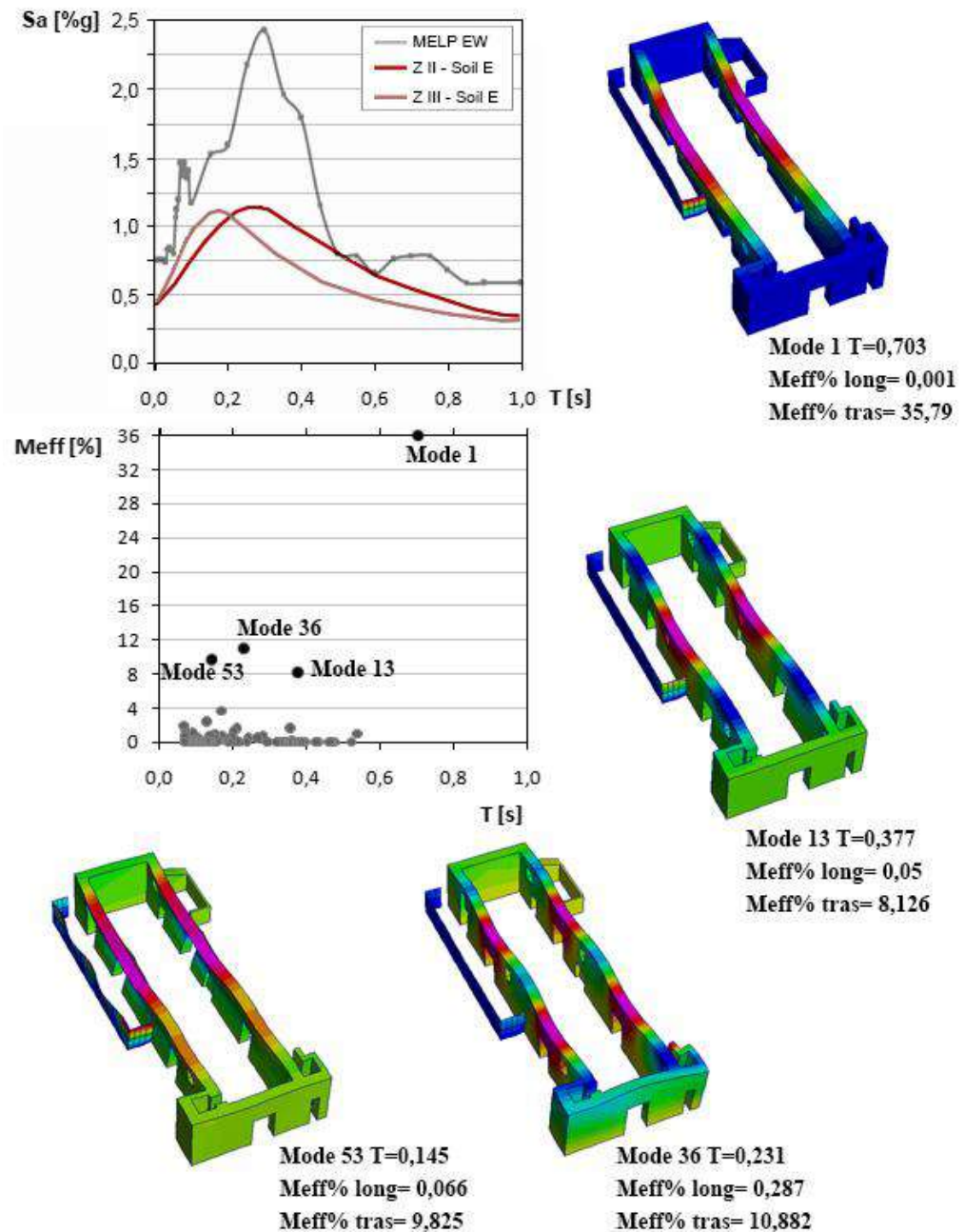
The first mode ( $T=0,703s$ ) involves the lateral walls of nave in the trasversal direction with an participating mass in the longitudinal direction ( $M_{eff}\%long$ ) equals to 35.79%. Also the deformed shapes of the other considered modes (13, 36 and 53) involve the lateral walls and in the case of the 36<sup>th</sup> mode farther adjacent walls of the bell tower base.

Considering the EW pseudo-acceleration response spectra, all modes with participating mass larger than 5% have a period within 0.155-0.24s, where the spectral demand ( $S_a$ ) is relevant. The 34<sup>th</sup> mode involves the main façade and rear façade in the longitudinal direction with an  $M_{eff}\%long$  equals to 32.78%. Also the other modes 37, 38 and 50 involve the same macro-elements and the bell tower base.

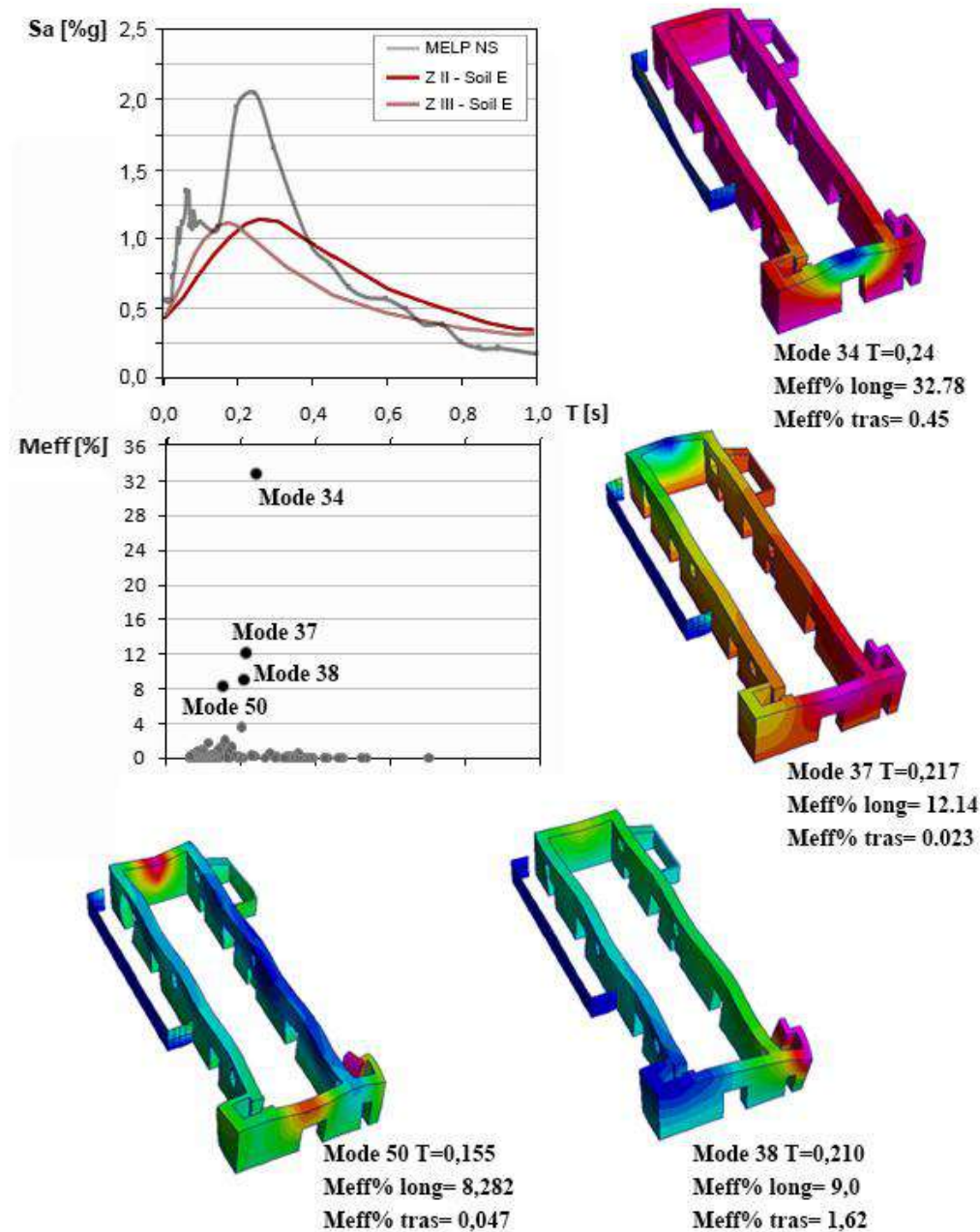
As observed by (Formisano et al., 2018), despite the obvious limitation of assuming that masonry behaves as an elastic material, the linear dynamic analysis (LDA) is able to suggest

the critical macroelements. In this case the results of LDA suggest the activation of out-of-plane mechanisms of the upper part of lateral walls and the main façade.

It is important to point out that out-of-plane behaviors of FA, LWw, LWe were observed following the 2010 Maule earthquake, and the crack pattern (analyzed in the Section 5.1.3) is coherent with the LDA results.



**Figure 5.1.16**—EW Pseudo-acceleration response spectra for the February 27th 2010 Maule earthquake for MELP station; elastic spectrum suggested by the NCh433.Of1996 for seismic zone II and III, soil type E; deformed shapes of the main modes with corresponding periods and participating mass ratios in the transversal direction.



**Figure 5.1.17** – NS Pseudo-acceleration response spectra for the February 27th 2010 Maule earthquake for MELP station; elastic spectrum suggested by the NCh433.Of1996 for seismic zone II and III, soil type E; deformed shapes of the main modes with corresponding periods and participating mass ratios in the longitudinal direction.

### 5.1.5 Summary

In this Chapter the seismic performance of a timber-reinforced CL church that survived strong earthquakes, the Malloa parish, has been assessed. Different structural analyses (LKA, IKA, LDA, and EFA) have been used to provide a more reliable seismic behavior of this parish. Through LKA and IKA analyses, the OOP overturning detected mechanisms are investigated

considering the contribution offered by frictional and tensile restrain forces. In general, results highlighted a good seismic response of this adobe parish under high PGAs, although the damages related to OOP capacity of the side wall upper parts, due to the absence of timber reinforcement at lintel level, were surveyed.

Local-level analysis have provided a reliable assessment of the OOP mechanisms of main façade, lateral walls and chapels. Results suggest that vulnerability could have been successfully reduced through punctual interventions that make use of traditional retrofitting technologies based on the use of wood, as presented in Chapter 6, instead of extensive and invasive solutions somehow partially incompatible.

Results of LKA for OOP failure of compound façade offered an unsatisfactory safety assessment (considering the lowest multiplier  $\alpha_t$ , the load multiplier which takes into account the resistive friction forces activated at the wood-masonry interfaces on orthogonal walls), safety index  $Is_{IKA}=0.555$ . While, IKA analysis provides a satisfactory safety index equal to  $Is_{LKA}=1.2$ .

Regarding the OOP simple overturning of west and east lateral walls the results of LKA analysis are unsatisfactory with a safety index between  $0.66 \leq Is_{IKA} \leq 0.93$ . For the same macroelements, IKA analysis offered a satisfactory safety assessment with  $Is_{LKA}$  comprises between  $1.22 \leq Is_{IKA} \leq 1.57$ .

In other words, the OOP mechanisms are activated but the macro-elements still have capacity in terms of displacement before collapsing, as confirmed by the crack pattern.

The findings of IKA, LKA, DLA, and EFA show the fundamental role of timber elements for a good seismic performance of this earthen church during earthquake. Indeed, the load coefficient of OOP overturning wall increases very rapidly when the timber reinforcement is considered. Moreover, shear failure of timber-to-timber joints, surveyed in the field, is crucial because it determines the segmentation of the ring beam, and consequently the loss of a box-like behaviour. In addition, shear failure of wood-to-wood joints transform the ring beam into a sort of corner key, thus, reducing its resistive capacity, which is based on the longitudinal length.

Lastly, global-level assessments confirmed somewhat *box-like* behavior due to ring-beam and corner-key timber elements. Indeed, the results of modal analysis showed the concentration of participating mass in a few vibration modes (reaching about  $M_{eff}=65\%$  in 4-5 modes), unlike what happens in buildings with preferential local behaviors. Thus, the structure not exhibit a preferential global behavior, despite the activation of some local mechanisms, which enforce and suggest simple and straightforward intervention strategies.



NC&amp;VStyle

## 5.2 Case study 2: San Francisco church

The San Francisco Church, with its three aisle basilica plan, is the oldest building in Santiago. It is the last surviving example of original sixteenth century architecture in Chile and has an adjoining adobe building housing a convent (Benavides, 1988). Having incurred local damages from an estimated 15 seismic events with intensities ranging from 7.1 to 9.5 (Chilean National Seismological Centro <http://sismologia.cl/> [accessed 10 October 2015]; Astroza et al. 2010), evidence of repairs and differentiation in building materials can be observed in the structure. While many of these earthquakes originated from distant epicentres, they were felt with strong to severe intensities in Santiago causing damages, although information about them remains incomplete. Pena(1969) provides a thorough but incomplete assessment of San Francisco's structural history with additional information about construction phases provided in Pereira Salas, 1965; Benavides, 1988; Villalobos et al., 1990; De Ramón, 2000; Rovegno, 2009; Sahady, 2015; and Gross, 2015. The combination of typological elements from indigenous Andean building culture and 17<sup>th</sup> century colonial architecture make the San Francisco Church a transition building that is wholly unique in Chile giving its study relevance. A full investigation, which considers the major seismic hazard in Chile and construction techniques employed, of the technological features enforcing the resilience of the structure has not been carried out yet. As a result, a comprehensive analysis, using already proposed and validated structural analysis methodologies for heritage buildings (Fratini et al. 2011; Gamrani et al. 2012; Rovero and Fratini 2013; Rovero and Tonietti 2012, 2014; Sani et al. 2012) was performed. A multi-level analysis incorporating local and global structural analysis, physical and mechanical characterization of materials, crack pattern analysis, in situ surveys, and historical research was utilized.

### 5.2.1 San Francisco church

The Basilica plan of the church is 30.3m in width and 64.6m in length with five transverse arcade walls subdividing lateral walls (Fig.5.2.1). The roof ranges from 9 to 18 m in height while the bell tower reaches 46.4 m at its top making it a feature of the city's skyline. Spanning centuries, many alterations have been performed resulting in several observable construction systems and materials.

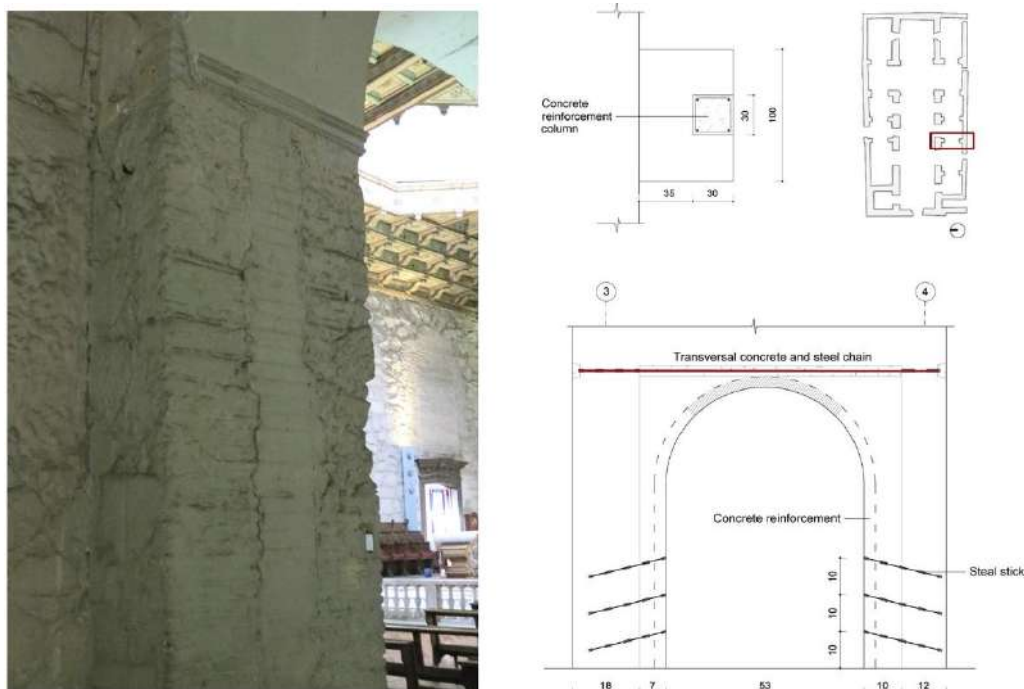


**Figure 5.2.1** - View of the façade, current plan, façade and section of the San Francisco church.

Rubble stone masonry makes up the original portions of the 1.65m thick longitudinal central nave walls. When the roof structure was unified some courses of adobe masonry were added to heighten the walls. One meter thick brickwork makes up the lateral nave walls around the North and South Perimeter. The original, 1.85 meter thick, stone masonry makes up the lower part of the façade while the top portion was rebuilt with bricks and adobe following earthquake damages. Similarly, the 1.7 m thick stone masonry wall behind the altar was rebuilt with brick and adobe courses and a wooden frame demonstrates the legacy of earthquake damage and repair.

Two arcades support the spatial connection between the central and lateral aisles along the latitudinal walls. The transept and the arches adjacent to it are made up of original stone masonry as well as the access arch to the lower tower. The arches near of the façade were built

of brick in addition to the lateral aisles. The five arcades partitioning the lateral aisles brick masonries reinforce by and RC frame cast within intrados and an RC tie-rod at the top (Fig.5.2.2).



**Figure 5.2.2** - Concrete reinforcements of arcs (Jorquera et al., 2016).

From base to top, the tower is composed of three sections, each with different materials: the base is original and is built of rubble stone masonry; the middle part above the base is built of bricks; and the third part is Olivillo (*Aextoxicon punctatum*) and Oak (*Nothofagus sp.*) wood frame assembly. The second and third parts are a 30 m high independent volume. No historical information is available to shed light the building's foundation. However, as part of the current research, which is being undertaken in conjunction with a team of archaeologists, a 4 m long excavation was dug near to the transept. This revealed a unique foundation system comprised of round river boulders, between 10 and 30 cm, placed without mortar and contained laterally by large hewn stones with dimensions of 60x60x60cm and a larger corner stone of 90x60x60 cm. During an earthquake the stones but do not scatter laterally due to the axis which partially isolates the building from seismic action. The church has had a strong horizontal "diaphragm" on the central nave under the roof, since the first build. The system is made of large cypress (*Austrocedrus chilensis*) beams (30x35 cm cross sections) securely fastened to the walls and spaced with 1.2m increasing to 2 m close to the walls providing evidence of reconstruction interventions, (De Ramon, 2000). While partially modified to accommodate the roof lantern which illuminates the altar, the original structure still exists to this day.

The structure of the roof is comprised of wood trusses (spacing 2.4 m) placed separately above each aisle and set on top of the adobe walls. Many diagonals and two horizontal beams make

up the central truss with the lower beam partially traversing the top of the walls. The slenderest lateral oak (*Nothofagus* sp.) trusses (inter-axes about 3 m) are assembled with one horizontal beam, a few diagonals and a vertical chain linking the trusses to the diaphragm. The roof is buttressed by a triangular adobe wall atop the traverse walls which rests on the longitudinal walls and is covered by cane and clay tiles.

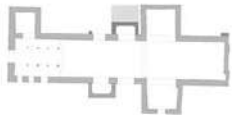
### 5.2.1.1 Seismic history and the main interventions

Atacama CL church



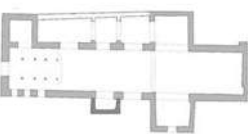
Over the 400 years of its use the church of San Francisco has undergone many changes including: adding adjoining structures to increase its size, stylistic changes and post-earthquake repairs. Having never completely collapsed, it has never needed to be demolished and has been in continuous use since its original construction. Each post-earthquake repair used construction techniques current to their day and transformed the structure. Five main construction phases were able to be recognized in accordance with historical data (Benavides 1988[1941]; De Ramón 2000; Gross 2015; Pena 1969; Pereira Salas 1965; Rovegno 2009; Sahady 2015; Villalobos et al. 1990) and visual inspections of areas that lack structural continuity and homogeneity or materials.

I. 1586-1618



The period between the original construction of the church (1586-1618) and the 1647 earthquake is the first phase. Built with cyclopean rubble stone masonry, the church had a Latin cross plan with two lateral chapels and a tower connected to the main façade (Fig.5.2.3a). The original section of the San Francisco church demonstrates many similarities with the vernacular Andean Churches in northern Argentina and Chile and southern Peru and Bolivia due to its typological and constructive features representative of Andean building culture. Furthermore, the recurring motifs of Andean Building culture include the cyclopean masonry texture with stones and earthen mortar (Fig.5.2.3b), the lateral chapels which function as buttresses for the longitudinal walls, the bell tower on the side of the main façade and the Latin cross plan (Benavides, Marquez de la Plata, and Rodriguez 1977; Montandón 1950; Rodríguez 2012). The evidence of Andean building culture's influence given by the structure itself and reinforced by documented accounts of an indigenous and *mestizo* employed in its construction (Pena 1969).

II. 1647-1698

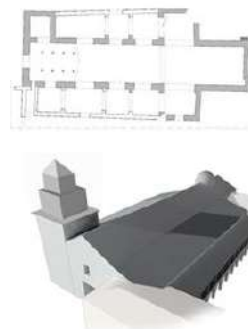


The Magnum earthquake which occurred in 1648 marked the beginning of the second construction phase (1647-1698). The earthquake is estimated to have had a magnitude of 8 and is widely regarded as being the strongest in the colonial period. The church lost its tower and most of its choir in the quake. However, the roof and walls were left structurally intact. Where every other building in Santiago was severely damaged or destroyed, San Francisco church remained as the sole structural survivor. The morphology of the building was changed in 1684 with the addition of the two lateral chapels to the Latin cross plan (Fig. 5.2.3c). The bell tower

was rebuilt in 1698, although no record was made of the building technologies used or architectural features incorporated in the new structure.

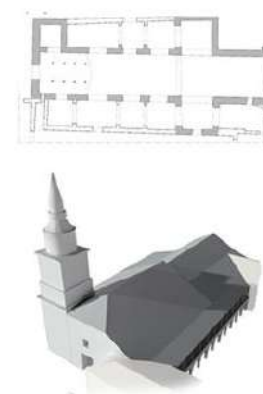
The third phase (1698-1799) was characterized by enlargements and reconstructions (Fig.5.2.3d). San Francisco survived two major earthquakes in this period. This first and second most destructive of the colonial period, in 1730, had an estimated strength of 8.5 to 9 and caused no serious structural damage. The second in 1751 (magnitude 8.5, Lomnitz 2004) damaged the bell tower resulting in the upper portion being demolished in 1754 and rebuilt with eclectically spirited brick masonry combining elements of 3 different styles (Rovegno 2009). New chapels attached to the main nave were built in 1779, resulting in the church having 8 chapels in total. The entryway was moved to the front façade from the north aisle wall, where it is to this day.

### III. 1698-1799



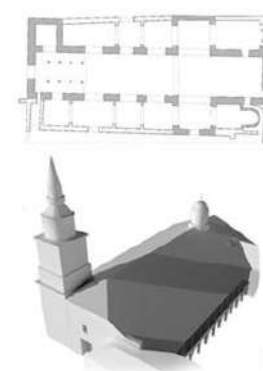
The fourth period of construction, which took place between 1800 and 1875 (Fig.5.2.3e), was marked by the 8.0-8.5 magnitude (Lomnitz 2004) La Ligua (Valparaíso) earthquake that damaged a portion of the roof and two arches of the longitudinal walls (Gazeta Ministerial de Chile 1966). The two arches were rebuilt in brick and repairs were carried out on a section of the presbytery behind the wall and the chapel at the end of the south aisle in 1825 (De Ramón 2000). The top of the tower was again reconstructed in 1857 with the presently existing wooden belfry after damages caused by the 1851 Huasco earthquake (Lomnitz 2004). This reduced inertial load and improved seismic resistance (De Ramón 2000). The renowned Chilean Architect Fermin Vivaceta designed the wooden framework as unifying the chapels in to brickwork lateral aisles. This intervention transformed the church into a basilica plan while the heightened tower (46.4m) became one of Santiago's urban landmarks.

### IV. 1800-1895



The most recent construction phase (1858-present day) saw a new brickwork chapel added to eastern wall behind the altar and the roof structure unified in 1895. The magnitude Mw 8.0 Algarrobo earthquake in 1985, with epicenter offshore and felt at 7.5 MMI in Santiago, caused extensive damage to the traverse arches of the lateral aisles of the church. These were reinforced (intervention designed by the engineer Santiago Arias (CMN 2010)) by inserting an RC frame (30x30 cm) and mixed RC-Steel tie-Rod system above the arches (Fig.5.2.3f). Due to the lack of intervention guidelines for historical masonry buildings, no principles of heritage conservation were followed during this intervention which was a common practice in most structural interventions done on historical monuments after the 1985 earthquake.

### V. 1896-today



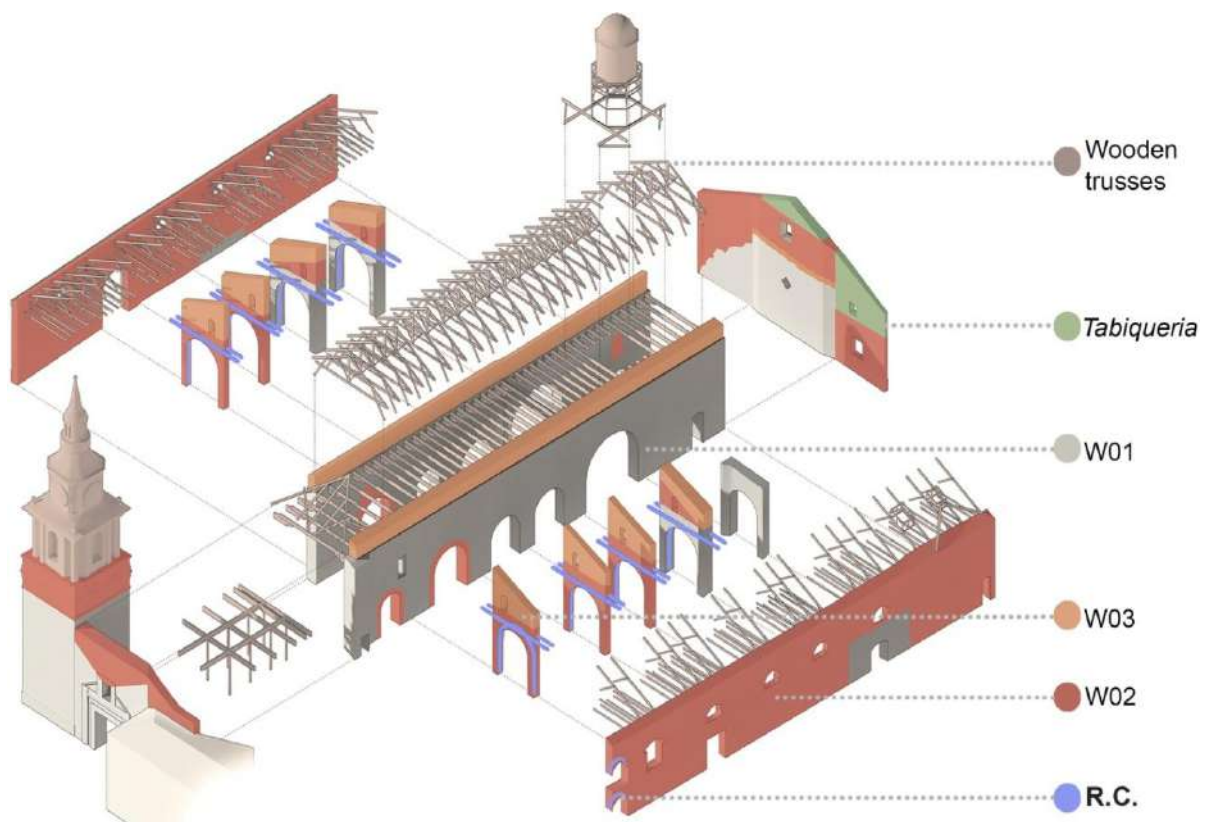
Significant damages were observed after the 2010 Maule earthquake Mw 8.8 (7.0 MMI in Santiago; Atkinson and Wald 2007) which included displacement of the arch intrados, deep cracks in the longitudinal stone walls and wall bulges at the spring level of the transverse arches. These crack patterns can still be observed. No significant deterioration of the 2010

**Figure 5.2.3 – History of San Francisco church**  
(Stefanini, 2016)

damage patterns was observed after the 2015 Illapel earthquake (Mw 8.3 and MMI 5.3–5.6 in Santiago; Atkinson and Wald 2007).

### 5.2.2 Properties of materials


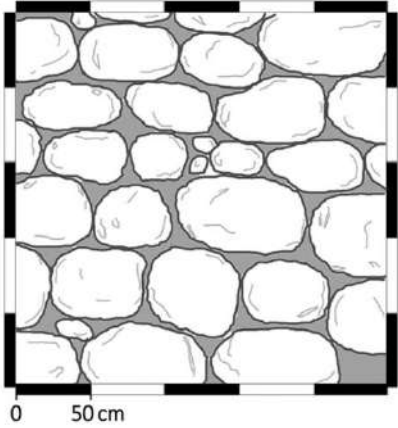
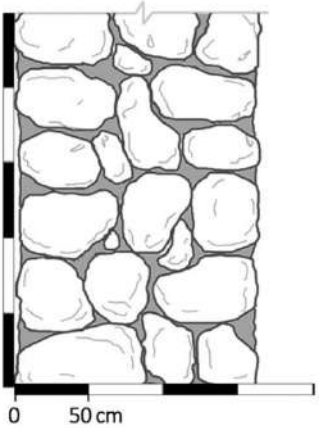




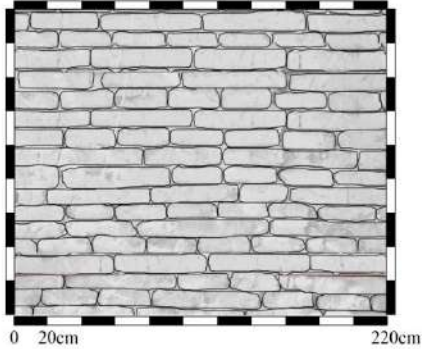
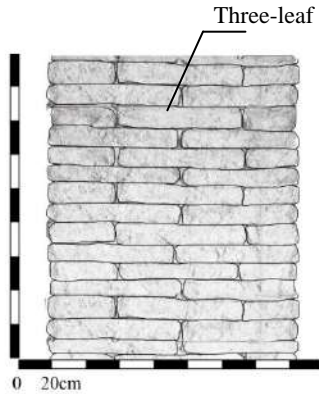
There are three types of masonry present in the church (M01, M02, and M03), reflecting the church's construction history. Redolent of typical Andean masonry, cyclopean rubble stone masonry makes up the Latin cross masonry walls (M01). The lateral aisles perimeter walls and the transverse arched walls are constructed of brick (M02). Adobe was used for the upper portion of the transverse walls and the stone central nave walls (M03) (Fig. 5.2.4).



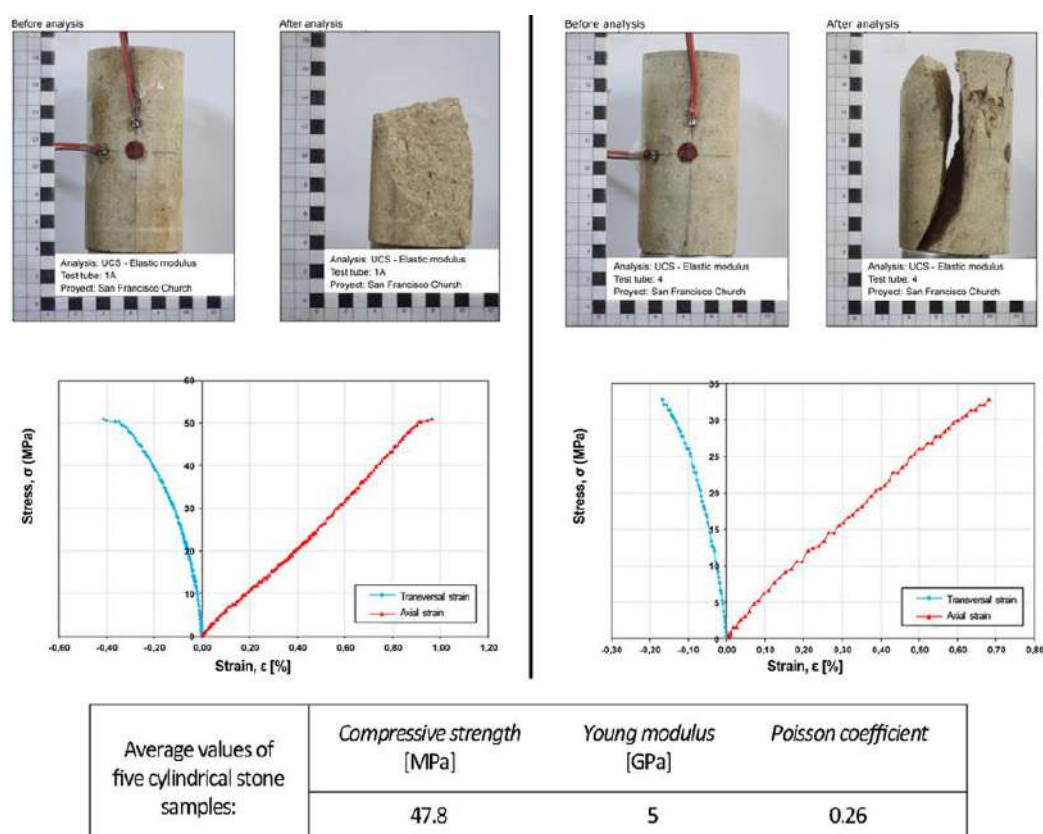
**Figure 5.2.4-** Exploded Axonometric of resistant structure (Stefanini, 2016).

In addition to extensive visual surveys, in situ and laboratory tests were considered in order to qualitatively categorize these 3 masonry types. Specifically, two standard core samples were extracted from the stone masonry walls complemented by a thorough series of rebound tests (Controls 45- D0561 Hammer) on the stone and brick walls. Uniaxial compression tests were performed on five stone samples from the removed cores which included observations of thin cross sections by an optical microscope in transmitted polarized light. In addition, the tests determined the mineralogical and clay mineral composition (through X-ray diffraction), the quantity of calcium carbonate (via the Dietrich Fröling calcimeter) and the grain size distribution through sieve analysis of the mortar and adobe samples.

Table 5.2.1- Masonry types of San Francisco church

<b>[M01]_Cyclopean stone rubble masonry wall</b>		
		
(a) M01 elevation	(b) M01 section	
<b>[M02]_Brick masonry wall of double-leaf</b>		
		
(c) M02 elevation	(d) M02 section	
<b>[M03]_Adobe wall three-leaf masonry</b>		
		
(e) M03 elevation	(f) M03 section	

As shown in Fig. 5.2.5 core samples C1 and C2 were extracted from the central nave and south transept walls penetrating over half of their width. Masonry constituted of large white igneous stones interleaved with smaller black igneous stone elements with a small quantity of mortar. The white stone was determined to be Biotite Andesite with a specific weight of  $23 \text{ KN/m}^3$ , while the black rock Clinopyroxene Basaltic Andesite with a specific weight of  $26 \text{ KN/m}^3$  by the mineralogical and petrographical tests. Both are hypo-crystalline equigranular and isotropic rocks with different alterations.



**Figure 5.2.5** - Laboratory Mechanical tests of stone samples from coring test samples (Jorquera et al., 2016).

Main lithological properties of the stones confirmed that the origin of the rocks used in the San Francisco church is stone quarries on Cerro Blanco. The five cylindrical Biotite Andesite samples extracted from the cores (74.4 mm diameter and 154 mm height) were subjected to uniaxial compression tests with the average values of the mechanical parameters shown in Fig. 5.2.5. A comprehensive experimental analysis using a rebound test was done to assess the compressive strength of a large number of the M01 masonry stone blocks. This determined that the Biotite stones have a compressive strength of 50 MPa. This test, being indirect, is not as reliable as the compression test as it overestimates the outcomes of the compression test by 4.6%. Since the results of rebound test are not dispersed (coefficient of variation 16%), it is possible to assert that the stone of M01 masonry are of the same type.

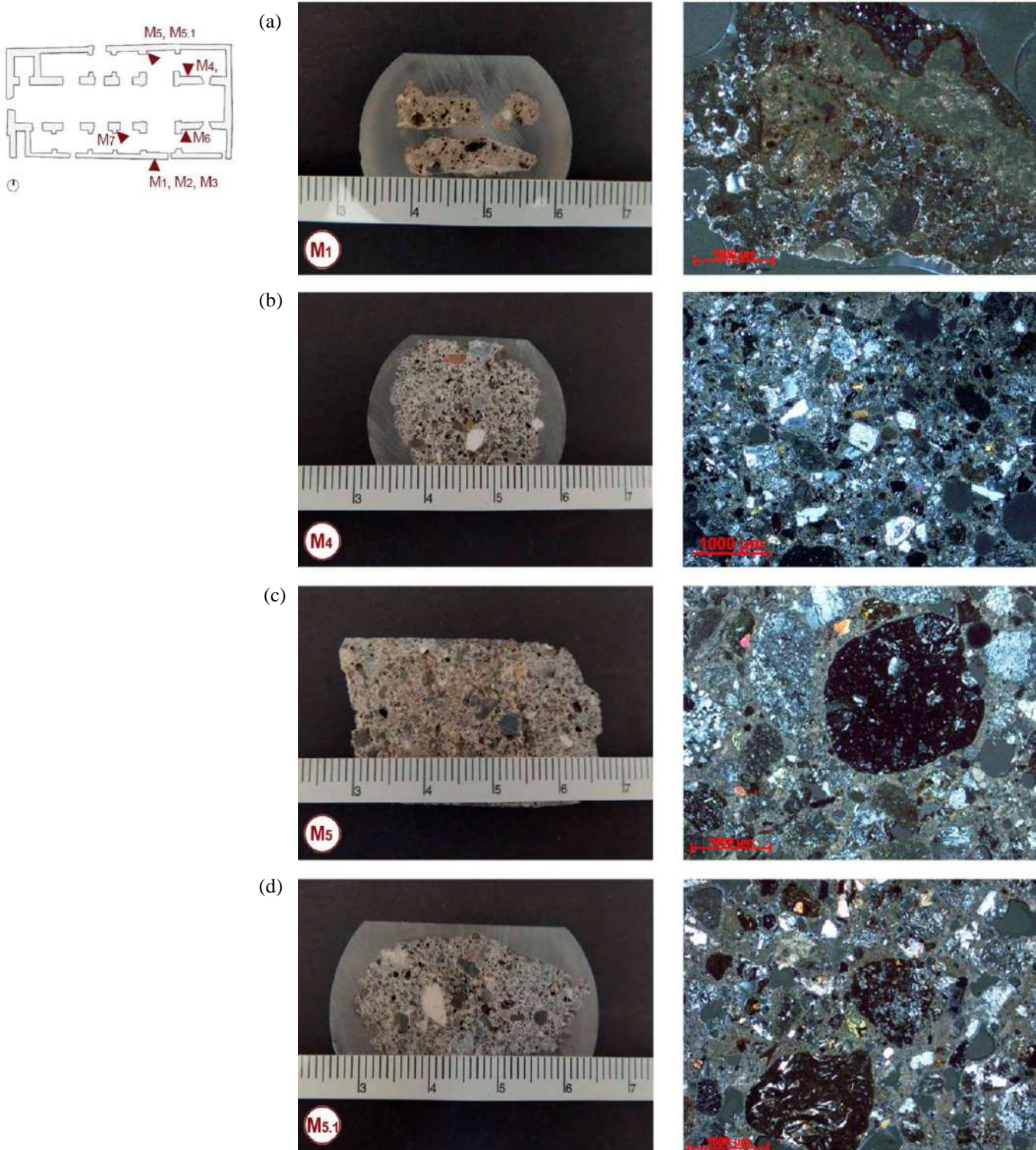
As regards mortar of the M01, three samples of the M01 mortar – M1, M2 and M3 – were extracted from the south transept wall near the wall openings while sample M4 was extracted from the core sample C2. Samples M5 and M5-1 were taken from the north transept wall behind a detached gravestone. Another sample, M8, was taken from the central nave's south wall just under the roof which is likely to have been where a surface improvement intervention took place.

Principle mineral compositions, clay minerals composition of earthen portions, calcimetry and granulometry of mortar samples are summarized in Table. 5.2.2. Thin mortar sample segments and an approximation of sampling positions are shown in Fig. 5.2.6. The M1, M2 and M3 mortar samples appear to have been result of mixing earth and lime (1 part lime/3 parts earth). The often lumpy composition of the mortar indicates that was not well mixed. The mixes are not very lean (the main class is represented by fine sand) in terms of aggregate grain size. High cohesion levels are not assured with this grain size composition so it must be attributed to inclusion of lime. Samples M4, M5 and M5-1 are comparable as they are low in binder (Binder/Aggregate 1/3) and have a bimodal grain size distribution and a binder composed of aerial lime. Regarding the amount (Sample M5-1 is somewhat richer in binder) and type of binder (minimal presence of chert fragments in samples M5 and M5-1) some small differences are evident in the type of binder (Fig. 5.2.6d-e). Made up of aerial lime binder and lacking aggregate the M8 sample is a different case (Fig. 5.2.6f). Two 2.5x25 m sections of the central nave wall were identified by thorough visual in situ surveys as being representative of the texture of M01 masonry type.

A hypothesis for the M01 wall section can be defined based on in situ surveys and results of tests on core samples (Table. 5.2.1) which determined the dimension ranges for the blocks from Cerro Blanco: 45-65 cm long, 45-65 cm high and 45 centimeters thick. The specific weight of this masonry was estimated from the wall section equal to  $22 \text{ KN/m}^3$ , assuming for biotite stone  $23 \text{ KN/m}^3$ , for basalt stone  $26 \text{ KN/m}^3$ , for mortar  $13.9 \text{ KN/m}^3$ , for pebbles  $20.6 \text{ KN/m}^3$  and evaluating a percentage of stone blocks at about 80%. In terms of masonry, the M01 cyclopean stones are typified by: irregular but homogeneous shape; intent of horizontal rows, staggered vertical joints; stone element size congruence; traverse blocks crossing half the wall width, the aforementioned assuring integrity and clamp behavior in the masonry (Table. 5.2.1).

The Masonry Quality Index (M.Q.I) for the rebuilt section of the cross wall was calculated according the method proposed by (Borri et al., 2015) which was applied and validated in (Rovero et al., 2015). When in situ Flat-Jack tests in conjunction with laboratory tests and robust homogenization techniques are impossible to perform or the results are untrustworthy, this method is helpful (Feo et al. 2016). Through the employ of qualitative profiles that can be applied to any type of wall, the M.Q.I. is able to obtain estimates of mechanical parameters (compressive strength, Young modulus, and shear strength) which evaluate the level of concurrence between masonry features and the rule art, or more specifically, the block shape and size, horizontal rows, staggering of vertical joints, traverse block presence (*diatonies*),

quality of mortar and stone durability. For the M01 and M02 stone masonry, Masonry Quality Index results are displayed in Table 5.2.3 accompanied by the M03 adobe masonry data which is assumed to be concurrent with Chilean Standard (INN, 2013).



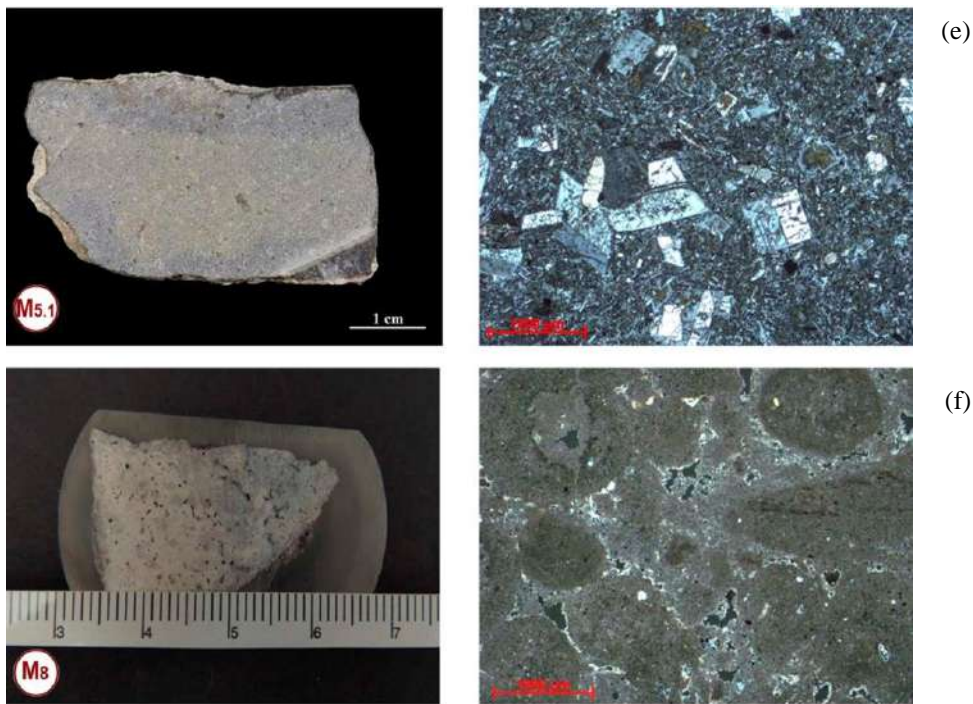


Figure 5.2.6 - Thin section of joint mortar samples (Jorquera et al., 2016).

Table 5.2.3 - Principal mineralogical composition, clay minerals composition of the earthen materials, calcimetry and grain sizes, of the mortar samples

Sample	Principal mineralogical composition			Clay minerals composition			Calcimetry	Granulometry		
	Quartz %	Feldspars %	Calcite* %	kaolinite	illite	smectite	CaCO <sub>3</sub>	Sand %	Silt %	Clay %
M 1	8	12	17.5	10	25	65	17.5	85.3	13.3	1.5
M 2	8	11	15.0	15	30	55	15.0	93.1	5.7	1.2
M 3	8	5	13.5	15	25	60	13.5	92.6	5.7	1.7
M 4	8	14	17.0	-	-	-	17.0	-	-	-
M 5	11	10	21.1	-	-	-	21.1	-	-	-
M 5-1	11	11	22.5	-	-	--	22.5	-	-	-
M 6	11	11	-	5	35	60	-	56.0	32.5	8.8
M 7	13	14	-	10	25	65	-	50.4	35.4	14.2
M 8	-	tr	79.4	-	-	-	79.4	-	-	-

In conclusion, the adobe masonry M03 around the triangular part on top of the traverse arcades and longitudinal nave walls is constructed of adobe (30x60x10 cm). Mineralogical analysis was carried out on two adobe samples (M6, M7) of M03 masonry. The results of the grain size analysis found that they were made of lean earth which was richer in silt and clay minerals than the M1, M2 and M3 earth samples. Given the similarity of clay mineral composition of these samples it could be contended that it was the same as in samples M1, M2 and M3 where a difference is found in sieving material to extract the coarser granules.

**Table 5.2.2** - Young module ( $E$ ) compressive strength ( $f'_m$ ), and shear strength ( $\tau_0$ ) of M01, M02 and M03

ID	Type of masonry	$\gamma$ [N/m <sup>3</sup> ]	$f'_m$ [MPa]	$E$ [GPa]	$\tau_0$ [MPa]
M01	Rubble stone masonry	22050	3.7	1.6	0.06
M02	Fire-brick masonry 40x22x7cm	17652	3.1	1.38	0.05
M03	Adobe masonry 30x60x10 cm	16671	1.2	-	0.025

### 5.2.3 Assessment of crack patterns

As a result of the dual factors of inherent structural defects and regular severe earthquake shaking, the San Francisco church has incurred several damages since its original construction. The previously mentioned interventions and additions are responsible for some of the structural frailties while others, such as in plane capacity of the walls and box like behavior, are due to wall detachment as well as insufficient interlocking among the orthogonal walls. The horizontal “diaphragm” is not enough to prevent the overturning of any of the side aisle walls or front and rear facades despite its essential role in transverse seismic response (Fig. 5.2.7). Expected earthquake damage patterns that have been observed are a result of gaps in masonry walls and inadequate linking between additions, which were built with different materials.

The San Francisco church has a complicated crack pattern. It has been analyzed on the basis of the most commonly occurring behaviors of basilica plan churches (Da Porto et al. 2010; Giresini 2016; Doglioni, Moretti, and Petrini 1994; Giuffrè 1991; Lagomarsino and Podestà 2004b, Lagomarsino et al., 2004) to more adequately grasp the extent of the damage with a view to the reaction of the structure in both longitudinal and transverse directions. In-plane behavior of the longitudinal and transverse arcade walls and out-of-plane behavior of the façade, rear presbytery wall and transept walls are taken into consideration.



**Figure 5.2.7** - Horizontal diaphragm placed on the central nave

As they are vitally linked phenomena, longitudinal arcade walls' out-of-plane behavior and the transverse arcade wall's in-plane behavior were analyzed together. Diagonal cracks in the arches and top triangular adobe section exhibit the in-plane behavior for the traverse arcade. Crack patterns characteristic of masonry arcades affected by earthquake shaking documented in historic churches in the downtown of Santiago (the Metropolitan Cathedral, the Agustín Church, the Merced Church, etc.), are present in the San Francisco Church. This is documented in historical archives of repairs (Consejo de Monumentos Nacionales—CMN, 2010).



**Figure 5.2.8**—In-plane behavior of the transverse arcades

At present, the repairs undertaken in 1988, which installed a reinforced concrete frame and upper tie-rod (Fig.5.2.8) decreasing deformations while causing a profound change in the masonry arches' behavior, have caused adaptation in the behavior of the transverse arcade. Racks can be observed at and around the intrados to the arcades and in the piers, which resulted from discontinuities and disunity amongst the masonry and concrete. Deep cracks provide evidence of the insufficient bonding between the transverse brick masonry arcades and the stone longitudinal nave walls (Fig.5.2.8a). Significant bulges in the stone work corresponding to the transverse arch springs, likely linked with an RC tie-rod, define the longitudinal walls' unique out-of-plane behavior during seismic action. Unsettlingly, deep cracks and deformations in some arch piers of the nave are related to these bulges (Fig.5.2.8b). The pounding effect between the transverse and longitudinal walls is congruous with the

aforementioned phenomena, resulting from the disparate building techniques used in construction, repairs and renovations (i.e. brickwork and stonework) which cannot be easily bound together. Additionally, deep cracks due to earthquake shaking have formed in the arch intrados of the longitudinal walls pointing to their separation into two leaves (Fig.5.2.9c-d). The introduction of reinforced concrete chains in the top section of the transverse arcade walls played an essential role in the bulging phenomenon observed in the longitudinal walls (Fig. 5.2.9e). The effect of the tie-rods is twofold in that they increase resistance to overturning while changing the collapse modalities of the vertical arch mechanism linked to the bulging.



**Figure 5.2.9-** Cracks in transverse arches(Jorquera et al., 2017).

In regard to the façade's out-of-plane behavior, a historical collapse is evident due to the presence of a brick reconstruction at its gable (Fig.5.2.10). The uneven thickness of the walls presents a risk of the apex wall overturning given the macro-element Length/Height ratio of 0.605 (D'Ayala and Speranza, 2003). Another vulnerability is inherent in the disjointedness amidst the main nave's orthogonal walls and the external orthogonal wall of the bell tower which is related to the unconventional bell tower producing inertia different than that of the main block. Regarding the rear wall of the presbytery's out-of-plane behavior, a collapse is

evidenced by the upper portion being reconstructed with wooden and brick elements (Fig.5.2.10). The subsequent aspects relate to these failure mechanisms: the notable distance between the walls; the walls' great slenderness ( $\lambda_c = 17.5$ ); the ratio between length of macro-element and height on ground  $L/H = 0.88$  (D'Ayala and Speranza, 2003); the absence of a connection with the roof covering; and the existence of a wide gap. Vertical fractures, evidencing the north and south transepts' walls out-of-plane behavior, denote the constructive incongruousness between the top sections of the transept facades and the lower sections, which pertain to the initial center of the Latin cross (Section 5.2.2). A previous collapse is made apparent by the reconstruction brick wedged in the original stone walls.



*Figure 5.2.10 –Upper part of façade and presbytery wall.*

#### 5.2.4 Structural analysis

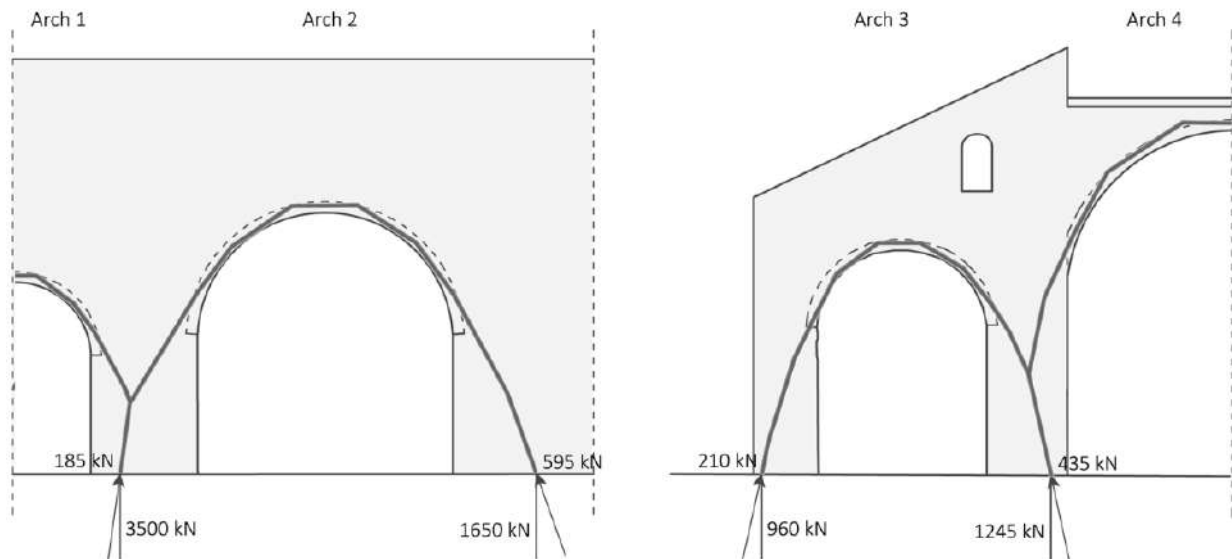
Safety assessment of monumental buildings requires a multi-level approach that should embrace local and global behaviors, linking causes of damage and related consequences that influence each other. Results outlined throughout Sections 5.2.2 and 3 suggest that accurate analysis has to focus on the response of those macro-elements that exhibited significant damage during past seismic events.

To this end, multiple analysis techniques have been employed. Regarding the response of those macro-elements that revealed a substantial vulnerability to out-of-plane actions, linear (LKA) and incremental kinematic (IKA) analyses addressed front façade, behind presbytery wall and transept walls, while rocking analyses focused on transepts walls. As for the in-plane response, LKA was exploited to evaluate the capacity of transverse arcade walls.

Moreover, a control on the global response of the church has also been carried out to define preferential displacement shapes. The global response of San Francisco has been addressed through LDA (code Straus 7).

The Chilean NCh433 code does not provide the possibility to verify the seismic behavior of existing non-confined-masonry buildings, although the Chilean Standard NCh3332.Of.2013 for the Structural Intervention of Earthen Historical Buildings (Instituto Nacional de

Normalización - INN 2013) provides general criteria for interventions intended to result in strengthening. For this reason, it was decided to address the gap in this standard with a combined analysis through the Italian Code NTC2008 (MIT 2008) and Circ.617/2009 (MIT 2009).



**Figure 5.2.11** - Thrust line for the arches 1, 2, 3, and 4.

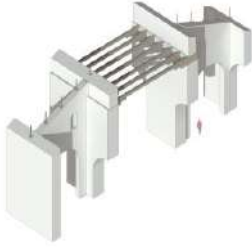
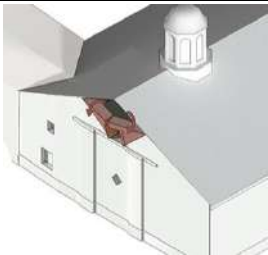
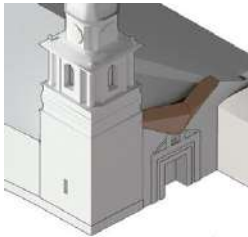
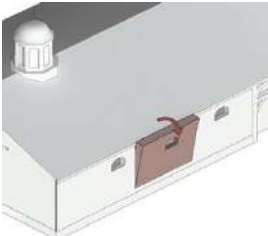
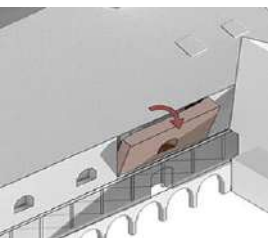
To achieve a safety estimation of the static consistency of the church, a preliminary graphical analysis for vertical loads has been first carried out on a significant portion of the main nave and transept wall through the Safe Theorem of Limit Analysis (Heyman 1966). An equilibrated solution has been found (drawn as a set of thrust lines) contained inside the masonry structure, compatible with the loads and which does not violate the yield conditions. This condition has guaranteed the safety of structure for vertical loads. Fig.5.2.11 shows the thrust line of each arch (1, 2, 3, and 4) with the related values of thrusts. It is worth noting that the thrust line of the transverse arcade F highlights a limit condition for the stability of portion F4, considering the thrust position at the ground. As expected from direct surveying activities, the thrust lines converging on pillar F3 are influenced by loads of both the longitudinal arcade (3) and the transverse wall facing the transept (wall F), determining a high loading level on a reduced portion of masonry which is in fact heavily damaged. Linear static analysis for vertical loads on the global 3D FEM has been carried out, and results show comparable stress levels ranging 1–1.2 MPa on portions F3 and F4.

#### 5.2.4.1 Linear and non-linear kinematic analysis




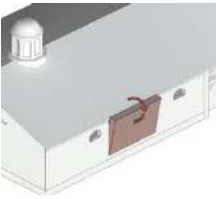
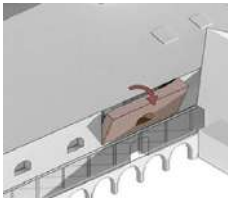
First, mechanisms that are most likely to be activated in San Francisco have been defined for both the current state and state prior to the brick additions or RC consolidation. In fact, response to past seismic events, denoted by still visible cracks, are deeply correlated with the expected future behavior since earthquake related damage has a progressive and relapsing

character (Doglioni, Moretti, and Petrini, 1994). Tables 5.2.4 and 5.2.5 show results and descriptions of the analyzed local mechanisms for the San Francisco church considering both the current state of the building and the state preceding the additions and RC insertion interventions.

**Table 5.2.4** - Results of Linear Kinematic Analysis current state: ID of analyzed macro-element; Mechanism types; Participating Mass  $M^*$ , Kinematic multiplier  $\alpha_0$ , Mechanism Activation Acceleration  $a_0^*$ , Dag Demand Acceleration at ground level, and  $Da1$  the Demand Acceleration at elevated level.

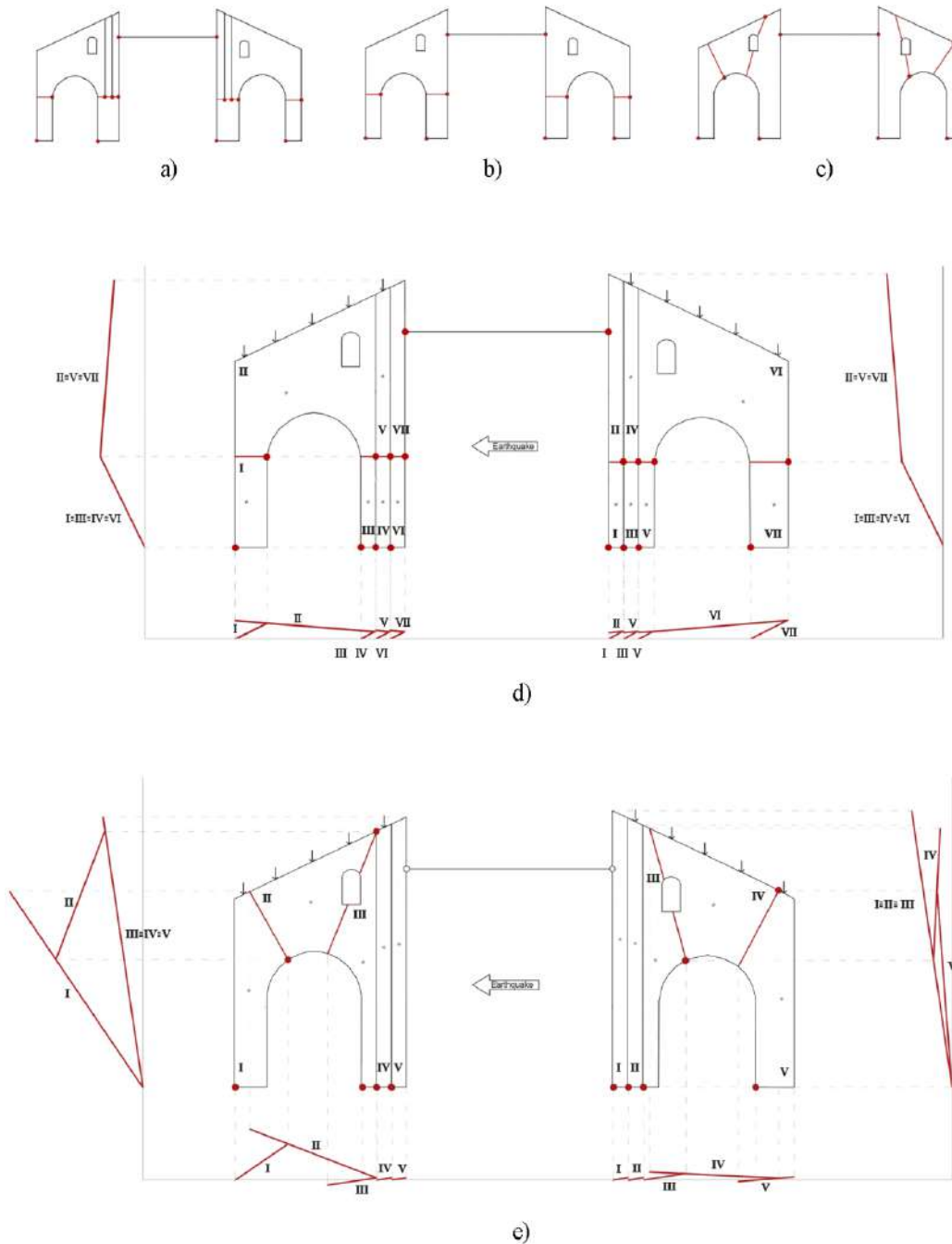
ID	Mechanism Type	Current State	$M^*$ [kN]	$\alpha_0$	$a_0^*$ [m/s <sup>2</sup> ]	$Da1$ [m/s <sup>2</sup> ]	$Da2$ [m/s <sup>2</sup> ]
TA1	In-plane behavior		1068	0.473	3.68	2.31	-
TA2	In-plane behavior		1054	0.2	1.57	2.31	-
TA3	In-plane behavior		1093	0.472	3.59	2.31	-
BP	Gable Overturning		60	0.286	2.468	2.31	2.22
MF	Gable Overturning		122	0.336	2.478	2.31	2.34
NT	Simple Overturning		172	0.113	0.866	2.31	1.01
ST	Simple Overturning		188	0.131	1.030	2.31	2.16

**Table 5.2.5** - Results of Linear Kinematic Analysis before the RC interventions: ID of analyzed macro-element; Mechanism types; Participating Mass  $M^*$  [kN], Kinematic multiplier  $\alpha_0$ , Mechanism Activation Acceleration  $a_0^*$  [ $m/s^2$ ], Dag Demand Acceleration at ground level [ $m/s^2$ ], and  $Da1$  the Demand Acceleration at elevated level [ $m/s^2$ ].

ID	Mechanism Type	State prior to the brick reconstructions or concrete framework reinforcements	$M^*$ [kN]	$\alpha_0$	$a_0^*$ [ $m/s^2$ ]	$Da1$ [ $m/s^2$ ]	$Da2$ [ $m/s^2$ ]
TA3	In-plane behavior		717	0.106	1.59	2.31	-
TA4	In-plane behavior		755	0.136	1.17	2.31	-
BP1	Gable Overturning		103	0.222	1.71	2.31	2.22
MF	Horizontal arch		156	0.271	2.06	2.31	2.34
NT	Simple Overturning		334	0.141	1.063	2.31	1.01
ST	Simple Overturning		303	0.166	1.282	2.31	2.16

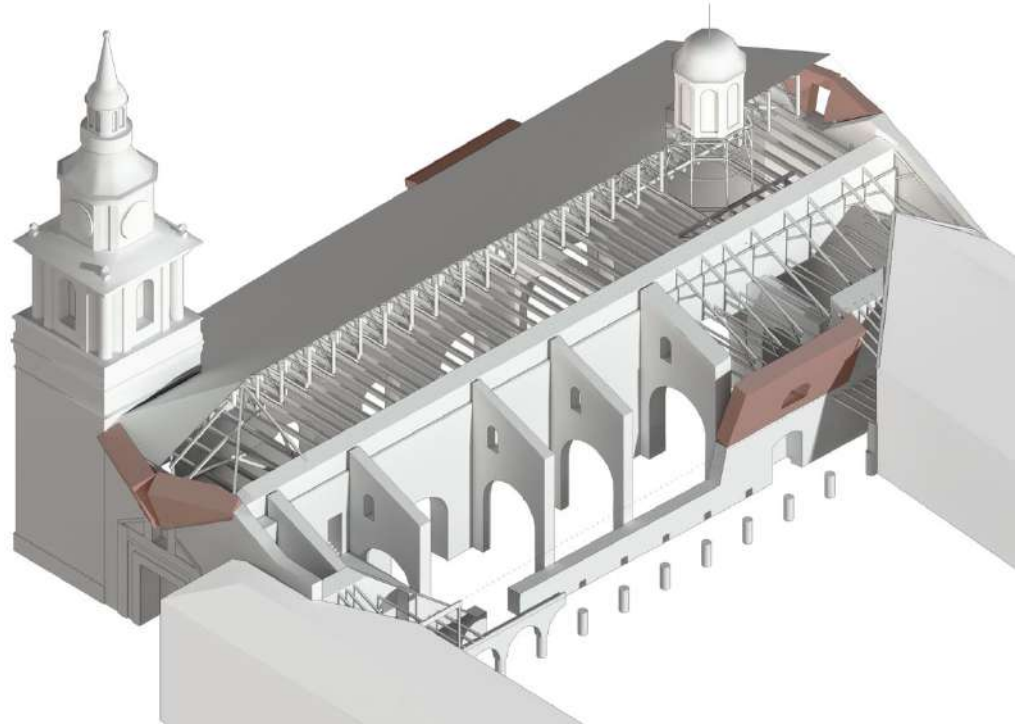
The response of the transversal arcade systems in the current state is analyzed through three mechanism scenarios, TA1, TA2, and TA3, based on visible crack patterns annotated during surveying activities (Fig.5.2.12). Different scenarios represent an increasing quality of the masonry of longitudinal walls (axis 2 and 3; see Fig.5.2.1). Mechanism TA1 represents walls 2 and 3 as a two-leaf masonry, thus by means of two blocks (Fig.5.1.12a), while mechanism TA2 assumes the same masonry quality for wall 2 and 3 but a complete effectiveness of the anchoring of the piers (Fig.5.1.12b).

Mechanism TA3 (Fig.5.1.12c) represents the longitudinal walls as a monolithic masonry with full effectiveness of the anchoring intervention on piers. The hypothesized direction of the action induces a counter- clockwise mono-lateral rotation of piers and a consequent clockwise rotation of upper blocks.

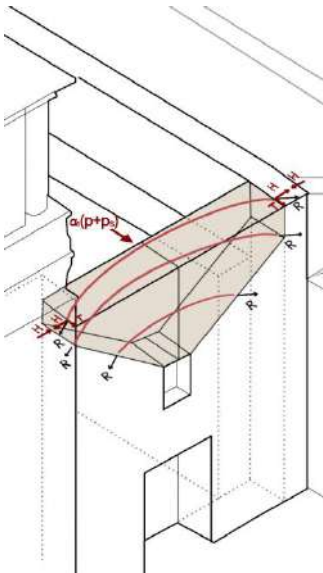


**Figure 5.2.12** - In-plane mechanism of the transverse arcade. Possible activated mechanisms: a) TA2 (current state) longitudinal wall made up of a two-leaf masonry and complete effectiveness of the anchoring of the piers; b) TA3 (current state) longitudinal walls as a monolithic masonry with complete effectiveness of the anchoring intervention on piers and c) TA5 (state before concrete reinforcements) longitudinal walls as a monolithic masonry. Horizontal and vertical virtual displacement diagram: d) TA1 (current state) longitudinal wall made up of two-leaf masonry and e) TA4 (state before concrete reinforcements) longitudinal wall made up of two-leaf masonry (Jorquera et al., 2017).

Fig.5.1.13 shows the out-of-plane mechanisms identified for the current state. Mechanisms represent the overturning of gables of façade, and behind presbytery wall, i.e., MF and BP in Table5.2.4, whose cuneiform macro-blocks rock around two oblique cylindrical hinges, and the overturning of the north and south transept walls around cylindrical hinges placed 60 cm off the ground, NT and ST (Table5.2.4).



**Figure 5.1.13** - Local mechanisms of collapse in current state (Stefanini, 2016).



**Figure 5.2.14**- Horizontal bending mechanism of main façade

In the state prior to the brick additions or RC consolidation the mechanisms evaluated are the same, but in different materials, with the exception of the mechanism characterizing the transverse arcades (TA4 and TA5 Table5.2.5) and the main façade (MF1), which also have different layouts. For the in-plane mechanisms of the transverse arcade, two layouts have been considered addressing the longitudinal walls as two-leaf masonry, TA4 Table5.2.4 and Fig.5.1.12d, or monolithic, TA5 Table5.2.4 and Fig.5.1.12e. The layout of both mechanisms places hinges at pier bases and on arch haunches so that a counterclockwise rotation of piers induce a clockwise rotation of the central block, which includes the keystone of the arch and the related portion of the wall above it.

In the mechanism named MF1, the gable of the main façade is considered confined by both adjacent walls and longitudinal walls, so that it becomes a horizontal bending mechanism also named the horizontal arch mechanism of confined walls (Fig.5.2.14). For this kind of mechanism the horizontal arch inside the wall reaches the limit state due to masonry crushing for compressive stress, here considered  $f_{m,min}=2.6$  MPa, according to M.Q.I. method, (Borri et al. 2015).

After having defined mechanism layouts and characteristics, the kinematic multiplier,  $\alpha_0$ , can be evaluated and converted into spectral acceleration  $a_0^*$  to get a homogeneous dimension with the demand, evaluating the participating mass as a modal form of vibration equations (5.1).

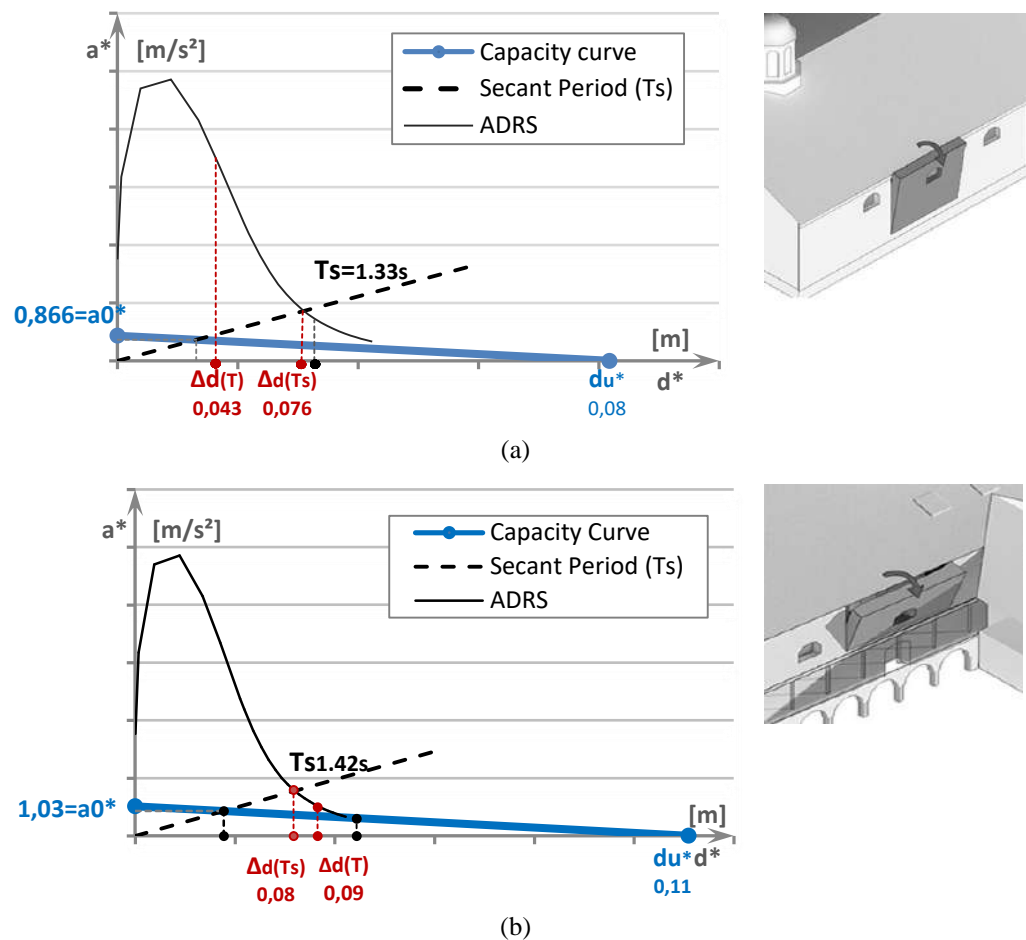
For all mechanisms, a slippage  $t = 0.66 \sum_{i=1}^n W_i (f d l)^{-1}$  of the cylindrical hinge is considered to take into account the finite compressive strength of the masonry and, after the onset of motion, the actual behavior of the blocks, which present considerable thickness. Slippage  $t$  depends on  $i$ -th self-weight,  $W_i$ , design compressive strength,  $f_{dc} = f_m$ , and width of wall,  $l$ . Safety assessment requires that the spectral acceleration must be equal or greater than the demand acceleration, with  $R=1.5$  is the acceleration reduction factor according to Eurocode8 (Eurocode8, 2014) and other coefficients defined in Section 5.1. Mechanisms involving the portion of masonry placed higher than ground level have an input demand amplified by the effect of height. The NTC 2008 (Ministro delle Infrastrutture e dei Trasporti—MIT, 2008) evaluates this amplification, with further verification imposing:  $a_0^* \geq S_e(T_1) \Psi(Z) \gamma$ . The amplification considers the design spectrum acceleration with respect to the period  $T_1$ ,  $S_e(T_1)$ , being  $T_1 = 0.05 H^{3/4}$  the first vibration period of the macro-block. Then  $\Psi(Z) = Z/H$  is a function depending on the height from the foundation of the centroid of the weight forces applied on the rigid bodies,  $Z$ , on the total height of the building from the foundation,  $H$ , and on  $\gamma = 3N/(2N+1)$ , which corresponds to a modal participation coefficient, depending on  $N$  number of floors.

The comparative analysis of the current state (fired bricks blocks) and state prior to the brick additions or RC consolidation (stones blocks) shows a significant improvement of resistant behavior for the mechanisms of the transverse arcade system TA1, TA2, and TA3 and for the Main and the Presbytery Façades, MF, PF.

These improvements, which lead to a satisfactory safety assessment for the current state, owe to a deeply different mechanism shape (arcade mechanisms and main façade mechanism) or a decrease in live loads (wooden gable on the presbytery gable). On the other hand, the walls of the north and south transepts, NT and ST, feature a worsening of the seismic behavior, due to the reduction of the resisting transverse section. Indeed, the crack pattern of transept walls, consisting of deep fractures between the transverse arcade-walls (Fig.5.2.1, plan F and G) and the longitudinal walls (Fig.5.2.1, plan 1 and 4) surveyed after the 2010 earthquake, confirms the activation of the mechanism without any collapse. While for the mechanisms involving the main façade and the presbytery façade, any crack pattern has been surveyed after the 2010 earthquake when the transept wall systems suffered severe damage, which requires a further investigation.

In order to enrich the understanding of the local response of the transept walls, considering the different nature of the mechanisms analyzed, further investigations have been carried out. In particular, the mechanisms regarding the transept walls are considered through incremental kinematic analysis (IKA). Incremental kinematic analysis (IKA) can be applied to evaluate the decrease of the kinematic multiplier  $\alpha_0$  due the increase of the displacement  $d_k$  of a control point

on varied geometrical configurations, repeatedly applying the principle of virtual works, assuming an increasing forcing action that cannot induce any transitory recovery of the block after the activation of motion (eq. 5.8 and 5.9). The displacement capacity curve obtained through IKA initiates with the value of acceleration necessary to activate the mechanism,  $a_0^*$ , and descends linearly, describing how the mechanism evolves until final failure, i.e., when the curve reaches nil value. Results of IKA can be used on properly damped response spectra but does not constitute an alternative to estimations offered by a nonlinear dynamic. Real out of plane mechanisms NT and ST are thus transformed into equivalent SDOF systems, whose capacity in displacement have to be compared with the related Acceleration Displacement Response Spectrum (ADRS) according to Nch2745Of.2013, as shown in Fig.5.2.15. From the comparison between the displacement Capacity and Demand (5.9) of both the transept walls, the tests are satisfied (Fig.5.2.15). Despite the activation of the mechanisms, both macro-elements (NT and ST) show a satisfactory capacity in displacement, which justifies the absence of the collapse.



**Figure 5.2.15** - Capacity and demand curves of incremental kinematic analysis: (a) north transept wall; and (b) south transept wall; and Acceleration Displacement Response Spectrum (ADRS) according to Nch2745Of.2013 (Palazzi et al., 2018c).

### 5.2.4.2 Global response model

In addition to the local analysis, FE models of the Church have been developed using the Straus 7 software (Strand 2004). The global structure was modeled considering homogeneous and elastic materials characterized by the mechanical proprieties as reported in Section 5.2.3. As for decorative elements, they are not included in the model, and the bell tower top and then on-structural loads of the roof have been applied as vertical forces. A linear static analysis of vertical loads was performed followed by a natural frequencies analysis for setting the spectral response. All loading configurations have been combined to evaluate stress and displacement. In agreement with the NCh433Of96 (Instituto Nacional de Normalización—INN 1996) the analysis included all the modes (100 vibration modes) necessary so that the sum of the equivalent masses, for each of the seismic action, is higher than 90% of the total mass.

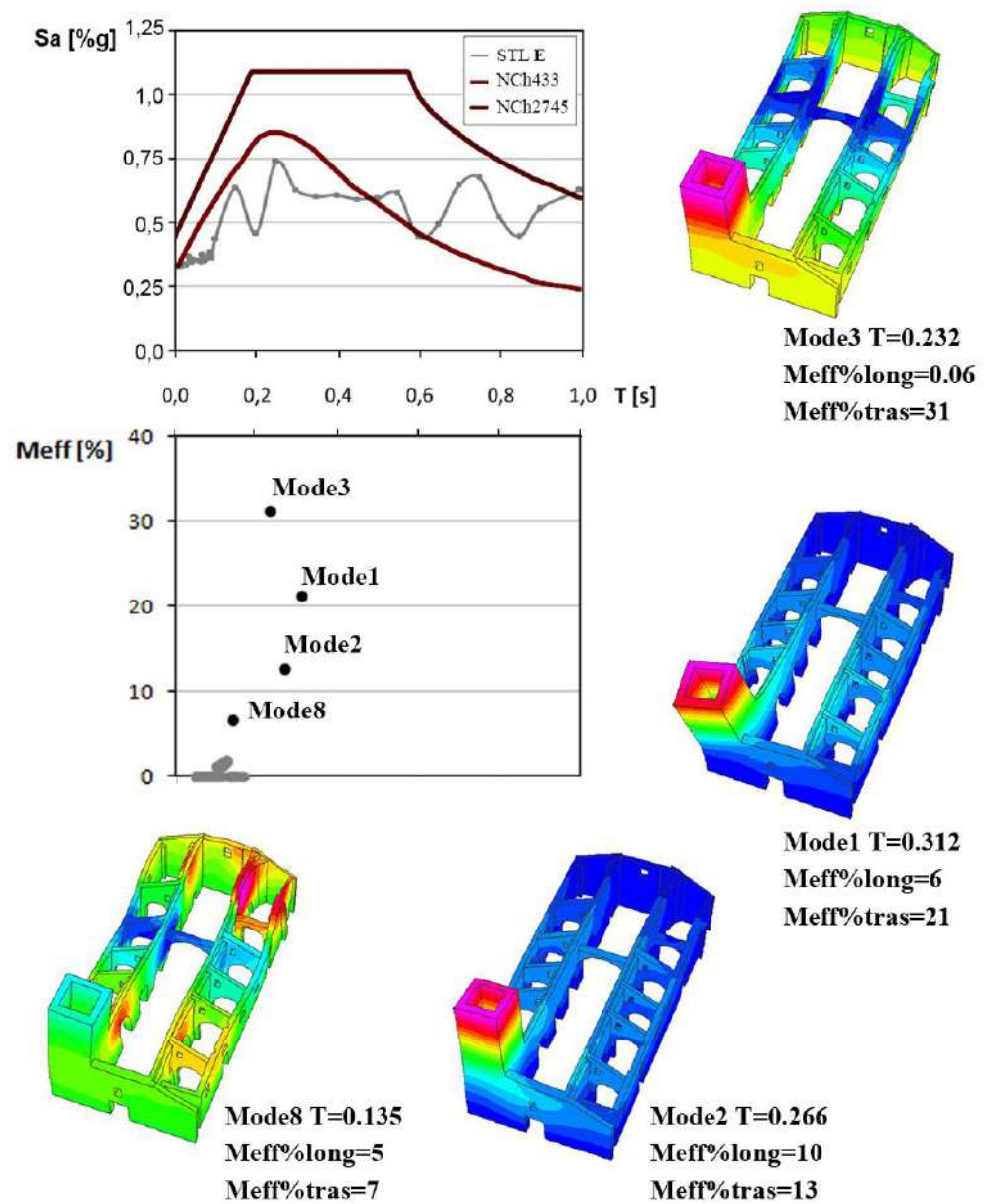
The results of EFA are plotted in Fig. 5.2.16, where the  $M_{eff}$ , the corresponding periods ( $T$ ), and the modal shapes of the first 100 vibration modes are shown.

Moreover, the results are compared with the pseudo-acceleration response spectra for the shock of February 27<sup>th</sup> 2010 Maule earthquake elaborated by (Liberatore, Sorrentino & Liberatore, 2012), and Chilean code values NCh4433of96 and NCh2745of2013. The Basilica is located at 490m from the STL station and characterized by the soil type B. N direction corresponds to the transversal direction of church, and E to the longitudinal direction.

Considering the N pseudo-acceleration response spectra, the four modes with participating mass larger than 5% have a period within 0.135-0.312s. This interval corresponds to the peaks of spectral demand, Fig. 5.2.16. The first mode ( $T=0.312s$ ) involves the transversal arcade walls, the façade and the bell-tower with a  $M_{eff}$  equal to 21%. The third mode ( $T=0.232s$ ) involves the transept walls, the transversal arcade walls, the façade and the bell-tower with a  $M_{eff}$  equal to 31%. The second mode ( $T=0.266s$ ) involves the façade and the bell-tower with a  $M_{eff}$  equal to 13%.

Considering the E pseudo-acceleration response spectra, six modes with  $M_{eff}$  larger than 5% have a period between 0.122-0.266s. This range correspond to a relevant spectral demand ( $S_a$ ), Fig. 5.2.17. The fifth mode ( $T=0.151s$ ) involves the upper part of presbytery wall and the base of bell-tower with a  $M_{eff}$  equal to 21%. The seventh mode ( $T=0.139s$ ) involves the upper part of façade and presbytery wall with a  $M_{eff}$  equal to 14%.

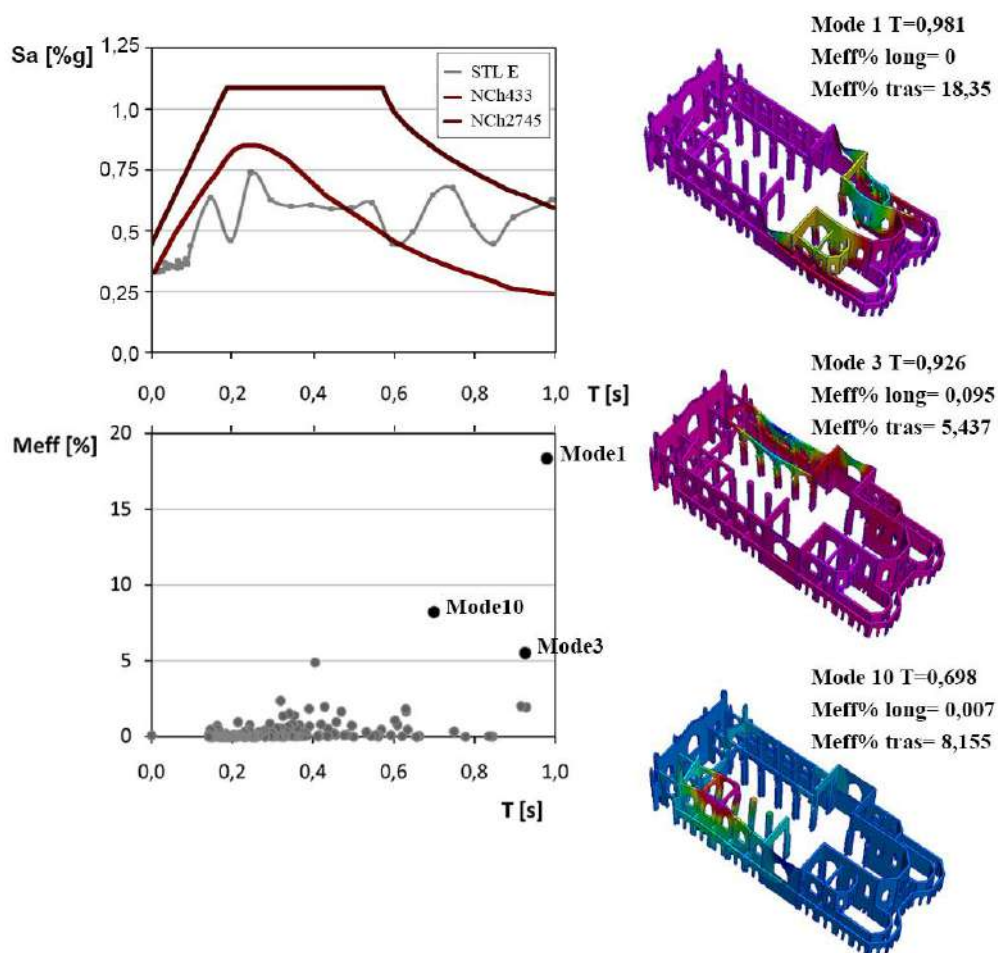
Displacement shapes and mass distribution among different vibration modes resulting from the Eigen frequency analysis (EFA) and linear dynamic analysis (LDA) are completely coherent with assumptions made for local response behavior (e.g., shapes of macro-elements) through linear kinematic analysis, even though linear elastic FEA may present significant limitations for any further investigation on masonry material.



**Figure 5.2.16** – E Pseudo-acceleration response spectra for the February 27th 2010 Maule earthquake for the STL station; deformed shapes of the main modes with corresponding periods and participating mass ratios in the longitudinal direction (Palazzi et al., 2018c).

In particular, the first vibration frequency evaluated through FEM is 3.21Hz and has a participating mass factor under 25%. Moreover, in the first ten vibration modes reported in Fig.5.2.16 and Fig.5.2.17 the participating mass is just 74% in y-direction and 64% in x-direction. In fact, the distribution of the effective mass is not prevalent in a single mode of vibration but is dispersed in numerous modes. This circumstance allows to assert that the structure does not exhibit a well-defined global behavior and that the evaluations based on local analysis are more significant. More specifically, the displaced configurations for modes 3

and 7 underline the intrinsic vulnerability and the related possible crack patterns of transept walls, transversal arcade systems and the gables of the main and presbytery facades.



**Figure 5.2.17** – *N* Pseudo-acceleration response spectra for the February 27th 2010 Maule earthquake for the STL station; deformed shapes of the main modes with corresponding periods and participating mass ratios in the transversal direction (Palazzi et al., 2018c).

### 5.2.5 Summary

The multidisciplinary approach proposed in this study allowed the identification of key factors that prevented the collapse of the monument, although recurrent damages caused by strong earthquakes occurred:

- suitable size ratios of structural and architectural elements;
- the efficient traditional constructive technique;
- the efficient transverse connection provided by the wooden beam;
- the addition of side aisles, operating as buttresses for the original Latin cross plan and use of triangular buttresses in the extrados of the arcades to ensure a better transverse response;
- and uninterrupted use and maintenance work.

Nevertheless, the high frequency of strong earthquakes over centuries caused recurrent and significant damage patterns and this study has highlighted main critical points.

Local-level evaluations have provided a robust assessment of the OOP behavior of front and rear gables and of upper parts of transept walls suggesting that vulnerability could be successfully reduced through light interventions. Indeed, results of LKA for the overturning of the gables offered a satisfactory safety assessment considering the blocks as if they actual position returns a negative assessment.

However, neither front gable nor gable of the wall behind presbytery suffered from any damage during the strong shake in 2010. For mechanisms of north and south transept walls, LKA offered an unsatisfactory safety assessment, safety index 0.375 for north transept and 0.445 for south transept, while IKA provided a safety index equal to 1.86 and 1.375 for north and south transept respectively. Rocking analysis showed indeed that rotations reached by transept walls for the strong motion of 2010 are far away from instability even when the roof mass transmitted on top of walls is considered. Regarding in-plane capacity, the main vulnerability is connected to the transverse response of the church. In fact, the presence of the transverse arcades undoubtedly has reduced the out-of-plane response of longitudinal nave walls and improved its stiffness, reducing the effective length to a single span.

However, the lacking connection between longitudinal nave wall and transverse arcade, first, reduced the retaining effect and, second, possibly eased a pounding effect amplifying the response of longitudinal wall and inducing vertical cracks of piers. Limit analysis and FE linear static analysis highlighted this weakness and the necessity of improving the lacking connections and the capacity of stone piers, given the severe load concentration levels clarified by thrust-line graphical analysis.

Lastly, global-level evaluations confirmed the prominent by-part response of the church. Indeed, results of modal analysis demonstrated that mass participating to the first Eigen mode is less than 25% and that any of the first ten modes do not excite more than 30% of the mass in a single direction. Thus, the structure does not exhibit a preferential global behavior, and it is better interpreted through local analyses, which enforce and suggest simple and straightforward intervention strategies.



NG style

### 5.3 Case study 3: Basilica del Salvador

This section of Chapter 5 focuses on the seismic behavior assessment of the Basilica del Salvador (Santiago, Chile), one of the most significant examples of the Chilean Neo-gothic architecture. This huge unreinforced brick church is a *Hallenkirche* basilica consisting of three aisles of the same height, three apses, an annular ambulatory, an outer gallery and a narthex. The Basilica was subjected to constructive changes, due to repaired damages, since the 1906 Valparaíso earthquake, and has suffered extensive structural failures during major Chilean seismic events over the past century. In particular, the church was heavily damaged with several local collapses following the 1985 Algarrobo and the 2010 Maule earthquakes. Since then, it has remained inaccessible and at the current state shows a severe and worrying crack pattern. Non-repaired damages, lack of maintenance and constant exposure to atmospheric agents have further jeopardized its precarious conditions, accelerating the deterioration of the masonries.

Even though previous studies aimed at characterizing the post-seismic scenarios of the Basilica have been conducted by (Moll & Sabanech, 1976; Joannon et al., 2003) and a preliminary retrofit project has been presented in (Rendel, et al. 2014), the current state of conservation of the building has not yet been completely investigated. As shown in (D'Ayala and Benzoni, 2012), the seismic action has caused the high loss of the Chilean heritage buildings and, therefore studies to preserve the scarce presence of unreinforced masonry monuments in the Country (Torres et al., 2017) must be done.

In this framework, a study aiming to define the actual seismic vulnerability of the *Basilica* and to provide the safeguard of its historical, architectural and social values, through seismic risk mitigation strategies, is necessary.

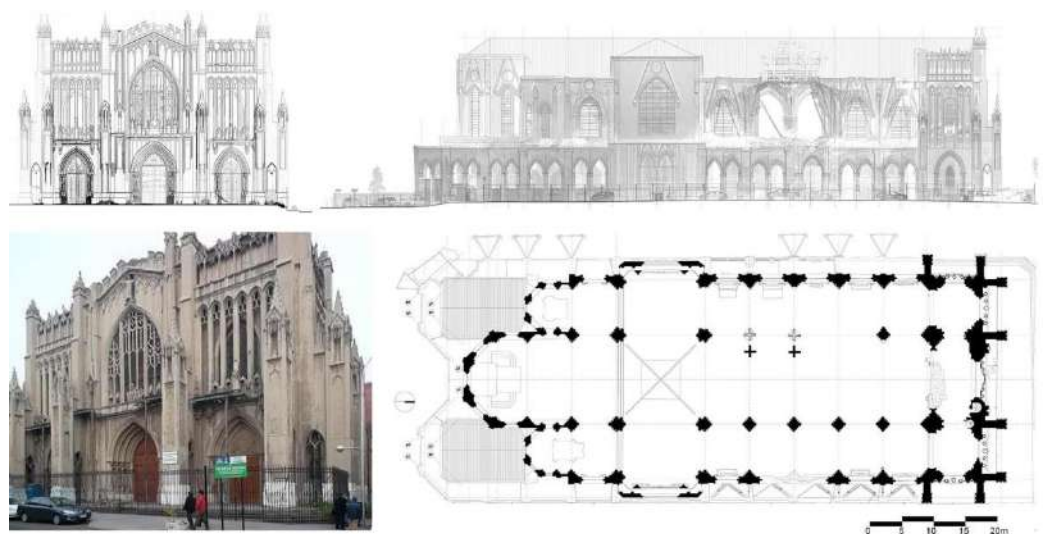
The assessment of the seismic behavior of the monument has been investigated by a multi-level approach such as historical researches, on-site observation, crack pattern analysis and laboratory testing for a mechanical characterization of materials. An integrated use of different structural analyses with different complexity levels is proposed: (1) as concerning numeric modal identification analysis, by finite element method, a linear dynamic analysis has been

carried out; while for concerning the local analyses by damage mechanisms, (2) linear and incremental kinematic analyses have been proposed.

### 5.3.1 Basilica del Salvador

In 8 December 1863 the *Compañía de Jesus* church, located on the foundational historical center of Santiago the Chile, was destroyed by a fire that caused the death of 2,000 faithful in a city that at the time had about 100,000 inhabitants (The New York Times, 1864). The tragedy touched the citizenship, settling in the collective memory of the City. Ten years later, the Bishop Rafael Valentín Valdivieso signed an ordinance for the construction of a memorial Basilica dedicated to the Savior. Thus, in 1873 the *Basilica del Salvador* was built and opened in 1892, becoming a great religious and civil Landmark of Santiago centre, declared National Monument through the decree D. N°933 of 24 November 1977.

The architectural complex was designed by the architect Teodoro Burchard and administered by the presbytery Ignacio Zuazagoita, executed in a neo-gothic style by German and local workers.



**Figure 5.3.1** - View of the Basilica and current plan, façade and section (Tandem Ltda, 2014).

The in-plan geometry is 90m long in the longitudinal, 40m wide in the transversal direction, and 25m maximum roof height, with a capacity to accommodate 5,000 people. The church features a *Hallenkirche* basilica of 3626 m<sup>2</sup>, having a narthex, three aisles of the same height with five rectangular spans (in the central nave of dimensions 13.5m x 6.8m and in the side aisles of 8.55m x 6.8m), a long nave crossed by a transept (13.5m x 37.15m), three semi-circular apses, an annular ambulatory and an outer gallery (Fig.5.3.1).

The naves and transept are covered by false cross vaults constituted of slender timber elements, while the outer gallery present dominical brick vaults (a unique architectural element in

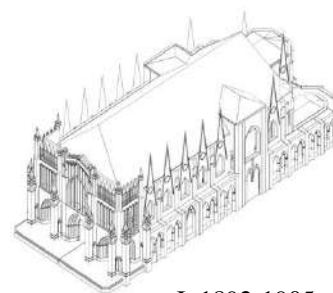
Santiago) and the system of light roof is supported by wooden trusses (Fig. 5.3.1) and covered by galvanized iron plates. The foundations are made of natural stone masonry, 2.1m high.

### 5.3.1.1 Seismic history and the main interventions

The actual configuration of the Basilica is the result of several interventions of seismic consolidation during the past centuries characterized by different construction techniques and materials, which change the structural behavior.

Historiographical, structural and chronological analyses (Moll & Sabanech, 1976; Joannon et al., 2003; Rendel et al., 2014; and Correa, 2015) allow describing the constructions phases of the Basilica del Salvador according to the most important seismic events that affected its structure (Fig.5.3.5, Tandem Ltda, 2014):

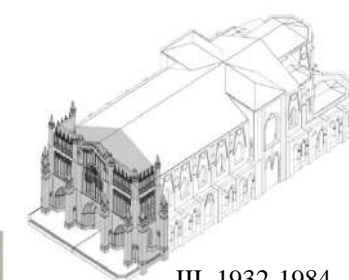
- The Valparaíso 1906 earthquake (8.2 Mw), the first major seismic event that shook the church, completely destroyed the original roof structure, determined heavy damages in the flying buttresses, caused deep cracks in the key of windows arches of the west side aisle and of central apse. Consequently, the gables of the lateral walls and the damaged flying buttresses were demolished, the roof was replaced, and the transverse arches of the west aisle and the central apse were confined with metallic stripes, to tie the upper part of the west wall to the longitudinal arcades of the central nave (Correa, 2015).
- Following the Mendoza 1927 earthquake (7.1 Mw), the church suffered several structural, moderate and heavy, damages. The architects Smith Solar and Smith Miller modified the original façade (1928-1945), introducing a reinforced concrete ring-beam, slab and two gables on the lateral bays of the narthex (Fig.5.3.2).



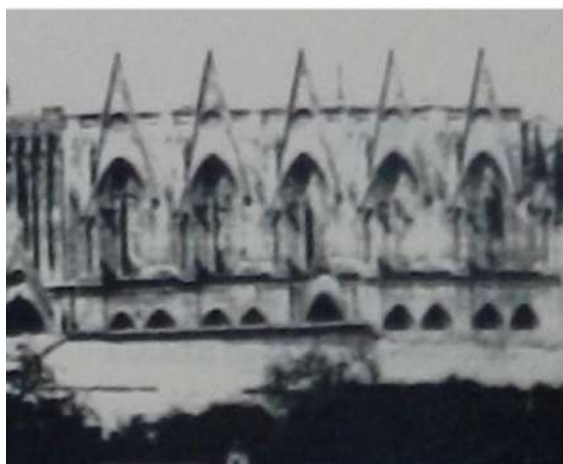
I. 1892-1905



II. 1906-1931

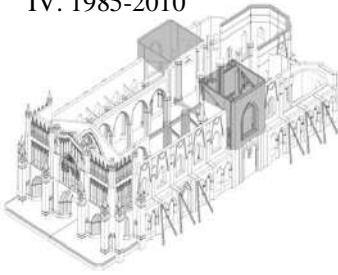


III. 1932-1984



**Figure 5.3.2** -Photo (a) original phase, and (b) uncertain date after 1906 (MOP)

## IV. 1985-2010



**Figure 5.3.2**– History of Basilica (Tandem Ltda, 2014)

- Before of the Algarrobo 1985 earthquake (8.0Mw), the old parish townhouse of the Basilica apse, built with adobe masonry, was demolished. Its layout is registered in the design of the pavement.

Following the 1985 seismic event, the upper part of the transept walls within two columns of the central nave arcades collapsed (Fig.5.3.3). The security measures started the same year and involved the reconstruction of the west and east transept walls with steel elements and gypsum structure, and the insertion of a ring-beam of reinforced concrete in the central apse. Two R.C. columns were erected, bound to the top of the lateral wall of west aisle. Since then, the church has remained inaccessible.



**Figure 5.3.3** - Photo (a) west transept wall, and (b) two central nave columns, collapsed after the 1985 earthquake (Ministry of Public Works).

- Additionally, the Maule 2010 earthquake (8.8Mw), the last megathrust earthquake that shook the Basilica, produced a worrying crack pattern and further local failures of the east side aisle wall, the central arch of the narthex, the arcades of the external gallery and of the columns of the central nave (Fig.5.3.4).

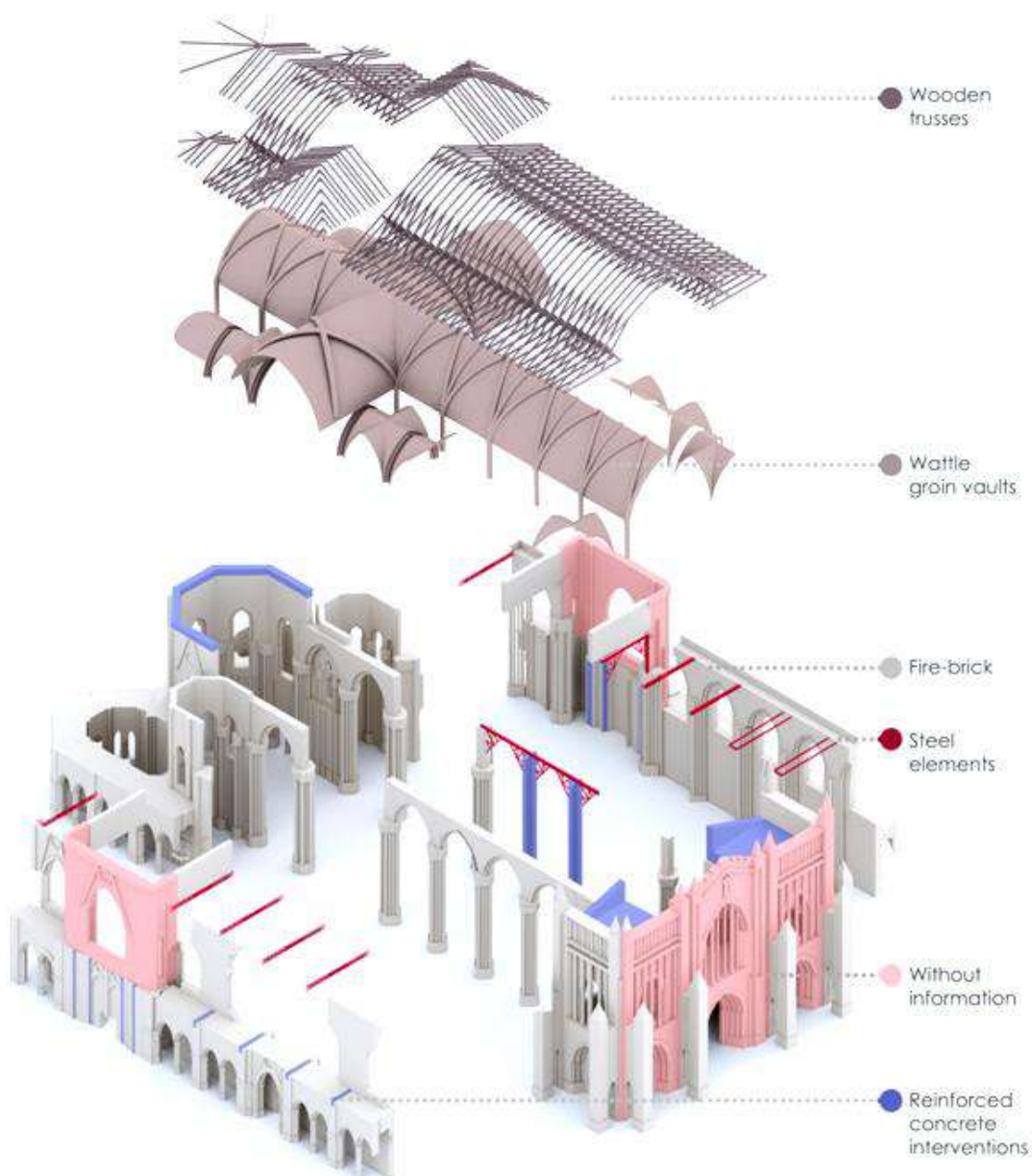


**Figure 5.3.4** - Photo (a) and (b): worrying crack pattern and local failures of east side aisle wall, central arch of narthex, arcades of the external gallery and columns of the central nave. (Ministry of Public Works).

At present, a temporary and preliminary reinforcement structure, consisting of steel braced frames with steel space trusses that span across the main nave, and designed by SIRVE S.A. (Rendel et al., 2014), is under construction.

### 5.3.2 Properties of materials

The Basilica complex comprises the original masonry structure of unreinforced brick, the light timber roof and punctual reinforced concrete elements introduced after several earthquakes (Fig. 5.3.6). Extensive visual surveys, in situ and laboratory destructive and non-destructive tests were carried out to evaluate the material proprieties of the building.



*Figure 5.3.6- Exploded Axonometric of resistant structure.*

The side aisles walls (thickness 70cm) consist of three head brickwork (brick dimensions 20.5x41.5x3.5cm) connected by a lime mortar, and polylobacter responds (maximum thickness 1.26cm). The compound piers of the central nave are made of an internal nucleus (diameter 140cm) composed by irregular rubble bricks of different dimensions and connected to each other with earth mortar joints, without a good bond between the attached responds (lobes diameters between 45cm and 21cm).

To define the mechanical proprieties of the fire-bricks, five different cubic samples of the nucleus of the piers (4.9x4.9cm), fourteen samples of the side aisle walls (4.1x4.1cm) and five samples of east transept wall (4.8x4.8cm) were tested, giving rise to an average ultimate strength of about 7.9MPa (CV=2.9%) and an average density  $\gamma=1660 \text{ daN/m}^3$  (CV=3.4%). Three point bend test (Fig.5.3.7) was used to measure the Young's modulus, E, of brick,  $\mu_E=1380 \text{ MPa}$ . Considering 2250N the maximum applied vertical force (brick length equal to 38cm, brick wide equal to 20cm, and brick thickness 6cm) the bending moment is  $M=22.5 \times 38/4=213.8 \text{ kgcm}$ , the inertial force is  $I=(1/12)bh^3=(1/12)20 \text{ cm} \times 6^3 \text{ cm}^3=360 \text{ cm}^4$ , compressive strength is  $f_m=(M/I)v=(214 \text{ kgcm}/360 \text{ cm}^4)3=17.8 \text{ kg/cm}^2$ .

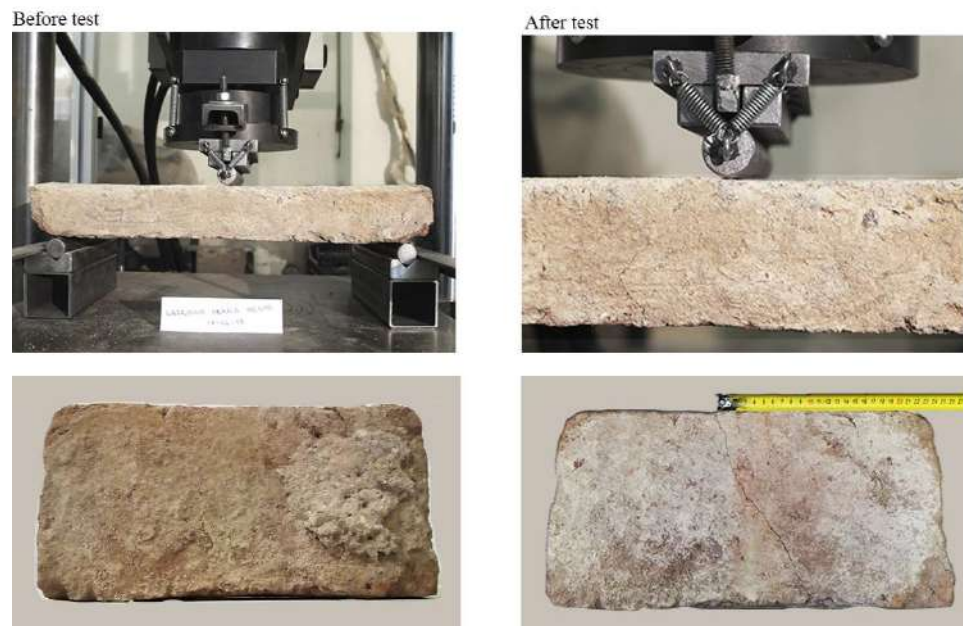


Figure 5.3.7– Three point bend test of brick.

Moreover, mineralogical and physical characterization of brick and mortar samples has been carried out. As regards bricks of the side aisle masonry walls (B1 and B2), and the nucleus of the piers (B2) three samples were collected. With respect to mortar joints of the side aisle masonry walls (M1, M2, M3), and the nucleus of the piers (M4), four samples were tested.

The following analyses have been performed:

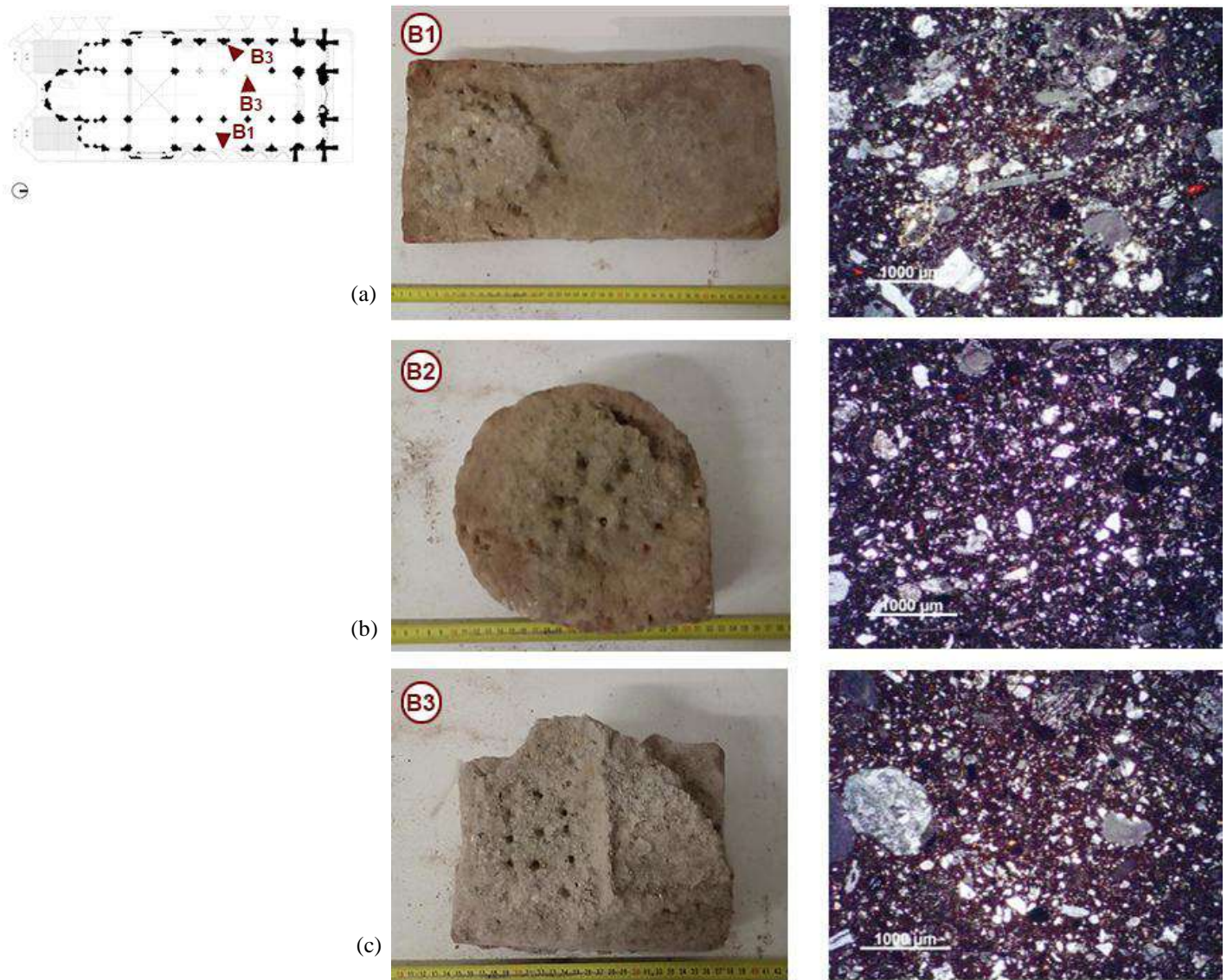
- Principal mineralogical composition was determined through powder X-ray Diffraction (XRD) (X'Pert diffractometer of PANALYticalcon antitode to copper) according to the following operating conditions: measuring range  $2\theta = 3-70$ , time for step = 60.325 sec, step size = 0.033, 40 KV, 30 mA.
- Clay minerals composition through powder X-ray Diffraction (XRD) was determined using the same instrument and scanning condition reported above.
- Granulometric analysis was carried out, according to NCh 2256-1-2001 and 165.
- Petrographic study, through observations thin sections in optical microscope in polarized transmitted light (Zeiss microscope AXIO Scope.A1).

Mineralogical analysis of the three bricks show that they are constituted by feldspar ((Al,B,Si) $4O_8$ ), quartz ( $SiO_2$ ), volcanic fragments (albite ( $Na(AlSi_3O_8)$ ), andesine ((Na,Ca)(Si,Al) $_4O_8$ )) and pyroxene (diopside sodian ( $CaMgSi_2O_6$ )). Quartz is present in a significant amount. The presence of other chemical compounds such as vanadium sulfate ( $VO_4$ ) was observed and is a common form of pathology, efflorescence (Martín del Río, 2014). The bricks are well cooked, as shown by the appearance of the groundmass that does not show signs of birefringence (index of low cooking temperature). Regarding the grain granulometry, always abundant, there are slight differences in the three bricks: the granulometry of B2 is fine and unimodal (200-300 $\mu m$ ), B1 is a little coarser but always unimodal (400-800 $\mu m$ ), and B3 is bimodal (prevalent 100-200 $\mu m$ , 700-800 $\mu m$ ).

Furthermore, the brick samples have included centimetric dimensions of a different clay mixture. The porosity is 33.78% (CV=0.08), but some difference can be observed, as for sample B3 that displays a higher porosity 36.3% (CV=0.03).

Table 5.3.1a summarizes principal results of analyses and, in Fig.5.3.8 thin sections of bricks and indication of sampling position are shown.

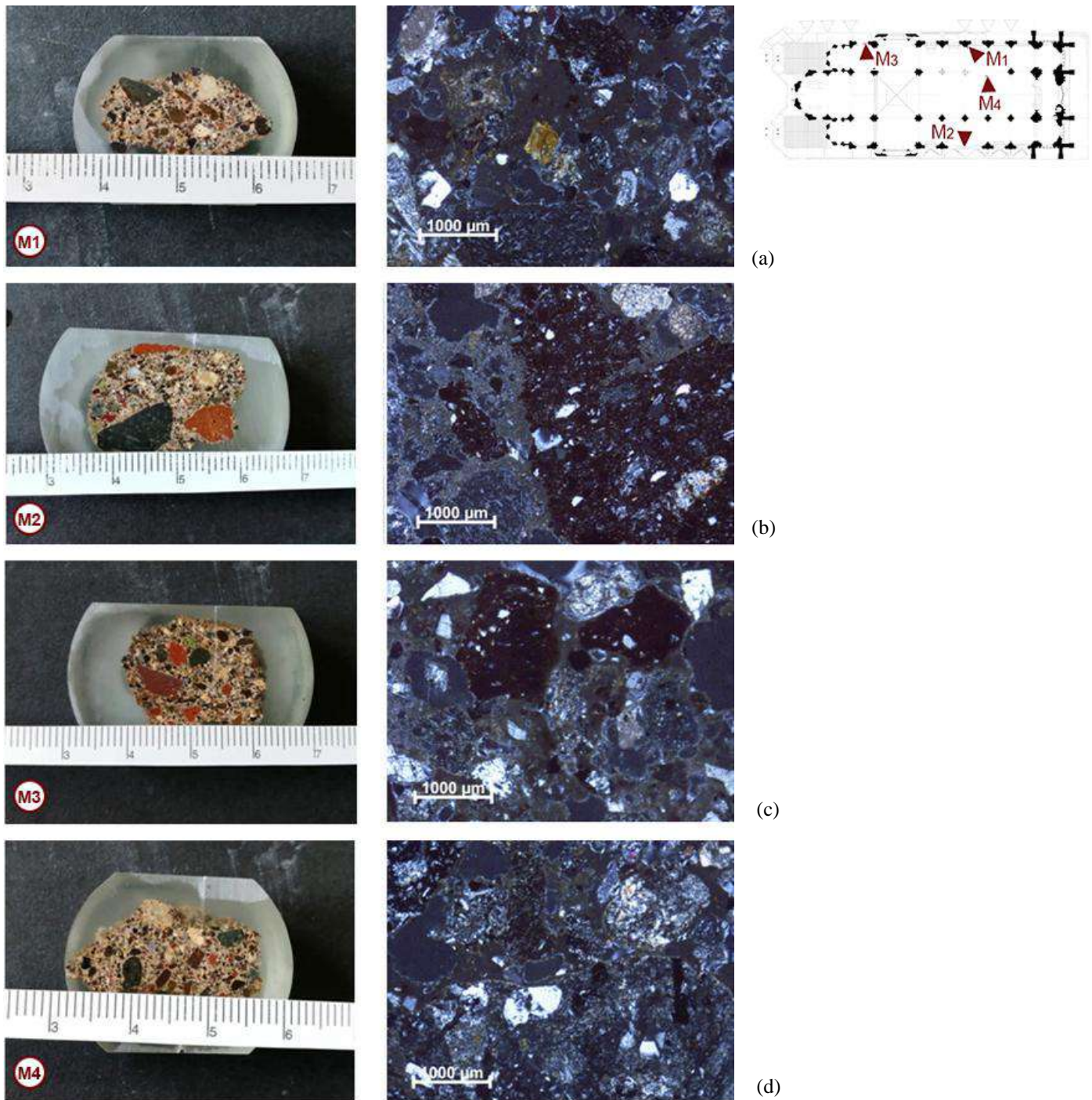
As regard the mortar samples (M1, M2, and M3) seems to have been made by mixing earth and lime (Fig.5.3.9). The mineralogical-petrographic study of the mortar samples showed that these consist of a particularly lean mixture (binder/aggregate 1/3-1/4) constituted by volcanic fragments (Andesine ((Na,Ca)(Si,Al) $_4O_8$ )), feldspars ((Al,B,Si) $4O_8$ ), and *cocciopesto*. The aggregate has a bimodal granulometry (prevalent 600-800 $\mu m$ , 1,5-3 secondary) with granules of a basically rounded shape, which indicates a fluvial origin. Compositions are predominantly of volcanic rock fragments compared to single granules. The presence of *cocciopesto* must also be reported except in the sample M1. The homogeneous distribution of the aggregate indicates that the mixture has been well mixed.



*Figure 5.3.8– Thin sections of brick samples.*

Furthermore, an extensive experimental analysis by PNT-G penetrometric test (Gucci&Barsotti, 1995) on a high number of mortar surfaces of the side aisles walls was carried out, providing a compressive strength of 1.4MPa. Based on these results, integrated with an M.Q.I. method (Borri et al. 2015) and with values suggested by the scientific literature (Tassios 1988; Hendry 1990), an estimation of mechanical features of brick masonry with lime mortar was assessed: compressive strength ( $f_{m,medium}=3.5\text{MPa}$ ), Young modulus ( $E_{medium} = 1380\text{MPa}$ ) and shear strength ( $\tau_{0,medium}=0.05\text{MPa}$ ), in agreement with Chilean Standard (INN, 2013). Additional laboratory tests, performed after the 2010 earthquake by (Joannon et al., 2003), have confirmed these values. As regards irregular brick masonry with earth mortar joints, characterized in the polylobate columns of the central nave, compressive strength equal to 1.0MPa ( $f_{m,min}$ ), Young modulus equal to 600MPa ( $E_{min}$ ) and shear strength equal to 0.025MPa ( $\tau_{0,min}$ ), have been assumed according to the requirements of the Chilean preliminary Code of

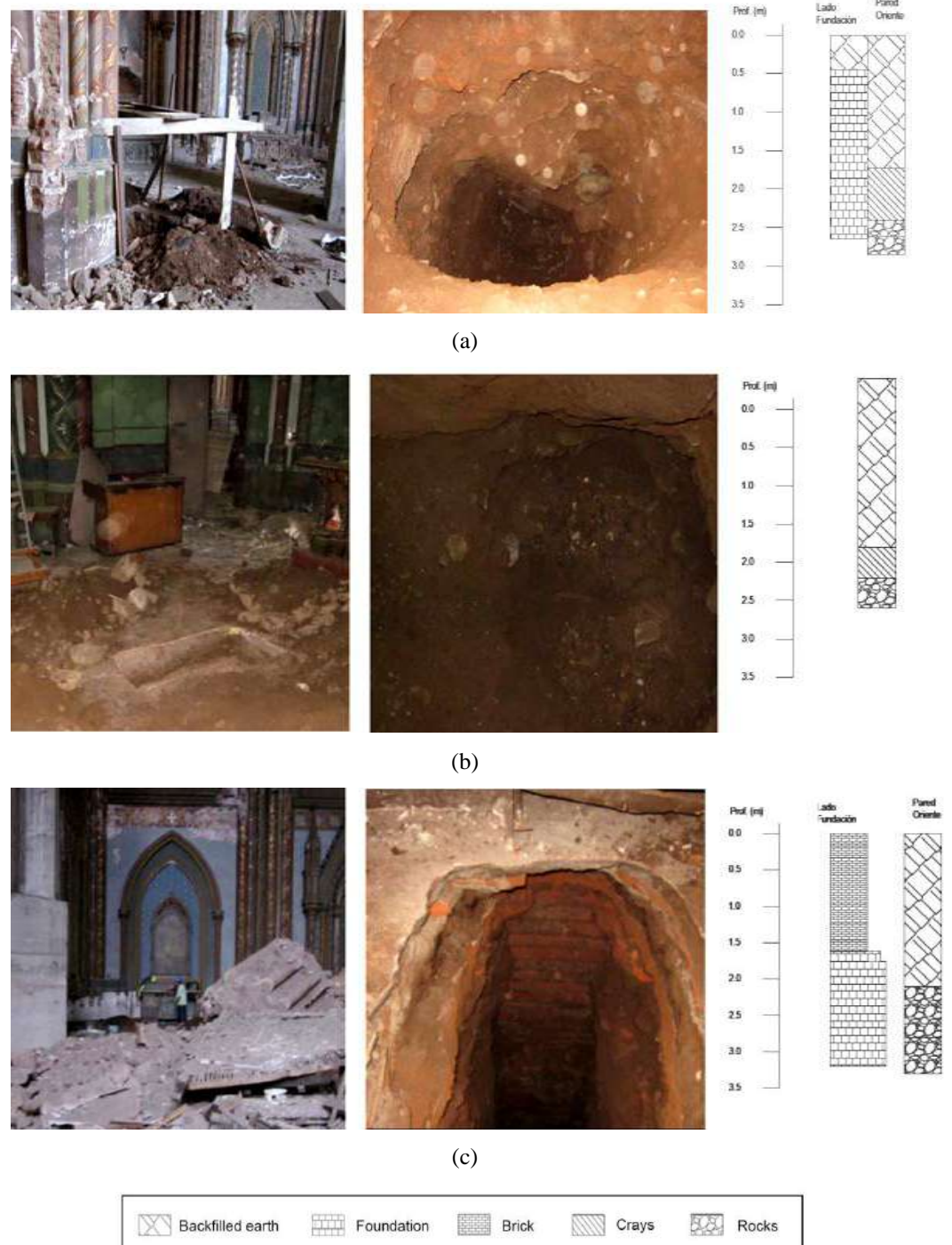
Intervención Estructural en Construcciones de Valor Patrimonial - Construcciones Históricas  
(INN, 2013).



*Figure 5.3.9– Thin sections of joint mortar samples.*

Finally, with the aim of characterize the soil mechanics and the foundation type, three excavations (Fig.5.3.10) located in the west side aisle [E1], the central nave [E2] and the east minor apse [E3], with a depth of 2.85m, 3.0m and 3.3m, were carried out by (DICTUC, 2013).

Based on the Chilean Code NCH433 of 96 (INN, 1996) and D.S.61, 2011 (MINVU, 2011), the soil having very dense and stable ground,  $V_{s30} > 500$  ms<sup>-1</sup>, was classified as soil type B, with soil coefficient  $S=1$ .



**Figure 5.3.10** –Localization and soil stratigraphy of (a) excavation E1 in the west side aisle; (b) excavation E2 in the central nave; and excavation E3 in the east minor apse, (DICTUC, 2013).

The foundation profundity measure was about 2.65m. The embedding of the foundation measured in the gravel was 25cm, consisting of quarry blocks of different shapes and

dimensions (about 8"), and sand filling part of the gaps between blocks. The stratigraphy of excavations is shown in Fig.5.3.10.

### 5.3.3 Assessment of crack patterns

Throughout its history, the *Basilica del Salvador* has suffered extensive and severe structural damages due to its inherent slenderness and constructional typology particularly sensitive to earthquake loading, as shows (De Matteis, 2007) in which the structural behavior of Gothic buildings in zones of low and moderate seismicity is analyzed.

The crack pattern of the monument is the result of the cumulative and non-repaired structural failures suffered following the several earthquakes of the 20<sup>th</sup> and 21<sup>th</sup> centuries in central Chile (as Valparaíso in 1906, Mw8.2; Algarrobo in 1985, Mw7.8; and Maule in 2010, Mw8.8). Moreover, the lack of maintenance and constant exposure to atmospheric agents has further worsened the precarious state of conservation of the church.

A first summary assessment of the damage state was performed by (Moll & Sabanech, 1976) and a more detailed survey was realized by E. Joannon in 2005 (CMN, 2005). From the analysis of both researches, the following structural weaknesses emerge:

- the in-plane capacity of transverse arcades;
- the absence of box-behavior of the structure, basically, determined by the lack of transverse connections between the longitudinal walls of the central and side aisles;
- the high conventional slenderness ( $\lambda_c = 16.8$ ) of the walls;
- the inefficient connections between wall and roof;
- the absence of rigid horizontal diaphragm.

To evaluate the severity of the damages at the current state, the crack pattern has been analyzed according to the dominant behavior of macro-elements of churches with basilica plan in the longitudinal and transverse directions, according to (Giuffrè 1991; Doglioni, Moretti, and Petrini 1994; Lagomarsino and Podestà 2004B; da Porto et al. 2010).

The most vulnerable structural sub-systems (macro-elements) have been identified and the following failure modes have been considered: (i) the in-plane behavior of the transverse arcades of the east side aisle and of the narthex; (ii) the punching mechanism of the wall of the west side aisle; and (iii) the out-of-plane behavior of the central apse, the laterals apses, the side aisles walls, the outer gallery walls, and the external transept walls.

- (i) Concerning the in-plane behavior, the activation of four-hinge collapse mechanisms has been detected in all the transverse arcades of the side aisles (Fig.5.3.11). As predicted by the theoretical models (Romano&Ochsendorf, 2009; Misseri&Rovero, 2017), this failure depends fundamentally on the thickness of arch (defined by the ratio of the thickness compared to the pointed radius,  $t/R_{point}$ , and the ratio of the eccentricity compared to the circular radius,  $e/R_{circ}$ ) and on the angle of embrace ( $\alpha$ ). In fact, the transverse arcades of the Basilica present a

thin pointed arch ( $t/R_{\text{point}}=0.143$ ;  $e/R_{\text{circ}}=0.536$ ) with a large angle of embrace ( $\alpha=90^\circ$ ), consistently with the values proposed in (Romano&Ochsendorf, 2009). These collapse phenomena were recorded in several neo-gothic churches of Santiago, made up in fire-brick: San Saturnino, Santa Filomena, Los Sacramentinos, San Pedro churches (CMN, 2008; 2010; 2014). All these buildings have reported deep cracks in the intrados at the crown and at the base extrados of the arches, developing the activation of the in-plane mechanisms of the arcades. Generally, the collapses occurred due to the formation of fourth hinge or to the sliding. As confirmed by historical sources (Berg et al., 1996), the in-plane mechanisms that have involved the transverse arcades of the Basilica del Salvador were iterative, relapsing and had triggered degenerative processes. At the current state all the transverse arches, which connected the walls of the aisles to those of the central nave, are collapsed together with the arches of the longitudinal west wall.



**Figure 5.3.11** -Collapses of the transverse arches and arches of the longitudinal west wall.

The first arches had already begun to crack after the 1906 earthquake; therefore, metal strips in galvanized iron ("confinement") were introduced for connecting the outer and inner walls of the west aisle (Figure 5.3.6).

Being the transverse arcades formed by thrusting arcs (without chains), the occurrence of these mechanisms have been conditioned by the eccentricity of the loading resultant at the base of the piers, already under static conditions.

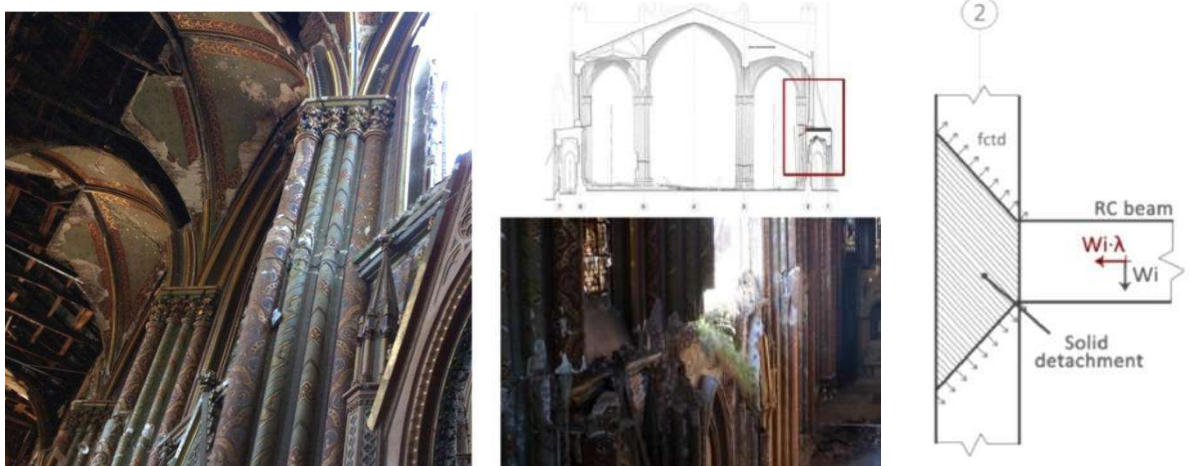
In relation to the in-plane behavior of the transverse arcade-walls of the narthex, dangerous disconnections occurred in the arches system during past seismic shake, both in the 1985 and 2010 earthquakes. If on one hand, the RC slab

located above the arches of the narthex (beams  $1\text{m} \times 1.5\text{m}$  and slab thickness  $25\text{cm}$ ) has improved the connection between the façade and the orthogonal walls, on the other, together with the RC tympanum, the different properties of concrete-masonry have represented an additional mass on the top of the building (Fig.5.3.12). During the mentioned seismic motions, these additional masses have proved negative effects to the structure, increasing the earthquake-induced inertia forces, severely damaging the underlying arches and determining the collapse of the central arc.



*Figure 5.3.12 - RC slab located above the arches of the narthex*

- (ii) As concerning the outer wall of the east aisle, the punching of the RC beams (characterized by higher stiffness than the masonry structure and located in correspondence to the outer cover gallery) has generated a state of strength on the masonry that have determined a portion of masonry in proximity of the contact surface to detach. The masonry that is detached has a truncated pyramidal shape with an inclination of approximately  $45^\circ$  (Fig.5.3.12).



*Figure 5.3.12 –Punching mechanism in the east aisle generate by RC beams*

As a consequence of the activation of the punching mechanism, the two central macro-elements were collapsed in two distinct times (after de Maule earthquake in 2010, and then in 2014), due to static instability. The condition of the two remaining macro-elements is highly unstable, indeed emergency works and safety measures to prevent further collapses were required.

About the seismic response of the side aisles walls, three different types of mechanisms have been detected, due to the structural asymmetries generated by post-earthquake retrofitting interventions: the in-plane, out-of-plane and the punching mechanisms.

- (iii) About the outer wall of the west aisle, the deep vertical cracks in the keystone of the windows, the absence of a ring-beam, the discontinuities between the narthex and transept walls, and a deep horizontal crack along the entire length of the nave (in coincidence of the outer cover gallery), show the decomposition of the upper part of masonry in four independent sub-portions. While, the out-of-plane behavior of two macro-elements in proximity of the narthex, is apparently in its outward rotation ( $\theta \sim 2^\circ$ , Fig. 5.3.12), the in-plane behavior of two macro-elements in proximity of the transept is guaranteed by the chains which bind the portions of masonry to the pillars in RC. In relation to the out-of-plane behavior of the central apse, the ring-beam in RC has averted the apse disassemble into further macro-elements preventing the activation of the simple overturning, as it has occurred in the minor apses (Fig. 5.3.13).

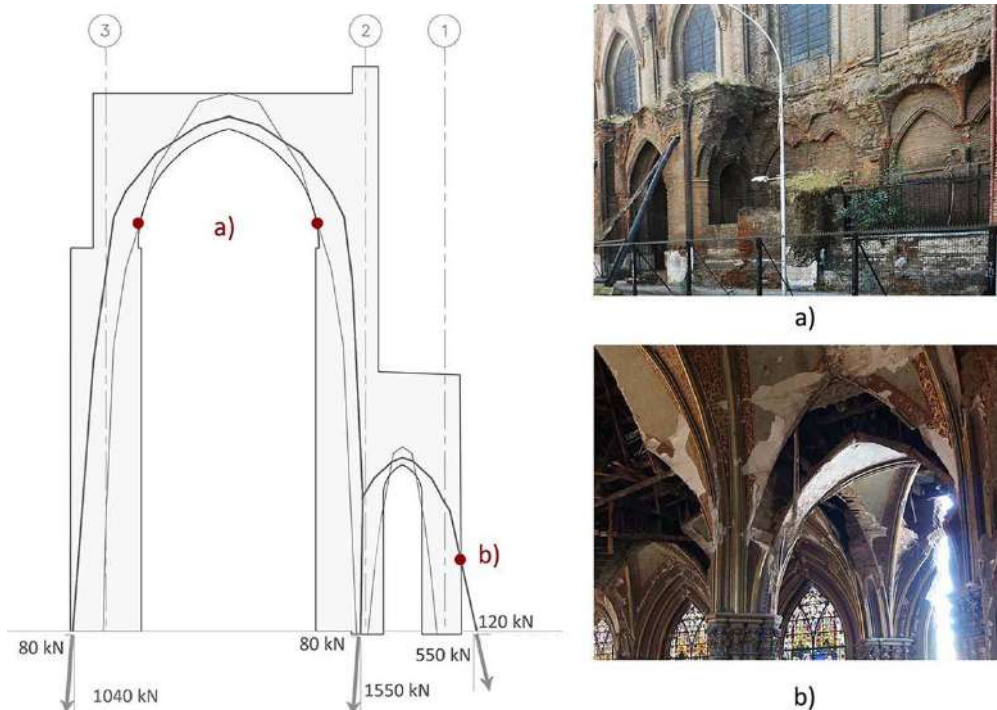


**Figure 5.3.13** - Deep cracks in the lateral apses (a) and (b), and in the central apse (c).

The out-of-plane behaviors of the external walls of the east and west gallery are associated with worryingly horizontal fractures along their entire length, present in the intrados of the firebrick vaults, indicating a separation of the external walls of the side aisles.

### 5.3.4 Structural analysis

The Chilean Codes for the evaluation and mitigation of seismic risk, the NCh433 (INN 1996) and the NCh2745 (INN 2013a), do not provide requirements for the assessment of the seismic behavior of existing non-confined-masonry buildings. Furthermore, the Standard for the Structural Intervention of Earthen Historical Buildings, NCh3332 (INN 2013b), provides generic criteria for the consolidation and restoration of the adobe constructions. Thus, in order to determine the structural safety of the Basilica, multi-level analyses that embrace local and global behavior have been employed, and the main collapse modes have been analyzed according to the prevision of the Italian Code NTC2008 (MIT 2008), Circ.617/2009 (MIT 2009) and the Guidelines of Cultural Heritage (BBCC, 1997; 2006), combined with Chilean Codes.



**Figure 5.3.13.** Thrusts line of wall portion in interception of longitudinal walls 3, 2 and 1, and transverse arcade D.

The results described in previous Sections (5.3.2 and 5.3.3) suggest that the analyses should be focused on the recurring failure modes of the observed macro-elements, which have exhibited significant damage during the past seismic events. With the aim of assessing the vulnerability

levels of identified macro-elements, considering the punching mechanisms, the out-of-plane and the in-plane behaviors, linear (LKA) and incremental (IKA) kinematic analyses were conducted. Moreover, a control on the global response of the church has also been carried out to define preferential displacement shapes. The global response of Basilica del Salvador has been addressed through nonlinear Dynamic Analyses of a 3D FE model with the commercial code STRAUS7. For a preliminary investigation of the static conditions of equilibrium of the Church, before to the collapses of the arches, the graphical statics analysis for vertical loads has been carried out on a representative transverse arcade of the original configuration, through the Safe Theorem of Limit Analysis (Heyman 1966). The thrust line (path of the resultants of the compressive forces) contained inside the masonry structure represents a possible equilibrate solution and is compatible with a safe condition for vertical loads. Fig.5.3.14 shows two potential internal thrust lines that allow a quick visualization of the precarious state of equilibrium of the structure, highlighting the limited condition for the stability at the bases of columns and at the springs of arches, as expected from direct surveying activities.

#### **5.3.4.1 Linear and non-linear kinematic analysis for the out-of-plane capacity**

The layout of the mechanisms that are most likely to be activated in the Basilica del Salvador has been defined for the current state and state one previous the RC consolidations. The selected macro-elements are shown in Fig.5.3.15.





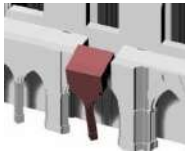


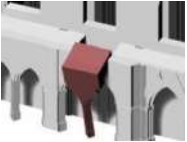

**Figure 5.3.15** - Identification of local mechanisms of collapse in the current state of Basilica.

In fact, the past seismic behaviors indicated by still visible “scars”, has to be correlated with the possible future behaviors since the damage pathology related to the earthquake has a progressive and relapsing character (Doglioni, Moretti, and Petrini, 1994).



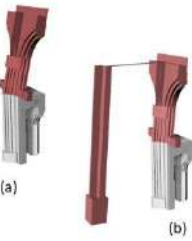


The main collapse failures detected in the Basilica at the current state are shown in Table 5.3.1, and the mechanisms characterized the state before the RC consolidations were analyzed in Table 5.3.2.

**Table 5.3.1** - Results of Linear Kinematic Analysis before the RC interventions: Kinematic multiplier  $\alpha_0$ , Participating Mass  $M^*$ , Mechanism Activation Acceleration  $a_0^*$ , equation (5.2) for the Demand Acceleration at ground level,  $Dag$ , equation (5.3) for the Demand Acceleration at elevated level,  $Dal$ .

ID	Mechanism Type	State Before RC interventions	$\alpha_0$	$M^*$ [kN]	$a_0^*$ [m/s <sup>2</sup> ]	$Dag$ [m/s <sup>2</sup> ]	$Dal$ [m/s <sup>2</sup> ]
APc1	Compost overturning		0.11	84.9	0.811	2.61	2.37
APc2	Compost overturning		0.088	50.9	0.654	2.61	2.37
APc3	Compost overturning		0.087	49.1	0.645	2.61	2.37
APc4	Compost overturning		0.108	82.4	0.796	2.61	2.37
APe-w1	Compost overturning		0.106	26.4	0.78	2.61	2.37
APe-w2	Compost overturning		0.084	22.2	0.62	2.61	2.37
APe-w3	Compost overturning		0.081	25.3	0.6	2.61	2.37
SAw1	In-plane mechanism		0.13	199.2	0.95	2.61	-
SAw2	In-plane mechanism		0.13	199.2	0.95	2.61	-
SAw3	In-plane mechanism		0.13	199.2	0.95	2.61	-
SAw4	In-plane mechanism		0.13	199.2	0.95	2.61	-
SAe1	Punching mechanism		0.117	125.59	0.852	-	-
SAe2	Punching mechanism		0.117	125.59	0.852	-	-
SAe3	Punching mechanism		0.117	125.59	0.852	-	-
SAe4	Punching mechanism		0.117	125.59	0.852	-	-
EAw1	Simple overturning		0.112	51.8	0.81	2.61	-
EAw2	Simple overturning		0.076	21.1	0.55	2.61	-

EAe1	Simple overturning		0.092	52	0.68	2.61	-
EAe2	Simple overturning		0.076	21.1	0.55	2.61	-
NA	In-plane mechanism		0.21	1565.2	1.64	2.61	-

**Table 5.3.2** - Results of Linear Kinematic Analysis of current state: Kinematic multiplier  $a_0$ , Participating Mass  $M^*$ , Mechanism Activation Acceleration  $a_0^*$ , equation (2) for the Demand Acceleration at ground level,  $D_{ag}$ , equation (3) for the Demand Acceleration at elevated level,  $D_{al}$ .

ID	Mechanism Type	State Current	$a_0$	$M^*$ [kN]	$a_0^*$ [m/s <sup>2</sup> ]	$D_{ag}$ [m/s <sup>2</sup> ]	$D_{al}$ [m/s <sup>2</sup> ]
APc	Compost overturning		0.311	201.2	2.29	3.14	2.37
APe-w1	Compost overturning		0.106	26.4	0.78	3.14	2.37
APe-w2	Compost overturning		0.084	22.2	0.62	3.14	2.37
APe-w3	Compost overturning		0.081	25.3	0.6	1.96	2.37
SAw1	Simple overturning		0.089	83.1	0.668	3.14	-
SAw2	Simple overturning		0.087	91.4	0.652	3.14	-
SAw3	In-plane mechanism		0.12	143.8	0.93	3.14	-
SAw4	In-plane mechanism		0.12	143.1	0.94	3.14	-
SAe1	Punching mechanism		0.117	125.59	0.852	3.14	-
SAe2	Punching mechanism		0.117	125.59	0.852	3.14	-
EAw1	Simple overturning		0.112	51.8	0.81	3.14	-
EAw2	Simple overturning		0.076	21	0.55	3.14	-

EAe1	Simple overturning		0.092	52	0.68	3.14	-
EAe2	Simple overturning		0.076	21.1	<b>0.55</b>	3.14	-
NA1	In-plane mechanism		0.19	771.1	1.49	3.14	-
NA2	In-plane mechanism		0.22	739.8	0.94	3.14	-

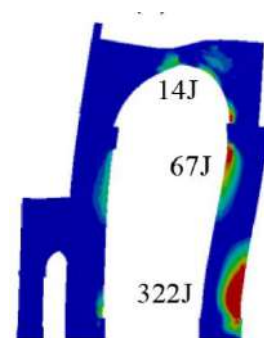
As introduced previously, the damages of the church can be essentially interpreted as the activation of three fundamental collapse mechanisms (i) the in-plane, (ii) the out-of-plane, and (iii) the punching mechanisms.

- (i) Concerning the in-plane response, at the current state, the transverse behavior of the west side aisle, SAw3-4, and narthex arcade walls, NA1-2, was analyzed taking into account the position of the disconnections (convencional hinges), as shown in Fig.5.3.17 and 18. In SAw3-4 most severe configuration (Fig.5.3.17a), the hypothesized seismic action induces clockwise mono-lateral rotation of columns piers and the upper part of the west sidewall, while in NA1-2 the configuration (Fig.5.3.18a) produces clockwise mono-lateral rotation of piers and a consequent counterclockwise rotation of upper blocks.

The 3D nonlinear ANSYS model by (Rendel et al., 2014) confirms the identified position of hinges (Fig.5.3.19), where cracking due to tensile stresses occurred. In particular, the Saw3 configuration is characterized by equivalent accumulated plastic strain energy at base of column is equal to 351J, at top of 88J, and in the intrados of the arch crow to 13J.

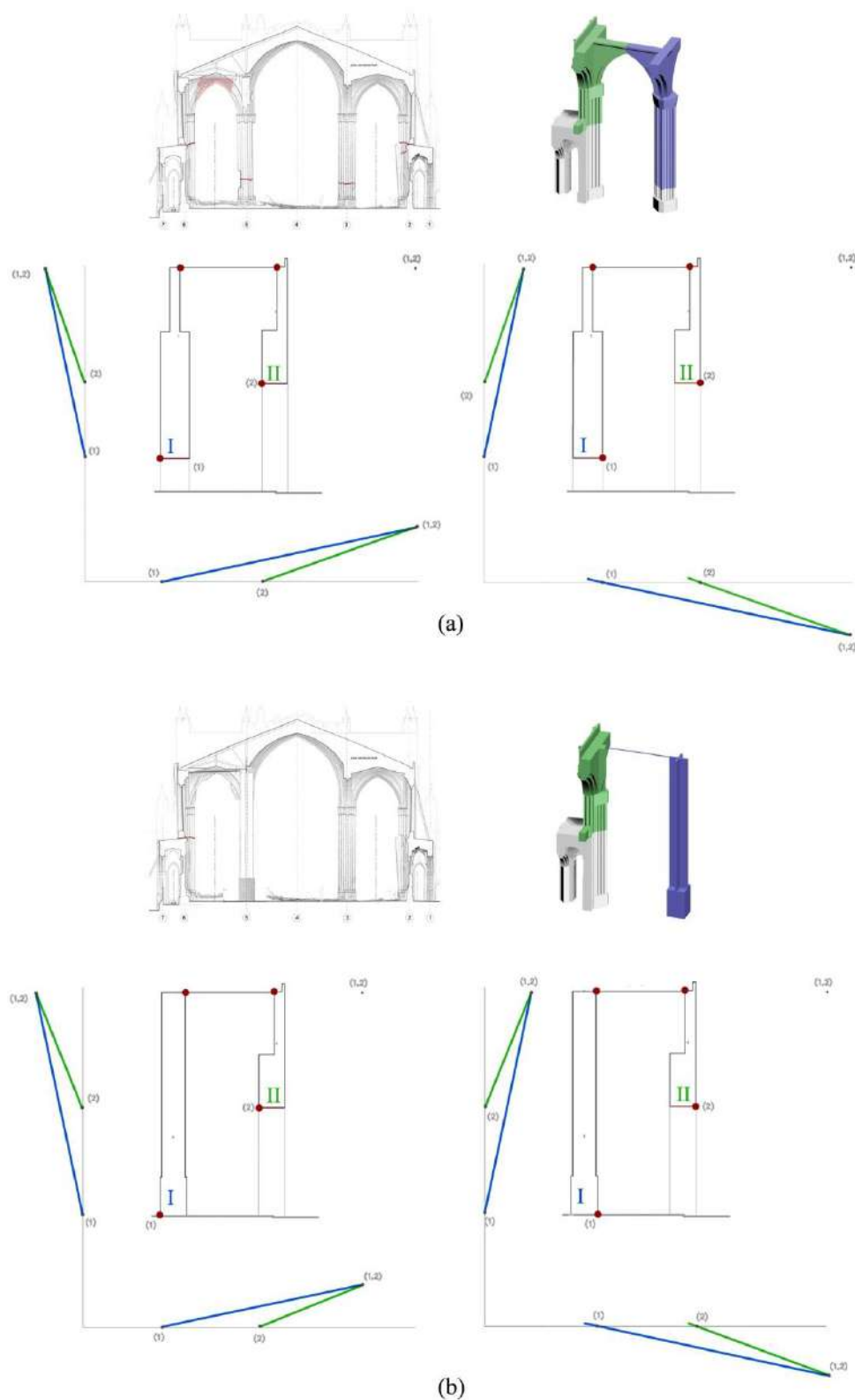
- (ii) All out-of-plane failures detected at the present state are identified in (Fig.5.3.15). The mechanisms represent the simple overturning of the rigid sub-blocks that made up the west side aisle, SAw1-2; the central, west and east lateral apses, APc, APe-w1, APe-w2, APe-w3, around cylinder hinge placed 8.5m off the ground at the level of the external gallery roof. The macro-blocks, that composed the outer walls of the gallery, EAw-e1 and EAw-e2, rock around cylinder hinge placed at ground level.

The central apse presented a different layout mechanism due to the absence of a ring-beam that has generated the decomposition of masonry in four independent sub-portions, APc1; APc2; APc3 and APc4.



**Figure 5.3.19 –**  
Equivalent  
accumulated plastic  
strain for arch  
(Values correspond to  
the total plastic strain  
energy [Joules] at the  
base and top of the  
column and the arch).

The main modes of vibration evaluated through FEM (frequency equal to 1.17Hz, 1.50 Hz and 1.71 Hz) underline the intrinsic vulnerability of the Saw1 and 2 configuracions, confirm the position of the identified disconnections.



**Figure 5.3.17** – In-plane mechanism of the transverse arcade of the side aisles: (a) SAw-e (original configuration) west and east side aisles; and (b) SAw3-4 (current state) west side aisle.

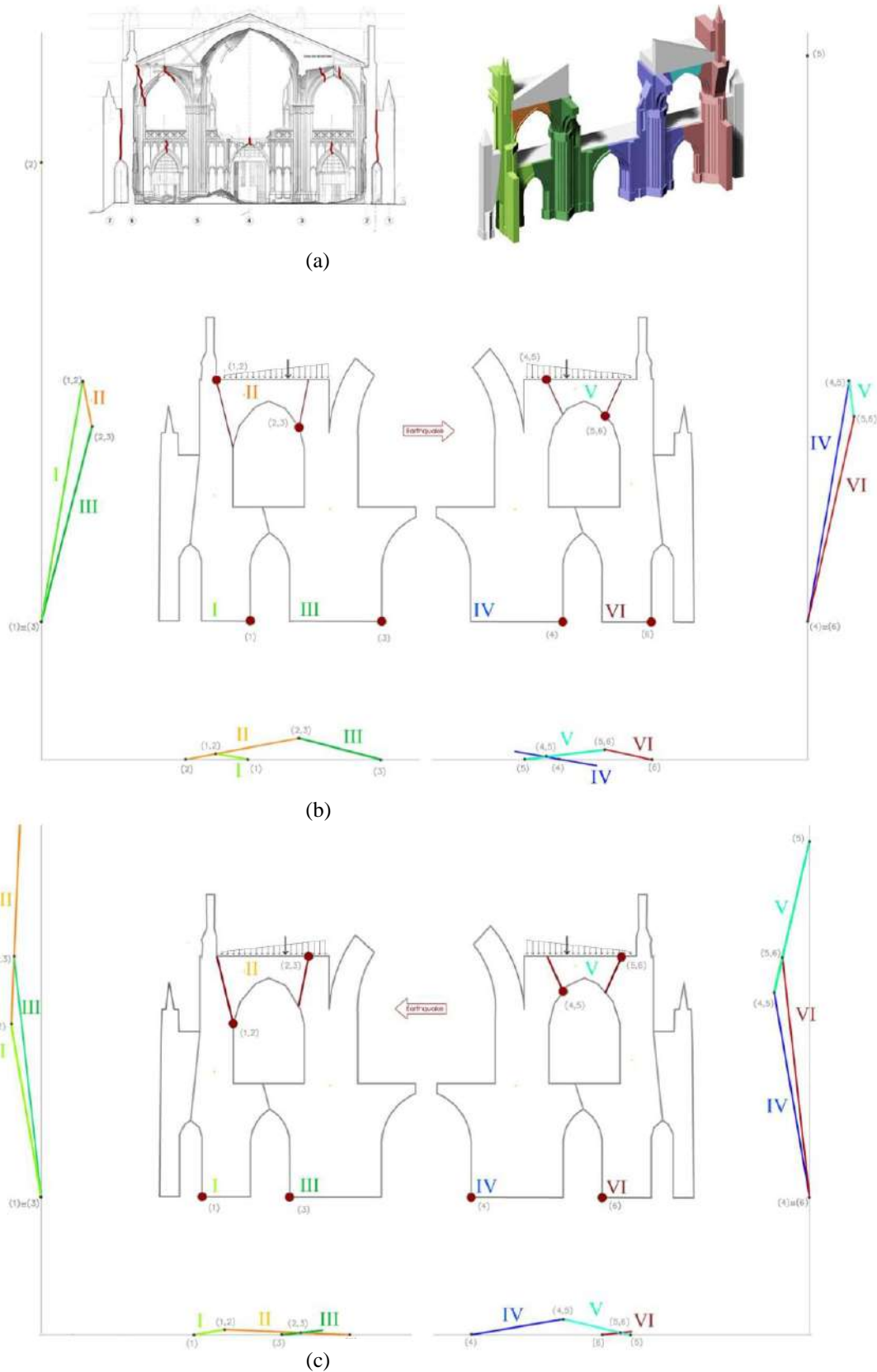


Figure 5.3.18– In-plane mechanism of the transverse arcade of the Narthex at the current state.

- (iii) Finally, dangerous punching mechanisms have been detected in the walls of east side aisle, SAe1-2-3-4. The RC beams introduced in 1906 in the extrados of the gallery arches, which are punching the wall of the east side aisle, have generated on the masonry a state of strength which determined a portion of masonry in the proximity of the contact surface to detach (Fig.5.3.11). The masonry that is detached has a truncated-pyramidal shape with an inclination of the sidewalls of approximately  $45^\circ$ . As effect of the force  $F$  ( $W \cdot \lambda$ ), transmitted from the beam on the detachment surface, a state of tensile stress is generated ( $f_{ctd}$ ). As long as the tension is lower than the limit, the system is in equilibrium. For strength values higher than the limit, it takes place the separation of the truncated-pyramidal block.

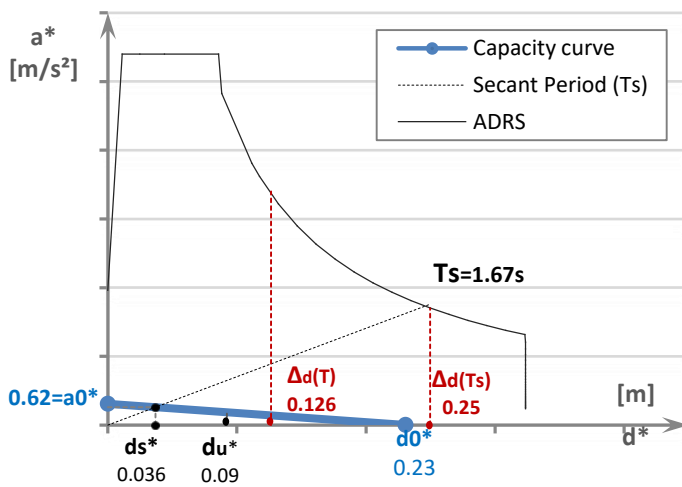
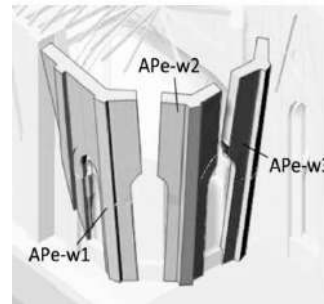
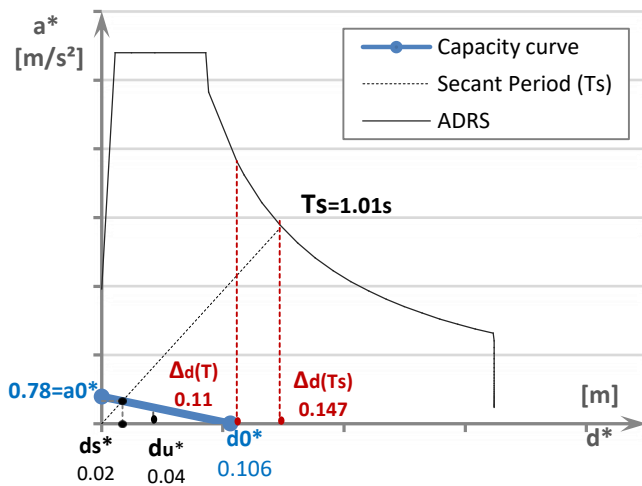
After having defined mechanism layouts and the forces involved in the failure, the kinematic multiplier of the horizontal equivalent forces producing the activation of the mechanisms,  $\alpha_0$ , has been evaluated according to Equation 5.1. Then,  $\alpha_0$  has been converted into acceleration capacity,  $a_0^*$ , according to the codified procedure (MIT, 2009; POLIMI, 2010; Sorrentino et al., 2017) based on the Equation 5.1.

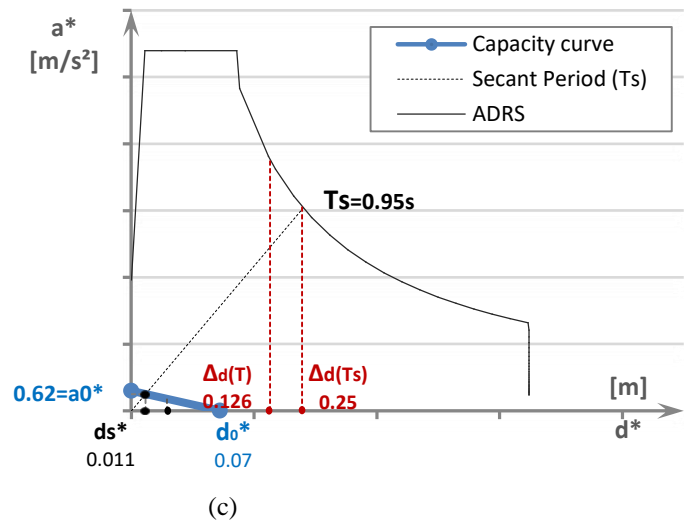
From a comparative analysis of the current state and the state prior to 1985, the mechanism that involves the central apse shows a significant improvement of the seismic response of the APc macro-element due to the introduction, after the Algarrobo earthquake, of the RC ring-beam (Fig.5.3.2). This retrofit leads to an unsatisfactory safety assessment for the current state, owed to a varied mechanism shape. On the contrary the collapse of two arches in the west side aisle, axes D and E, following Maule 2010 earthquake have determined a varied configuration of the failures type of the sub-blocks, SAw1 and SAw2, and a worsening of the resistant behavior that features the current state. The collapses of the two arches and columns, axis F and G, after the 1985 earthquake and the consequent rebuilding of the pilars in RC and the introduction of the tie-rods, have determined the varied mechanism shape of the transverse arcades of the west side aisle, macro-elements SAw3 and SAw4, evidencing a minimum reduction of the in-plane response capacity. At the present, the most dangerous condition of damage is represented by the static instability that features the sub-blocks of the east side aisle, SAe1 and SA2, which has already determined the collapse, even in absence of the seismic actions, of the macro-elements SA3 and SA4. The insertion of the RC beams in the outer gallery cover has greatly weakened both the outer wall of the east aisle and the gallery, due to exceeding the limit of the tensile strength of masonry in the first case and the reduction of the resisting transverse section in the second case.

In order to obtain a more accurate assessment of the expected seismic response in relation to the analyzed kinematics (local mechanisms), the tests have been also conducted through incremental kinematic analysis, IKA, in terms of pushover curve (Sorrentino et al., 2017). The capacity curve has been obtained assessing the decrease of the kinematic multiplier,  $\alpha$ ,

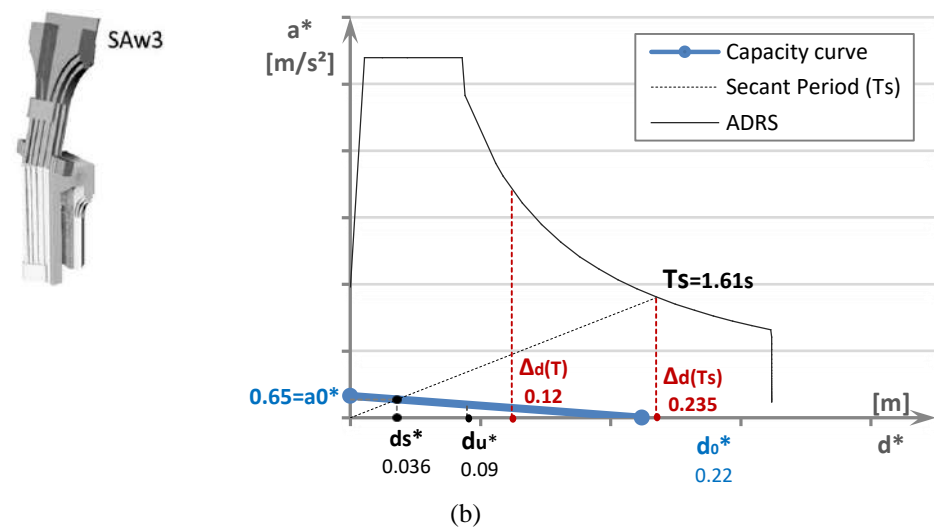
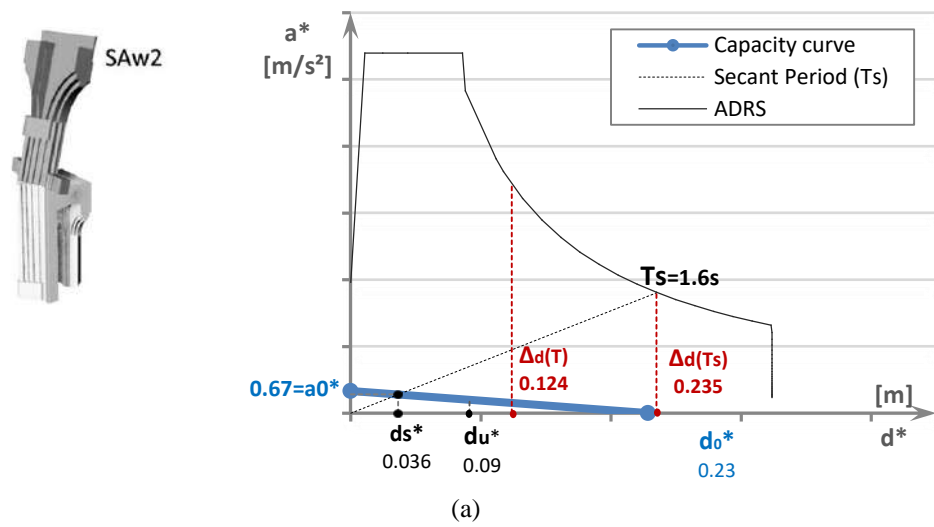
estimated applying the Virtual Work Theorem through the eq. (5.6) and the increase of the displacement  $d_k$  of a control point for any varied configurations of the kinematic chain representatives of the mechanism's evolution. From the unchanged initial configuration, a succession of finished displacements has been applied, and the multiplier associated with each varied configurations has been obtained.

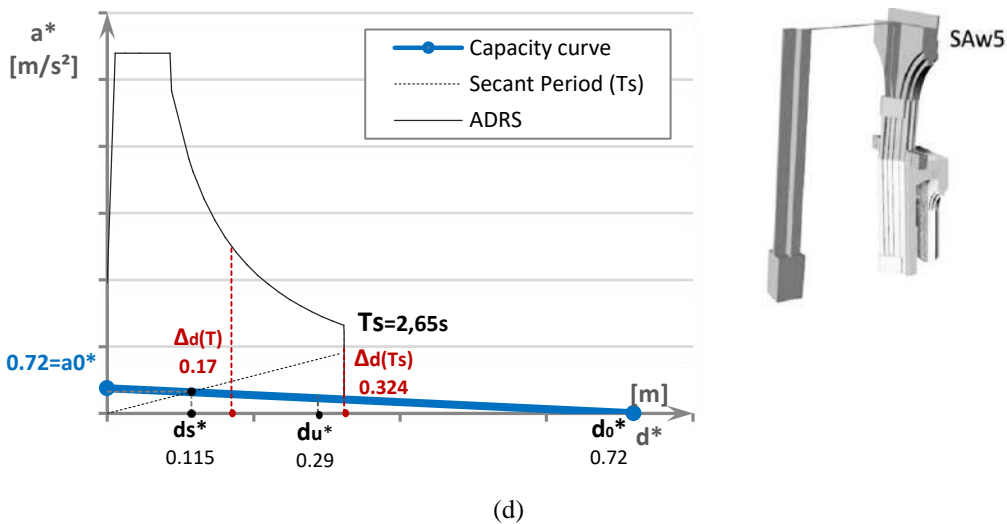
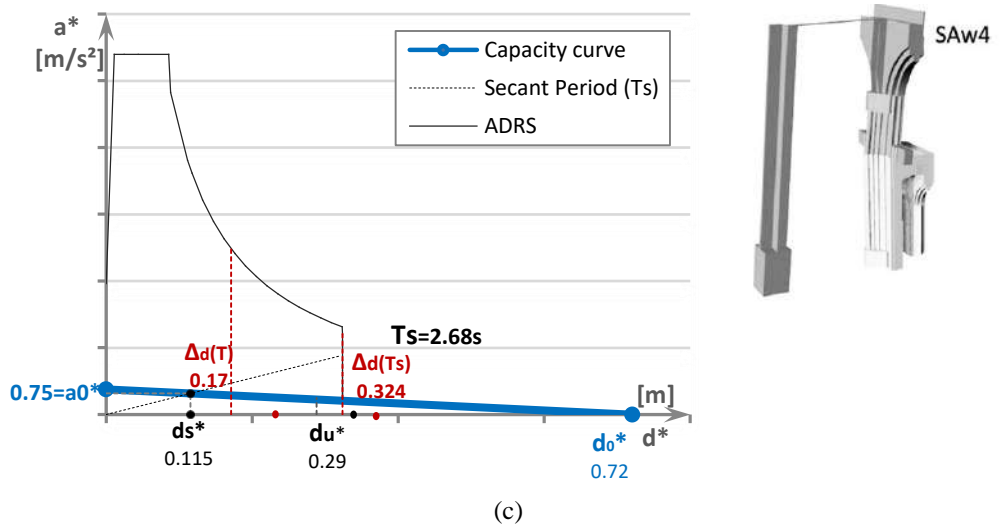
From the comparison between the displacement Capacity and Demand, eq. (5.9), of each mechanisms analyzed, the checks no are satisfied (Fig. 5.3.19, 20 and 21). The Capacity Spectrum highlights the limit condition in terms of displacement of the all macro-elements, coming to collapse. The damage scenario is in concord with the crack pattern annotated during the surveying.



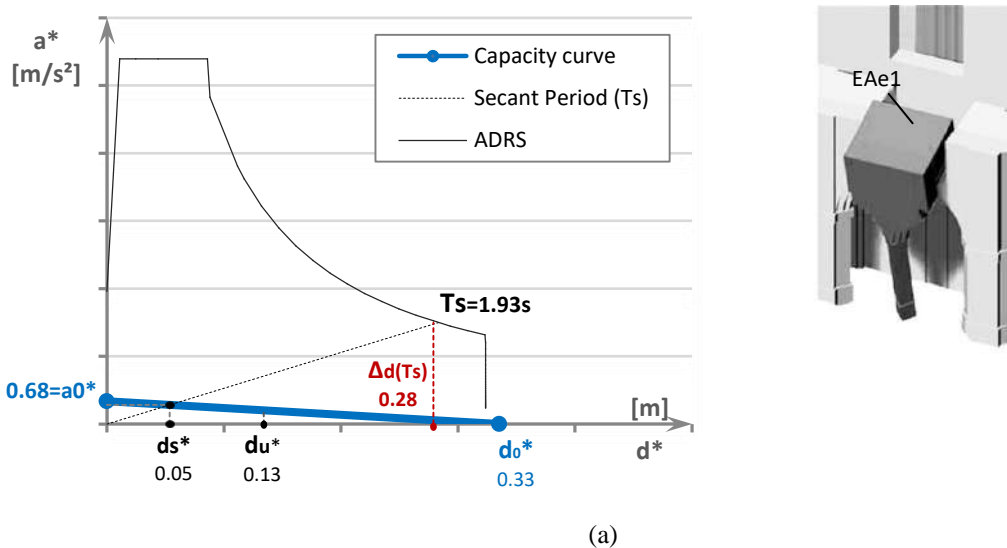


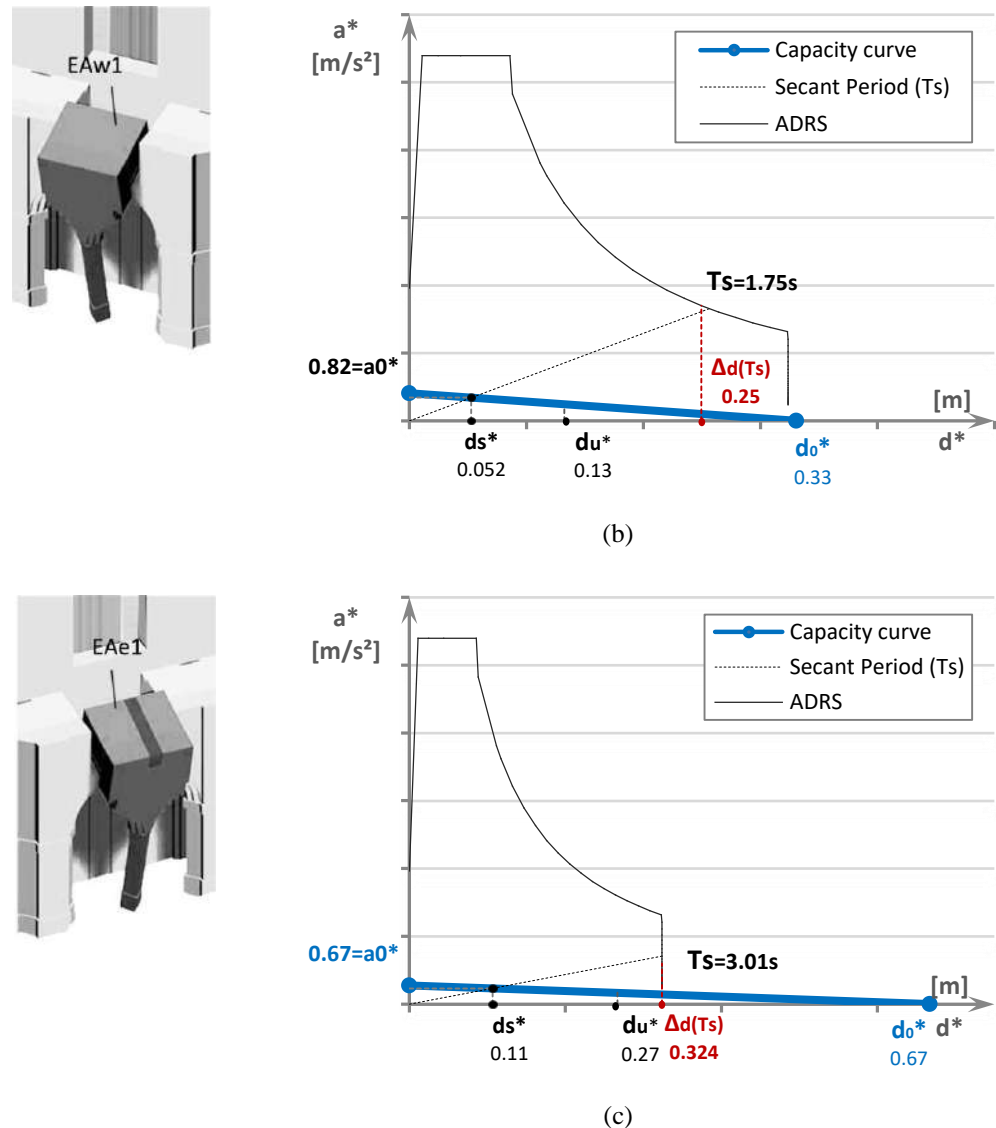
**Figure 5.3.19-** Capacity and demand curves of incremental kinematic analysis of the three sub-portions of the lateral apses: (a) Ape-w1 (b) Ape-w2 and (c) Ape-w3; and Acceleration Displacement Response Spectrum (ADRS) according to Nch2745Of.2013.





**Figure 5.3.20** - Capacity and demand curves of incremental kinematic analysis, four sub-portions of the west side aisle wall: (a) SAw1 (b) SAw 2, (c) SAw 3, and (d) Saw4; and Acceleration Displacement Response Spectrum (ADRS) according to Nch2745Of.2013.





**Figure 5.3.21-** Capacity and demand curves of incremental kinematic analysis, three sub-portions of the west and east external gallery: (a) EAe-w2, (b) EAw 1, and (c) EAe1; and Acceleration Displacement Response Spectrum (ADRS) according to Nch2745Of.2013.

#### 5.3.4.2 Global response models

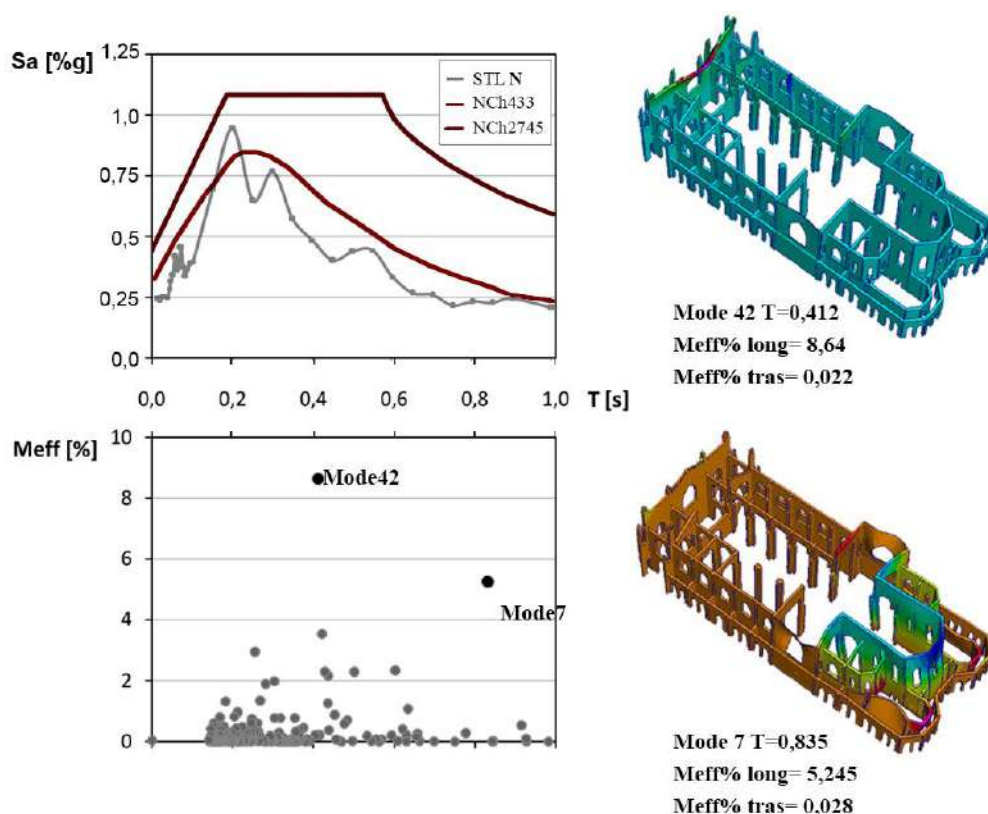
With the aim of obtaining a control on the global response of the structure, the LDA has been carried out using the commercial computer software Straus 7 (HSHs.r.l.). An accurate 3D numerical model composes of 27,559 shell elements for the masonry walls, 1,428 beams for wooden structure of roof, and 30,279 nodes, was generated. According to Section 5.3.3, the FEM model of the Basilica was obtained assuming the mechanical proprieties indicated in (Table 5.3.3).

LDA analysis was carried out using the elastic spectrum suggested by the NCh2745.Of2013 (INN, 2013), and the design inelastic spectrum is plotted considering a reduction factor  $R$  equal to 1.5, with takes into account the dissipative capacity of the structure.

**Table 5.3.3** – Mechanical proprieties of materials

Element	Young modulus [MPa]	Poisson modulus	Specific weight [kN/m <sup>3</sup> ]
Masonry walls	1380	0.25	17
Masonry piers	600	0.25	16
Wooden beams		0.25	
R.C. elements	25,000	0.2	23.5

Eigen frequency analysis (EFA) was carried out to identify the modal shapes of the main vibration modes and calculate the effective participating Mass ( $M_{eff}$ ). The results of EFA are plotted in Fig.5.3.22 and 23, where the  $M_{eff}$ , the corresponding periods ( $T$ ), and the modal shapes of the first 200 vibration modes are shown.

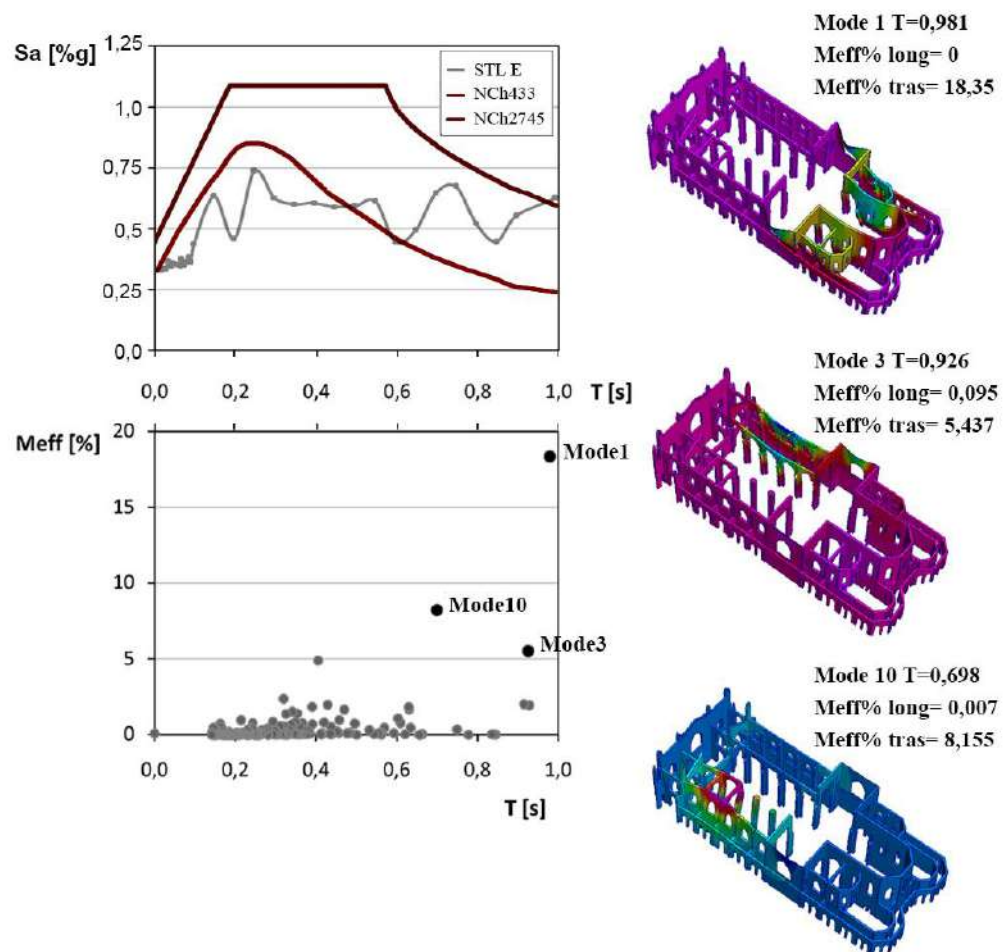


**Figure 5.3.22**– N Pseudo-acceleration response spectra for the February 27th 2010 Maule earthquake for the STL station; deformed shapes of the main modes with corresponding periods and participating mass ratios in the longitudinal direction.

Moreover, the results are compared with the pseudo-acceleration response spectra for the shock of February 27<sup>th</sup> 2010 Maule earthquake elaborated by (Liberatore, Sorrentino & Liberatore, 2012), and Chilean code values. The Basilica is located at 2.5km from the STL station and

characterized by the same type of soil. N direction corresponds to the longitudinal direction of Basilica, and E to the transversal direction.

Considering the N pseudo-acceleration response spectra, the two modes with  $M_{eff}$  larger than 5% have a period within 0.4-0.8s. Both periods correspond to a relevant spectral demand ( $S_a$ ), Fig. 5.3.22. The mode42 ( $T=0.412s$ ) involves the upper part of main façade with a  $M_{eff}$  equal to 8.64%. The mode7 ( $T=0.835$ ) involves the central and lateral apses with a  $M_{eff}$  equal to 5.245%.



**Figure 5.2.23** – E Pseudo-acceleration response spectra for the February 27th 2010 Maule earthquake for the STL station; deformed shapes of the main modes with corresponding periods and participating mass ratios in the transversal direction.

Considering the E pseudo-acceleration response spectra, all modes with participating mass larger than 5% have a period within 0.7-1.0s. This interval corresponds to the peaks of spectral demand, Fig. 5.3.23. The first mode ( $T=0.981s$ ) involves the transept walls, the central and lateral apses with a  $M_{eff}$  equal to 18.35%. The third mode ( $T=0.926s$ ) involves the external wall of east side nave and the east columns of central nave, with a  $M_{eff}$  equal to 5.437%.

Finally the mode10 ( $T=0.689s$ ) involves the external wall of west side nave and the west columns of central nave, with a  $M_{eff}$  equal to 8.155%.

### 5.3.5 Summary

A seismic assessment by limit analysis of a masonry neo-gothic church, the Basilica del Salvador, struck by 2010 Maule earthquake has been presented. The post-earthquake crack pattern and the failure mechanisms, consequence of several seismic events of the XX and XXI centuries in central Chile, have been compared with the results derived by the numerical analysis. Local-level evaluations confirm the possibility of identifying possible collapse mechanisms of churches and assess the seismic safety levels. The outputs of LKA for the overturning of the central apse offered a satisfactory safety assessment, safety index ( $I_s$ ) 1.68, confirming the appropriateness of the retrofit intervention introduced in 1985. For the OOP mechanisms of the west and east lateral apses, LKA afforded unsatisfactory safety assessment ( $I_{sLKA}=0.3$ ) as the IKA, less conservative than the linear kinematic analysis, that provided a safety index equal to 0.52. Likewise, the results of LKA and IKA for the bending failures of side west aisle wall ( $I_{sLKA}=0.34$  and  $I_{sIKA}=0.4$ ), and west and east walls of external gallery ( $I_{sLKA}=0.28-0.41$  and  $I_{sIKA}=0.4-0.83$ ), showed unsatisfactory safety assessment.

As concerning the IP behavior of west side aisle and transverse arcades of the narthex, both kinematic analyzes offered an unsatisfactory performance provided a safety indexes  $I_{sLKA}=0.47$  and  $I_{sIKA}=0.89$  for the transverse arcades of the aisle and  $I_{sLKA}=0.48-0.76$  for the narthex macro-element respectively. Regarding the pushing mechanism of the wall of east side aisle, also in this case the LKA afforded unsatisfactory safety assessment with safety index equal to 0.43. The results of the analysis showed a deficient seismic response of several structural subsystems, which exhibited significant weaknesses in terms of box-like behavior, coherently with the actual collapse processes.

As noted for the two previous case studies, sections 5.1.4.2 and 5.2.4.2, despite the limitations of LDA with FEM model for the masonry structure, the results of global response are able to suggest the critical macro-elements. In this case the results of LDA suggest the activation of out-of-plane mechanisms of the upper part of external walls of side aisles, of the columns of central nave, and the central and lateral apses. The O-O-P behavior of LWw, LWe, AP, APw, APe and FA were observed following the 2010 Malue earthquake, and the crack patten (analyzed in the section 5.3.3) is coherent with the LDA results.

Nevertheless, the global model has not able to fully capture the damage state and in-plane behavior of trasverse walls of the narthex.

# Chapter 6

## SEISMIC RETROFIT INTERVENTIONS

### 6. 1 Restoration project

From results of the seismic fragility assessment at macro-scale (Chapter4), and single-building-scale (Chapter5) it emerged that several URM churches, even those consolidated and repaired after prior Chilean earthquakes, demonstrated inadequate performance during the 2010 Maule earthquake.

For this reason, following Maule seismic event, considerable efforts were made to develop guidelines and standards to repair, consolidate and strengthen URM built heritage while respecting ICOMOS conservation philosophy. The Chilean *Standard for the Structural Intervention of Earthen Historical Buildings* (INN, 2013) is one of the preliminary outcomes from these efforts, in which generic criteria for strengthening interventions is provided.

Another set of guidelines for conservation and repair of earthen constructions, *Recuperación de Patrimonio de Arquitectura en Tierra*, was published by Fundación Altiplano (Fundación Altiplano, 2010). These guidelines present a set of criteria to assess damage types and levels, correlating the post-seismic scenarios to possible traditional and modern repair and strengthening techniques. More recently, as of August 2 2017, the Chilean commission for heritage construction (*Comisión de Construcción Patrimonial*) has been working on the draft bill for "Structural interventions on historical heritage buildings". This draft bill introduces the suggestions of the ICOMOS-ISCARSAH, 2004, European code for Design of structures for earthquake resistance (Eurocode8, 2004), and the Italian Code NTC2008 (MIT, 2008), Circ.617/2009 (MIT, 2009). It is still not known when the draft bill will become law, and in any case the seismic hazard mitigation of Chilean Built Heritage remains a complex task. In this high seismicity context it is very difficult to balance the needs of structural retrofit while preserving heritage value.

In this conclusive Chapter strengthening solutions are proposed for improving the seismic performance of Chilean URM churches. These solutions take into account the unique architectural, structural, and constructive features of this Heritage, as analyzed in the previous Sections. Therefore, it intends to give general guidelines to improve the design for the classes of churches analyzed, taking into account more specific experiences in relation to the local building culture. The criteria used in the consolidation and repair interventions for the three cases studies representative of each fragility class, will be the basis for general guidelines for post-earthquake retrofit programmes of URM churches belonging to the same architectural style.

This Chapter does not claim to exhaust this complex problem, but it is a first contribution to develop a state-of-art for URM church evaluations in central Chile.

From this perspective, traditional techniques (belonging to local constructive culture) and modern retrofit (which can be implemented when the traditional methods are insufficient, according to Venice Charter, 1964<sup>2</sup>) are proposed in accordance with the ICOMOS Principles to the greatest extent possible.

The building knowledge (Sections 5.1.1-2-3; 5.2.1-2-3; and 5.3.1-2-3) and the fragility assessment phases (Sections 5.1.4; 5.2.4; and 5.3.4) represent the first two steps of the procedure for defining seismic improvement interventions, i.e. the restoration project (Table 6.1):

Table 6.1 – Steps of a conservation project (Giaretton et al., 2016)

Step (1) KNOWLEDGE OF THE BUILDING	<ul style="list-style-type: none"> <li>• Constructive and seismic historical documentation necessary to identify the original layout, the construction phases, and consolidation interventions;</li> <li>• Geometrical, constructive and structural survey;</li> <li>• Characterization of material with non-destructive and destructive tests;</li> <li>• Identification of soil properties.</li> </ul>
Step (2) FRAGILITY ASSESSMENT	<ul style="list-style-type: none"> <li>• Local analyses through damage mechanisms: Linear and incremental kinematic analysis (LKA and IKA)</li> <li>• Global analysis: Eigen frequency analysis (EFA) and Linear dynamic analysis (LDA)</li> </ul>
Step (3) SEISMIC RETROFITTING INTERVENTIONS	<ul style="list-style-type: none"> <li>• Design seismic retrofit interventions taking into account local, traditional, and modern retrofitting techniques</li> <li>• Monitoring and ordinary maintenance program</li> </ul>

Steps (1) and (2) shown in Table 6.1 constitute the *anamnesis* of the building, which is the fundamental base for the design of any seismic retrofit intervention.

<sup>2</sup>Venice Charter, article 10 page2: “Where traditional techniques prove inadequate, the consolidation of a monument can be achieved by the use of any modern technique for conservation and construction, the efficacy of which has been shown by scientific data and proved by experience”.

## 6.2 ICOMOS Principles and seismic retrofit project

The conservation philosophy has a direct consequence on seismic retrofit projects. As introduced in Chapter 1, the most generic principles of conservation are: authenticity, minimal intervention and intrusiveness, compatibility, recognizability, and reversibility. Following, from an engineering standpoint, these criteria are analyzed considering their influence on the structural behavior of the building when applied:

- *Authenticity* [Au] of the original features of the building (materials, geometry), which must be preserve “ensuring that the original mechanical and resisting principles governing the structure response are not altered and original structural elements are not made redundant” (D’Ayala, 2014);
- *Minimal intervention and intrusiveness* [Mi], which consist of an intervention where the human safety and conservation requirements are balanced, through a cost-benefit analysis that also includes intangible value losses;
- *Compatibility* [Co] between new retrofitting materials and existing elements is related to chemical, physical and mechanical performances. The retrofits and structural elements “not only do no harm to the original ones, but they also act as sacrificial elements in precence of external actions, i.e. they should act as fuses of the Structural system” (D’Ayala, 2014).

Furthermore, the *constructive compatibility* allows for reduction of structural discontinuities that are the preferencial ways of damage in case of seismic motion, and guarantee a greater level of monolithicity of masonry wall and integration among structural elements;

- *Recognizability* [Rc] of retrofitting interventions allows to easily detect the original constructive systems of the building and also possible structural heterogeneities due to post-earthquake repairs (main vulnerability feature in URM structures subject to seismic motions), especially when the historical documentation is absent.
- *Reversibility* [Rv] of interventions considers the possibility of removing retrofits if better solutions are found in the future (ICOMOS, 2003 and Petzet, 2004). Currently, this is one of the most debated conservation issues because new technologies are often invasive and non-reversible. Thus, least harmful solutions should be chosen in accordance with minimum intervention and compatibility principles.

In order to define a judgement of analyzed retrofitting techniques, in the next section, the degree of agreement with ICOMOS Principles will be qualitatively evaluated through a category of judgement defined as: respect (R), partial respect (PR), and no respect (NR) of a

given conservation principle. These judgement categories (JCs) are directly related to the performance levels (PLs) based on experts' judgment, Table 6.2.

**Table 6.2** - ICOMOS principle ID, judgement category (JC), conservation's principle score ( $\gamma_k$ ) given to each JC, and description for each conservation principles of performance levels.

ID	JC	$\gamma_k$	Performance level description
<b>Au</b>	R	2	Original static and dynamic behaviors are not altered.
	PR	1	Original static behavior is not altered, but dynamic behavior is substantially altered
	NR	0	Original static and dynamic behaviors are altered
<b>Min</b>	R	3	Human safety and conservation requirements are balanced. Cost-benefits are balanced
	PR	1.5	Human safety and conservation requirements are partially balanced.
	NR	0	Human safety and conservation requirements are not balanced.
<b>Co</b>	R	3	Retrofitting intervention is compatible mechanically (e.g. stiffness, weight, cohesion and deformability similar to the original structure), physically (e.g. very similar porosity and pore size distribution, very low variation of the moisture transport as absorption and drying rate, no thermal and hygric expansion), and chemically (e.g. identical chemical composition, no harmful chemical reaction, similar solubility) with existing structure.
	PR	1.5	Retrofitting intervention is mechanically compatible with the original ones, but it has slightly or moderately different physically and chemical features (e.g. moderate variation of the porosity and pore size distribution and moderate variation of drying and hygroscopic behavior, different chemical features, no harmful chemical reaction or byproducts).
	NR	0	High level of conflict between the original structure and the retrofitting intervention under dynamic actions, and use of material physically, chemically different from the original ones.
<b>Rec</b>	R	2	Relevant differences between the original structure and new intervention in term of thickness, material, tactile and color consistency.
	PR	1	The features of new intervention are similar to the original, whereas the tactile and color consistency is different.
	NR	0	Thickness, material, tactile and color consistency are similar to the original.
<b>Rev</b>	R	2	New intervention can be completely removed.
	PR	1	New intervention can be removed generating minor damage to the original structure.
	NR	0	New intervention cannot be removed.

Based on the assessment of the agreement level between the selected intervention and the ICOMOS Principles, a numerical score is proposed to each judgement category.

These numerical scores associated with the categories of judgement presented in Table 6.2 are used in Equation (6.1) to evaluate the level of conformity of new intervention with ICOMOS philosophy, through the Intervention Quality Index (IQI). The IQI index assesses the restoring intervention quality in relation to the: (i) Current state of conservation of the monument and the seismic intensity, through the  $\Delta I_s$  index which takes into account the difference between the safety index of building after ( $I_{s2}$ ) and before ( $I_{s1}$ ) the intervention; (ii) Level of compliance given by the conservation's principle score  $\gamma_k$  related to each conservation's principle,  $PI_k$ . The IQI index is computed by the following equation:

$$IQI = \sum_{k=1}^N \hat{\gamma}_{PI_k} \cdot \Delta I_s \quad \text{where} \quad \Delta I_s = \frac{I_{s2} - I_{s1}}{Dag} \quad (6.1)$$

where  $N$  is the number of considered ICOMOS principles;  $\hat{\gamma}_{PI_k}$  is the normalized weight associated with the influence of each  $PI_k$  on the global behavior of structure (ranges between 0 and 3);  $PI_k$  is the  $k$ -th ICOMOS Principle, in this research Au, Mi, Co, Re, and Rev; and  $\Delta I_s$  is the difference of the safety index of structure after ( $I_{s2}$ ) and before ( $I_{s1}$ ) the intervention. In particular, the safety index is given by the ratio between the acceleration capacity  $a_0^*$  of the structure (Equation 5.1) and seismic demand when the macro-element is placed at the ground level  $Dag$  and higher than ground level  $Dal$  (as defined in Chapter 5.1.4.1).

Finally, according to IQI index values, the retrofitting interventions can be classified in three categories as shown in Table 6.3 :

Category A, the intervention meets safety requirements (alignment) and guarantees full compliance with the conservation principles;

Category B, the intervention meets safety requirements (improvement) and guarantees compliance with the conservation principles;

Category C, the intervention meets safety requirements (alignment/improvement) but does not guarantee complete compliance with the conservation principles.

Category D, the intervention does not meet safety requirements and does not guarantee compliance with the conservation principles.

**Table 6.3 - Intervention conformity level to ICOMOS principles**

Intervention conformity level			
A	B	C	D
$1.8 < IQI \leq 2.4$	$1.0 < IQI \leq 1.8$	$0.6 < IQI \leq 1.0$	$0 < IQI \leq 0.6$

A state of poor conservation of the materials in the structure (i.e. degradation of materials due to continuous exposure to the elements which generates degradation phenomena reducing

structural efficiency), the presence of poor quality materials (i.e. irregular textures and/or incoherent and friable mortar), and design errors in the original structure (i.e. lack of wall-to-wall and wall-to-roof connections, excessive slenderness, wall pattern not respectful of the rule-of-the-art etc) inevitably require invasive and consolidation projects which depart from ICOMOS principles.

In these cases, the priority is to guarantee the minimum safety level. Therefore, it is necessary to evaluate the invasiveness of the project considering the initial conservation state of the building, and related with the required safety level to the ICOMOS principles.

In particular, considering a highly seismic context, a conservation project which is minimally invasive could be insufficient, and hence more invasive solutions must be needed. The International Council on Monuments and Sites is aware of the complexity of this issue, and for this reason it is explicit that the principles are non-binding recommendations. Thus, ICOMOS principles are not an absolute requirement, but recommendations for the definition of optimal retrofit interventions. In this regard, the Eurocode8 (Eurocode8, 2004) gives the following directives:

- “The intervention should always be designed so that the architectural and constructional identity of the building is preserved”;
- “Only when the original structure is clearly insufficient against earthquakes should the addition of structural elements contributing to seismic resistance be considered. Nevertheless, such additional elements should fulfil the requirement of compatibility with the original architectural and mechanical features of the construction”.

### 6.3 From the diagnosis of vulnerability to the conservation project

The passage from the analytical and diagnostic phases, i.e. steps (1) and (2), to the intervention project, step (3), consists of designing a unified strategy of interventions considering the identified vulnerabilities and structural deficiencies. The main goals of Step (3) are to prevent the activation of local collapse mechanisms (OOP and IN failures), and guarantee a *box-like behavior* respecting the conservation philosophy.

The design improvement devices and interventions must be able to:

- collaborate with existing elements and contrast local vulnerability;
- systematically increase the dissipative capacity and ductility of the structure, admitting partial deformations and cracks;
- restore the structural resistance of the initial system;
- avoid introducing concentrated and relevant stiffness (R.C. slab and injections etc.);
- increase the tensile resistant connections.

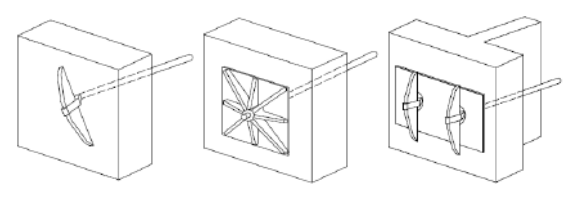
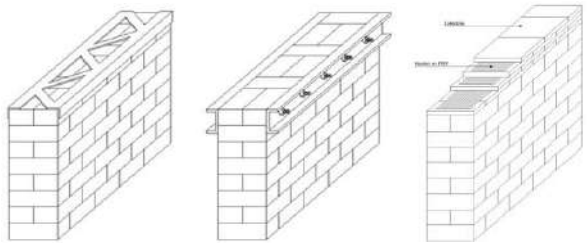
These requirements, at the base of the seismic “improvement” concept, are applicable to URM churches characterized by moderate post-seismic damage, level D<sub>3</sub> as shown in Table 4.2. In buildings with heavy crack patterns, with partial or near total collapses of different macro-elements, (i.e., damage levels D<sub>4</sub> and D<sub>5</sub>), the improvement interventions and partial

reconstructions are required to guarantee the safety levels. In (Giaretton et al., 2016) two main classes of complementary retrofitting interventions are distinguished: I) Stability-based techniques, which reduce the deficit connections and thrust of arches and vaults; and II) Strength-based techniques, which restore and increase the resistance of masonry wall.

### 6.3.1 Stability-based techniques

The stability-based techniques reduce deficiency between connections and thrust of structural elements (arches, vaults etc.), stabilizing the structure as a whole, in order to increment *box-like-behavior*. Common stability-based techniques for URM buildings are presented and analyzed below. Traditional systems (such as tie-rods, ring-beam, *frenelli*, enlargement and buttresses), and modern retrofitting techniques (such as cross-bracing, tie-rods and plywood diaphragm) are taken into account considering the features of architectural styles. The possible retrofit measures for each seismic vulnerability are generally more of one with different characteristics in terms of effectiveness, invasiveness, reversibility, compatibility, durability and costs. Thus, a qualitative judgment on total, partial or absence of the respect of conservation principles, previously analyzed, is provided. Generally the implementation of traditional solutions is advantageous from both from a cost and compatibility point of view. But, in highly seismic regions these techniques could result insufficient and modern devices should be employed. A summary of the main stability-based analyzed techniques is provided in (Table 6.4).

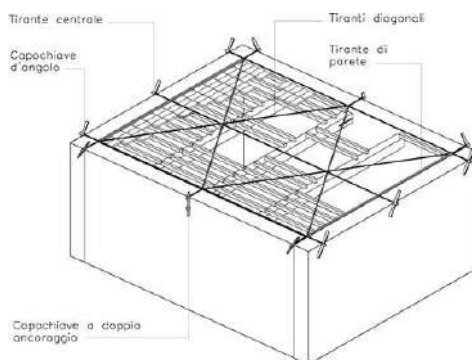
*Table 6.4 – Stability-bases techniques*

I) STABILITY-BASED TECHNIQUES		
Device	Main goal	Example of device
<b>[TR]</b>  Tie-rod and anchor plate (made of timber and steel)	Prevent the two walls from spreading apart	 (i) anchor-post      (ii) anchor plate      (iii) double-tie-rod
<b>[RB]</b>  Ring beam (made of timber, reinforced brick masonry, steel)	Prevent overturning, proving strength and stiffness	 (i) and (ii) Steel RB      (iii) Reinforced masonry RB

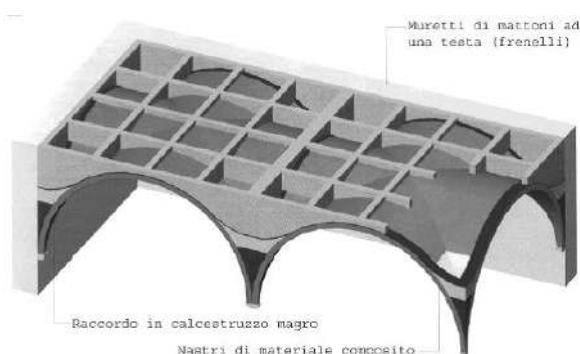
**[FR-CB]**

*Frenelli* or  
Cross  
bracing

Reduce roof  
structure  
deformability



Cross bracing in extrados of vault (Giovanetti, 1998)

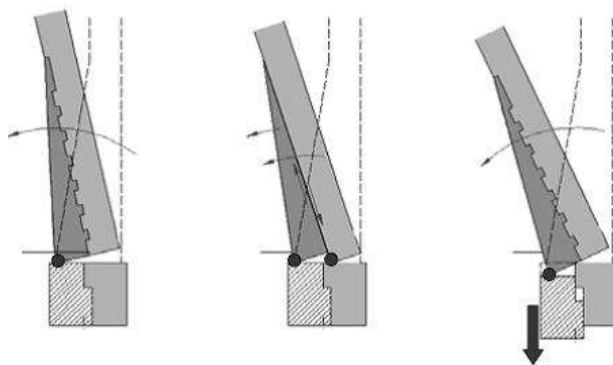


Brick frenelli in the extrados of cross vault (Gurrieri, 1999)

**[EN-BT]**

Enlargement  
or  
Buttresses

Improve  
global  
behavior and  
increase the  
load bearing  
capacity of  
wall



(i) Optimal configuration, (ii) lack of bond, and (iii) ineffective configuration (Cangi, 2009)

The stability-based techniques present in Table 6.4 are analyzed in the following paragraphs.

### 6.3.1.1 [TR] \_ Ties-rods and anchor plate

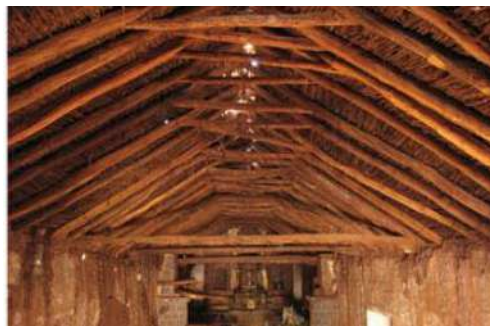
The *tie-rods* were widely used in historical structures to connect wall-to-wall and wall-to-floor and to improve the building integrity. In the URM churches this device is positioned at the roof level. The tie and anchor dimensions are related to the tensile force of tie-rod, anchor and masonry. The anchors have different shapes: circular, rectangular or square plates or simple

bar positioned at 45°. The simple bar anchor is the higher arm against the orthogonal wall in order to distribute the load to both the diaphragm and the wall. Moreover, the low cost, easy installation, maintenance and repair are advantages of this technique. Table 6.5 shows that overall Au, Min, Rec and Rev Conservation principles are achieved (respect “R” or partial respect “PR” of principle), taking into account the different material solutions relative to architectural style Fig.6.1.

**Table 6.5** - TR, check of respect: total (R), partial (PR), or absence (A) of ICOMOS principles and individuation of material device considering the architectural style.

TIE-ROD [TR]															
Architectural style	CL					NC&V					NG				
Material device	Timber TR					Steel TR					Steel TR				
ID	Au	Min	Co	Rec	Rev	Au	Min	Co	Rec	Rev	Au	Min	Co	Rec	Rev
JC	PR	R	R	R	R	PR	R	R	R	R	PR	R	R	R	R
$\sum_{k=1}^N \hat{\gamma}_{PI_k}$	11					11					11				

In seismic areas, tie-rods were widely used to connect wall-to-wall and wall-to-floor, since Byzantine times (4<sup>th</sup> and 5<sup>th</sup> centuries, wood made) and during the 15<sup>th</sup>, 17<sup>th</sup> 18<sup>th</sup> and 19<sup>th</sup> centuries (Milizia, 1785; Rondelet, 1832), both wood and steel made.



**Figure 6.1** - (a) Tie beams in the Kuño Tambo church, one of the prototype buildings of the SRP (image by C. Cancino, 2010); (b) exterior view of connections of tie beams in Cuzco (image by S. Lardinois, 2012).

While in Europe and Asia this traditional device is widespread and its effectiveness has been proven during the past 200 years, in the central area of Chile is not frequently implemented. Only in earthen buildings, in particular Andean CL religious structures, the tie-rods are a traditional device (Fig.6.1), in wooden material (Michiels, 2014).

Only recently, the tie-rods have been introduced in some historical buildings, such as the Divina Providencia and San Vicente churches in Santiago, both NCL&V style damaged after

the 2010 Maule earthquake. In particular, the reluctance to introduce steel tie-rods at spring of arches is due to the fact that the intervention is considered aesthetically very invasive. Nevertheless, the use of tie-rods is particularly suitable to Chilean URM buildings and is strongly recommended. The use of [TR] for reinforce Chilean URM churches represents a compatible traditional solution, respectful of conservation principles (Table 6.5).

According to (DPCM, 2011) the tensile value in the tie-rods, required for design of the tie-rods, is given by the expression:

$$T_{TR} = \alpha_0(W yg + Psh) - \frac{1}{h_T} [W xg + Psd] \quad (6.2)$$

where  $\alpha_0$  is the multiplier of load coefficient,  $W$  is the wall masonry load;  $Ps$  is the roof load;  $h$  is the wall height;  $t$  is the wall thickness;  $d$  is the horizontal distance between the point of application of roof load and the plastic hinge; and  $P_{so}$  is the horizontal force due to the thrust action of vault or roof. The tensile value of TR must be equal to the minimum value of  $T_{TR} = \min(T_t, T_m, T_c)$ , where  $T_{TR}$  is the maximum applicable normal tensile force;  $T_t$  is the maximum tensile force of tie-rod ( $T_t = f_{yd} A_t$ );  $T_m$  is the tensile force of masonry ( $T_m = f_{yd} [2(b+t) + 2a+tt]$ ); and  $T_c$  is the tensile force of anchor plate ( $T_c = \sigma_r ab$ ); where  $f_{yd}$  is the design tensile strength of the tie-rod material;  $A_t$  the area of cross-section of tie-rod;  $a$  is the anchor height and  $b$  anchor length;  $\sigma_r$  is the compressive strength of the masonry; and  $f_{vd}$  is the design shear strength of masonry. Assuming the presence of tie-rods the multiplier of load coefficient is:

$$\alpha_{0,TR} = \frac{W xg + Psd + Th_T}{Psh + W yg} \quad (6.3)$$

where  $\alpha_{0,TR}$  is the multiplier of load coefficient,  $W$  is the wall masonry load;  $xg$  is the horizontal distance between the center of gravity and the plastic hinge;  $Ps$  is the roof load;  $t$  is the wall thickness;  $d$  is the horizontal distance between the point of application of roof load  $Ps$  and the plastic hinge; and  $yg$  is the vertical distance between the wall's center of gravity and the plastic hinge.;  $T$  is the tensile force of tie-rod; and  $h_T$  is the vertical distance between the point of application of  $T$  and the plastic hinge.



**Figure 6.2** – Deep cracks in the transverse arches of external gallery of Basilica del Salvador.

As mentioned previously, in Chilean context, the implementation of steel TRs would be a very effective device in countering the arch thrusts and avoiding the trigger of out-of-plane (OOP) failure of the NG and NC&V churches.

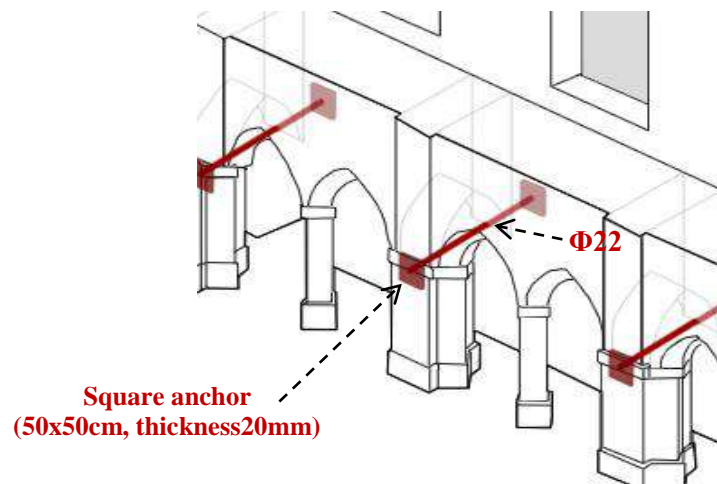
For example, in the case of the Basilica del Salvador (Chapter 5.3), the introduction of TRs would effectively counteract the activation of overturning mechanism of the EAw-e1 macro-elements that compose the outer walls of the external gallery (Fig.6.2).

The kinematic multiplier of the horizontal equivalent forces producing the activation of the mechanisms,  $\alpha_0$ , is equal to 0.112 and the corresponding spectral acceleration  $a_0^*$  equal to  $0.815 \text{ [m/s}^2\text{]}$ , (Table5.3.1).

With the aim of averting triggering the OOP failures of EAw-e1 macro-blocks, TR introduction is proposed, imposing  $a_0^*$  equal to the Demand Acceleration at ground level ( $2.61 \text{ m/s}^2$ , according to Nch2745Of.2013). Considering a circular section of tie (length 5.91m, diameter 22mm, Young modulus  $210000 \text{ daN/cm}^2$ ,  $f_y=2350 \text{ daN/cm}^2$ , and  $\gamma=7850 \text{ daN/m}^3$ ), a square anchor (50x50cm, thickness 20mm, Young modulus  $210000 \text{ daN/cm}^2$ ,  $f_y=2350 \text{ daN/cm}^2$ , and  $\gamma=7850 \text{ daN/m}^3$ ) the  $\alpha_{OTR}$  is 0.359 for  $T_{TR} = \min(T_t, T_m, T_c) = \min(89.3 \text{ kN}, 344 \text{ kN}, \mathbf{86.2 \text{ kN}})$ . The comparative analysis of the current state and the state after the retrofitting intervention (Table6.6) shows a significant improvement of acceleration capacity of the OOP mechanism of EAw-e1. This improvement leads to safety satisfactory assessment, safety index after the intervention  $Is_2 = 1$ . According to Equation 6.1 the IQI index is equal to 1.6 (Table 6.6), leading to an intervention conformity level type “B”.

**Table.6.6** - Effectiveness of steel TR in terms of acceleration for Basilica del Salvador

	Mechanism Activation Acceleration $a_0^*$ [m/s <sup>2</sup> ]		Safety index (DPCM, 2011)	
	Before interv.	After interv.	$Is_1$	$Is_2$
EAw1- OOP	0.815	2.61	0.31	1

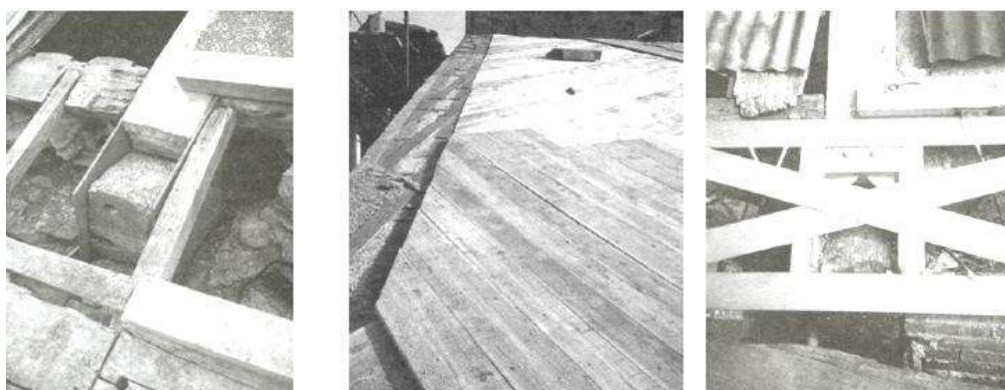


**Figure 6.3**– Retrofitting intervention for Basilica del Salvador: steel tie-rod

### 6.3.1.2 [RB-CK]\_Ring beam and/or corner-key

The *ring beam* (also bond beam or collar beam) is one of the most effective stability-based techniques for improving the seismic behavior of URM structures. The RB is placed on top of the walls to guarantee box-like behavior and prevent the activation of out-of-plane mechanisms, providing strength and stiffness against bending. Moreover, this continuous element along the entire length of the walls creates in-plane continuity.

The use of timber RB in Chilean CL structures is a common and traditional practice. This material is compatible with earth and easily available (Tolles et al., 2000). Moreover, wooden RBs at different heights of wall were generally used (vertical distance between 80 and 120cm), as in the case of Malloa parish. In addition to RB devices, corner keys, wooden elements to connect the wall-to-wall, can be commonly found. Concerning NC&V and NG buildings in the central valley, after 1985 Algarrobo earthquake the RB made of reinforced concrete (R.C.), was frequently introduced. Often, oversized RB associated with R.C. slab has proved to be ineffective and destructive in seismic events (see Chapter 2). In fact, despite R.C. elements performing the same structural function of wooden or reinforced-brick RBs, the different stiffness between concrete and masonry can cause significant failures during seismic events. Thus, to guarantee a minimum impact on the existing masonry structures, timber, reinforced brick masonry and steel ring-beams (Fig. 6.4) are recommended as a valid alternative to R.C. ring-beam (DPCM, 2011 and Borri et al., 2009). A consolidation intervention with oversized R.C. ring-beam associated with R.C. slab, besides not always guaranteeing an improvement in structural performance, does not comply with the ICOMOS principles insofar as: static and dynamic behavior is altered (Au, NR, 0); human safety and conservation requirements are partially balanced (Min, PR, 1.5); R.C. material is not compatible with masonry (Co, NR, 0); and, although the RB can be removed, it generates minor damage to the original structure (Rev, PR, 1). The only principle that the RB made of R.C. respects is the recognizability (Re, R, 2). Therefore, the  $\sum_{k=1}^N \hat{\gamma}_{PI_k}$  is equal to 4.5.



**Figure 6.4** - Steel ring beam: a) connection between the wood roof element and the walls; b,c) partial strengthening of the plywood panel diaphragm and its connection with the steel ring beams (Regione Marche 2000). (Frumento et al., 2006).

In the case of timber RBs for CL buildings, overall Au, Min, Co, Rec and Rev Conservation principles are achieved (R, respect of principle and PR partial respect). The  $\sum_{k=1}^N \hat{\gamma}_{PI_k}$  is 10.

In Table 6.7 different material solutions for ring-beam device of NC&V and NG structures are analyzed. The  $\sum_{k=1}^N \hat{\gamma}_{PI_k}$  for Reinforced brick RB is 10 and for Steel RB is 9.5-10.

**Table 6.7**– RB, check of the respect: total (R), partial (PR), or absence (A) of ICOMOS principles and individuation of materials considering the architectural style.

RING-BEAM DEVICE [RB]															
Architectural style	CL					NC&V					NG				
Material device	Timber RB					Reinforced brick or Steel RB					Reinforced brick or Steel RB				
ID	Au	Min	Co	Rec	Rev	Au	Min	Co	Rec	Rev	Au	Min	Co	Rec	Rev
JC	PR	R	R	R	PR	PR	R	R-PR	R	PR	PR	R	R-PR	R	R
$\sum_{k=1}^N \hat{\gamma}_{PI_k}$	10					10 - 9.5					10 - 9.5				

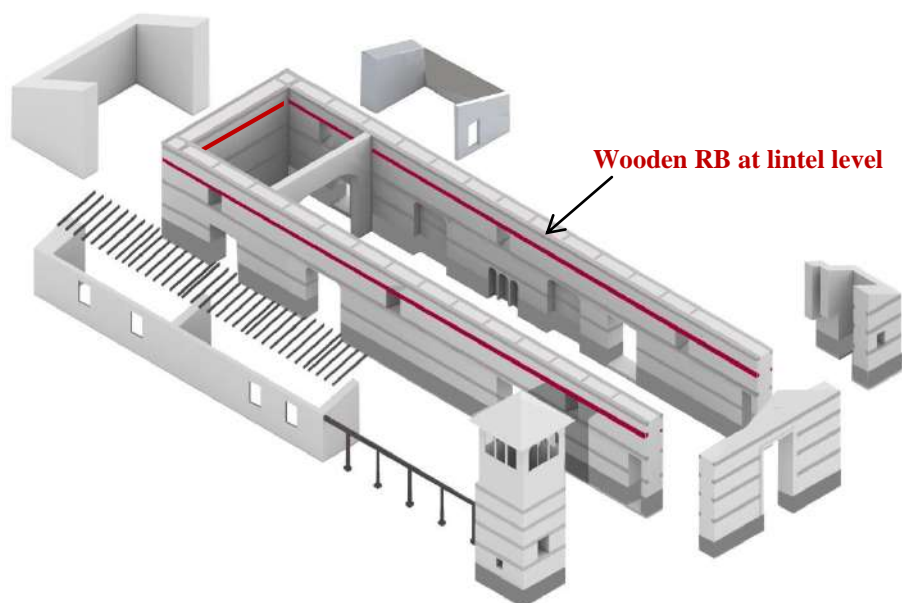
The requirements for a preliminary RB elements design are provided by the following parameters: the maximum ring-beam strength,  $R_{RB}$ , is given by the minimum value between the tensile strength of the RB,  $R_{c,t}$ , and sliding strength between the ring-beam and masonry,  $R_{c,m}$ .  $R_{RB} = \min(R_{c,t}; R_{c,m})$ , where  $R_{c,t} = \sum_{i=1}^n f_y d A_i$  and  $R_{c,m} = \frac{f_{vk}}{FC \gamma_m} A$ ; where  $n$  is the number of tensile-strength elements;  $f_y$  is the yield strength of RB material;  $A_i$  is the area of cross-section of elements with tensile strength;  $f_{vk}$  is the shear resistance of masonry;  $A$  is the contact surface between the masonry and the RB;  $FC$  is the confidence factor (DPCM, 2011), that takes into account the level of knowledge about the construction; and  $\gamma_m$  partial safety coefficient for masonry equal to 2 (DPCM, 2011). Assuming the presence of a ring-beam, the multiplier of load coefficient is:

$$\alpha_{0,RB} = \frac{W xg + Psd + n R_{RB} h_{RB}}{Psh + W yg} \quad (6.4)$$

where  $\alpha_{0,RB}$  is the multiplier of load coefficient,  $W$  is the wall masonry load;  $Ps$  is the roof load;  $xg$  is the horizontal distance between the wall's center of gravity and the plastic hinge;  $d$  is the horizontal distance between the point of application of the roof load and the plastic hinge;  $h_{RB}$  is the vertical distance between the center of gravity of RB and the plastic hinge;  $n$  is the number of tensile-strength elements;  $h$  is the wall height; and  $yg$  is the vertical distance between the wall's center of gravity and the plastic hinge.

As seen in Chapter 5.1, a critical aspect of the effectiveness of this device in CL buildings is the vertical distance between the ring-beams (greater than 1.2m), the dimensions of the

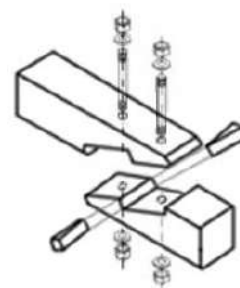
restraint device, and the length of the timber element which depends on the presence of carpentry links. In the case of the Malloa church, the distance between the top ring-beam and the next one is 2.72m, due to the presence of big openings.



**Figure 6.5** - Retrofitting intervention for Malloa church: wooden ring-beam at lintel level

This excessive distance between the two RBs resulted in the devices being ineffective and leads to the activation of out-of-plane collapse mechanisms in the masonry portions between them. Thus, an effective consolidation intervention would introduce a new RB among the original ones in order to reduce the free inflection length of the wall (Fig.6.5).

Moreover, the strength of carpentry links, in particular of hooked scarf joints, is indispensable to guarantee the effectiveness of RB device (Fig. 6.6). As shown in the crack pattern and the collapse mechanisms analyses of Malloa church, the hooked scarf joints were the most vulnerable structural element after the 2010 Maule earthquake. The comparative analysis of the current state and the state after the retrofitting intervention, consisting on the introduction of a new RB between the top RB and the next one, shows a significant improvement in acceleration capacity for the OOP mechanism of LW1e macro-element (Table 6.8). The IKA analysis has demonstrated the RB to be the most vulnerable macro-element, i.e. with the lowest load kinematic multiplier,  $\alpha_i$  (Table 5.1.5). This improvement leads to satisfactory safety assessments, safety index equal to 1 and an Intervention Quality Index equal to 1.5.



**Figure 6.6** - Reinforced hooked scarf joint.

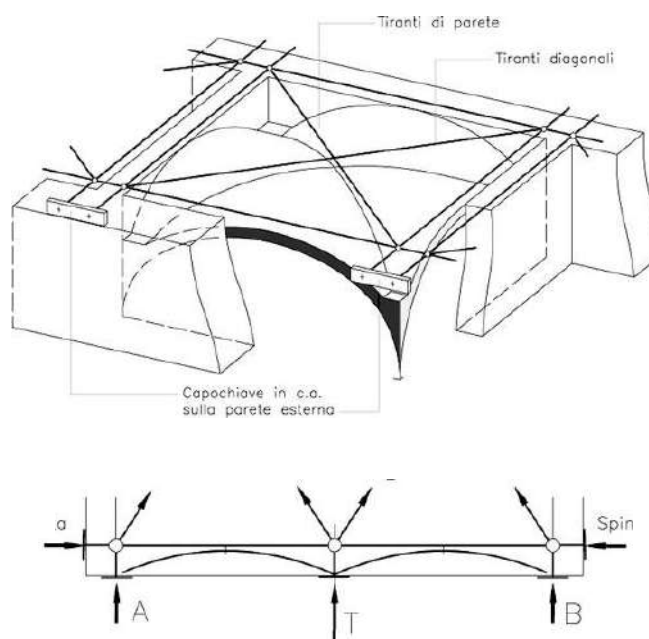
**Table 6.8** - Effectiveness of wooden RB in terms of acceleration for Malloa parish.

	Mechanism Activation Acceleration $a_0^*$ [m/s <sup>2</sup> ]		Safety index (DPCM, 2011)	
	Before interv.	After interv.	$Is_1$	$Is_2$
Lw1e - OOP	1.44	5.3	0.27	1

### 6.3.1.3 [FR-CB] *Frenelli* or Cross bracing

In general, to make the timber roof diaphragm rigid or partially-flexible, mutual connections between the upper part of masonry wall and the roof structure should be introduced. In addition to prevent translation, wooden or metal ring-beam-rods, suitably connected both to walls and wooden roof structure (metallic caps) must be used to evenly distribute the concentrated loads of the roof. Moreover, cross bracing, two diagonal supports placed in an X shape, can be utilized to reinforce the roof structure preventing sideways deflection and supporting compression and tension forces. This device, known as herringbone strutting is commonly used in masonry buildings increasing the capacity of vaults to withstand seismic actions. The cross bracings are located on the extrados of vaults as shown in Fig.6.7.

A traditional reinforcement technique, which performs the same structural behavior of CB, is masonry *frenelli*. The FRs reduce the high loads acting on the vault, mainly linked to the abutment, and the thrust forces.



**Figure 6.7-** Steel cross bracing in extrados of vault (Giovanetti, 1998).

Table 6.9 shows that the use of steel CB in NC&V and NG masonry structures guarantees respect for all conservation principles (R, respect of principle), with the exception of Au, for which the check is partial respect due to the change of dynamic behavior determined by the introduction of CB device, and the Co principles. Regarding CL structures, the implementation of plywood CB at roof level guarantees the respect of all ICOMOS recommendations with exception of Au because the original static behavior is not altered, but dynamic performance is substantially altered.

**Table 6.9-** CB, check of respect: total (R), partial (PR), or absence (A) of ICOMOS principles and individuation of material device considering the architectural style.

CROSS BRACING DEVICE [CB]															
Architectural style	CL					NC&V					NG				
Material device	Plywood					Steel CB					Steel CB				
ID	Au	Min	Co	Rec	Rev	Au	Min	Co	Rec	Rev	Au	Min	Co	Rec	Rev
JC	PR	R	R	R	R	PR	R	R	R	R	PR	R	R	R	R
$\sum_{k=1}^N \hat{\gamma}_{PI_k}$	11					11					11				

**Table 6.10-** FR, check of respect: total (R), partial (PR), or absence (A) of ICOMOS principles and individuation of material device considering the architectural style.

FRENELLI DEVICE [FR]										
Architectural style	NC&V					NG				
Material device	Brick					Brick				
ID	Au	Min	Co	Rec	Rev	Au	Min	Co	Rec	Rev
JC	NR	R	R	R	R	NR	R	R	R	R
$\sum_{k=1}^N \hat{\gamma}_{PI_k}$	10					10				

An Alternative to the use of CB for strengthening masonry vaults (a rare structural element in the churches in the Chilean central valley but more common in the northern area), is the use of masonry *frenelli*. In Table 6.10 the analysis of the  $\sum_{k=1}^N \hat{\gamma}_{PI_k}$  is carried out for NC&V and NG buildings because, as seen in Chapter 2, the CL churches do not have the vault macro-element.

The requirements for a preliminary design of RB elements are provided as follows: the maximum tensile value in the cross bracing, required for design of the CB element, must be equal to the minimum value of  $T_{CB,i} = \min(T_{ti}, T_{mi})$ , where  $T_{CB}$  is the maximum applicable normal tensile force;  $T_t$  is the maximum tensile force of the tie-rods equal to  $T_t = f_{yd} A_t$ ; and  $T_m$  is the tensile force of the masonry, equal to  $T_m = f_{yd}[2(b+t) + 2(a+t)]t$ . The  $f_{yd}$  is the tensile design strength of the tie-rod material;  $A_t$  the area of cross-section of tie-rod; and  $f_{vd}$  is the design shear strength of masonry. Assuming the presence of cross bracing, the multiplier of load coefficient is:

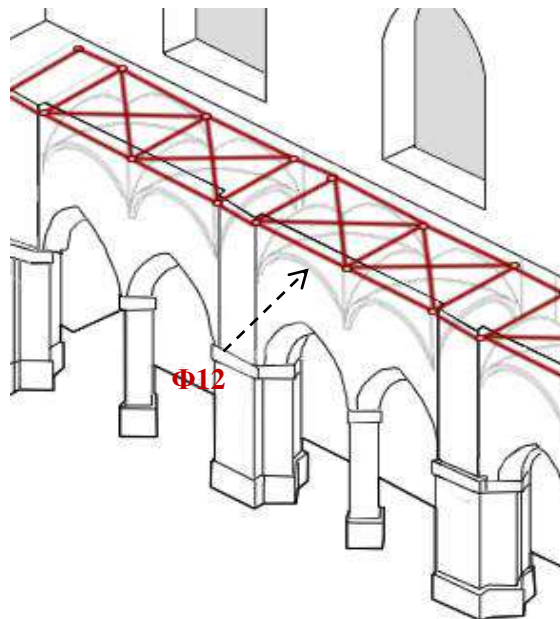
$$\alpha_{0,CB} = \frac{Psd + Wxg + T_{CB,A}d_A + T_{CB,T}d_T + T_{CB,B}d_B}{Psh + Wyg} \quad (6.5)$$

Where  $\alpha_{0,CB}$  is the multiplier of the load coefficient,  $W$  is the wall masonry load;  $Ps$  is the roof load;  $x_g$  is the horizontal distance between the wall's center of gravity and the plastic hinge;  $d$  is the horizontal distance between the point of application of roof load and the plastic hinge;  $y_g$  is the vertical distance between the wall's center of gravity and the plastic hinge;  $h$  is the wall height;  $T_{CB,A,B,C}$  are the tensile forces of the bracings at points A,B,C; and  $h_{A,B,C}$  are the horizontal distances between the points A,B,C and the plastic hinge.

The current seismic performance of Basilica del Salvador gallery vaults, the only one building with masonry vaults between the 106 churches analyzed in Chapter 2 and 4, and the modified behavior due to the introduction of CBs devices are checked in Table 6.11, Fig.6.8, using IKA analysis. The load kinematic multiplier,  $\alpha_0$ , of EAw-e1 macro-blocks is equal to 0.112 and the spectral acceleration,  $a_0^*$ , is equal to  $0.815 \text{ [m/s}^2\text{]}$ , (Table5.3.1). The Demand Acceleration at ground level is  $2.91 \text{ m/s}^2$  according to Nch2745Of.2013. For each bay it is considered a circular section of four cross bracings (two transversal CBs with length 5.91m, two diagonal CBs with length 8.36m, all CBs with diameter 12mm, Young modulus  $2100000 \text{ daN/cm}^2$ ,  $f_y=2350 \text{ daN/cm}^2$ , and  $\gamma=7850 \text{ daN/m}^3$ ). The  $\alpha_{0CB}$  is 0.401 for  $T_{CB} = \min(T_t, T_m) = \min(106 \text{ kN}$ , and  $344 \text{ kN})$ .

**Table6.11** - Effectiveness of CB in terms of acceleration for Basilica del Salvador.

	Mechanism Activation Acceleration $a_0^*$ [m/s <sup>2</sup> ]		Safety index (DPCM, 2011)	
	Before interv.	After interv.	$Is_1$	$Is_2$
EAw1- OOP	0.815	2.91	0.3	1.12



**Figure 6.8** - Retrofitting intervention for Basilica del Salvador: steel tie-rod.

The comparative analysis of the current state and the state after the retrofitting intervention (Table 6.11) shows the achievement of the required safety levels ( $I_s=1$ ) for the OOP mechanism of EAw-e1. The IQI Index results equal to 1.8.

#### 6.3.1.4 EN-BT\_Enlargement & Buttresses

The enlargement consists of a new massive local masonry addition in order to increase the wall section and prevent out-of-plane failures. While the enlargement generally involves the entire length of the wall, the buttresses support the wall corner and/or projecting from the section of an internal transverse wall, providing resistance to lateral thrusts.

In the 1746 earthquake, a decree of the Spanish Viceroyalty imposed the use of buttresses in the Andean region. Thus, the use of EN-BT was widely employed in the CL and NC&V architectures with different materials and shapes (Fig.6.9).

Historically, EN-BT were part of the original construction and had a very efficient performance during the seismic motion. Consequently, these systems were introduced as a seismic device corresponding to masonry enlargements or buttresses added to original masonry structures. Therefore, the strengthening efficiency depends on good interlocking and bonding between the original and new material, and mechanical compatibility in regard to strength and stiffness, as far as mortars and resistant elements (adobe, brick, and stone) are concerned. Ensuring the efficiency of intervention, which lies in the ability to constitute a homogeneous and monolithic wall-device system, is in contrast with the principle of reversibility because the EN-BT cannot be removed in several cases.



**Figure 6.9** – Santo Domingo church in Santiago and Socaire church in Atacama.

Table 6.12 shows that the use of EN-BT as seismic device in masonry structures guarantees respect for all conservation principles (R, respect of principle) with the exception of the authenticity and reversibility principles (Rev and Au). In fact, the EN-BT intervention determines the alteration of original static and dynamic behavior, not respecting the Au principle. Nevertheless, these devices obtain an intervention conformity level class “B”. Thus, they can be considered retrofitting interventions in conformity with ICOMOS philosophy.

The *Guidelines for wall construction with buttresses and pilasters* (Arya et al., 2014) provide some specifications respect to the geometrical features of walls and devices:

The buttress thickness must be equal or greater than the wall thickness ( $t_{\text{wall}}$ ); the length of buttress must be equal or larger than  $3t_{\text{wall}}$ ; the length ( $L$ ) between two buttresses must be  $L \leq 10 t_{\text{wall}}$  and  $L \leq 64 t_{\text{wall}}^2/h$ , where  $h$  is the height of reinforced wall (Fig.6.10).

**Table 6.12** - EB, check of respect: total (R), partial (PR), or absence (A) of ICOMOS principles and individuation of material device considering the architectural style.

ENLARGEMENT-BUTTRESS DEVICES [EB]										
Architectural style	CL					NC&V				
Material device	Adobe or stone					Brick				
ID	Au	Min	Co	Rec	Rev	Au	Min	Co	Rec	Rev
JC	NR	R	R	R	PR	NR	R	R	R	PR
$\sum_{k=1}^N \hat{Y}_{PI_k}$	9					9				

The requirements for a preliminary design of EN-BT elements are provided as follows:

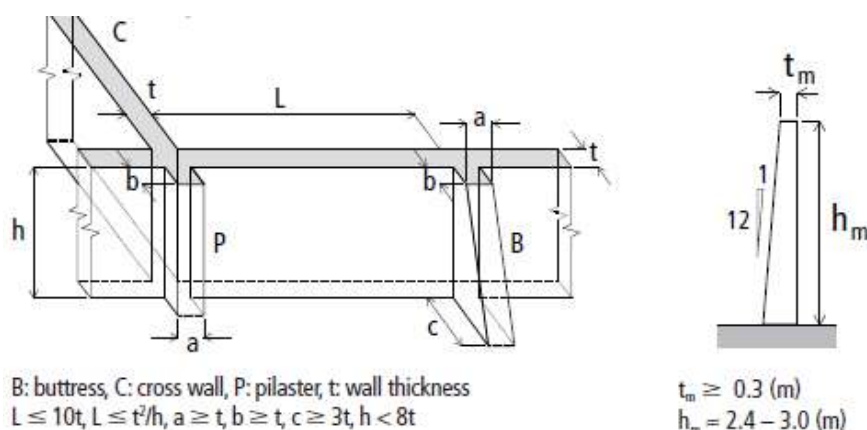
Assuming the presence of enlargement or buttresses the multiplier of load coefficient is:

$$\alpha_{0,EB} = \frac{P_s d + W_{xg} + W_{EF} x_{EF}}{P_s h + W_{yg} + W_{EF} y_{EF}} \quad (6.6)$$

Where  $\alpha_{0,EB}$  is the multiplier of the load coefficient,  $W$  is the wall masonry load;  $P_s$  is the roof load;  $x_g$  is the horizontal distance between the wall's center of gravity and the plastic hinge;  $d$  is the horizontal distance between the point of application of roof load and the plastic hinge;  $y_g$  is the vertical distance between the wall center of gravity and the plastic hinge;  $h$  is the wall height;  $W_{EF}$  is the weight of EN-BT;  $x_{EF}$  is the horizontal distance between the rotation hinge and the gravity center of EN-BT element; and  $y_{EB}$  is the vertical distance between the rotation hinge and the gravity center of EN-BT element.

From the historiographical analysis of the San Francisco church, different sources (Stefanini, 2016, Jorquera et al., 2017) agree that at the beginning of the 20<sup>th</sup> century the buttresses of the aisles were cut.

As seen in Chapter 5.2 the most vulnerable macro-element in San Francisco church after the 2010 Maule earthquake were the transverse arcades (TA). In particular, preliminary safety estimation, through Safety Theorem of Limit Analysis (Fig.5.2.11) of the static consistency of the church, showed the limit condition of the thrust line of the transverse arcade F. Moreover, corresponding to this macro-element, LKA and LDA analyses show the activation of OOP mechanisms in the transept walls.



**Figure 6.10** - Recommendations for buttresses design of Guidelines for earthquake resistant non-engineered construction. UNESCO (Arya et al., 2014).

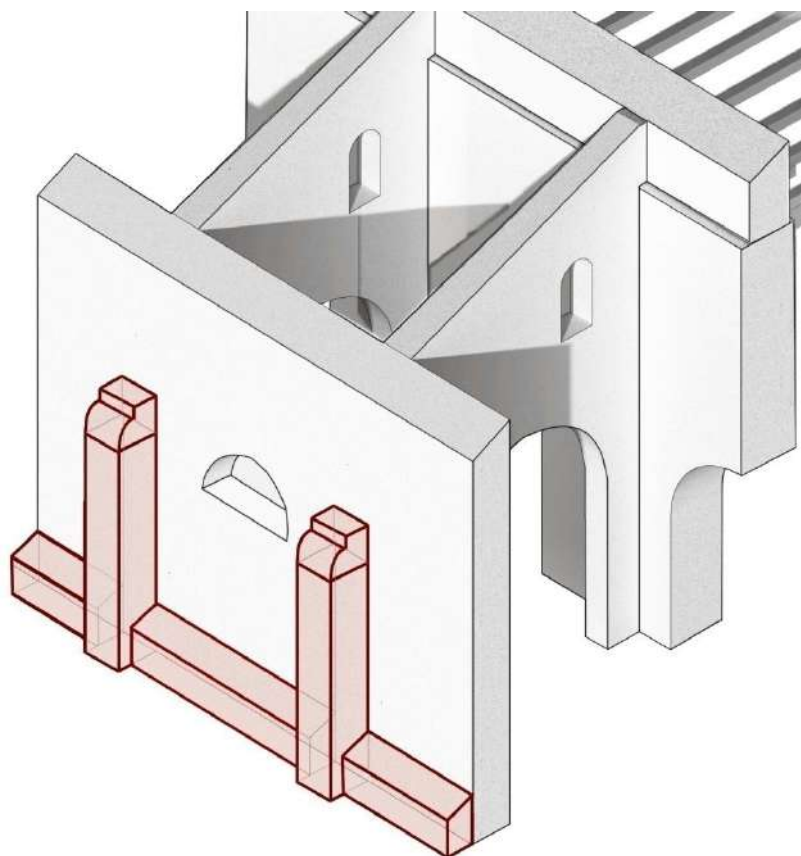
With the aim of averting the triggering of the OOP failures of the NT macro-element and the in-plane behavior of transverse arcade TA, the introduction of buttresses is proposed, Fig.6.11, imposing  $a_0^*$  equal to the Demand Acceleration at ground level ( $2.31 \text{ m/s}^2$ , according to Nch2745Of.2013).

Considering a shape coherent with the architectural style (partially visible, a thickness of  $1 \text{ m} \times 1 \text{ m}$ , with the same masonry brickwork and mechanical, chemical and physical features of brick and mortar compatible with the original, the improvement in the seismic behavior due to the BT device is assessed through LKA analysis for the consolidation of San Francisco church. In both cases of north and south transept walls, NT and ST, comparative analyses of the current state and the reinforced state (Table 6.13) show an increase in the safety index (respectively equal to 68% and 75%). These improvements lead to an IQI equal to 1.2 and 1.4 respectively, and an intervention conformity level type “B”.

**Table 6.13** - Effectiveness of BT in terms of acceleration for San Francisco church.

	Mechanism Activation Acceleration $a_0^*$ [ $\text{m/s}^2$ ]		Safety index (Cir.n.26, 2010)	
	Before interv.	After interv.	$Is_1$	$Is_2$
NT	0.866	2.34	0.33	1.01
ST	1.03	2.63	0.394	1.14

Considering the recommendations for buttresses design of Guidelines for earthquake resistant non-engineered construction (Arya et al., 2014), the only requirement not met is  $a \geq 3t$ , due to the need to realize an intervention respectful of the stylistic typology (NC&V), that has  $a = t$ . For practical reasons due to the lack of sufficient transit space in the sidewalk adjacent to the church wall:  $L = 8.65 \text{ m} \leq 10t = 10 \text{ m}$ ,  $L = 8.65 \text{ m} \geq t^2/h = 0.095 \text{ m}$ ,  $a = 1 \text{ m} \geq t = 1$ ,  $c = 1 \text{ m} \geq t = 1 \text{ m}$ ,  $h = 10 \text{ m} < 8t = 8 \text{ m}$ .



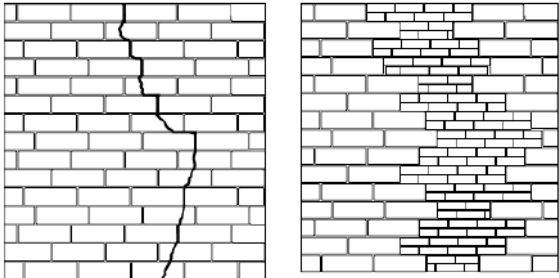
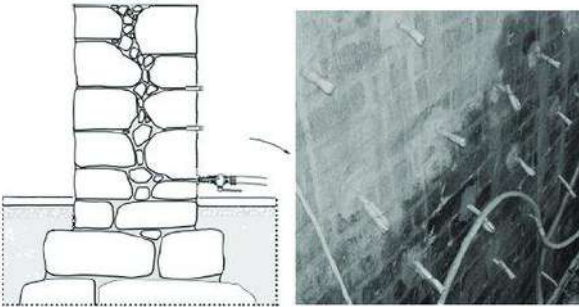
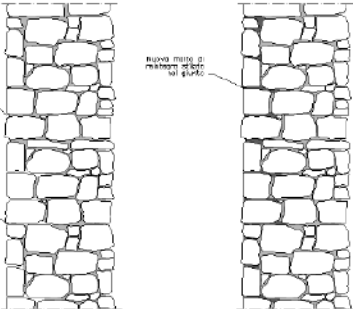
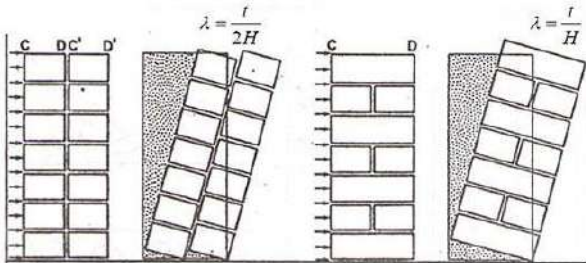
*Figure 6.11 - Retrofitting intervention for San Francisco church: Brick Buttresses.*

### 6.3.2 Strength-based techniques

Strength-based techniques improve the strength of the walls by providing better “monolithic” behavior to masonry. Common strength-based techniques for URM buildings are presented and analyzed below. Traditional systems (such as unstitch-stitch, *diatones*, and bed joint re-pointing), and modern retrofitting techniques (such as grout injection, artificial headers and fiber jackets) are taken into account considering the features of architectural styles of Chilean buildings. As in the case of stability-based techniques, possible retrofit devices for each seismic vulnerability vary with different characteristics in terms of effectiveness, invasiveness, reversibility, compatibility, durability and costs. Thus, a qualitative judgment on total, partial or absence of respect for conservation principles, previously analyzed, is provided. Generally the implementation of traditional solutions is advantageous from both a cost and compatibility point of view. However, in highly seismic regions these techniques may be insufficient and making necessary the implementation of modern devices.

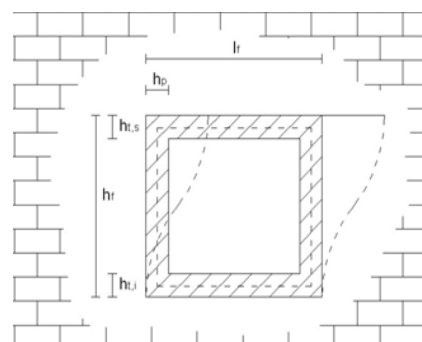
A summary of the main analyzed techniques is provided in (Table 6.14).

Table 6.14 – Strength-bases techniques.

I) STRENGTH-BASED TECHNIQUES		
Increase the resistance of masonry wall		
Device	Main goal	Example of device
<b>[US]</b>  Unstitch-stitch technique for regular brickwork	Structural continuity and uniform load distribution	 Unstitch-stitch (Dolce& Manfredi, 2011)
<b>[GI]</b>  Grout injection for masonry, stone, adobe and brick made	Enhance homogeneity and increase strength	 Grout injection (Baltazar et al., 2019)
<b>[BJR]</b>  Bed joint re-pointing for masonry, stone, adobe and brick made	Increase in strength of masonry and prevent water penetration in mortar joints	 BJR in stone masonry (Dolce& Manfredi, 2011)
<b>[D-AH]</b> Diatones or Artificial headers for masonry, stone, adobe and brick made	Increase monolithicity of masonry panel and global behavior of structure	 Diatones in brick masonry (Giuffré, 1991)

**[OC]**  
Openings  
confinement

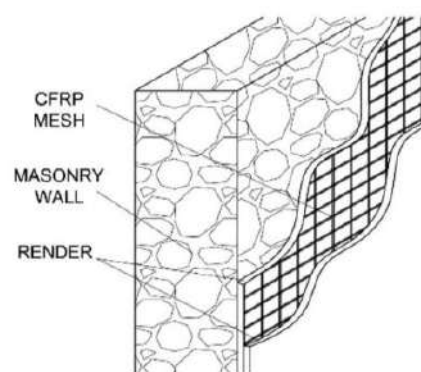
Increase the  
strengthening  
of masonry



Window confinement (Dolce& Manfredi, 2011)

**[JC]**  
Jacketing of  
masonry  
with steel or  
CFRP or  
inorganic  
matrix and

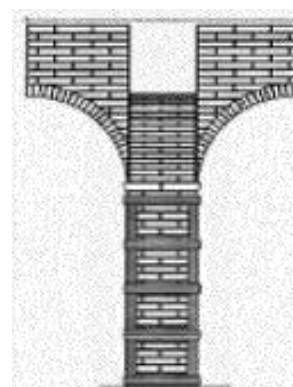
Increase  
strength  
capacity and  
ductility of  
wall



CFRP jacketing of masonry wall  
(Guerreiro et al., 2017)

**[CF]**  
Confinement  
of columns  
and pillars  
with  
composite or  
steel  
materials

Increase  
strength  
capacity and  
ductility of  
columns and  
pillar



Pillar confinement with steel elements (POLIMI, 2010)

### 6.3.2.1 [US]\_Unstitch-stitch technique

The local unstitch-stitch intervention consists of dismantling and rebuilding a portion of a cracked wall, with the aim of restoring continuity and structural integrity. For unstitch-stitch interventions, the principle of *Compatibility* is essential to guarantee an effective consolidation of the masonry wall: use of materials with similar shape, dimensions, stiffness and strength. In fact, the effectiveness of this intervention is strictly connected to recovering previous wall properties; otherwise the seismic actions could expel the intervention (Fig.6.12). Adequate connections should be provided to obtain a “monolithic” behavior. With this technique it is possible to: (1) intervene individually, to compensate for a crack in the masonry or less several lesions spaced apart, or, less frequently, and (2) to intervene in a more extensive way, in the case of cracks spread throughout the structure and located close to each other.



**Figure 6.12** - Masonry replacement intervention. The repairs are ineffective due to the lack of compatibility between the masonry portions (Frumento et al., 2006).

Table 6.15 shows that the use of US compatible masonry with the original for CL, NC&V and NG URM structures guarantees respect for all conservation principles (R, respect of principle), with exception of Rev, for which the check is not respected due to the fact that the efficiency of the intervention is strictly related to good bonds between the original and the new masonry, i.e. good bonds do not guarantee that the intervention can be removed without any damage to the original structure.

Particular attention must be paid to the use of strategies that guarantee the intervention's recognition, such as use of a pigmentation tone different from the original, or stylization of ornamentation among others.

When a masonry wall has local cracks, this can be considered as being composed of two sub-walls (“A” and “B” walls) whose stiffness ( $k_A$  and  $k_B$ ) and resistance ( $V_{uA}$  and  $V_{uB}$ ) to press-flexion and shear have to be analyzed (Fig.6.13).

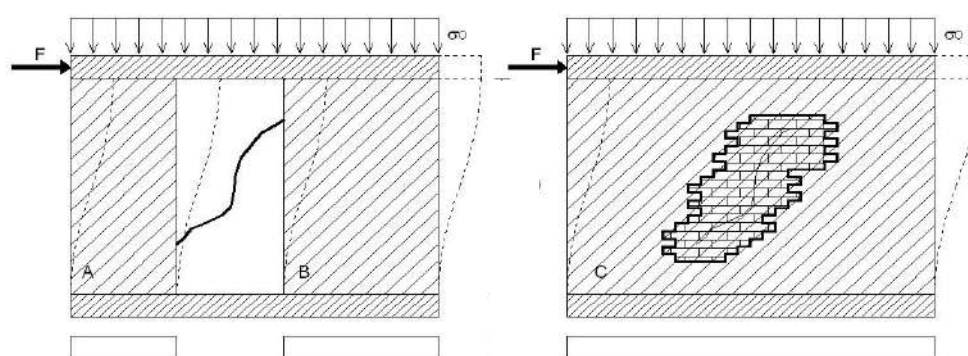
**Table 6.15-** US, check of respect: total (R), partial (PR), or absence (A) of ICOMOS principles and individuation of material device considering the architectural style.

UNSTITCH-STITCH DEVICE [US]															
Architectural style	CL					NC&V					NG				
Material device	Adobe and earth mortar*					Brick or stone and lime mortar*					Brick and lime mortar*				
ID	Au	Min	Co	Rec	Rev	Au	Min	Co	Rec	Rev	Au	Min	Co	Rec	Rev
JC	R	R	R*	R**	PR	R	R	R*	R**	PR	R	R	R*	R**	PR
$\sum_{k=1}^N \hat{\gamma}_{PI_k}$	10					10					10				

\* The use of materials with same shape, dimensions, stiffness and strength and compatibles from the chemical, physical and mechanical point of view is implied.

\*\* Different strategies must be considered to guarantee this principle such as different tones of pigmentation, or stylization of ornamentation among others.

In a case where an element is free to translate only in the head (a degree of freedom), the stiffness is equal to  $k = \left( \frac{h^3}{12EI} + \frac{1.2h}{GA} \right)^{-1}$ . In a case where it is free to translate and rotate the stiffness is equal to  $k = \left( \frac{4h^3}{12EI} + \frac{1.2h}{GA} \right)^{-1}$ , where  $h$  is the height of the masonry wall;  $E$  is the normal Young modulus of the masonry;  $G$  is the tangential elastic modulus of the masonry;  $I$  is the moment of inertia with respect to the gravity center, orthogonal to the plane of the wall, of the cross section of the masonry wall;  $A$  is the area of the cross section of the masonry wall.



**Figure 6.13** - Schematization of masonry wall (a) with a localized lesion, and (b) with an unstitch-stitch intervention (Vinci, 2012).

The resistance to press-flexion failure mechanism,  $V_f$ , of the masonry wall is  $V_f = M_u/h_0$ , where  $M_u$  is the bending moment, and  $h_0$  is the distance between the verification section and the null-moment section. The resistance to shear failure mechanism,  $V_t$ , of the masonry wall is equal to  $V_t = f_{vd} l_t t$ , where  $V_t$  is the shear resistance to sliding failure;  $l_t$  is the length of the compressed base of the wall; and  $t$  is the thickness of the wall. For both masonry walls the

failure occurs due to bending. The elastic,  $\delta_0$ , and ultimate,  $\delta_u$ , displacements of the analyzed elements are obtained by  $\delta_0 = V_u/k$  and  $\delta_u = d \delta_0$ , where  $V_u$  is the maximum shear;  $k$  the masonry wall stiffness; and  $d$  the ductility.

From the crack pattern assessment of the Basilica del Salvador, Chapter 5.3.3, the deep vertical cracks in the keystone of the windows show the decomposition of the upper part of masonry in independent sub-portions, subjected to the activation of OOP mechanisms.

Therefore, the Unstitch-stitch interventions are provided, in the entire structure, for the reconstruction of the arch haunches of the windows.

### 6.3.2.2 [GI]\_Grout injection

In Italy, after the Friuli (1976) and Irpinia (1980) earthquakes the grout injections were largely applied to fill the holes, cavities and internal voids. The aim of this technique is to reconstitute the structural continuity and increase the mechanical properties of masonry wall. The physical, chemical, and mechanical *Compatibility* of grout injections with original elements of masonry (brick or stone and mortar) is essential for the effectiveness of intervention.

**Table 6.16-** GI, check of respect: total (R), partial (PR), or absence (A) of ICOMOS principles and individuation of material device considering the architectural style.

GROUT INJECTION DEVICE [GI]															
Architectural style	CL					NC&V					NG				
Material device	Earth mortar*					Hydraulic-lime or ternary grouts *					Hydraulic-lime or ternary grouts *				
ID	Au	Min	Co	Rec	Rev	Au	Min	Co	Rec	Rev	Au	Min	Co	Rec	Rev
JC	PR	PR	R*	R	NR	PR	PR	R*	R	NR	PR	PR	R*	R	NR
$\sum_{k=1}^N \hat{Y}_{PI_k}$	7.5					7.5					7.5				

The common GIs for masonry walls are made of binder, water and additives, injecting into the masonry mortar (Fig.6.14). In (Valluzzi et al., 2004; Vintzileou & Miltiadou, 2008; Kalagriet et al., 2010) hydraulic-lime or ternary grouts, inorganic binders, are suggested (Table 6.16). When this intervention is carried out with compatible materials is not intrusive technique.

In order to guarantee material compatibility with URM structures, only lime-based grouts should be used. Nevertheless, epoxy additives and/or cement are often used to obtain faster setting.

It is now known that these additives, despite at short-term increase the strength and cohesion of the masonry, in the long-term create problems which are, not monitorable, such as the

*decomposition of the original materials due to the different hydrothermal behavior and the release of salt content (D'Ayala, 2014).*



**Figure 6.14** – Grout injections (Source POLIMI-UNIPD)

The Italian Code for existing building (DPCM, 2011, C8A.2) provides correction coefficients to consider the contribution of mortar injections to the masonry wall strength. The correction coefficients are in accordance with the masonry type. The values of the correction coefficients for the masonry types present in Chile are shown below, Table 6.17. To take into account the effect of consolidation, the mechanical parameters of the masonry must be multiplied by the corrective coefficients corresponding to the type of wall shown in Table 6.17 equal to  $f_{mGI} = fm \gamma_{CO}$ ,  $\tau_{odGI} = \tau_{od} \gamma_{CO}$ ,  $E_{GI} = E \gamma_{CO}$ ,  $G_{GI} = G \gamma_{CO}$ , where  $fm$  is the compressive strength;  $\tau_{od}$  is the shear strength;  $E$  is the normal Young modulus; and  $G$  is the tangential Young modulus.

**Table 6.17** – Correction coefficients are in accordance with the masonry type (DPCM, 2011, C8A.2)

Masonry type	Correction coefficient for mortar injections $\gamma_{CO}$
Rubble-Stone-Masonry	2.0
Brick-masonry with lime mortar	1.5

With the aim of improving the cohesion and coherence of the Basilica's masonry columns (Fig.6.15), Chapter 5.3, grout injections are proposed. Mineralogical and petrographic studies of column mortar sample (M4, Chapter 5.3.2) were carried out to define the grout injection features. The results of the analysis showed that the M4 sample consists of a particularly lean mixture (binder/aggregate 1/3-1/4), comprised of volcanic fragments (Andesine ((Na,Ca)(Si,Al)4O8)), feldspars ((Al,B,Si)4O8), and *cocciopesto*. The aggregate has a bimodal granulometry (prevalent 600-800 $\mu$ m, 1,5-3 secondary) with granules of a basically rounded shape, which indicates a fluvial origin. Composition is predominantly of volcanic rock

fragments compared to single granules. Thus, inorganic binders such as hydraulic-lime or ternary grouts are suggested for GI intervention.

After the study of mortar grout composition, the GI procedure comprises: choice of injection points (2-3 injection points/m<sup>2</sup>), plaster removal, drilling of 40mm diameter spaced on a 400mm grid, sealing and repointing of the mortar joints, assessment of the injection pressure, and GI with fluid lime-based grout through a ultra-fine aggregate and low salt content.



**Figure 6.15** – Column section of Basilica del Salvador

**Table 6.18-** Effectiveness of AH in terms of Masonry quality index for Malloa Parish

	Mechanical properties of columns		Safety index (Cir.n.26, 2010)	
	Before interv.	After interv.	$Is_1^*$	$Is_2^*$
$f_m$ [MPa]	3.5	5.25	0.875	1.31
$\tau_0$ [MPa]	0.05	0.075	0.33	0.83
$E$ [MPa]	1380	2070	0.77	1.11

\*In this case the safety indexes ( $Is_1$  and  $Is_2$ ) are calculated through the ratio between the mechanical properties  $f_m$ ,  $\tau_0$ , and  $E$ , at present or reinforced states, and the maximum ranges recommended by the standard (Cir.n.26, 2010) for brick masonry, equal to  $f_{m, max}=400$ MPa,  $\tau_{0, max}=0.09$ MPa, and  $E_{max}=1800$ MPa.

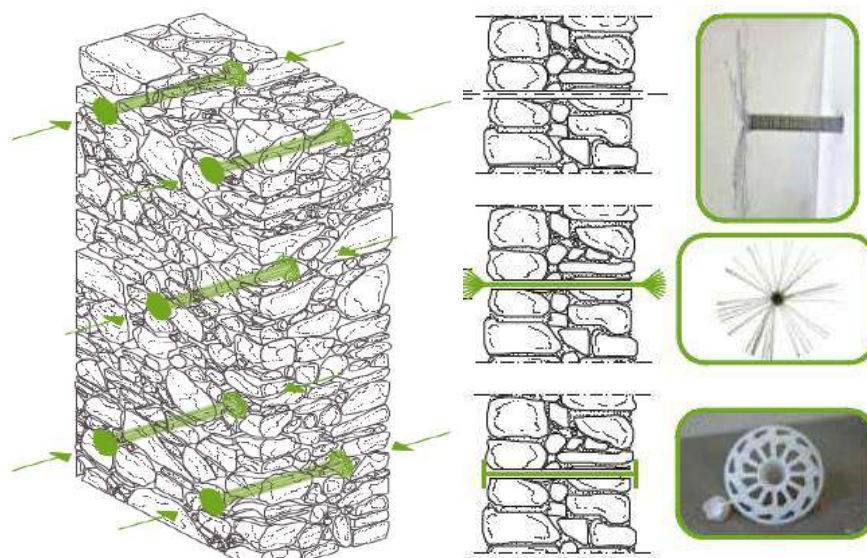
### 6.3.2.3 Artificial headers

Artificial headers consist of transversal locking in the wall thickness, *diatones*, which connect the adjacent wall leaves, increasing the monolithicity of masonry panel and the global behavior of structure. AH permits the load distribution along the entire width of the masonry. In historic brick, stone, and adobe masonries, the *diatones* are a traditional construction device, which form the “rule of the art” of building (Borri et al., 2015).

Historically, this device was part of the original masonry and demonstrated to have very efficient performance during the past earthquakes. Consequently, *artificial headers* were introduced as device in existing buildings using different solutions: R.C. elements, steel bars, and fiber bars (carbon, glass, polyvinylalcohol, and galvanized steel materials) impregnated in a matrix (Fig.6.16).

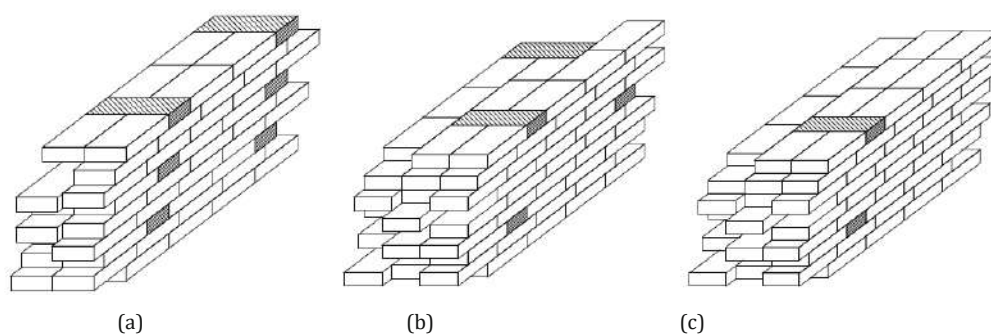
Physical, chemical, and mechanical *Compatibility* of the device must be guaranteed with original masonry for the effectiveness of the intervention. In (Valluzzi et al., 2004; Vintzileou & Miltiadou, 2008; Kalagri et al., 2010), for example, hydraulic-lime or ternary grouts, inorganic binders, are suggested.

Moreover, to be efficient, this device must be generalized to the entire wall. Systematic presence of headers  $<4\text{-}5\text{m}^2$ , with constant horizontal and vertical distance is suggested.



**Figure 6.16** –Example of Galvanized steel diatones of KERAKOLL

Table 6.19 shows that the use of AH as seismic device in masonry structures guarantees respect for all conservation principles (R or PR), with the exception of the Authenticity (Au). In fact, the AH intervention determines the alteration of original static and dynamic behavior, permitting the loads to be distributed along the entire width of the wall and preventing the activation of mechanisms OOP mechanism (Borri et al., 2015).



**Figure 6.17** - Wall leaf connections: (a) Systematic presence of headers ( $>4-5/m^2$ ) with wall thickness similar to the stone/brick larger dimension; (b) Double leaf walls with limited number of headers ( $2-5/m^2$ ) and all thickness is larger than the brick larger dimension; and (c) No headers or less than  $2/m^2$  (Borri et al., 2015).

According to the masonry type characterizing the CL, NC&V, and NG churches, different types of AH are considered for reinforcing URM structures with respect to their architectural styles. Regarding the CL buildings, in adobe masonry, timber or adobe transverse elements are proposed for wall leaf connections given their chemical, physical and mechanical compatibility with the original materials. The  $\sum_{k=1}^N \hat{\gamma}_{PI_k}$  is equal to 10.

In the case of two or three leaves wall reinforcement of NC&V and NG buildings, the use of R.C. elements, steel bars, and fiber bars with different matrices are the most common devices. This technique is considered rather invasive and its removal can cause minor damage to the original structure. Thus, as shown in **Table 6.19**, Min and Rev principles for NC&V and NG structures are partially respected. Moreover, the AH intervention determines the alteration of original static and dynamic behavior as not respecting the Au principle. The use of AH devices fall in  $\sum_{k=1}^N \gamma_{PI_k}$  equal to 7.5. Thus, they can be considered retrofitting interventions in conformity with ICOMOS philosophy.

**Table 6.19**—AH, check of respect: total (R), partial (PR), or absence (A) of ICOMOS principles and individuation of material device considering the architectural style.

ARTIFICIAL HEADER DEVICE [AH]																
Architectural style	CL					NC&V					NG					
Material device	Adobe-Timber					R.C.-Fiber-Steel					R.C.-Fiber-Steel					
ID	Au	Min	Co	Rec	Rev	Au	Min	Co	Rec	Rev	Au	Min	Co	Rec	Rev	
JC	NR	R	R	R	R	NR	PR	R	R	PR	NR	PR	R	R	PR	
$\sum_{k=1}^N \hat{\gamma}_{PI_k}$	10					7.5					7.5					

As seen in Chapter 5.1.4.1, the most vulnerable macro-elements in Malloa parish after the 2010 Maule earthquake were the chapel walls (LW5e, LW6e, LW7e, and LW5w). In fact, they were the only macro-elements where several local collapses involving the external leaf of the two-leaf adobe masonry (W03) were observed. Two double-leaf-wall overturning mechanisms were triggered, determining the collapse of the external leaf due to the absence of transverse connections between wall leaves. For this reason, the reconstruction of the collapsed leaf and the introduction of wooden *diatones* were proposed.

Calculating the Masonry Quality Index (MQI method, presented in Chapter 5, Borri et al., 2015), a comparison between the masonry quality before and after the AH intervention can be assessed. The MQI method allows for an estimation of masonry quality using a qualitative description applicable to any type of wall, evaluating the agreement of the masonry features with the rule of art, (i.e., block shape and size, horizontal rows, staggering of vertical joints, presence of transverse blocks *diatones*, mortar quality, and the stone/brick/adobe strength). Three different value of MQI for vertical actions (V), out-of-plane actions (OOP), and in-plane actions (IP) are obtained, and the results before and after the intervention AH are compared in Table 6.20.

Considering the minimum safety  $MQI_{Demand}$  value requirement for each action (Borri et al., 2015, considering for vertical action  $MQI_{demand} \geq 5$ ; for OOP action  $MQI_{demand} \geq 7$ ; and IP action  $MQI_{demand} \geq 5$ ), the safety index is calculated as a ratio between  $MQI_{Capacity} / MQI_{Demand}$ . Table 6.20 gives the safety indexes of the W03 masonry in Malloa parish, before and after the AH intervention.

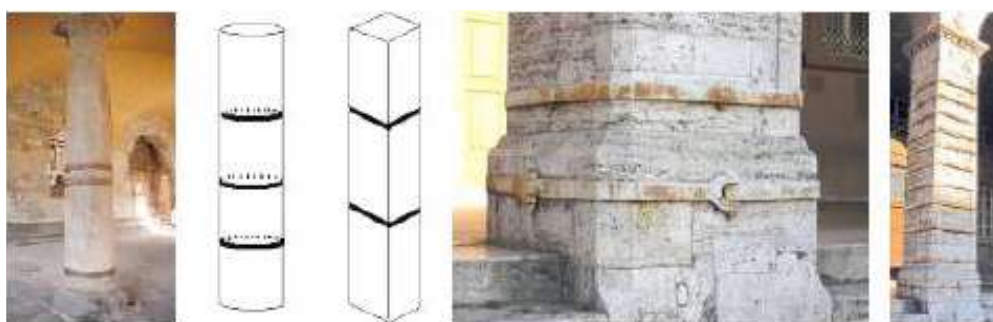
Although the safety index after the intervention  $Is_2$  is greater than  $Is_1$  at the current state, the safety check is not yet satisfied, due to the very low strength of the adobe masonry. Thus the MQI very low: 0.1, 0.2, and 0.4 respectively for vertical, OOP and IN actions. Therefore, a consolidation intervention complementary to the introduction of *diatones* is required such as a ring-beam at the roof and lintel levels, and jacketing with natural fiber and earth matrix.

**Table 6.20** - Effectiveness of AH in terms of Masonry quality index for Malloa Parish.

Action	M.Q.I <sub>Capacity</sub>		Safety index	
	Before interv.	After interv.	$Is_1^*$	$Is_2^*$
Vertical	2.1	2.4	0.42	0.48
Out-of-plane	1.8	2.4	0.26	0.34
In-plane	2.1	3	0.42	0.6

### 6.3.2.4 [CF] Confinement or jacketing of columns, pillars and walls

In order to control local compressive strength concentrations and improve stability of columns and pillar, *confinement* is an effective technique. These devices are located in critical sections of vertical elements, generally in the lower part of shaft where vertical cracks are present, to contain transversal dilatation. The most commonly used materials are steel ring and polymers or FRP strips.



**Figure 6.18** – Confinement of column and pillar (Source UNIPD)

In Fig.6.18 retrofitting interventions with steel CF of column and a pillar are shown.

The main goal of confinement is to restore the bearing capacity of the element, conferring an increase in resistance and deformation capacity. The confinement is undertaken with steel elements respecting (R) all conservation principles analyzed in Table 6.21, while the use of polymers or FRP does not guarantee respect of compatibility (PR\*), due to the delamination process, and reversibility (NR\*). Nevertheless, in many cases due to the damage level, diffuse cracks and the shape of the element, polymers or FRP strips represent a valid alternative.

**Table 6.21**- CN, check of respect: total (R), partial (PR), or absence (A) of ICOMOS principle and individuation of material device considering the architectural style.

CONFINEMENT DEVICE[CN]															
Architectural style	NC&V and NG														
Material device	Steel					FRP with inorganic polymer					FRCM with organic polymer				
ID	Au	Min	Co	Rec	Rev	Au	Min	Co	Rec	Rev	Au	Min	Co	Rec	Rev
JC	NR	R	R	R	R	NR	PR	PR	R	PR	NR	PR	R	R	PR
$\sum_{k=1}^N \hat{\gamma}_{PI_k}$	10					6					7.5				

The effectiveness of confinement is relative to the damage state of elements and the distance between strips. In (Grimaz et al., 2010), solutions of confinement are identified considering different shape and dimensions. In particular:

- masonry columns with diameters  $d \leq 90\text{cm}$ ;
- and masonry pillars with minor side  $s_{\min} < 90\text{cm}$  and the ratio between the minor and larger side equal to  $L/l_{\min} \leq 2$ .

These limitations are due to the ineffectiveness of devices on slender and stumpy elements.

The requirements for a preliminary design of CF elements are provided as follows:

The relation who expresses the resistance increase of vertical element due to confinement intervention (Borri & Graziani, 2004) is:  $N_u = N + \Delta N$ , where  $N$  is the compression resistance of the vertical element section without confinement equal to  $N = A f_{m,do}$ , and  $\Delta N$  is the increase of the normal resistant force due to the confinement, equal to  $\Delta N = A k_l f'_l$ , where  $A$  is the area of vertical element section;  $f_{m,do}$  the masonry compressive strength;  $k_l$  is the coefficient of increase of the compressive strength due to the confinement, equal to  $k_l = 2.4 (f'_l / f_{m,do})^{-0.17}$ ; and  $f'_l$  is the effective confinement pressure, equal to  $f'_l = k_H k_v f_l$  eq.6.8, where  $k_H$  is the horizontal efficient coefficient equal to the ratio between the area of vertical element section with confinement and the area of vertical element section ( $A_m$ ), equal to  $k_H = 1 - [(b'^2 + d'^2) / (3A_m)]$ ;  $k_v$  is the vertical efficient coefficient equal to  $k_v = [1 - (p_f b_f) / (2_{\min} b, d)]^2$ .



**Figure 6.19** - Worrying deep vertical crack in arch piers of central nave pillar axis F.

As shown from the crack pattern analysis and safety estimation of the static consistency of San Francisco church, in Chapter 5.2, the columns of central nave subject to compression have generated vertical tensile crack with a brittle fracture of the stone material (Fig.6.19). This type of crack is very worrying because, when it occurs the effectiveness of the original

section of pillar is lost. Moreover, it is worth noting that the thrust line of transverse arcade F highlights a limit condition for stability. Thus, it is necessary to intervene promptly eliminating the cause of the damage, i.e. the load above and the thrusts of the arches must be immediately contrasted. For these reasons, the reinforcement of the damaged pillars of central nave of San Francisco is strongly recommended. For example, the confinement with FRP of the most damaged pillar, pillar F, is assessed. The masonry pillar under examination is 2.61m in width and 1.9m thickness and at 5.94m receives the thrust of three masonry arches.

According to CNR-DT 200 (CNR-DT,2013), the axial capacity of the FRP strengthened member,  $N_{Sd}$ , must be lower than the design axial force due to the applied loads,  $N_{Rmc,d}$ , as follows  $N_{Sd} \leq N_{Rmc,d}$ , where  $N_{Rmc,d} = (1/\gamma_{Rd})A_m f_{mcd}$ , where the partial factor ( $\gamma_{Rd}$ ) is equal to 1.25.

**Table 6.22-** Effectiveness of CF in terms of design axial force  $N_{Rmc,d}$  and axial capacity of the FRP strengthened member,  $N_{Sd}$  for San Francisco church

	M.Q.I <sub>Capacity</sub>		Safety index	
	Before interv.	After interv.	$Is_1^*$	$Is_2^*$
$N_{Rmc,d}$ [kN]	1056	3600	029	1

Considering a dimensionless coefficient of increase in resistance,  $k'$ , equal to 2.8; a coefficient of efficiency,  $k_H$ , equal to 0.77; the coefficient of vertical efficiency,  $k_v$ , equal to 0.75; The confining pressure,  $f_l$ , equal to 494.5; the strain for FRP,  $\epsilon_{fd}$ , equal to 0.0086; the confined area and the total area of the masonry column,  $A_m$ , equal to 14.97; the  $b'$  and  $d'$  equal to 1.88m and 2.59m respectively; the center-to-center spacing of FRP strips,  $pf$ , equal to 0.5m; the Young modulus of elasticity in the fiber direction,  $E_f$ , equal to 230GPa; the FRP strip width,  $bf$ , equal to 0.01m; the FRP thickness,  $tf$ , equal to 0.00165m; the  $r$  equal to 0.01m, of equal to 3.47E-05.

The increase of the normal resistant force due to the confinement is equal to  $\Delta N = 3600 \text{ kN}$  and  $N_{Sd}$  axial capacity of the FRP strengthened member is 1050kN. Moreover, the design compressive strength,  $f_{mcd}$ , for members confined with FRP subjected to a lateral confining pressure is equal to 1.5MPa, while the design compressive strength of unconfined masonry  $f_{mdo}$  0.7MPa.

The comparative analysis of the current state and the state after the CN retrofitting intervention (Table 6.22) shows the achievement of the required safety levels ( $Is_2=1$ ), and the IQI Index results equal to 1.1, leading to an intervention conformity level type “B”.

## 6.4 Summary

This last Chapter synthesizes the work of this thesis, while the results obtained in the previous Sections allow answering the general research question: How can the seismic risk of URM Built Heritage be mitigated in a highly seismic region, while respecting the conservation principles such as those given by ICOMOS?

In this chapter, a preliminary proposal was provided to introduce evaluation criteria for the reinforcement interventions in relation to the level of compatibility with the conservation principles. In order to define the assessment methodology, the conservation ICOMOS principles have been reinterpreted in a purely structural manner considering the impact that a specific retrofit intervention has on the church from a conservation point of view.

The degree of agreement between each retrofit technique and conservation principles has been evaluated through judgement categories (respected, partially respected, and not respected), and then transformed into scores. These scores allow to assign a weight relative to the degree of importance that each principle, interpreted in structural terms, assumes in the evaluation procedure. In particular, the respect for *compatibility* and *minimum intervention* principles have been assessed as being more significant than *reversibility* and *recognition*.

The proposed scores represent a preliminary hypothesis that should be better specified in future works, considering further factors influencing the choice of intervention, such as for example: the required safety levels, the state of conservation of the asset, the symbolic importance and the social value, the costs and the duration of the intervention. Moreover, the method applied here to the Chilean context, must be statistically validated for its application to a wider range of construction contexts.

The three case studies, representative of the fragility classes, made it possible to apply this method by, considering specific intervention proposals, such as tie-rods for Basilica del Salvador arches, wooden ring-beams for the Malloa parish, and pillar confinements for the San Francisco church, among others.

Generally, the proposed stability-based techniques arise from the rediscovery of traditional earthquake-resistant practices of Chilean constructive culture (extensively documented in Chapter 2), while the strength-based techniques arise from the use of modern retrofit strategies. The results obtained have confirmed the overall hypothesis assumed: “The rediscovery of traditional earthquake resistant practices, together with the use of modern retrofit strategies, allow preserving and reinforcing the built heritage without harming its identity”.

In fact, the application of the evaluation methodology proposed leads to very high values of conformity for the stability-based techniques, while it leads to lower values and partial assessment relative to the respect of conservation principles for the strength-based techniques.



# Chapter 7

## CONCLUSION

### 7.1 Main findings

Considering main findings and related discussions reported in the summary of each Chapter, this dissertation achieved the objectives listed in Section 1.4.

In particular at territorial-scale, this research provides the following findings:

- The main variables controlling the seismic fragility of URM churches of central Chile have been determined. These are: (a) masonry type (Stone, Brick, Adobe); (b) architectural layout (Basilica, Single Nave, Latin Cross); (c) architectural style (Colonial Style, Neo-classic Style & Variants, Neo-gothic Style); and (d) foot-print area ( $90\text{m}^2 < A1 \leq 500\text{m}^2$ ;  $500\text{m}^2 < A2 \leq 900\text{m}^2$ ; and  $A3 > 900\text{m}^2$ ). (Chapter 2).
- Somewhat homogeneous fragility classes have been identified. There are: Colonial (CL), Neo-classical & Variants (NC&V), and Neo-gothic (NG) churches. (Chapter 2).
- Probability Mass Functions, considering the global and local structural behavior of Chilean URM churches, have been developed to quantify their seismic fragility. Good agreement has been observed between the Probability Mass Functions and Binomial Probability Density Functions. (Chapter 4).
- Fragility Curves of whole stock have been developed to quantify the seismic fragility of Chilean URM churches. The FCs have been obtained using generalized linear model (GLM) fitting by maximum likelihood estimation (MLE), and lognormal distribution fitting by weighted sum of squared error (SSE). (Chapter 4).

Moreover at single building-scale, this research provides the following findings:

- A methodology to assess the seismic performance of a single URM structure (case study), based on a multidisciplinary approach that exploited historical researches, direct surveys on building techniques and crack pattern, in situ and laboratory testing and multilevel structural analysis has been provided. (Chapter 5).
- The seismic response and risk of three case studies, representative of fragility classes, have been quantified through: as concerning the local analyses by damage mechanisms, the LKA and IKA analyses have been carried out; and as concerning the global analysis LDA and EFA have been carried out. (Chapter 5.1, 5.2, and 5.3).
- A new preliminary methodology for the individuation of seismic retrofitting strategies related to ICOMOS conservation principles is proposed. (Chapter 6).

- General guidelines for seismic retrofitting interventions, deduced through the new methodology, are presented for the case studies representative of homogenous fragility classes. (Chapter6).

### 7.2 Future research

Based on the achieved results, further objectives for future research tasks can be identified.

At territorial-scale:

- To collect data in order to obtain Empirical Fragility Curves for CL, NC&V, and NG classes;
- To develop seismic scenarios for whole churches of central valley of Chile ( Valparaiso, Metropolitan, Bernardo Hogging's, and Maule regions);
- And to add site effects to seismic scenarios, by considering the subsoil under each church location, undertaking 1D site response analysis.

Moreover, at single building scale it includes:

- To assess the seismic behavior of three case studies through non-linear static and dynamic analysis;
- To develop Analytical Fragility Curves for three case studies;
- To develop the preliminary methodology for the analysis of the accordance between seismic retrofitting intervention and the conservation principles.

## References

- ❖ Arias Arquitectos, and Fercovic, G. 2011. Ficha técnica de daño y oferta de servicios. Informe de la Evaluación Preliminar de Daños Provocados por el sismo de 2010, Chile: Ilustre municipalidad de Malloa, Departamento de Proyecto.
- ❖ Arias Arquitectos. 2013. *Reparación y Consolidación estructural Iglesia San F.co el Monte*. Santiago: Consejo de Monumentos Nacionales. Dirección de Arquitectura del Ministerio de Obras Publicas.
- ❖ Arnold, C., Reitherman, R. 1982. *Building Configuration and Seismic Design*. New York: John Wiley.
- ❖ ARQUIPA, Arquitectura y Patrimonio SPA, 2017. *Informe de diagnóstico estructural Iglesia del San Ignacio, Santiago*. Santiago de Chile: Consejo de Monumentos Nacionales, Dirección de Arquitectura del Ministerio de Obras Publicas.
- ❖ Arya, A. S., Boen, T., & Ishiyama, Y. (2014). Guidelines for earthquake resistant non-engineered construction. UNESCO.
- ❖ Astroza, M., F. Cabezas, M. Moroni, L. Massone, S. Ruiz, E.Parra, F. Cordero, and A. Mottadelli. 2010. Intensidades sísmicas en el área de Daños del Terremoto del 27 de Febrero de 2010. Santiago, Chile: Departamento de Ingeniería Civil, Universidad de Chile.
- ❖ Astroza, M., S. Ruiz, and R. Astroza. (2012). Damage assessment and seismic intensity analysis of the 2010 (Mw 8.8) Maule earthquake. *Earthquake Spectra* 28 (S1):145–64.
- ❖ Atkinson, G., and D. Wald. 2007. Modified Mercalli Intensity: A surprisingly good measure of ground motion. *Seism Researcher L* 78:362–68. doi:10.1785/gssrl.78.3.362.
- ❖ Augusti, G., Ciampoli, M., & Zanobi, S. (2002). Bounds to the probability of collapse of monumental buildings. *Structural safety*, 24(2-4), 89-105.  
Available at:  
[http://openarchive.icomos.org/432/1/Monuments\\_and\\_Sites\\_1\\_Charters\\_Petzet.pdf](http://openarchive.icomos.org/432/1/Monuments_and_Sites_1_Charters_Petzet.pdf).
- ❖ Bahamondez, P., Muñoz, G., E., Morales, A., M. 2012. Patrimonio religioso en Chile: su valoración un proceso en desarrollo. *Conserva: Revista del Centro Nacional de Conservación y Restauración* , 17.
- ❖ Baltazar, L. G., Henriques, F., & Cidade, M. T. (2019). Rheology of Natural Hydraulic Lime Grouts for Conservation of Stone Masonry—Influence of Compositional and Processing Parameters. *Fluids*, 4(1), 13.
- ❖ Barazangi, M., & Isacks, B. L. (1976). Spatial distribution of earthquakes and subduction of the Nazca plate beneath South America. *Geology*, 4(11), 686-692.

## REFERENCES

---

- ❖ Barrientos, S. 2007. Earthquakes in Chile. In *The Geology of Chile*, edited by T. Moreno, and W. Gibbons, 263–87. London, UK: Geological Society.
- ❖ Benavides, A. 1988[1941]. *La arquitectura en el virreinato del Perú y en la capitanía general de Chile*. Santiago, Chile: Andrés Bello.
- ❖ Benavides, J., R. Márquez De La Plata, and L. Rodríguez. (1977). *Arquitectura del altiplano. Caseríos y villorrios ariqueños*. Santiago, Chile: Facultad de Arquitectura y Urbanismo Universidad de Chile.
- ❖ Berg L, Boldrini P, Gonzalez P, Lappé P, Vivaldi R (1996). Estudio preliminar para un proyecto de restauración de la Basílica del Salvador. Santiago de Chile: Oficina Ministerio Obra Pública
- ❖ Bergami, A. V., and C. Nuti. (2013). A design procedure of dissipative braces for seismic upgrading structures. *Earthquake and Structures* 4:85–108. doi:10.12989/eas.2013.4.1.085.
- ❖ Bernardini A., Gori R, Modena C. (1990); “An application of coupled analytical models and experiential knowledge for seismic vulnerability analyses of masonry buildings”; In A. Koridze (ed) *Engineering Aspects of Earthquake Phenomena*, Vol. 3: 161-180. Oxon: Omega Scientific, 1990
- ❖ Boroschek RL, Contreras V, Kwak DY, Stewart JP (2012). Strong Ground Motion Attributes of the 2010 M w 8.8 Maule, Chile, *Earthquake. Earthquake Spectra*, 28 (S1), S19–S38.
- ❖ Boroschek, R., Soto, P., and Leon, R., (2010a). Red Local de Registros Edificio Camara Chilena de la Construcción. Universidad de Chile, Facultad de Ciencias Fisicas y Matematicas, Departamento de Ingeniería Civil, Informe Renadic 10/03 Rev. 2.
- ❖ Boroschek, R., Soto, P., and Leon, R., (2010b). Registros del Terremoto del Maule Mw = 8.8 27 de Febrero de 2010, Universidad de Chile, Facultad de Ciencias Fisicas y Matematicas, Departamento de Ingeniería Civil, Informe Renadic 10/05 Rev. 2 (in Spanish).
- ❖ Borri, A., & Grazini, A. (2004). Masonry columns strengthening with FRP materials. In *Proceedings of the 2nd national symposium on mechanics of masonry structures strengthened with FRP materials* (pp. 193-202).
- ❖ Borri, A., Castori, G., & Grazini, A. (2009). Retrofitting of masonry building with reinforced masonry ring-beam. *Construction and Building Materials*, 23(5), 1892-1901.
- ❖ Borri, A., Corradi, M., Castori, G., & De Maria, A. (2015). A method for the analysis and classification of historic masonry. *Bulletin of Earthquake Engineering*, 13(9), 2647-2665.
- ❖ Borri, A., Castori, G., Grazini A. (2009). Retrofitting of masonry building with reinforced masonry ring-beam. *Construction and Building Materials*, 23: 1892-1901

- ❖ Braga F, Dolce M, Liberatore D (1982). A statistical study on damaged buildings and ensuing review of the MSK-76 scale. In: Proceedings of 7th European conference on earthquake engineering, Athens, September
- ❖ Braga, F., R. Gigliotti, G. Monti, F. Morelli, C. Nuti, W. Salvatore, and I. Vanzi. (2015). Post-seismic assessment of existing constructions: Evaluation of the shake maps for identifying exclusion zones in Emilia. *Earthquake and Structures* 8 (1):37–56. doi:10.12989/eas.2015.8.1.037
- ❖ Brandonisio, G., Lucibello, G., Mele, E. and De Luca, A., (2013). Damage and performance evaluation of masonry churches in the 2009 L'Aquila earthquake. *Engineering Failure Analysis*, 34: 693-714.
- ❖ Cáceres, O. (2007). *La arquitectura de Chile independiente*, Universidad del Bío-Bío. Concepción: Editorial Universitaria.
- ❖ Calvi GM, Pinho R, Magenes G, Bommer JJ, Restrepo-Veléz LF, Crowley H. (2006). The development of seismic vulnerability assessment methodologies for variable geographical scales over the past 30 years. *ISET J Earthq Technol* 43(3):75–104; Paper No. 472.
- ❖ Cancino, C. (2010). Damage assessment of historic earthen sites after the 2007 earthquake in Peru. *Adv Mater Res*, 133–134:665–670
- ❖ Cancino, C., Farneth, S., Garnier, P., Neumann, J.,V., and Webster, F.,D. (2009). Damage Assessment of historic earthen buildings after the August 15, 2007 Pisco Earthquake, Peru. Los Angeles: The Getty Conservation Institute, LA.
- ❖ Cancino, C., S. Lardinois, T. Michiels, and P. Balakrishnan. 2013. Earthen architecture initiative seismic retrofitting project: A bibliography. Los Angeles, CA: Getty Conservation Institute. <http://aata.getty.edu/browse>
- ❖ Cangi, G. (2009). Murature tradizionali e terremoto-Analisi critica del danno come presupposto per il recupero e la ricostruzione dell'edilizia storica danneggiata dal sisma in Abruzzo. ARCo–Associazione per il Recupero del Costruito. Restaurare dopo Terremoto, 27.
- ❖ Cárdenas, A. P. (2010). *Informe de la Evaluación Preliminar de Daños Provocados por el sismo de 2010, Chile: Iglesia del Santísimo*. Santiago de Chile: Consejo de Monumentos Nacionales, Dirección de Arquitectura del Ministerio de Obras Publicas.
- ❖ Carocci, C. F. (2001). Guidelines for the safety and preservation of historical centres in seismic areas. *Historical constructions*, 145-166.
- ❖ Carrasco, G. and Rodríguez, A., (2010<sup>a</sup>). *Informe de la Evaluación Preliminar de Daños Provocados por el sismo de 2010, Chile: Antigua Iglesia de Las Agustinas*. Snatiago de Chile: Ilustre Municipalidad de Santiago, Departamento de Proyecto.
- ❖ Carrasco, G. and Rodríguez, A., (2010<sup>b</sup>). *Informe de la Evaluación Preliminar de Daños Provocados por el sismo de 2010, Chile: Antigua Iglesia de Santo Domingo*. Santiago de Chile: Ilustre Municipalidad de Santiago, Departamento de Proyecto.

## REFERENCES

---

- ❖ Carrasco, G., Rodríguez, A., and Muñoz, J. (2010). *Informe de la Evaluación Preliminar de Daños Provocados por el sismo de 2010, Chile: Antigua Iglesia de Santa Ana*. Santiago de Chile: Ilustre Municipalidad de Santiago, Departamento de Proyecto
- ❖ Casapulla, C., and D. D'Ayala. (2006). In-plane collapse behavior of masonry walls with frictional resistances and openings.
- ❖ Casarin, F., and C. Modena. (2008). Seismic assessment of complex historical buildings: Application to Reggio Emilia cathedral. *International Journal of Architectural Heritage* 2 (3):304–27. doi:10.1080/15583050802063659.
- ❖ Casolo, S., and C. Sanjust. (2009). Seismic analysis and strengthening design of a masonry monument by a rigid body spring model: The “Maniace Castle” of Syracuse. *Engineering Structures* 31 (7):1447–59. doi:10.1016/j.engstruct.2009.02.030.
- ❖ Cazanova, F. (1998). *Historia de la Recoleta I*. Santiago:Publicaciones del Archivo Franciscano.
- ❖ CEN – EN 1998-1 (2005), Eurocode 8: Design of structures for earthquake resistance, Part 1: General rules, seismic action and rules for buildings
- ❖ Chilean National Seismological Centre web <http://sismologia.cl/> [08/09/2017]
- ❖ Cisternas, M. (2012). El terremoto de 1647 de Chile central como un evento intraplaca: ¿otra amenaza para Chile metropolitano?. *Revista de Geografía Norte Grande* 53:23–33.
- ❖ CnR, D. T. (2013). 200 R1–2013,“. *Guide for the Design and Construction of Externally Bonded FRP Systems for Strengthening Existing Structures,*” *National Research Council, Rome, 10*.
- ❖ Codes (IBC2015), International Building Code; ASCE 7-2010, Minimum Design Loads for Buildings and other Structures
- ❖ Colombi, M., Borzi, B., Crowley, H., Onida, M., Meroni, F., & Pinho, R. (2008). Deriving vulnerability curves using Italian earthquake damage data. *Bulletin of Earthquake Engineering*, 6(3), 485-504.
- ❖ Comte, D. (2010). Sismicidad y Peligro Sísmico en Chile. Ponencia 2do Congreso Nacional de Recursos Hídricos. APR Chile.
- ❖ Conferencia Episcopal de Chile, (2010). Magnitud de los Daños en Templos y Otros Recintos Católicos, No. 11535, [http://www.iglesia.cl/breves\\_new/archivos/20100325\\_catastro.pdf](http://www.iglesia.cl/breves_new/archivos/20100325_catastro.pdf) (in Spanish).
- ❖ Consejo de Monumentos Nacionales – CMN (Chile). 2010. Catastro Sismo 27 de Febrero 2010, VII Región del Maule, Consejo de Monumentos Nacionales, Ministerio de Educación. 1970. Chilean Law of Monuments 17.288. <http://monumentos.cl> (accessed March23, 2017).
- ❖ Correia, M., Dipasquale, L., & Mecca, S. (2014). *VERSUS: Heritage for Tomorrow*. Firenze University Press

- ❖ Corvalan, I., David Infante, C., and Montoya, S. (2010). *Informe de la Evaluación Preliminar de Daños Provocados por el sismo de 2010, Chile: Iglesia Dulce nombre de Maria*. Santiago de Chile: Ilustre Municipalidad de Santiago, Departamento de Proyecto.
- ❖ Criber, E., Brando, G., De Matteis, G. (2015). The effects of L'Aquila earthquake on the St. Gemma church in Goriano Sicoli: part I—damage survey and kinematic analysis. *Bulletin of Earthquake Engineering*, 13 (12), pp. 3713-3732.
- ❖ Cruz, E. (1995). Importancia de la configuración estructural. In *IX Congreso Nacional de Ingeniería Estructural*. Mexico City: Mexico. Instituto Tecnológico y de Estudios Superiores de Monterrey, 280–287.
- ❖ D. M. LL. PP., (2008), Norme Tecniche per le Costruzioni, 14 Gennaio, Roma (in Italian).
- ❖ D'Ayala, D. (2000). Establishing correlation between vulnerability and damage survey for churches. In *12th World Conference on Earthquake Engineering*, paper no. 2237. New Zealand.
- ❖ D'ayala, D. (2005). Force and displacement based vulnerability assessment for traditional buildings. *Bulletin of Earthquake Engineering* 3 (3):235–65. doi:10.1007/s10518-005-1239-x.
- ❖ D'Ayala, D. (2014). Conservation principles and performance based strengthening of heritage buildings in post-event reconstruction. In *Perspectives on European Earthquake Engineering and Seismology* (pp. 489-514). Springer, Cham.
- ❖ D'Ayala, D. F. (1999). Correlation of seismic damage between classes of buildings: churches and houses. In *Seismic Damage to Masonry Buildings*, edited by Bernardini A. Rotterdam: Balkema, 41–58.
- ❖ D'Ayala, D., & Speranza, E. (2003). Definition of collapse mechanisms and seismic vulnerability of historic masonry buildings. *Earthquake Spectra*, 19(3), 479-509.
- ❖ Da Porto, F., B. Quelhas Da Silva, F. Lorenzoni, P. Girardella, and M. R. Valluzzi. (2010). New integrated knowledge based approaches to the protection of cultural heritage from earthquake-induced risk. In *4th structural engineers world congress*. Italy: At Villa Erba, Como, Italy.
- ❖ D'Ayala, D. & Benzoni, G. (2012). Historic and traditional structures during the 2010 Chile Earthquake: Observations, codes, and conservation strategies. *Earthquake Spectra* 28, No. S1, S425-S451
- ❖ de Cracovia, C. (2000). Principios para la conservación y restauración del patrimonio construido. In *Preámbulo. La Carta de Cracovia fue elaborada por los participantes de la conferencia internacional Cracovia*.
- ❖ De Felice, G., and R. Giannini. (2001). Out-of-plane seismic resistance of masonry walls. *Journal of Earthquake Engineering*, Taylor and Francis 5 (5):253–71. doi:10.1080/13632460109350394.

## REFERENCES

---

- ❖ De Matteis, G., & Mazzolani, F. M. (2010). The Fossanova Church: seismic vulnerability assessment by numeric and physical testing. *International Journal of Architectural Heritage*, 4(3), 222-245.
- ❖ De Matteis, G., Colanzi, F., Viskovic, A., Mazzolani F.M. (2007). Structural behaviour of gothic style churches in the earthquake prone Mediterranean area. In *Proceedings of the International Symposium Studies on Historical Heritage*, Antalya: Turkey, TA-MIR.
- ❖ De Matteis, G., Criber, E. and Brando, G. (2016). Damage probability matrices for three-nave masonry churches in abruzzo after the 2009 l'aquila earthquake. *International Journal of Architectural Heritage* 10:120–145.
- ❖ De Matteis, G., & Zizi, M. (2019). Seismic Damage Prediction of Masonry Churches by a PGA-based Approach. *International Journal of Architectural Heritage*, 1-15.
- ❖ De Natale, G., Madariaga, R., Scarpa, R., & Zollo, A. (1987). Source parameter analysis from strong motion records of the Friuli, Italy, earthquake sequence (1976-1977). *Bulletin of the Seismological Society of America*, 77(4), 1127-1146.
- ❖ De Ramón, A. (2000). *Santiago de Chile (1541-1991). Historia de una sociedad urbana*. Santiago: editorial Sudamericana.
- ❖ Decanini, L., D., Liberatore, D., Liberatore, L., Magenes, G., Penna, A. and Sorrentino, L. (2012). *Report on the Maule (Chile) February 27<sup>th</sup>, 2010 earthquake*. Pavia: IUSS Press.
- ❖ Di Pasquale, G., Orsini, G. and Romeo, R.W. (2005). New Developments in Seismic Risk Assessment in Italy, *Bulletin of Earthquake Engineering*, Vol. 3, No. 1, pp. 101-128
- ❖ Díaz, D., (2016). *Diseño de herramientas de evaluación del riesgo para la conservación del patrimonio cultural inmueble. Aplicación en dos casos de estudio del norte andino chileno*. México: Publicaciones ENCRYM/INAH.
- ❖ DICTUC (2013). Informe de Mecanica de Suelos.Basílica del Salvador y de Nuestra Señora del Carmen Huérfanos con Almirante Barroso. Santiago de Chile: Oficina DICTUC – in Spanish.
- ❖ Direttiva del Presidente del Consiglio dei Ministri (DPCM, 2011). “Valutazione e riduzione del rischio sismico del patrimonio culturale con riferimento alle Norme tecniche per le costruzioni di cui al DM 14 gennaio 2008,” Gazzetta Ufficiale della Repubblica Italiana n. 47 del 26 febbraio 2009, Supplemento Ordinario n. 54. In Italian.
- ❖ Doglioni, F. (2000). Codice di Pratica (Linee Guida) per la progettazione degli interventi di riparazione, miglioramento sismico e restauro dei beni architettonici danneggiati dal terremoto umbro marchigiano del 1997. Bollettino Ufficiale Regione Marche, (15).

- ❖ Doglioni, F., A. Moretti, and V. Petrini. 1994. Le chiese e il terremoto: Dalla vulnerabilità constatata nel terremoto del Friuli al miglioramento antisismico nel restauro, verso una politica di prevenzione. Trieste, Italy: Lint Editoriale.
- ❖ Doherty, K., M. Griffith, N. Lam, and J. Wilson. (2002). Displacement-based seismic analysis for out-of-plane bending of unreinforced masonry walls. *Earthquake Engineering and Structural Dynamics* 31 (4):833–50. doi:10.1002/eqe.126.
- ❖ Dolce, M., & Manfredi, G. (2011). Linee guida per riparazione e rafforzamento di elementi strutturali, tamponature e partizioni. ReLUIS Doppiavoce Ed.
- ❖ Dolce, M., Masi, A., Marino, M. and Vona, M. (2003). Earthquake Damage Scenarios of the Building Stock of Potenza (Southern Italy) Including Site Effects. *Bulletin of Earthquake Engineering*, Vol. 1, No. 1, pp. 115-140.
- ❖ Dowling, D. (2004). Adobe housing in El Salvador: Earthquake performance and seismic improvement. *Society of America Special Papers*, 281–300.
- ❖ EERI, Earthquake Engineering Research Institute. (2010). The Mw 8.8 Maule Chile Earthquake of 27th February, 2010. EERI A preliminary field report – February 2010.
- ❖ Elnashai, S., and Sarno, L., D. (2008). *Fundamentals of Earthquake Engineering*. Wiley: United Kingdom.
- ❖ Engdahi, R. Y A. Villaseñor. (2003). Global catalog of earthquake magnitude > 7. Handbook International Association of Seismology and Physics of the Earth's Interior. Vol 1.
- ❖ Eurocode 6, (2006). Design of masonry structures – Part 1-1: General rules for reinforced and unreinforced masonry structures (EN 1996-1-1), European Committee of Standardization. Brussels, Belgium; 2006.
- ❖ Eurocode 8, (2004). Design of structures for earthquake resistance – Part 1: General rules, seismic actions, and rules for buildings (EN 1998-1), European Committee of Standardization. Brussels, Belgium; 2004.
- ❖ Fajfar, P. (2000). A nonlinear analysis method for performance-based seismic design. *Earthquake spectra*, 16(3), 573-592.
- ❖ Fajfar, P., (1999). Capacity spectrum method based on inelastic demand spectra. *Earthquake Engineering & Structural Dynamics*, 28(9), pp.979-993.
- ❖ Feo, L., R. Luciano, G. Misseri, and L. Rovero. (2016). Irregular stone masonries: Analysis and strengthening with glass fibre-reinforced composites. *Composites Part B: Engineering* 92:84–93. doi:10.1016/j.compositesb.2016.02.038.
- ❖ Fonseca, F., C. and D'Ayala, D. (2012). Seismic assessment and retrofitting of Peruvian earthen churches by means of numerical modelling. In *Proceedings of 15th World Conference on Earthquake Engineering 15WCEE*, Lisbon: Portugal.
- ❖ Formisano, A., Vaiano, G., Fabbrocino, F., & Milani, G. (2018). Seismic vulnerability of Italian masonry churches: The case of the Nativity of Blessed Virgin Mary in Stellata of Bondeno. *Journal of Building Engineering*, 20, 179-200.

## REFERENCES

- ❖ Fratini, F., E. Pecchioni, L. Rovero, and U. Tonietti. (2011). The earth in the architecture of the historical centre of Lamezia Terme (Italy): Characterization for restoration. *Applied Clay Science* 53 (3):509–16. doi:10.1016/j.clay.2010.11.007.
- ❖ Freeman, S. A. (1978). Prediction of response of concrete buildings to severe earthquake motion. *Special Publication*, 55, 589-606.
- ❖ Freeman, S. A. (1998). The capacity spectrum method. In *Proceedings of the 11th European conference on earthquake engineering*, Paris.
- ❖ Frumento, S., Giovinazzi, S., Lagomarsino, S., & Podestà, S. (2006). Seismic retrofitting of unreinforced masonry buildings in Italy. In *NZSEE Conference*
- ❖ G.U. no.55, 7/03/2006. Approval of forms for the seismic damage assessment of cultural heritage buildings, Decree of the Prime Minister, Rome 23/02/2006. (in Italian).
- ❖ Gamrani, N., K. R. Chaham, M. Ibnoussina, F. Fratini, L. Rovero, U. Tonietti, M. Mansori, L. Daoudi, C. Favotto, and N. Youbi. (2012). The particular “rammed earth” of theSaadian sugar refinery of Chichaoua (XVIth century, Morocco): Mineralogical, chemical and mechanical characteristics. *Environmental Earth Sciences* 66 (1):129–40.doi:10.1007/s12665-011-1214-6.
- ❖ Gazeta Ministerial de Chile 1822-1823 III. 1966. Documentos relativos a los efectos del terremoto del día 19 de noviembre. Santiago, Chile.
- ❖ Giaretton, M., Dizhur, D., da Porto, F., & Ingham, J. (2016). Seismic assessment and improvement of unreinforced stone masonry buildings: literature review and application to New Zealand.”. *Bulletin of the New Zealand Society for Earthquake Engineering*, 49(2).
- ❖ Giovanetti F. (1998). *Manuale del Recupero: Città di Castello*. DEI, Tipografia del GenioCivile.
- ❖ Giresini, L. (2016). Energy-based method for identifying vulnerable macro-elements in historic masonry churches. *Bulletin of Earthquake Engineering* 14 (3):919–42. doi:10.1007/s10518-015-9854-7.
- ❖ Giuffré A (1989). *La meccanica nell'architettura: la statica*. La Nuova Italia Scientifica, Rome.
- ❖ Giuffrè, A. (1991). *Lettura sulla meccanica delle murature storiche*. Rome: Kappa.
- ❖ Giuffrè, A., & Carocci, C. (1993). *Statica e dinamica delle costruzioni murarie storiche*. Atti del Convegno internazionale CNR “Le pietre da costruzione: il tufo calcareo e la pietra leccese”. Mario Adda Editore, Bari, 539-598.
- ❖ Grases J., López, O., Hernández, J. (1987). *Edificaciones Sismorresistentes: Manual de aplicación de las normas*. Caracas: Fundación Juan José Aguerrevere. FONDUR.
- ❖ Gross, P. (2015). *Arquitectura en Chile. Desde la prehispanidad al centenario*. Santiago, Chile: Editorial Sa Cabana
- ❖ Grünthal, G. (1998). *European Macroseismic Scale 1998 (EMS-98)*. Cahiers du Centre Européen de Géodynamique et de Séismologie 15, Luxembourg, 99 pp

- ❖ Gucci N, Barsotti R (1995). A non-destructive technique for the determination of mortar load capacity in situ. *Materials and Structures*, 28(5):276-83
- ❖ Guerreiro, J., Proença, J. M., Ferreira, J. G., & Gago, A. S. (2017). Bonding and anchoring of a CFRP reinforced render for the external strengthening of old masonry buildings. *Construction and Building Materials*, 155, 56-64.
- ❖ Hendry AW(1990). *Structural masonry*. Basingstoke: Macmillan Leipzig, Klinkhardt, Biermann.
- ❖ Heyman, J. (1966). The Stone skeleton. *International Journal of Solids and Structures* 2 (2):249–79. doi:10.1016/0020-7683(66) 90018-7.  
<http://eqclearinghouse.org/co/20100227-chile/wp-content/uploads/2010/>
- ❖ Huneeus, A.(1968). *La Catedral de la Arquidiócesis de Santiago de Chile. Sus principales objetos sagrados y recuerdos*. Santiago de Chile: Impr. San José.
- ❖ Iglesias, A., and Porte, E. (1955). *La Catedral de Santiago de Chile. Estudio monográfico*. Santiago de Chile: Publicaciones del Instituto de Historia de la Arquitectura.
- ❖ Indirli M. (2006). Natural multi-hazard and building vulnerability assessment in the historical centers: the examples of San Giuliano di Puglia(Italy) and Valparaíso (Chile). Proc. 7th European Commission Conference “SAUVEUR”, Safeguarded Cultural Heritage, Prague, May 31 – June 3, 2006.
- ❖ Indirli, M., Razafindrakoto, H., Romanelli, F., Puglisi, C., Lanzoni, L., Milani, E., Munari, M. and Apablaza, S. (2011). Hazard evaluation in Valparaíso: the MAR VASTO Project. *Pure and applied geophysics*, 168(3-4)543-582.
- ❖ Instituto Nacional de Normalización (INN), 1996. Earthquake resistant design of buildings, Official Chilean Code NCh433.Of96.
- ❖ Instituto Nacional de Normalización (INN), 2013. Estructuras –Intervención de construcciones patrimoniales de tierra cruda– Requisitos del Proyecto Estructural. Santiago, Chile NCh3332.Of2013.
- ❖ International Council on Monuments and Sites (ICOMOS) Principles for the analysis, conservation and structural restoration of architectural heritage (2003). Available at: [https://www.icomos.org/charters/structures\\_e.pdf](https://www.icomos.org/charters/structures_e.pdf).
- ❖ International Scientific Committee for Analysis And Restoration Of Structures Of Architectural Heritage (ISCARSAH) Recommendations for the analysis, conservation and structural restoration of architectural heritage. ICOMOS,2003. Available at: <https://iscarsah.files.wordpress.com/2014/11/iscarsah-guidelines.pdf>.
- ❖ Joannon R, Gatica U, Larrain, A (2003). Factibilidad de Recuperación Basílica del Salvador. Informe Final. Santiago: Oficina de Arquitectura Joannon – in Spanish.
- ❖ Jorquera, N., Misseri, G., Palazzi, N., Rovero, L. and Tonietti, U. (2017). Structural characterization and seismic performance of San Francisco church, the most ancient monument in Santiago, Chile. *International Journal of Architectural Heritage* 11(8),1061-1085.

## REFERENCES

- ❖ Jorquera, N., Vargas, J., Lobos, M.L., and Cortez, D. (2016). Revealing Earthquake-Resistant Geometrical Features in Heritage Masonry Architecture in Santiago, Chile. *International Journal of Architectural Heritage* 11(4),519-538.
- ❖ Kalagri A, Miltiadou-Fezans A and Vintzileou E (2010). Design and evaluation of hydraulic lime grouts for the strengthening of stone masonry historic structures. *Materials and Structures*, 43(8): 1135–1146.
- ❖ Kausel, E.; J. CampoS. (1992). The Ms = 8 Tensional earthquake of December 9, 1950 of northern Chile and its relation to the seismic potential of the region. *Phys. Earth. Planet. Int.* 72: 220-235.
- ❖ Khazaradze. G. and Klotz, J. (2003). Short and long-term effects of GPS measured crustal deformation rates along the South-Central Andes. *Journal of Geophysical Research Atmospheres* 108 (B6)
- ❖ Kircher, C. A., Nassar, A. A., Kustu, O., and Holmes, W. T. (1997). Development of building damage functions for earthquake loss estimation, *Earthquake Spectra* 13(4), 663–682. doi:10.1193/1.1585974.
- ❖ Kishor J., Wald D., and D'Ayala D. (2011). Developing empirical collapse fragility functions for global building types." *Earthquake Spectra* 27.(3): 775-795.
- ❖ Lagomarsino S. (2012). Damage assessment of churches after L'Aquila earthquake (2009). *Bull Earthquake Eng* 10:73–92. doi:10.1007/s10518-011-9307-x
- ❖ Lagomarsino S. and Giovinazzi S. (2006). Macroseismic and mechanical models for the vulnerability and damage assessment of current buildings"; *Bulletin of Earthquake Engineering*, 4, 25 August: pp. 415-443
- ❖ Lagomarsino S. and Podestà S. (2004a). Seismic Vulnerability of Ancient Churches: I. Damage Assessment and Emergency Planning. *Earthquake Spectra* 20(2): 377-394.
- ❖ Lagomarsino S. and Podestà S. (2004b). Seismic Vulnerability of Ancient Churches: II. Statistical Analysis of Surveyed Data and Methods for Risk Analysis, *Earthquake Spectra*, 20(2): 395–412
- ❖ Lagomarsino, S. (2006). On the vulnerability assessment of monumental buildings. *Bulletin of Earthquake Engineering* 4 (4):445–63. doi:10.1007/s10518-006-9025-y.
- ❖ Lagomarsino, S., and S. Podestà. (2004c). Damage and vulnerability assessment of churches after the 2002 Molise, Italy, earthquake. *Earthquake Spectra* 20:S271–S283. doi:10.1193/1.1767161.
- ❖ Lagomarsino, S., and S. Resemini. (2009). The assessment of damage limitation state in the seismic analysis of monumental buildings. *Earthquake Spectra* 25 (2):323–46. doi:10.1193/ 1.3110242.
- ❖ Lagomarsino, S., S. Podestà, G. Cifani, and A. Lemme. (2004). The 31st October 2002 Earthquake in Molise (Italy): A new methodology for the damage and seismic vulnerability survey of churches. 13th World Conference on Earthquake Engineering. August 1–6 2004, Vancouver, Canada. Paper 1366

- ❖ Lallemand D., Kiremidjian A., Burton H. (2015). Statistical procedures for developing earthquake damage fragility curves. *Earthquake Engng Struct. Dyn.*
- ❖ Leyton, F.; S. Ruiz and s. Sepulveda. (2009). Preliminary revaluation of Probabilistic Seismic Hazard Assessment in Chile: from Arica to Taitao Peninsula. *Advances in Geosciences* (22): 147-153.
- ❖ Leyton, F.; S. Ruiz; S. Sepúlveda. (2010). Reevaluación del peligro sísmico probabilístico en Chile Central. *Andean Geology*. 37(2): 455-472.
- ❖ Liberatore, L., Sorrentino, L., & Liberatore, D. (2012). Engineering analysis of ground motion records of Chile, 2010 earthquake. In *Proc. of the 15th World Conf. on Earthq. Eng.*
- ❖ Lira, C., and Arévalo, C. (2010). *Informe de la Evaluación Preliminar de Daños Provocados por el sismo de 2010, Chile: Iglesia de San Agustín de Melipilla*. Santiago de Chile: Consejo de Monumentos Nacionales. Dirección de Arquitectura del Ministerio de Obras Publicas.
- ❖ Lomnitz, C. (2004). Major earthquakes of Chile: A historical survey, 1535-1960. *Seismological Research Letters* 75(3):368–78. doi:10.1785/gssrl.75.3.368.
- ❖ Lourenco, P. (2005). Assessment, diagnosis and strengthening of Outeiro Church, Portugal. *Construction and Building Materials* 19 (8):634–45. doi:10.1016/j.conbuildmat.2005.01.010.
- ❖ Lourenço, P. B., & Roque, J. A. (2006). Simplified indexes for the seismic vulnerability of ancient masonry buildings. *Construction and Building Materials*, 20(4), 200-208.
- ❖ Lourenço, P. B., Oliveira, D. V., Leite, J. C., Ingham, J. M., Modena, C., & Da Porto, F. (2013). Simplified indexes for the seismic assessment of masonry buildings: International database and validation. *Engineering Failure Analysis*, 34, 585-605.
- ❖ Lourenco, P., K. Krakowiak, F. Fernandes, and L. Ramos. 2007. Failure analysis of Monastery of Jeronimos, Lisbon: How to learn from sophisticated numerical models. *Engineering Failure Analysis* 14 (2):280–300. doi:10.1016/j.engfailanal.2006.02.002.
- ❖ Mallardo, V., Malvezzi, R., Milani, E., & Milani, G. (2008). Seismic vulnerability of historical masonry buildings: a case study in Ferrara. *Engineering Structures*, 30(8), 2223-2241.
- ❖ Marotta, A., Goded, T., Giovinazzi, S., Lagomarsino, S., Liberatore, D., Sorrentino, L., and Ingham, J. M. (2015). An inventory of unreinforced masonry churches in New Zealand. *Bulletin of the New Zealand Society for Earthquake Engineering*, 48(3): 170–189.
- ❖ Marotta, A., Sorrentino, L., Liberatore, D. and Ingham, J. (2016). Statistical seismic vulnerability of New Zealand unreinforced masonry churches. In *10th International Conference on Structural Analysis of Historical Constructions*. CRC Press, Taylor & Francis Group.

## REFERENCES

- ❖ Marotta, A., Sorrentino, L., Liberatore, D. and Ingham, J.M. (2017). Vulnerability assessment of unreinforced masonry churches following the 2010–2011 Canterbury earthquake sequence. *Journal of Earthquake Engineering*, 21(6), pp.912-934.
- ❖ Martinelli, A., Cifani, G., Cialone, G., Corazza, L., Petracca, A. and Petrucci, G. (2008). Building vulnerability assessment and damage scenarios in Celano (Italy) using a quick survey data-based methodology, *Soil Dynamics and Earthquake Engineering*, 28, 875–889.
- ❖ MARVASTO (2007). Risk Management in Valparaíso/Manejo de Riesgos en Valparaíso, Servicios Técnicos acronym MAR VASTO, funded by BID/IDB (Banco Inter Americano de Desarrollo / Inter-American Development Bank). Project ATN/II-9816-CH, BID/IDB-ENEA Contract PRM.7.035.00-C, March 2007–June 2008
- ❖ Masonry Standards Joint Committee, (1999). “Building Code Requirements for Masonry Structures,” ACI-530-99/ASCE 5-99/TMS 402-99, American Concrete Institute, American Society of Civil Engineers, and The Masonry Society, Detroit, New York, and Boulder.
- ❖ Mele, E., De Luca, A., & Giordano, A. (2003). Modelling and analysis of a basilica under earthquake loading. *Journal of cultural Heritage*, 4(4), 355-367.
- ❖ Mezzi, M., (2003). Optimum Structural Configurations of Seismic Isolated Buildings. Inc 2nd International Specific Conference on The Conceptual Approach to Structural Design. Milan: Italy.
- ❖ Ministerio de Vivienda y Urbanismo – MINVU (Chile). 2011. Reglamento que fija el diseño sísmico de edificios y deroga D.S. N°117 MINVU of 2010.
- ❖ Ministerio de Vivienda y Urbanismo – MINVU (Chile). 2011. Reglamento que fija el diseño sísmico de edificios y deroga D.S. N°117 MINVU of 2010.
- ❖ Ministerio Obra Pública (2008). Proyecto de restauración Basílica del Salvador. Perfil Etapa de Ejecución. Cod.n° 300-87203-0. Santiago de Chile: Oficina Ministerio Obra Pública – in Spanish.
- ❖ Misseri G, Rovero L (2017). Parametric investigation on the dynamic behaviour of masonry pointed arches. *Archive of Applied Mechanics*, 87 (3): 385-404.
- ❖ Misseri, G., Palazzi N.C., Rovero, L. (2019). Local seismic cultures and earthen architectural heritage: limit analysis for the safety assessment of traditional retrofitting techniques. (Under submission).
- ❖ Misseri, G., Rovero, L., Stipo, G., Barducci, S., Alecci, V., & De Stefano, M. (2019). Experimental and analytical investigations on sustainable and innovative strengthening systems for masonry arches. *Composite Structures*, 210, 526-537.
- ❖ Modena, C., Valluzzi, M. R., da Porto, F., & Casarin, F. (2011). Structural aspects of the conservation of historic masonry constructions in seismic areas: remedial measures and emergency actions. *International Journal of Architectural Heritage*, 5(4-5), 539-558.

- ❖ Moll P, Sabanech J (1976). *Basilica del Salvador*, Thesis, Facultad de Arquitectura y Urbanismo Departamento de Diseño Arquitectónico, Universidad de Chile, Santiago.
- ❖ Montandón, R. (1950). *Iglesias y capillas coloniales en el Desierto de Atacama*. Santiago, Chile: Cuadernos del
- ❖ Montessus de Ballore, F. (1912). *Historia sísmica de los Andes Meridionales al sur del paralelo XVI*. Santiago de Chile: Imprenta Cervantes.
- ❖ Muñoz M., J., and Ojeda del Río, P. (2010). *Informe de la Evaluación Preliminar de Daños Provocados por el sismo de 2010, Chile: Parroquia San Saturnino*. Santiago de Chile: Ilustre Municipalidad de Santiago, Departamento de Proyecto.
- ❖ Naderzadeh, A. (2009). Application of seismic base isolation technology in Iran. *Menshin* 63 (2):40–47.
- ❖ Nelsen, A., (2010). Chile earthquake takes heavy toll on historical sites, *The Christian Science Monitor*, 31 March 2010, <http://www.csmonitor.com/World/Americas/2010/0331/Chileearthquake-takes-heavy-toll-on-historical-sites>.
- ❖ Neumann Vargas, J., Bardiola Bernales, J. and Blondet, M. (1986). Resistencia Sísmica de la Mampostería de Adobe. 4as Jornadas Chilenas de Sismología e Ingeniería Antisísmica, Ministerio de Vivienda y Urbanismo, pp. J.40-53 (in Spanish)
- ❖ Orsini G (1999) A model for buildings' vulnerability assessment using the parameterless scale of seismic intensity (PSI). *Earthquake Spectra* 15(3):463–483. doi:10.1193/1.1586053
- ❖ Ortega, J., Vasconcelos, G., Rodrigues, H., Correia, M. (2018). Assessment of the efficiency of traditional earthquake resistant techniques for vernacular architecture, *Engineering Structures*, 173:1-27.
- ❖ Ortega, J., Vasconcelos, G., Rodrigues, H., Correia, M., Lourenço, P.B. (2017). Traditional earthquake resistant techniques for vernacular architecture and local seismic cultures: a literature review. *Journal of Cultural Heritage* 27, 181-196
- ❖ Palazzi, N.C., Rovero, L., Tonietti, U., de la Llera, J.C., Sandoval, C. (2018a). Kinematic limit analysis of Basilica del Salvador, a significant example of the neo-gothic architecture in Santiago, Chile. In *16<sup>th</sup> European Conference on Earthquake Engineering*, Thessalonica, Greece 18-21 June 2018.
- ❖ Palazzi, N.C., Rovero, L., Tonietti, U., de la Llera, J.C., Sandoval, C. (2018b). Seismic vulnerability assessment of unreinforced masonry churches in central Chile. In *11<sup>th</sup> International Conference on Structural Analysis of Historical Constructions*, Cuzco, Peru, 11-13 September 2018.
- ❖ Palazzi, N.C., Sandoval, C., Martínez, P. (2018c). Análisis estructural. Colecciones de Referencia para el Patrimonio Construido – Identificación Microestructural de Materiales y Macroestructural de Sistemas Constructivos. Proyecto FONDEF ID14I20187

## REFERENCES

---

- ❖ Palazzi, N. C., Rovero, L., De La Llera, J. C., Sandoval, C. (2019). Preliminary Assessment on Seismic Vulnerability of Masonry Churches in Central Chile. *International Journal of Architectural Heritage*, 1-20.
- ❖ Parisi M.A. and Piazza M. (2002). Traditional timber joints in seismic areas: cyclic behaviour, numerical modelling, normative requirements, *European Earthquake Engineering*, Vol 1, 40-49
- ❖ Pena, M. J. (1969). *Restauración de la Iglesia y Convento de San Francisco*. París, France: UNESCO.
- ❖ per le Antichità, C. S., & Arti, B. (1932). *Norme per il restauro dei monumenti*. Carta Italiana del Restauro.
- ❖ Pereira Salas, E. (1965). *Historia del Arte en el Reino de Chile*. Santiago, Chile: Eds. de la Universidad de Chile.
- ❖ Peters, G., & Verdugo, R. (2003). Seismic design considerations of tailings dams. In *Soil rock America 2003: proceedings of the 12th panamerican conference on soil mechanics and geotechnical engineering* (Vol. 2, pp. 2241-2246).
- ❖ Petzet M. (2004). *Principles of preservation: an introduction to the international charters for conservation and restoration 40 years after the Venice Charter*.
- ❖ Pinto, J.I. (2011). *Informe de la Evaluación Preliminar de Daños Provocados por el sismo de 2010, Chile: Iglesia de Loica*. Santiago de Chile: Ilustre Municipalidad de San Pedro, Departamento de Proyecto.
- ❖ POLIMI, (2010). New integrated knowledge based approaches to the protection of cultural heritage from earthquake-induced risk. NIKER Grant Agreement n°244123
- ❖ Pudjisuryadi, P., B. Lumantarna, and Y. Lase. (2007). Base isolation in traditional building. Lesson learned from Nias March 28, 2005 earthquake. Paper presented at EACEF: 1st International Conference of European Asian Civil Engineering Forum, September 26–27, 2007, Petra Christian University, Surabaya, and Civil Engineering Department, University of Indonesia, Depok.  
<http://wiryanto.files.wordpress.com/2007/11/131.pdf>
- ❖ R&V Ingeniero, (2012). *Informe de mecánica de suelos. Iglesia San Judas Tadeo. VI región del Libertador Bernardo O'Higgins*
- ❖ Recabarren, V. (2009). *Fijación de Límites Monumento Histórico Iglesia la Viñita*. Santiago de Chile: Consejo de Monumentos Nacionales, Dirección de Arquitectura del Ministerio de Obras Públicas.
- ❖ Rendel, M., Lüders, C. Greer, M., Vial, I., Westenank, B., de la Llera, J.C., Perez, F., Bozzi, D., Prado, F. (2014). Retrofit, using seismic isolation, of the heavily damaged Basílica del Salvador in Santiago, Chile. In *New Zealand Society for Earthquake Engineering, 14NZEE*. Aotea: New Zealand.
- ❖ Restrepo-Vélez LF, Magenes G. (2004). A mechanics-based procedure for the seismic risk assessment of masonry buildings at urban scale. *Proceedings of the XI Convegno Nazionale ANIDIS*, Genova.

- ❖ Roca, P., Cervera, M., & Gariup, G. (2010). Structural analysis of masonry historical constructions. Classical and advanced approaches. *Archives of Computational Methods in Engineering*, 17(3), 299-325.
- ❖ Rodríguez, A., and Carrasco, G. (2010). *Informe de la Evaluación Preliminar de Daños Provocados por el sismo de 2010, Chile: Iglesia San Agustín*. Santiago de Chile: Ilustre Municipalidad de Santiago, Departamento de Proyecto.
- ❖ Rodríguez, H. (2012). Iglesias de Atacama. Nueva arquitectura para antiguas creencias. In Atacama, edited by C. A. Del Solar, 158–97. Santiago, Chile: Museo Chileno de Arte Precolombino.
- ❖ Romano A, Ochsendorf J A (2009). The Mechanics of Gothic Masonry Arches, *International Journal of Architectural Heritage*, 4(1): 59-82
- ❖ Rossetto, T., Ioannou, I., and Grant, D. N. (2013). Existing Empirical Vulnerability and Fragility Functions: Compendium and Guide for Selection, GEM Foundation, Pavia, Italy.
- ❖ Rossetto, T., Ioannou, I., Grant, D.N., Maqsood, T. (2014). *Guidelines for empirical vulnerability assessment*. Pavia, Italy.
- ❖ Rota M., Penna A., Strobbia C. (2006). Typological fragility curves from Italian earthquake damage data. *Proceedings 1st European conference on earthquake engineering and seismology*, Geneva, paper no. 386
- ❖ Rovegno, J. R. (2009). La casa de fray Pedro de Bardeci. El convento de San Francisco. Santiago de Chile. Ensayo
- ❖ Rovero, L., and F. Fratini. (2013). The Medina of Chefchaouen (Morocco): A survey on morphological and mechanical features of the masonries. *Construction and Building Materials* 47:465–79. doi:10.1016/j.conbuildmat.2013.05.025.
- ❖ Rovero, L., and U. Tonietti. (2012). Structural behavior of earthen corbelled domes in the Aleppo's region. *Materials and Structures* 45 (1):171–84. doi:10.1617/s11527-011-9758-1.
- ❖ Rovero, L., V. Alecci, J. Mechelli, U. Tonietti, and M. De Stefano.(2015). Masonry walls with irregular texture of L'Aquila (Italy) seismic area: Validation of a method for the evaluation of masonry quality. *Materials and Structures* 49 (6):2297–314. doi:10.1617/s11527-015-0650-2.
- ❖ Sahady, A. (2015). Mutaciones del patrimonio arquitectónico de Santiago de Chile. Una revisión del del centro histórico. Santiago, Chile: Editorial Universitaria.
- ❖ Sánchez, M. I. (2013). *Vulnerabilidad Sísmica de Construcciones Patrimoniales Históricas de Mampostería en Chile: Aplicación a los Torreones Españoles de Valdivia*. Facultad de Ciencias de la Ingeniería, Universidad Austral de Chile. Valdivia: Editorial Universitaria.
- ❖ Sandoval, C.,Valledor, R., Lopez-Garcia, D. (2017). Numerical assessment of accumulated seismic damage in a historic masonry building. A case study. *International Journal of Architectural Heritage* 11 (8), 1177-1194.

## REFERENCES

- ❖ Sani, F., G. Moratti, M. Coli, P. Laureano, L. Rovero, U. Tonietti, and N. Coli. (2012). Integrated geological-architectural pilot study of the Biet Gabriel-Rufael rock hewn church in Lalibela, northern Ethiopia. *Italian Journal of Geosciences* 131 (2):171–86.
- ❖ Saragoni, G. R., Astroza, M., & Sturm, T. (2009). Vulnerability analysis of two centennial buildings that survived undamaged the two large Valparaíso earthquakes of 1906 and 1985. In *Protection of Historical Buildings: Proceedings of the International Conference on Protection of Historical Buildings PROHITECH 09*. Rome: Italy, 1547-1552.
- ❖ Silva, N. (2008). Caracterización y determinación del peligro sísmico en la Región Metropolitana. Tesis Ing. Civil. Santiago, Universidad de Chile. 148 p.
- ❖ Singhal, A. and Kiremidjian, A. S. (2004). Empirical fragility functions from recent earthquakes, In *Proc. of the 13th World Conference on Earthquake Engineering, Vancouver, Canada*, Paper No.1211.
- ❖ Singhal, Ajay, and Anne S. Kiremidjian. (1998). Bayesian updating of fragilities with application to RC frames. *Journal of structural Engineering* 124.8: 922-929.
- ❖ Sorrentino L, D'Ayala D, de Felice G, Griffith M C, Lagomarsino S, Magenes G. (2017). Review of out-of-plane seismic assessment techniques applied to existing masonry buildings. *International Journal of Architectural Heritage*, 11(1), 2-21.
- ❖ Stagno, H. (2011). Informe de diagnóstico estructural Iglesia del Santuario San Jose, Santiago. Santiago de Chile: Consejo de Monumentos Nacionales, Dirección de Arquitectura del Ministerio de Obras Publicas.
- ❖ Staniscia, S, Spacone, E, and Fabietti, V. (2017). Performance-Based Urban Planning: Framework and L'Aquila Historic City Center Case Study. *International Journal of Architectural Heritage*, 11(5):656-669
- ❖ Stefanini, S. (2016). La Chiesa di San Francisco a Santiago del Cile. 400 anni di resistenza ai terremoti. Analisi ed ipotesi per interventi di consolidamento. Master's thesis in Achitectural science Università deli Studi di Firenze.
- ❖ Stehberg, R. (1995). *Instalaciones incaicas en el norte y centro de Chile*. Santiago: Dirección de Bibliotecas, Archivos y Museos. ISBN 956-244-035-4. Retrieved February 5, 2014.
- ❖ Strand, 7. 2004. Straus 7.2: User's manual. Sidney, Australia: Strand 7. [www.strand7.com](http://www.strand7.com).
- ❖ Sturm, T. (2008). *Valparaíso: su patrimonio histórico y los sismos. Memoria para optar al título de Ingeniero Civil*, Universidad de Chile. Santiago de Chile: Editorial Universitaria.
- ❖ Surtierra (2011). Recuperación de la Iglesia San Juda Tadeo de Malloa. Informe Final. Santiago: Oficina de Arquitectura Surtierra – in Spanish.
- ❖ Tandem Ltda (2014). Recuperación de la Basilica del Salvador. Informe Final. Santiago: Oficina de Arquitectura Tandem Ltda – in Spanish.

- ❖ Tassios TP(1988). *Meccanica delle murature*. Liguori Editore. Naples, Italy.
- ❖ The New York Times (1894). Terrific tragedy in chili; Two Thousand Five Hundred Persons Roasted to Death in a Church. January 18
- ❖ Tolles, E. L., Kimbro, E. E., Webster, F. A., & Ginell, W. S. (2000). Seismic stabilization of historic adobe structures: Final report of the Getty seismic adobe project
- ❖ Torrealva, D., Vicente, E. (2013). *Testing results, SRP-Seismic Retrofitting Project in Perú Internal Report*, Pontificia Universidad Católica del Perú. Lima: Editorial Universitaria
- ❖ Torres, W., Almazán, J. L., Sandoval, C., & Peña, F. (2018). Fragility analysis of the nave macro-element of the Cathedral of Santiago, Chile. *Bulletin of Earthquake Engineering*, 16(7): 3031-3056.
- ❖ Torres, W., Almazán, J. L., Sandoval, C., Boroschek, R. (2017). Operational modal analysis and FE model updating of the Metropolitan Cathedral of Santiago, Chile. *Engineering Structures*, 143, 169-188.
- ❖ Udías, A., Madariaga, R., Bufo, E., Muñoz, D., & Ros, M. (2012). The large Chilean historical earthquakes of 1647, 1657, 1730, and 1751 from contemporary documents. *Bulletin of the Seismological Society of America*, 102(4), 1639-1653.
- ❖ United States Geological Survey's (USGS) Earthquake Hazards Program Shakemap us2010tfan.  
<https://earthquake.usgs.gov/archive/product/shakemap/atlas20100227063414/atlas/1491981213321/download/grid.xml>
- ❖ Valdebenito, G. E., M. I. Sánchez, and C. Sandoval. (2011). Seismic vulnerability of historical masonry structures in chile: a state-of-the-art review." 6th International Institute of Earthquake Engineering and Seismology 2011, Iran (Tehran)
- ❖ Valluzzi MR, da Porto F and Modena C (2004). Behavior and modeling of strengthened three-leaf stone masonry walls. *Materials and Structures*, 37(267): 184–192.
- ❖ Varum, H., Tarque, N., Silveira, D., Camata, G., Lobo, B., Blondet, M., Figueiredo, A., Masood Rafi, M., Oliveira, C., Costa, A. (2014). *Structural behaviour and retrofitting of adobe masonry buildings, Structural Rehabilitation of Old Buildings, Building Pathology and Rehabilitation 2*. Berlin: HeidelbergSpringer-verlag.
- ❖ Venice Charter (1964) International charter for the conservation and restoration of monuments and sites. In: Proceeding, 2nd international congress of architects and technicians of historic monuments, Venice (accessed at [http://www.international.icomos.org/charters/venice\\_e.pdf](http://www.international.icomos.org/charters/venice_e.pdf) in June 2018)
- ❖ Villalobos, S., L. Méndez, C. Canut De Bon, S. Pinto, S. Serrano, L. Parentini, L. Ortega, E. Cavieres, R. Sagredo, and J. Plass. 1990. *Historia de la ingeniería en Chile*. Santiago, Chile: Hachette.

## REFERENCES

---

- ❖ Vintzileou E and Miltiadou-Fezans A (2008). Mechanical properties of three-leaf stone masonry grouted with ternary or hydraulic lime-based grouts. *Engineering Structures*, 30(8): 2265–2276.
- ❖ Whitman RV, Reed JW, Hong ST. (1973). Earthquake damage probability matrices. *In: Proceedings of the Fifth World conference on earthquake engineering*. Fundación Altiplano, 2010. Guía Práctica para Talleres de Capacitación de Restauración en Adobe, <http://fundacionaltiplano.cl/archivo/publicaciones/> (in Spanish).

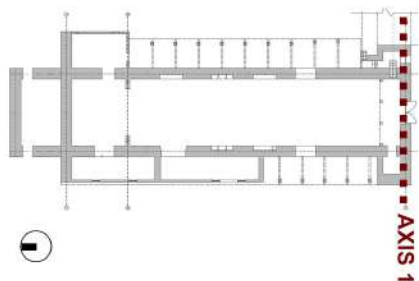
# **Annex1**

**SAN TADEO MALLOA PARISH**



## INDIVIDUATION AND LOCATION ANALYZED AXIS:

### AXIS 1 NORTH AND SOUTH



### CRACK PATTERN

**c.a.i** Capillar crack, Initial, c.i.i, and Advanced, c.a.i  
In the first phase of an initial capillary crack, it is not possible to directly determine the corresponding points of the edge, but only the shape of crack, while in the advanced step it is possible to identify both elements of analysis.

**P.H.** Crack corresponding to plastic hinge, P.H.  
A macro-element undergoes a rigid rotation around a plastic hinge, P.H., generally corresponding to horizontal or diagonal crack.

**c.r.i** Rotating crack, c.r.i  
The block during cracking undergoes a rigid rotation by which the two edges of the crack move away.

**c.d.i** Detachment crack, c.d.i  
The block is completely separated from the rest of the building.

**co.i** Partial collapse or loss of material  
**Co.i** Total collapse, localized decomposition of wall pieces

**D.b.i** Detachment of beam or metal tie  
Detachment of beam or tie-rod and loss of operability or, and / or severe deformation of a key

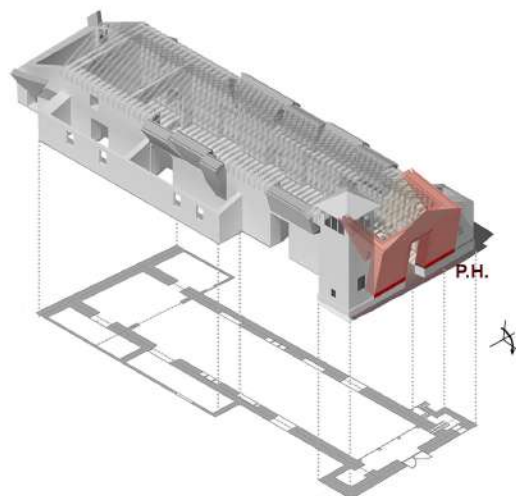
— Crack pattern after 2010 Maule earthquake

### DEGRADATION PHENOMENA THAT REDUCES STRUCTURAL EFFICIENCY

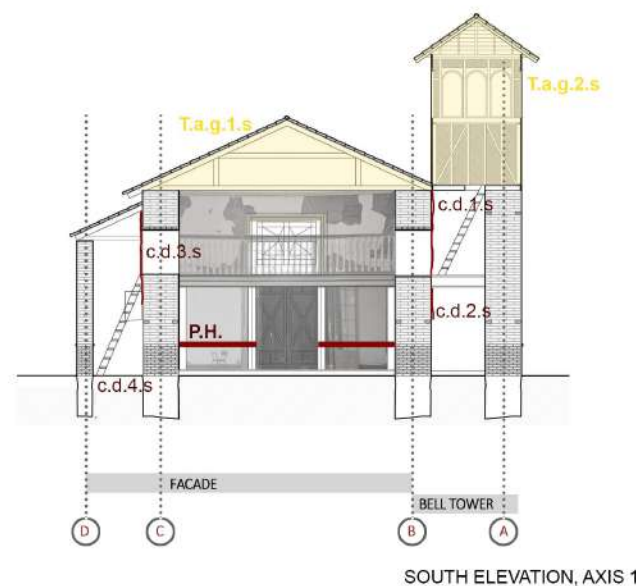
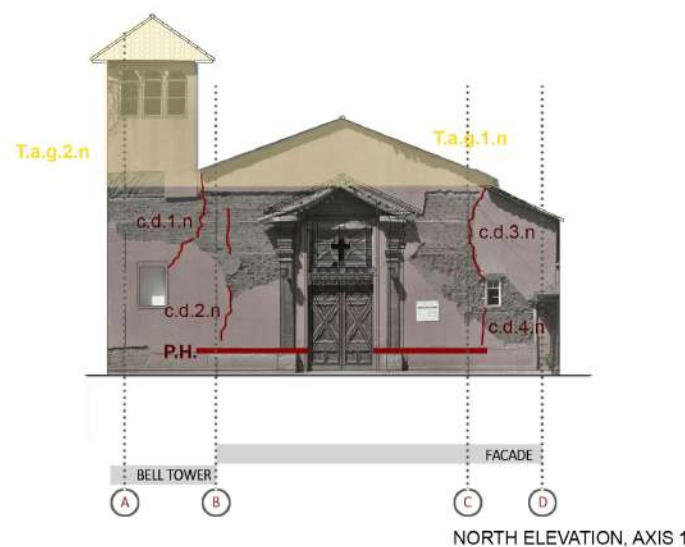
Degradation of the masonry  
Erosion, Er.i, and Mosses lichens and fungi, M.I.h.i

Presence of vegetation, Vi

Structural discontinuities  
Heterogeneous materiality (Reinforced Concrete, R.C., Concrete C, Steel, S., Tabique, T.a.g.i, Masonry type 1-2-3, M01-2-3, and Incannucciato, I.i)

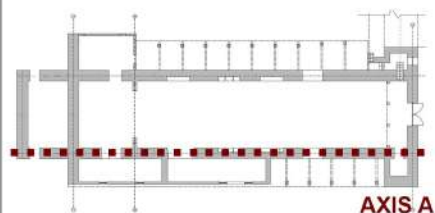


## CRACK PATTERN OF MALLOA PARISH\_MP01



## INDIVIDUATION AND LOCATION ANALYZED AXIS:

AXIS A WEST AND EAST



AXIS A

## CRACK PATTERN

c.a.i

Capillary crack, Initial, c.i.i, and Advanced, c.a.i  
In the first phase of an initial capillary crack, it is not possible to directly determine the corresponding points of the edge, but only the shape of crack, while in the advanced step it is possible to identify both elements of analysis.

P.H.

Crack corresponding to plastic hinge, P.H.  
A macro-element undergoes a rigid rotation around a plastic hinge, P.H., generally corresponding to horizontal or diagonal crack.

c.r.i

Rotating crack, c.r.i  
The block during cracking undergoes a rigid rotation by which the two edges of the crack move away.

c.d.i

Detachment crack, c.d.i  
The block is completely separated from the rest of the building.

co.i

Partial collapse or loss of material

Co.i

Total collapse, localized decomposition of wall pieces

D.b.i

Detachment of beam or metal tie  
Detachment of beam or tie-rod and loss of operability or, and / or severe deformation of a key

—

Crack pattern after 2010 Maule earthquake

## DEGRADATION PHENOMENA THAT REDUCES STRUCTURAL EFFICIENCY

—

Degradation of the masonry  
Erosion, Er.i, and Mosses lichens and fungi, M.i.h.i

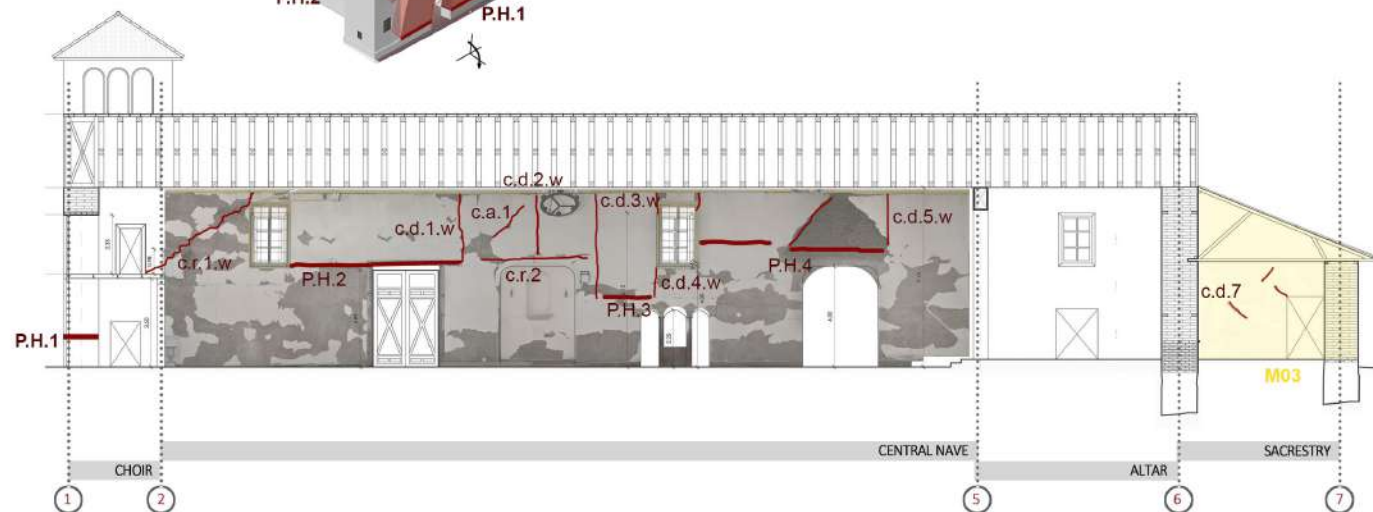
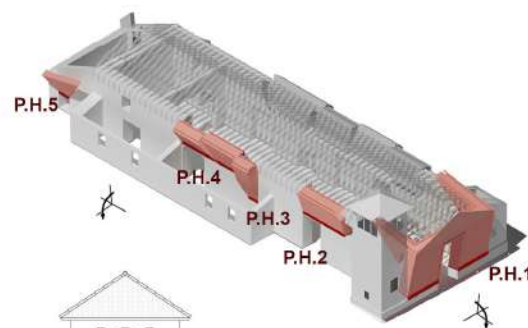
\*

Presence of vegetation, Vi

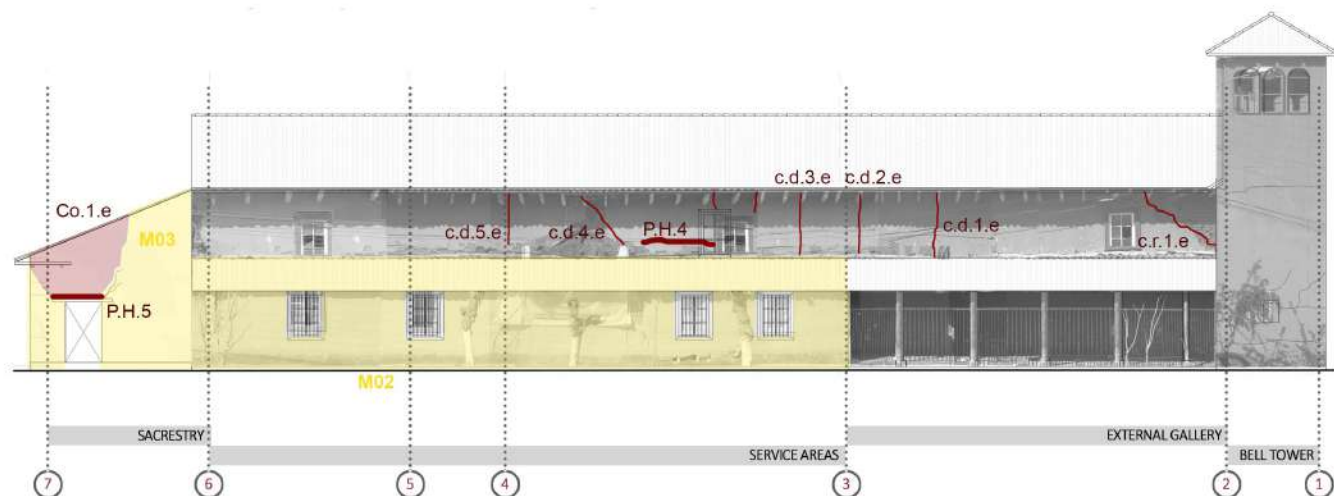
—

Structural discontinuities  
Heterogeneous materiality (Reinforced Concrete, R.C., Concrete C., Steel, S., Tabique, T.a.g.i. Masonry type1-2-3, M01-2-3, and Incannucciato, i.i)

## CRACK PATTERN OF MALLOA PARISH\_MP02



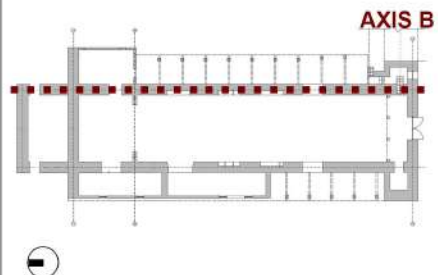
WEST ELEVATION, AXIS A



EAST ELEVATION, AXIS A

## INDIVIDUATION AND LOCATION ANALYZED AXIS:

AXIS B WEST AND EAST



## CRACK PATTERN

**c.a.i** Capillar crack, Initial, c.i.i, and Advanced, c.a.i  
In the first phase of an initial capillary crack, it is not possible to directly determine the corresponding points of the edge, but only the shape of crack, while in the advanced step it is possible to identify both elements of analysis.

**P.H.** Crack corresponding to plastic hinge, P.H.  
A macro-element undergoes a rigid rotation around a plastic hinge, P.H., generally corresponding to horizontal or diagonal crack.

**c.r.i** Rotating crack, c.r.i  
The block during cracking undergoes a rigid rotation by which the two edges of the crack move away.

**c.d.i** Detachment crack, c.d.i  
The block is completely separated from the rest of the building.

**co.i** Partial collapse or loss of material  
**Co.i** Total collapse, localized decomposition of wall pieces

**D.b.i** Detachment of beam or metal tie  
Detachment of beam or tie-rod and loss of operability or, and / or severe deformation of a key

— Crack pattern after 2010 Maule earthquake

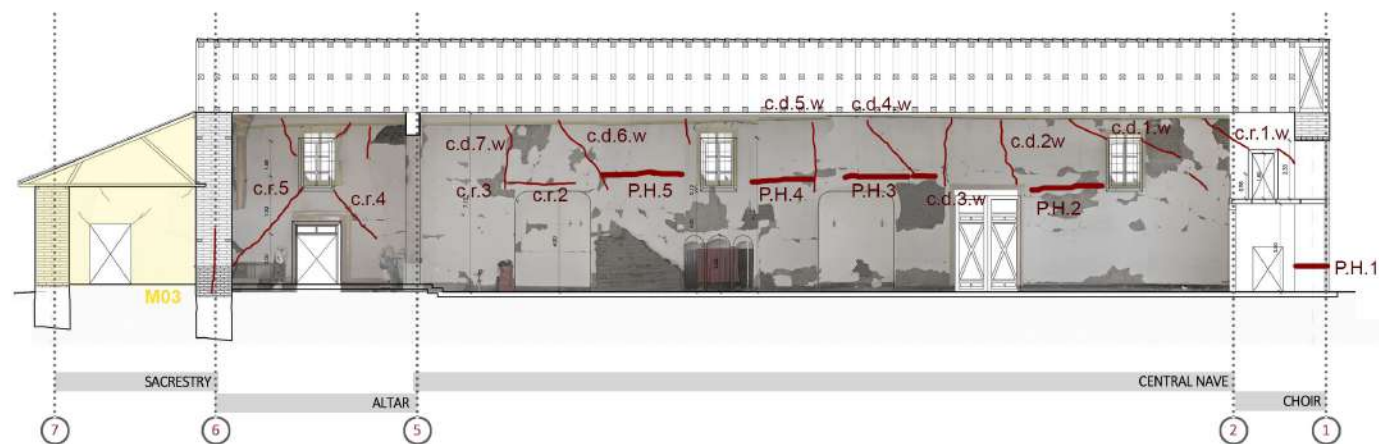
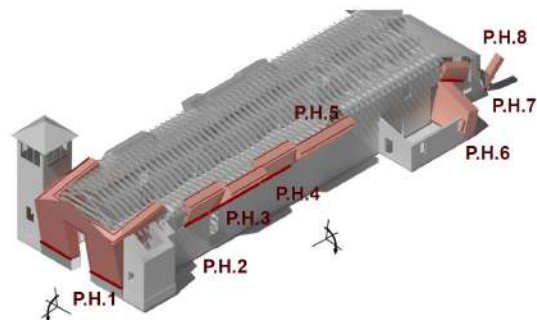
## DEGRADATION PHENOMENA THAT REDUCES STRUCTURAL EFFICIENCY

**Erosion, Er.i, and Mosses lichens and fungi, M.I.h.i**

**Presence of vegetation, Vi**

**Structural discontinuities**  
Heterogeneous materiality (Reinforced Concrete, R.C., Concrete C., Steel, S., Tabique, T.a.g.i. Masonry type1-2-3, M01-2-3, and Incannucciato, I.i)

## CRACK PATTERN OF MALLOA PARISH\_MP03



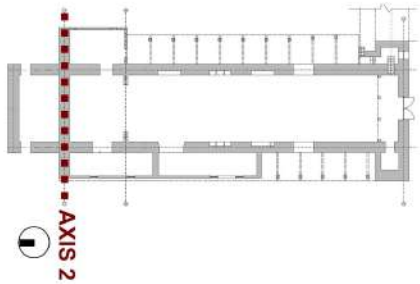
WEST ELEVATION, AXIS B



EAST ELEVATION, AXIS B

## INDIVIDUATION AND LOCATION ANALYZED AXIS:

### AXIS 2 NORTH AND SOUTH



### CRACK PATTERN

**c.a.i** Capillar crack, Initial, c.i.i, and Advanced, c.a.i  
In the first phase of an initial capillary crack, it is not possible to directly determine the corresponding points of the edge, but only the shape of crack, while in the advanced step it is possible to identify both elements of analysis.

**P.H.** Crack corresponding to plastic hinge, P.H.  
A macro-element undergoes a rigid rotation around a plastic hinge, P.H., generally corresponding to horizontal or diagonal crack.

**c.r.i** Rotating crack, c.r.i  
The block during cracking undergoes a rigid rotation by which the two edges of the crack move away.

**c.d.i** Detachment crack, c.d.i  
The block is completely separated from the rest of the building.

**co.i** Partial collapse or loss of material  
**Co.i** Total collapse, localized decomposition of wall pieces

**D.b.i** Detachment of beam or metal tie  
Detachment of beam or tie-rod and loss of operability or, and / or severe deformation of a key

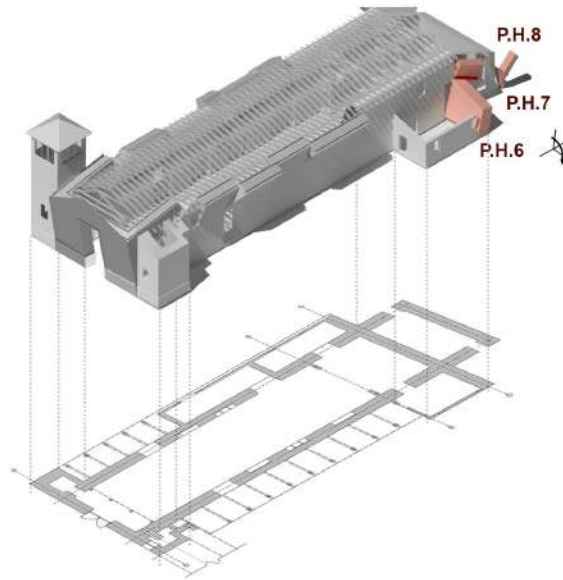
— Crack pattern after 2010 Maule earthquake

### DEGRADATION PHENOMENA THAT REDUCES STRUCTURAL EFFICIENCY

**Erosion, Er.i, and Mosses lichens and fungi, M.I.h.i**

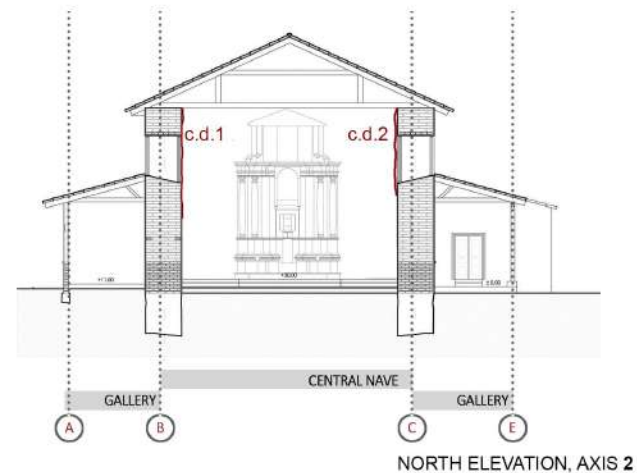
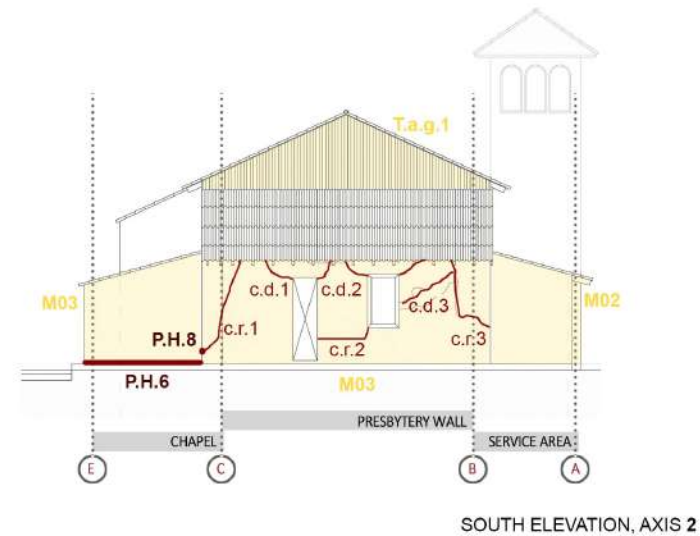
**Presence of vegetation, Vi**

**Structural discontinuities**  
Heterogeneous materiality (Reinforced Concrete, R.C., Concrete C., Steel, S., Tabique, T.a.g.i, Masonry type1-2-3, M01-2-3, and Incannucciato, I.i)



0 5 10 15m

## CRACK PATTERN OF MALLOA PARISH\_MP04



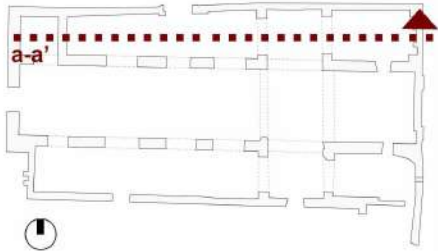
## **Annex2**

**SAN FRANCISCO CHURCH**



## INDIVIDUATION AND LOCATION ANALYZED AXIS:

SOUTH ELEVATION and SECTION a-a'



## CRACK PATTERN



Capillar crack, Initial, c.i.i, and Advanced, c.a.i

In the first phase of an initial capillary crack, it is not possible to directly determine the corresponding points of the edge, but only the shape of crack, while in the advanced step it is possible to identify both elements of analysis.

**P.H.**

Crack corresponding to plastic hinge, P.H.

A macro-element undergoes a rigid rotation around a plastic hinge, P.H., generally corresponding to horizontal or diagonal crack.



Rotating crack, c.r.i

The block during cracking undergoes a rigid rotation by which the two edges of the crack move away.



Detachment crack, c.d.i

The block is completely separated from the rest of the building.



co.i Partial collapse or loss of material



Co.i Total collapse, localized decomposition of wall pieces

**D.b.i**

Detachment of beam or metal tie



Detachment of beam or tie-rod and loss of operability or, and / or severe deformation of a key



Crack pattern after 2010 Maule earthquake

## DEGRADATION PHENOMENA THAT REDUCES STRUCTURAL EFFICIENCY



Degradation of the masonry  
Erosion, Er.i, and Mosses lichens and fungi, M.i.h.i



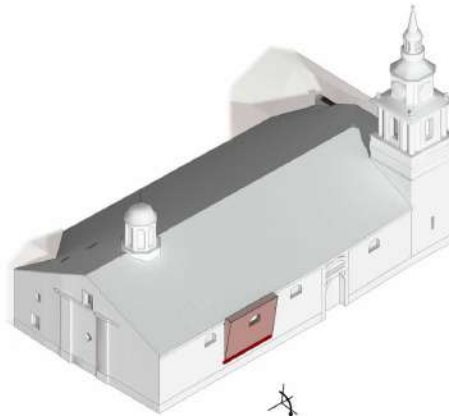
Presence of vegetation, Vi



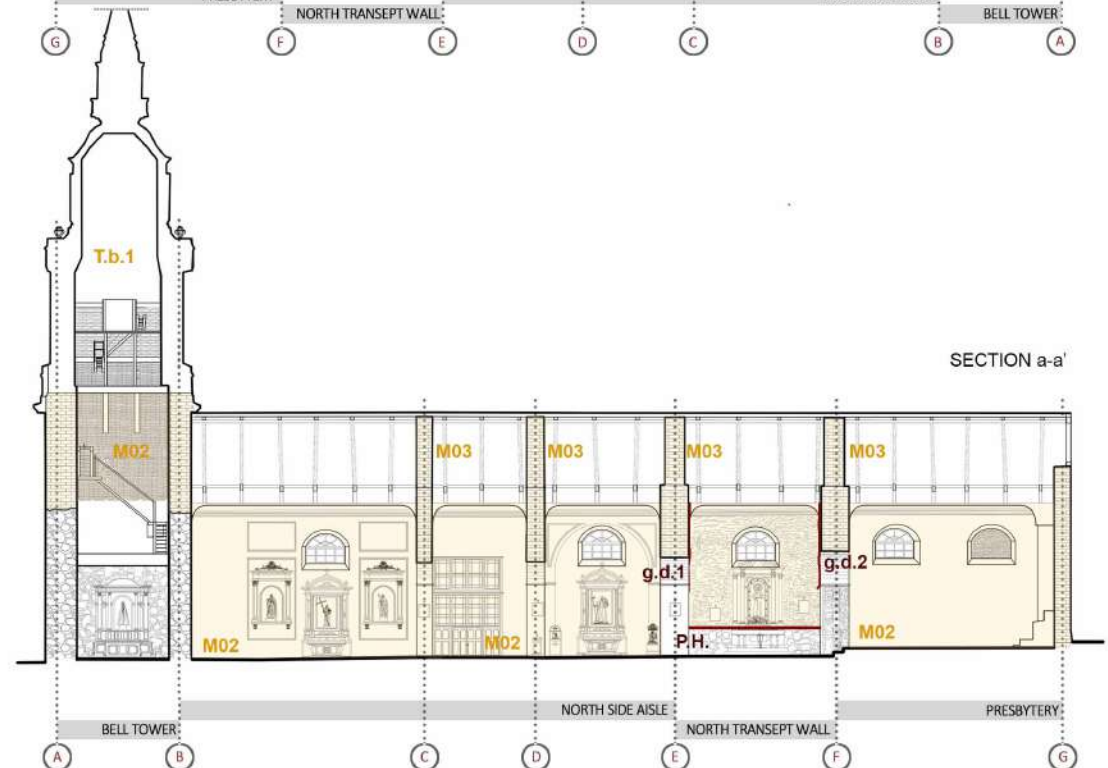
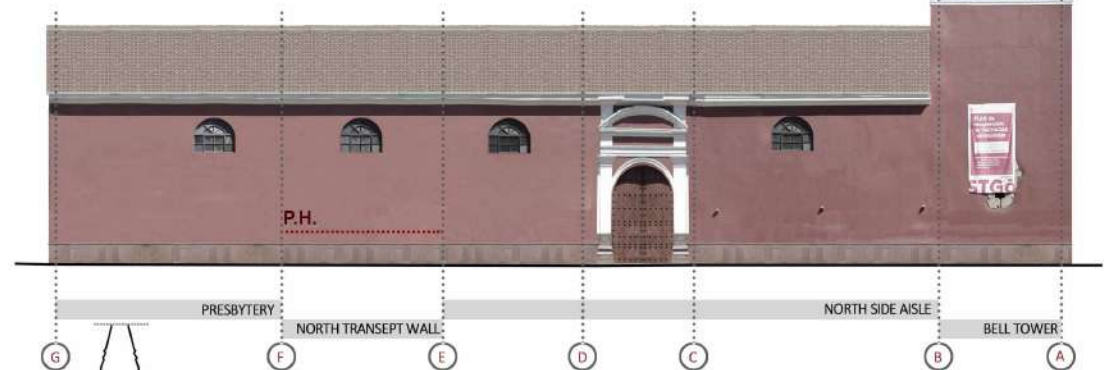
Structural discontinuities

Heterogeneous materiality (Reinforced Concrete, R.C., Concrete C, Steel, S., Tabique, T.a.g.i, Masonry type 1-2-3, M01-2-3, and Incannucciato, I.i.)

## CRACK PATTERN OF SAN FRANCISCO CHURCH\_SF01

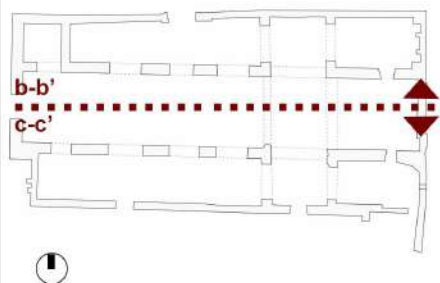


SOUTH ELEVATION, AXIS 1



## INDIVIDUATION AND LOCATION ANALYZED AXIS:

### SECTION b-b' and c-c'



### CRACK PATTERN

**c.a.i** Capillar crack, Initial, c.i.i, and Advanced, c.a.i  
In the first phase of an initial capillary crack, it is not possible to directly determine the corresponding points of the edge, but only the shape of crack, while in the advanced step it is possible to identify both elements of analysis.

**P.H.** Crack corresponding to plastic hinge, P.H.  
A macro-element undergoes a rigid rotation around a plastic hinge, P.H., generally corresponding to horizontal or diagonal crack.

**c.r.i** Rotating crack, c.r.i  
The block during cracking undergoes a rigid rotation by which the two edges of the crack move away.

**c.d.i** Detachment crack, c.d.i  
The block is completely separated from the rest of the building.

**co.i** Partial collapse or loss of material  
**Co.i** Total collapse, localized decomposition of wall pieces

**D.b.i** Detachment of beam or metal tie  
Detachment of beam or tie-rod and loss of operability or, and / or severe deformation of a key

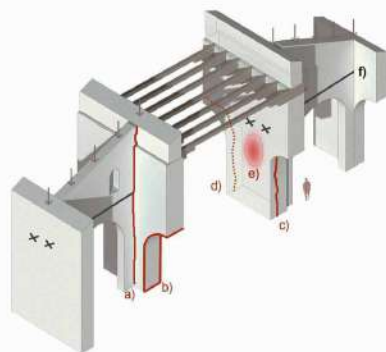
— Crack pattern after 2010 Maule earthquake

### DEGRADATION PHENOMENA THAT REDUCES STRUCTURAL EFFICIENCY

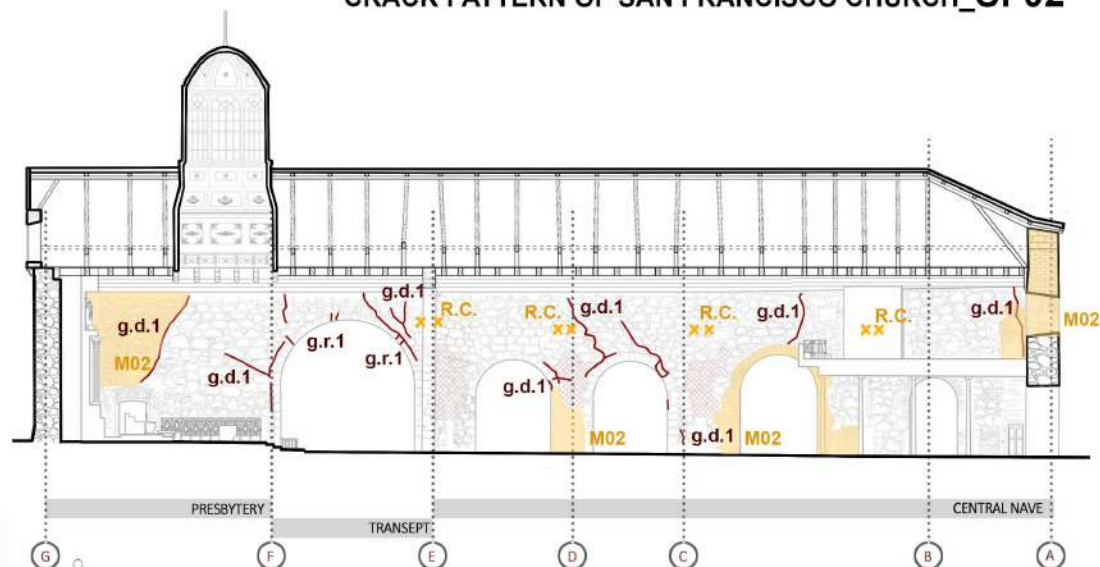
Degradation of the masonry  
Erosion, Er.i, and Mosses lichens and fungi, M.I.h.i

Presence of vegetation, Vi

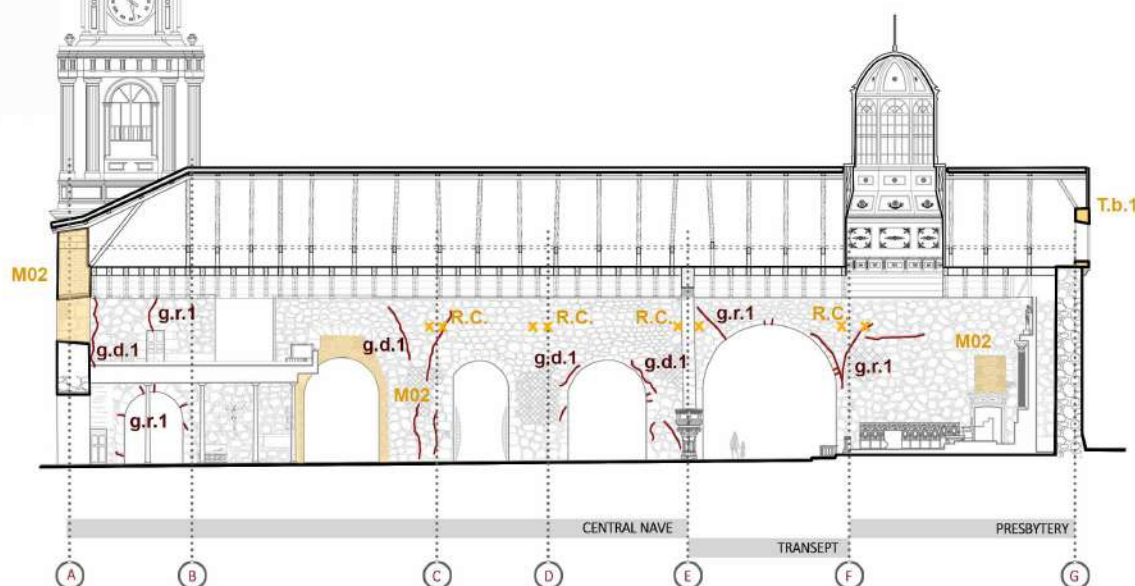
Structural discontinuities  
Heterogeneous materiality (Reinforced Concrete, R.C., Concrete C, Steel, S., Tabique, T.a.g.i, Masonry type 1-2-3, M01-2-3, and Incannucciato, I.i)



## CRACK PATTERN OF SAN FRANCISCO CHURCH\_SF02



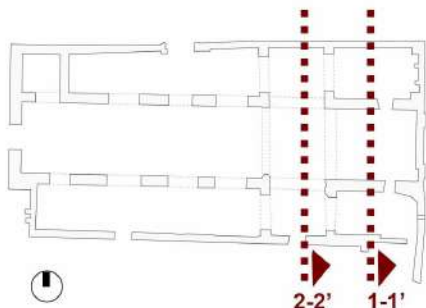
SECTION b-b'



SECTION c-c'

## INDIVIDUATION AND LOCATION ANALYZED AXIS:

SECTIONS 1-1' and 2-2'



## CRACK PATTERN

**c.a.i** Capillar crack, Initial, c.i.i, and Advanced, c.a.i  
In the first phase of an initial capillary crack, it is not possible to directly determine the corresponding points of the edge, but only the shape of crack, while in the advanced step it is possible to identify both elements of analysis.

**P.H.** Crack corresponding to plastic hinge, P.H.  
A macro-element undergoes a rigid rotation around a plastic hinge, P.H., generally corresponding to horizontal or diagonal crack.

**c.r.i** Rotating crack, c.r.i  
The block during cracking undergoes a rigid rotation by which the two edges of the crack move away.

**c.d.i** Detachment crack, c.d.i  
The block is completely separated from the rest of the building.

**co.i** Partial collapse or loss of material

**Co.i** Total collapse, localized decomposition of wall pieces

**D.b.i** Detachment of beam or metal tie

**X** Detachment of beam or tie-rod and loss of operability or, and / or severe deformation of a key

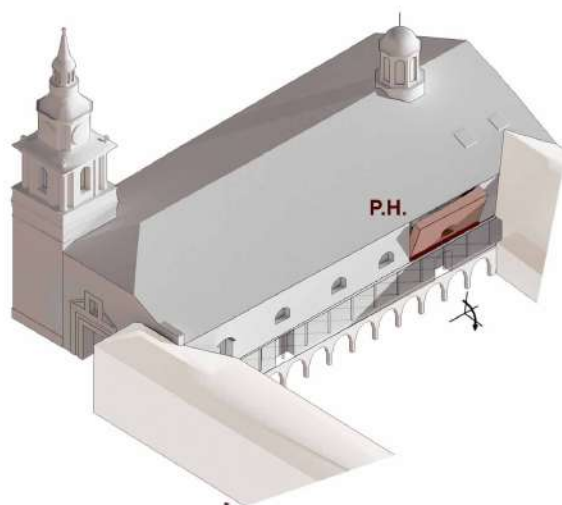
**—** Crack pattern after 2010 Maule earthquake

## DEGRADATION PHENOMENA THAT REDUCES STRUCTURAL EFFICIENCY

**///** Degradation of the masonry  
Erosion, Er.i, and Mosses lichens and fungi, M.i.h.i

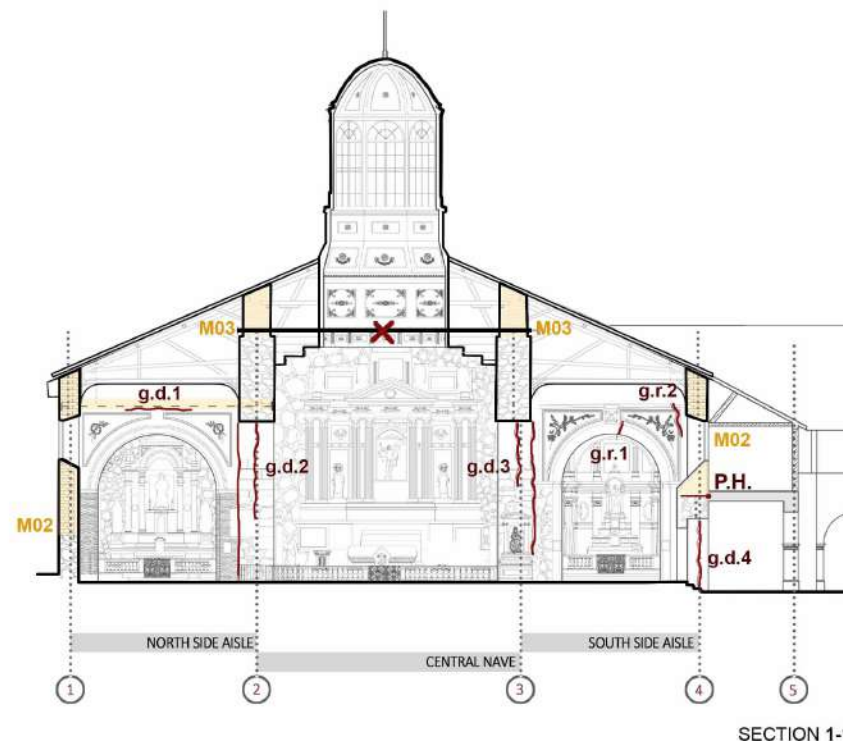
**\*** Presence of vegetation, Vi

**■** Structural discontinuities  
Heterogeneous materiality (Reinforced Concrete, R.C., Concrete C., Steel, S., Tabique, T.a.g.i, Masonry type 1-2-3, M01-2-3, and Incannucciato, I.i)

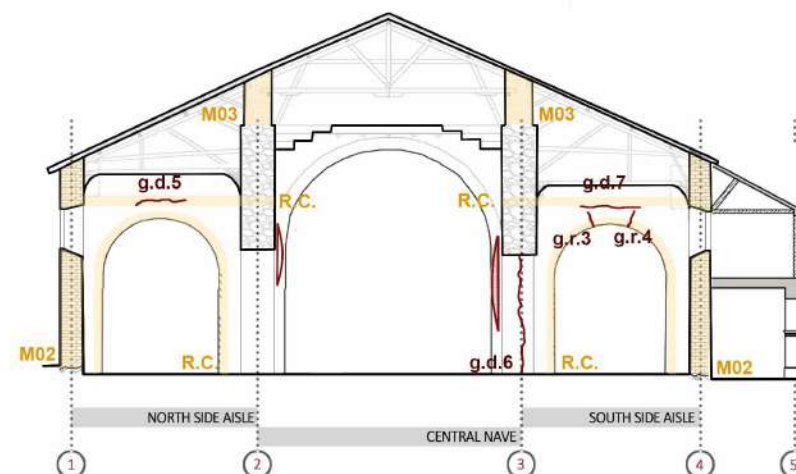


0 2.5 5.0 10.0 mts.

## CRACK PATTERN OF SAN FRANCISCO CHURCH\_SF03



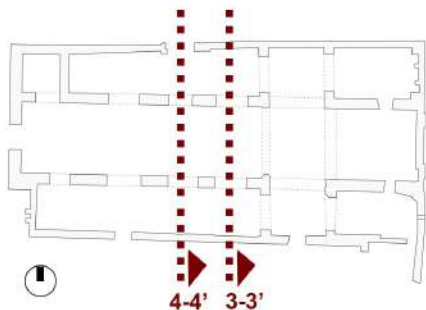
SECTION 1-1'



SECTION 2-2'

## INDIVIDUATION AND LOCATION ANALYZED AXIS:

SECTIONS 1-1' and 2-2'



## CRACK PATTERN



Capillar crack, Initial, c.i.i, and Advanced, c.a.i

In the first phase of an initial capillary crack, it is not possible to directly determine the corresponding points of the edge, but only the shape of crack, while in the advanced step it is possible to identify both elements of analysis.

**P.H.**

Crack corresponding to plastic hinge, P.H.

A macro-element undergoes a rigid rotation around a plastic hinge, P.H., generally corresponding to horizontal or diagonal crack.



Rotating crack, c.r.i

The block during cracking undergoes a rigid rotation by which the two edges of the crack move away.



Detachment crack, c.d.i

The block is completely separated from the rest of the building.



Partial collapse or loss of material



Total collapse, localized decomposition of wall pieces



Detachment of beam or metal tie

Detachment of beam or tie-rod and loss of operability or, and / or severe deformation of a key



Crack pattern after 2010 Maule earthquake

## DEGRADATION PHENOMENA THAT REDUCES STRUCTURAL EFFICIENCY



Degradation of the masonry

Erosion, Er.i, and Mosses lichens and fungi, M.i.h.i

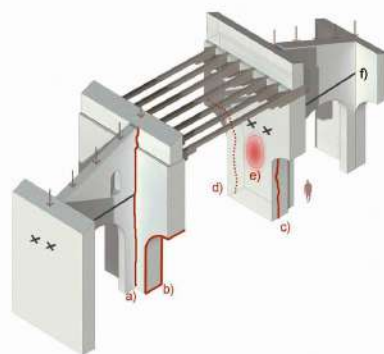


Presence of vegetation, Vi

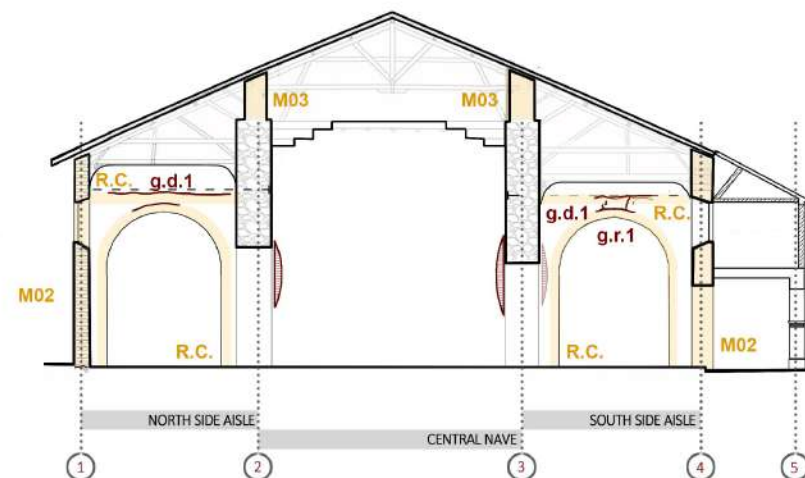


Structural discontinuities

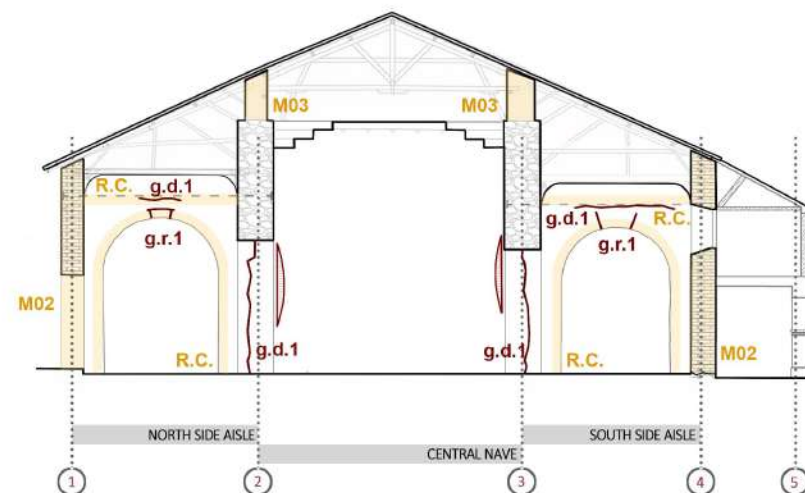
Heterogeneous materiality (Reinforced Concrete, R.C., Concrete C., Steel, S., Tabique, T.a.g.i, Masonry type 1-2-3, M01-2-3, and Incannucciato, I.i.)



## CRACK PATTERN OF SAN FRANCISCO CHURCH\_SF04



SECTION 3-3'



SECTION 4-4

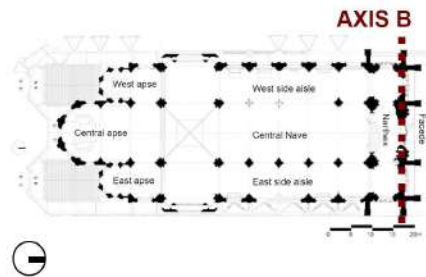
## **Annex3**

**BASILICA DEL SALVADOR**



## INDIVIDUATION AND LOCATION ANALYZED AXIS:

### AXIS B SOUTH AND NORTH

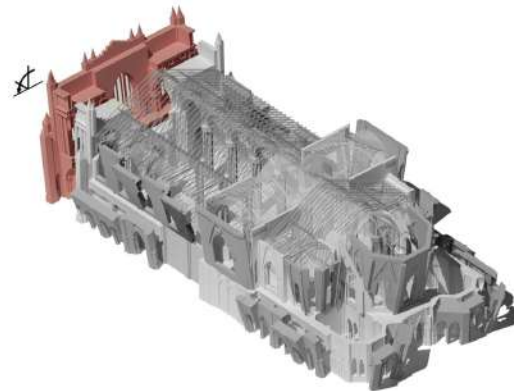


### CRACK PATTERN

- c.a.i** Capillar crack, Initial, c.i.i, and Advanced, c.a.i  
In the first phase of an initial capillar crack, it is not possible to directly determine the corresponding points of the edge, but only the shape of crack, while in the advanced step it is possible to identify both elements of analysis.
- P.H.** Crack corresponding to plastic hinge.  
A macro-element undergoes a rigid rotation around a plastic hinge, P.H., generally corresponding to horizontal or diagonal crack.
- c.r.i** Rotating crack, c.r.i  
The block during cracking undergoes a rigid rotation by which the two edges of the crack move away.
- c.d.i** Detachment crack, c.d.i  
The block is completely separated from the rest of the building.
- co.i** Partial collapse or loss of material  
**Co.i** Total collapse, localized decomposition of wall pieces
- D.b.i** Detachment of beam or metal tie  
Detachment of beam or tie-rod and loss of operability or, and / or severe deformation of a key
- Crack pattern after 2010 Maule earthquake

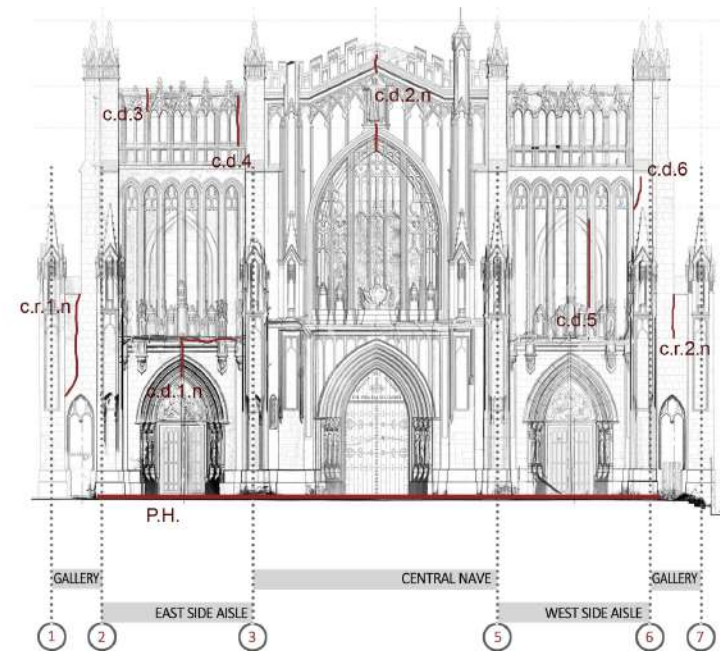
### DEGRADATION PHENOMENA THAT REDUCES STRUCTURAL EFFICIENCY

- Erosion, Er.i, and Mosses lichens and fungi, M.I.h.i**  
Degradation of the masonry
- Presence of vegetation, Vi**
- Structural discontinuities**  
Heterogeneous materiality (Reinforced Concrete, R.C., Concrete C., Steel, S., Tabique, T.a.g.i, Masonry type1-2-3, M01-2-3, and Incannucciato, I.i)

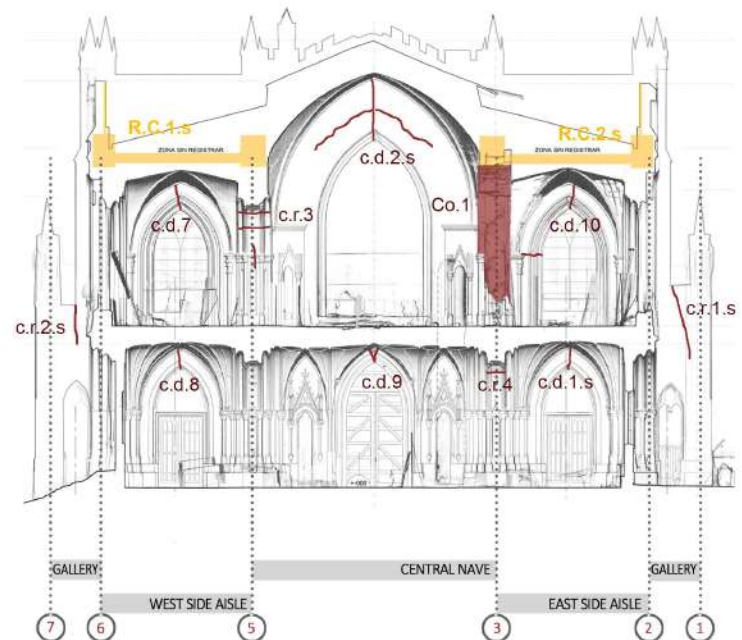


0 5 10 15m

## CRACK PATTERN OF BASILICA DEL SALVADOR\_BS01



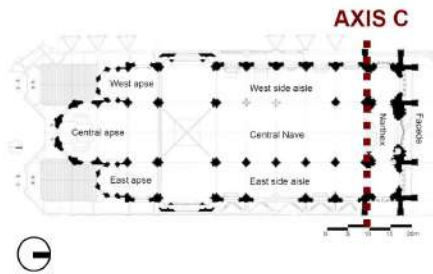
NORTE ELEVATION, AXIS B



SOUTH ELEVATION, AXIS B

## INDIVIDUATION AND LOCATION ANALYZED AXIS:

### AXIS C SOUTH AND NORTH



### CRACK PATTERN

**c.a.i** Capillar crack, Initial, c.i.i, and Advanced, c.a.i  
In the first phase of an initial capillary crack, it is not possible to directly determine the corresponding points of the edge, but only the shape of crack, while in the advanced step it is possible to identify both elements of analysis.

**—** Crack corresponding to plastic hinge, P.H.  
A macro-element undergoes a rigid rotation around a plastic hinge, P.H., generally corresponding to horizontal or diagonal crack.

**c.r.i** Rotating crack, c.r.i  
The block during cracking undergoes a rigid rotation by which the two edges of the crack move away.

**c.d.i** Detachment crack, c.d.i  
The block is completely separated from the rest of the building.

**co.i** Partial collapse or loss of material  
**Co.i** Total collapse, localized decomposition of wall pieces

**D.b.i** Detachment of beam or metal tie  
Detachment of beam or tie-rod and loss of operability or, and / or severe deformation of a key

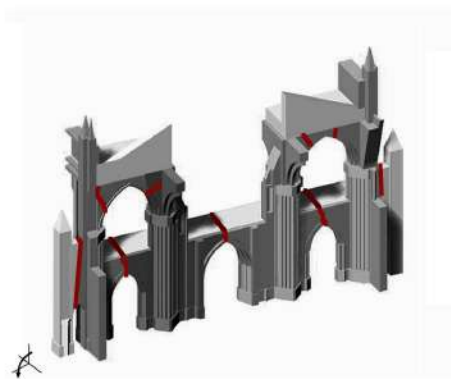
**—** Crack pattern after 2010 Maule earthquake

### DEGRADATION PHENOMENA THAT REDUCES STRUCTURAL EFFICIENCY

**///** Degradation of the masonry  
Erosion, Er.i, and Mosses lichens and fungi, M.I.h.i

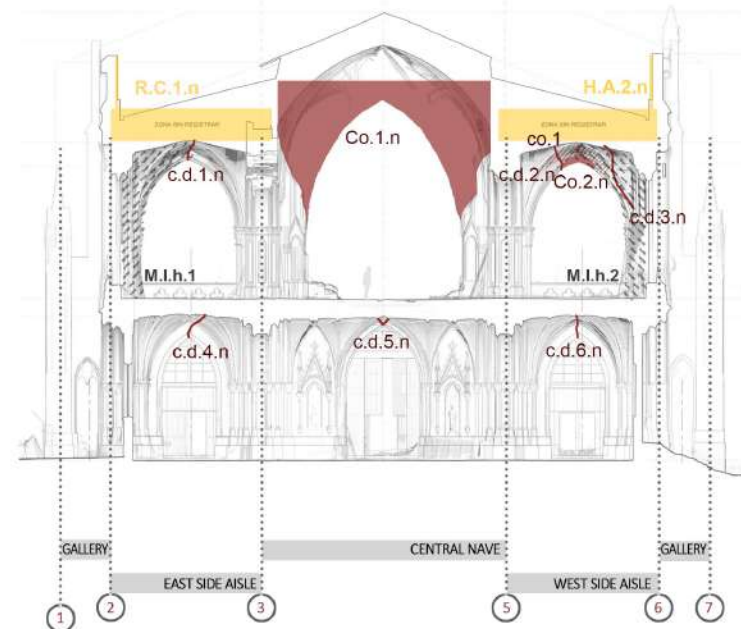
**\*** Presence of vegetation, Vi

**■** Structural discontinuities  
Heterogeneous materiality (Reinforced Concrete, R.C., Concrete C., Steel, S., Tabique, T.a.g.i, Masonry type 1-2-3, M01-2-3, and Incannucciato, I.i)

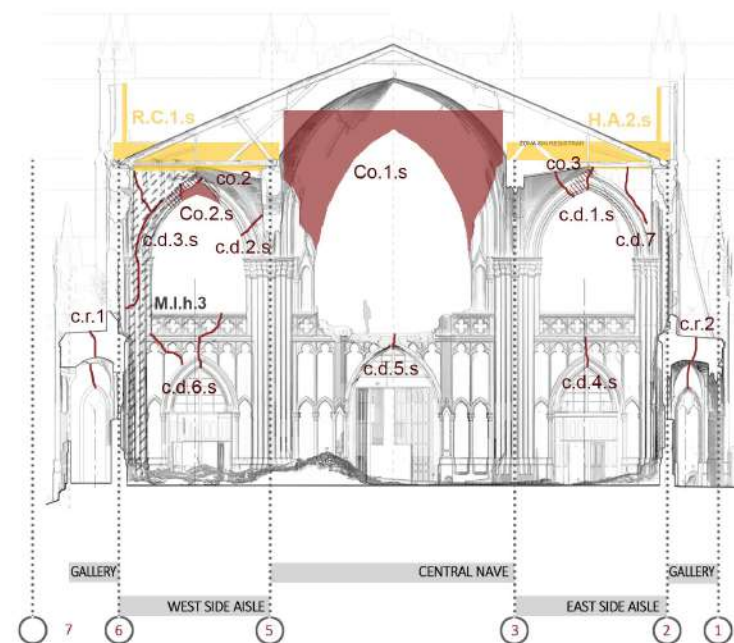


0 5 10 15m

## CRACK PATTERN OF BASILICA DEL SALVADOR\_BS02



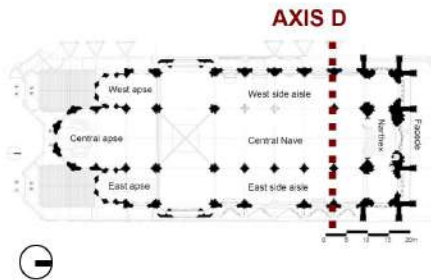
NORTH ELEVATION, AXIS C



SOUTH ELEVATION, AXIS C

## INDIVIDUATION AND LOCATION ANALYZED AXIS:

### AXIS D SOUTH



## CRACK PATTERN

**c.a.i** Capillar crack, Initial, c.i.i, and Advanced, c.a.i  
In the first phase of an initial capillary crack, it is not possible to directly determine the corresponding points of the edge, but only the shape of crack, while in the advanced step it is possible to identify both elements of analysis.

**P.H.** Crack corresponding to plastic hinge, P.H.  
A macro-element undergoes a rigid rotation around a plastic hinge, P.H., generally corresponding to horizontal or diagonal crack.

**c.r.i** Rotating crack, c.r.i  
The block during cracking undergoes a rigid rotation by which the two edges of the crack move away.

**c.d.i** Detachment crack, c.d.i  
The block is completely separated from the rest of the building.

**co.i** Partial collapse or loss of material  
**Co.i** Total collapse, localized decomposition of wall pieces

**D.b.i** Detachment of beam or metal tie  
Detachment of beam or tie-rod and loss of operability or, and / or severe deformation of a key

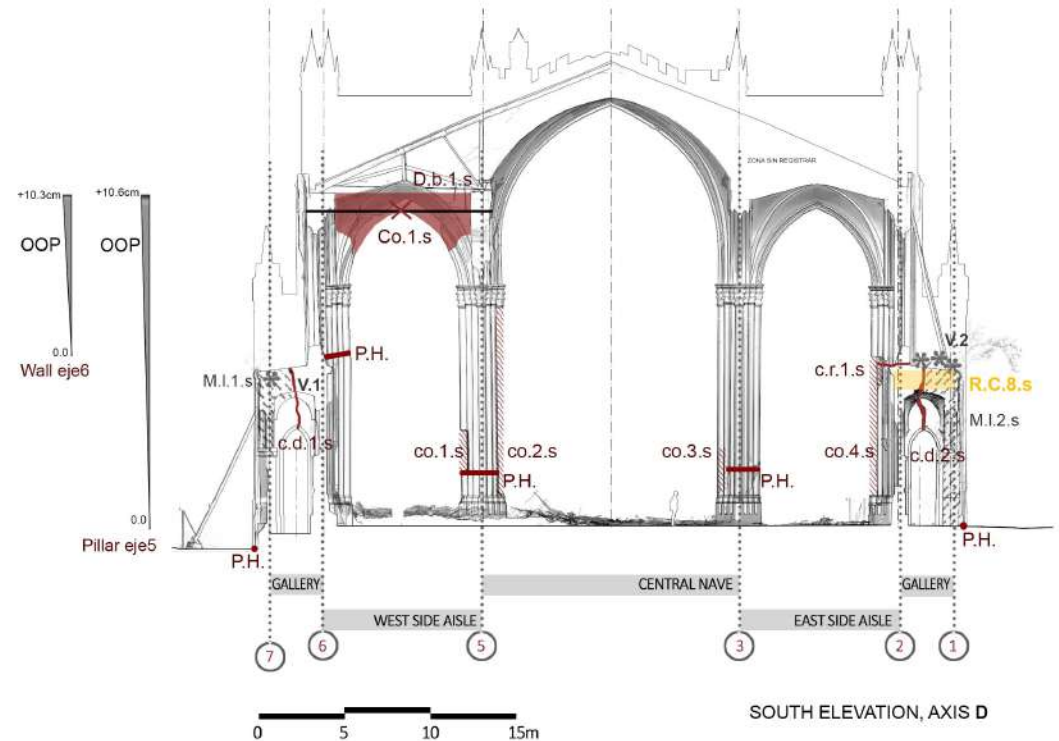
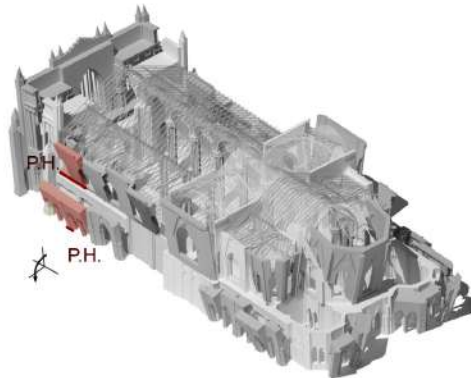
— Crack pattern after 2010 Maule earthquake

## DEGRADATION PHENOMENA THAT REDUCES STRUCTURAL EFFICIENCY

**Erosion, Er.i, and Mosses lichens and fungi, M.I.h.i**

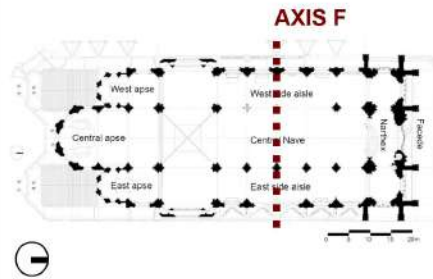
**Presence of vegetation, Vi**

**Structural discontinuities**  
Heterogeneous materiality (Reinforced Concrete, R.C., Concrete C., Steel, S., Tabique, T.a.g.i, Masonry type 1-2-3, M01-2-3, and Incannucciato, I.i.)



## INDIVIDUATION AND LOCATION ANALYZED AXIS:

### AXIS F NORTH



## CRACK PATTERN

**c.a.i** Capillar crack, Initial, c.i.i, and Advanced, c.a.i  
In the first phase of an initial capillary crack, it is not possible to directly determine the corresponding points of the edge, but only the shape of crack, while in the advanced step it is possible to identify both elements of analysis.

**P.H.** Crack corresponding to plastic hinge, P.H.  
A macro-element undergoes a rigid rotation around a plastic hinge, P.H., generally corresponding to horizontal or diagonal crack.

**c.r.i** Rotating crack, c.r.i  
The block during cracking undergoes a rigid rotation by which the two edges of the crack move away.

**c.d.i** Detachment crack, c.d.i  
The block is completely separated from the rest of the building.

**co.i** Partial collapse or loss of material  
**Co.i** Total collapse, localized decomposition of wall pieces

**D.b.i** Detachment of beam or metal tie  
Detachment of beam or tie-rod and loss of operability or, and / or severe deformation of a key

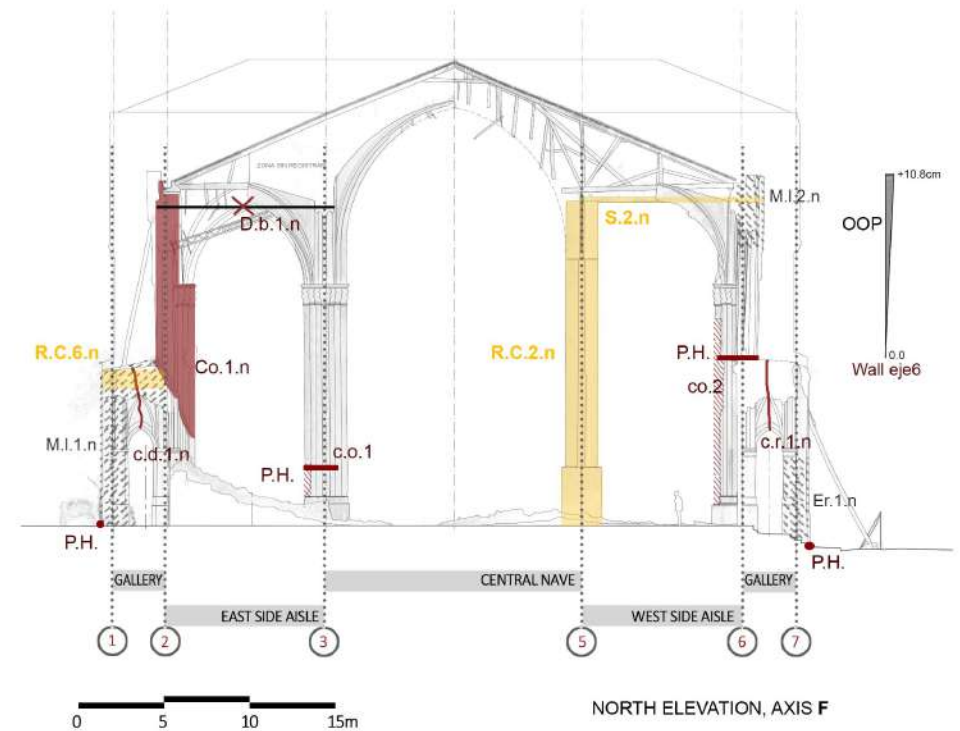
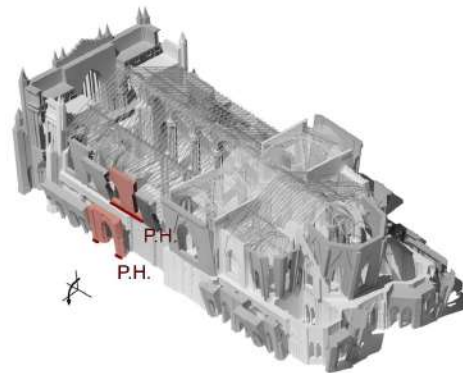
Crack pattern after 2010 Maule earthquake

## DEGRADATION PHENOMENA THAT REDUCES STRUCTURAL EFFICIENCY

**Er.i, M.I.h.i** Degradation of the masonry  
Erosion, Er.i, and Mosses lichens and fungi, M.I.h.i

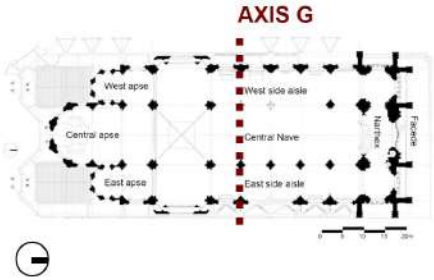
**Vi** Presence of vegetation, Vi

**S, R.C., C., T.a.g.i, I.i** Structural discontinuities  
Heterogeneous materiality (Reinforced Concrete, R.C., Concrete C., Steel, S., Tabique, T.a.g.i, Masonry type 1-2-3, M01-2-3, and Incannucciato, I.i)





INDIVIDUATION AND LOCATION  
ANALYZED AXIS:


AXIS G NORTH






CRACK PATTERN



 c.a.i. Capillar crack, Initial, c.i.i, and Advanced, c.a.i  
In the first phase of an initial capillary crack, it is not possible to directly determine the corresponding points of the edge, but only the shape of crack, while in the advanced step it is possible to identify both elements of analysis.

 Crack corresponding to plastic hinge, P.H.  
A macro-element undergoes a rigid rotation around a plastic hinge, P.H., generally corresponding to horizontal or diagonal crack.

 c.r.i. Rotating crack, c.r.i  
The block during cracking undergoes a rigid rotation by which the two edges of the crack move away.


 c.d.i. Detachment crack, c.d.i  
The block is completely separated from the rest of the building.

 co.i Partial collapse or loss of material  
 Co.i Total collapse, localized decomposition of wall pieces


 D.b.i Detachment of beam or metal tie  
 Detachment of beam or tie-rod and loss of operability or, and / or severe deformation of a key

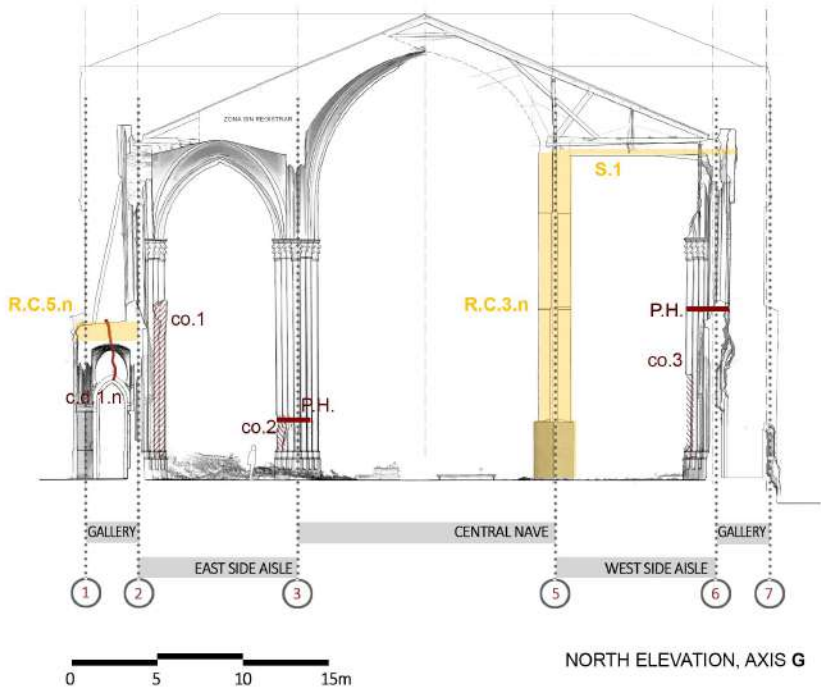
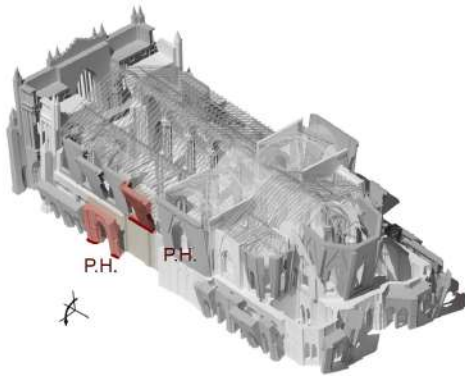
 Crack pattern after 2010 Maule earthquake

DEGRADATION PHENOMENA THAT REDUCES  
STRUCTURAL EFFICIENCY

 Degradation of the masonry  
Erosion, Er.i, and Mosses lichens and fungi, M.I.h.i

 Presence of vegetation, Vi

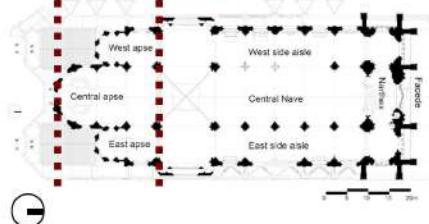
 Structural discontinuities  
Heterogeneous materiality (Reinforced Concrete, R.C., Concrete C., Steel, S., Tabique, T.a.g.i, Masonry type 1-2-3, M01-2-3, and Incannucciato, I.i)



## INDIVIDUATION AND LOCATION ANALYZED AXIS:

### AXIS P-J NORTH AND SOUTH

#### AXIS P AXIS J



### CRACK PATTERN

**c.a.i** Capillar crack, Initial, c.i.i, and Advanced, c.a.i  
In the first phase of an initial capillary crack, it is not possible to directly determine the corresponding points of the edge, but only the shape of crack, while in the advanced step it is possible to identify both elements of analysis.

**P.H.** Crack corresponding to plastic hinge, P.H.  
A macro-element undergoes a rigid rotation around a plastic hinge, P.H., generally corresponding to horizontal or diagonal crack.

**c.r.i** Rotating crack, c.r.i  
The block during cracking undergoes a rigid rotation by which the two edges of the crack move away.

**c.d.i** Detachment crack, c.d.i  
The block is completely separated from the rest of the building.

**co.i** Partial collapse or loss of material

**Co.i** Total collapse, localized decomposition of wall pieces

**D.b.i** Detachment of beam or metal tie

**X** Detachment of beam or tie-rod and loss of operability or, and / or severe deformation of a key

**—** Crack pattern after 2010 Maule earthquake

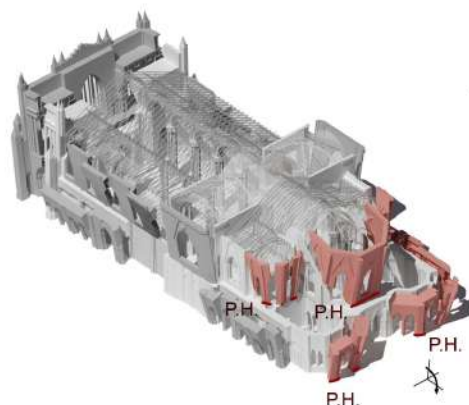
### DEGRADATION PHENOMENA THAT REDUCES STRUCTURAL EFFICIENCY

**Erosion, Er.i, and Mosses lichens and fungi, M.I.h.i**  
Degradation of the masonry

**Vi** Presence of vegetation, Vi

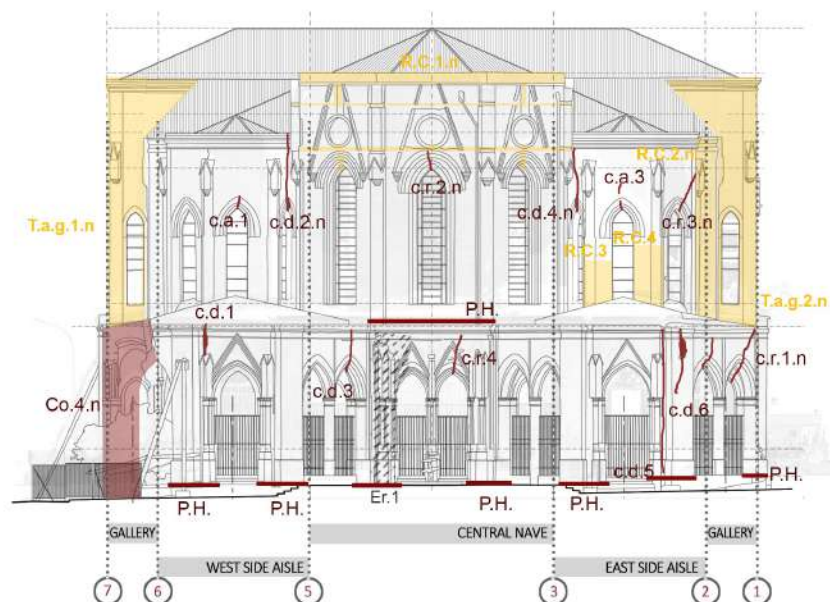
**—** Structural discontinuities

**—** Heterogeneous materiality (Reinforced Concrete, R.C., Concrete C., Steel, S., Tabique, T.a.g.i, Masonry type 1-2-3, M01-2-3, and Incanuatiato, I.i)

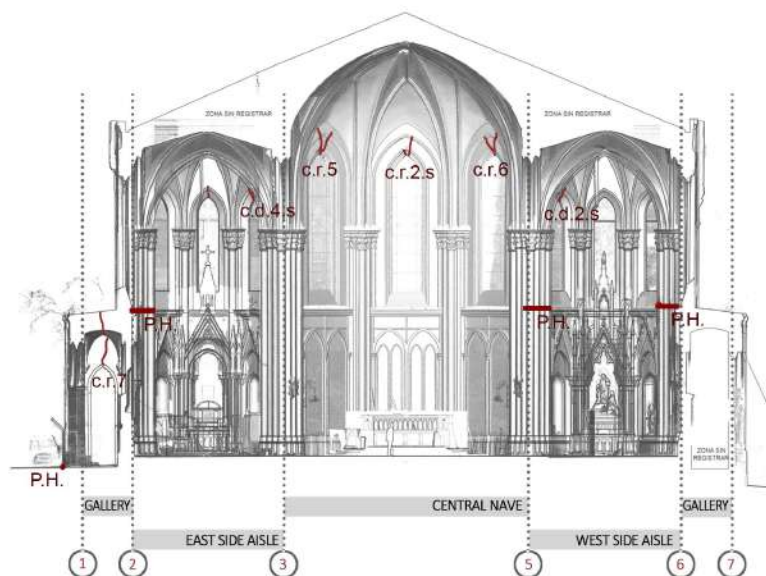


0 5 10 15m

## CRACK PATTERN OF BASILICA DEL SALVADOR\_BS6



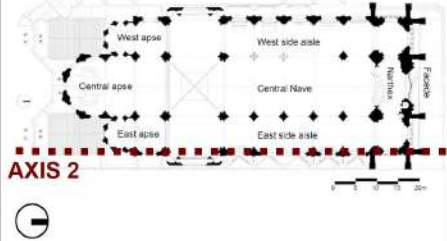
NORTH ELEVATION, AXIS P-J



SOUTH ELEVATION, AXIS J-N

## INDIVIDUATION AND LOCATION ANALYZED AXIS:

### AXIS 2 EAST AND WEST



### CRACK PATTERN

**c.a.i** Capillar crack, Initial, c.i.i, and Advanced, c.a.i  
In the first phase of an initial capillary crack, it is not possible to directly determine the corresponding points of the edge, but only the shape of crack, while in the advanced step it is possible to identify both elements of analysis.

**—** Crack corresponding to plastic hinge, P.H.  
A macro-element undergoes a rigid rotation around a plastic hinge, P.H., generally corresponding to horizontal or diagonal crack.

**c.r.i** Rotating crack, c.r.i  
The block during cracking undergoes a rigid rotation by which the two edges of the crack move away.

**c.d.i** Detachment crack, c.d.i  
The block is completely separated from the rest of the building.

**co.i** Partial collapse or loss of material  
**Co.i** Total collapse, localized decomposition of wall pieces

**D.b.i** Detachment of beam or metal tie  
Detachment of beam or tie-rod and loss of operability or, and / or severe deformation of a key

**—** Crack pattern after 2010 Maule earthquake

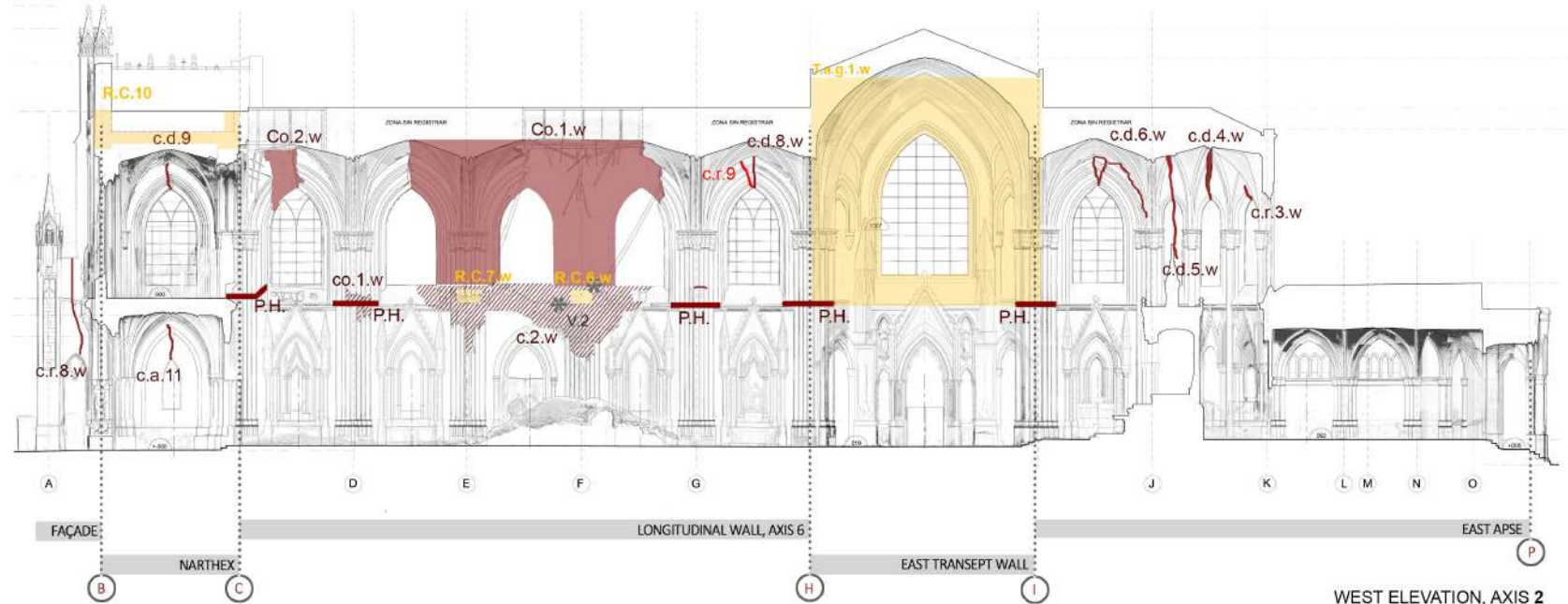
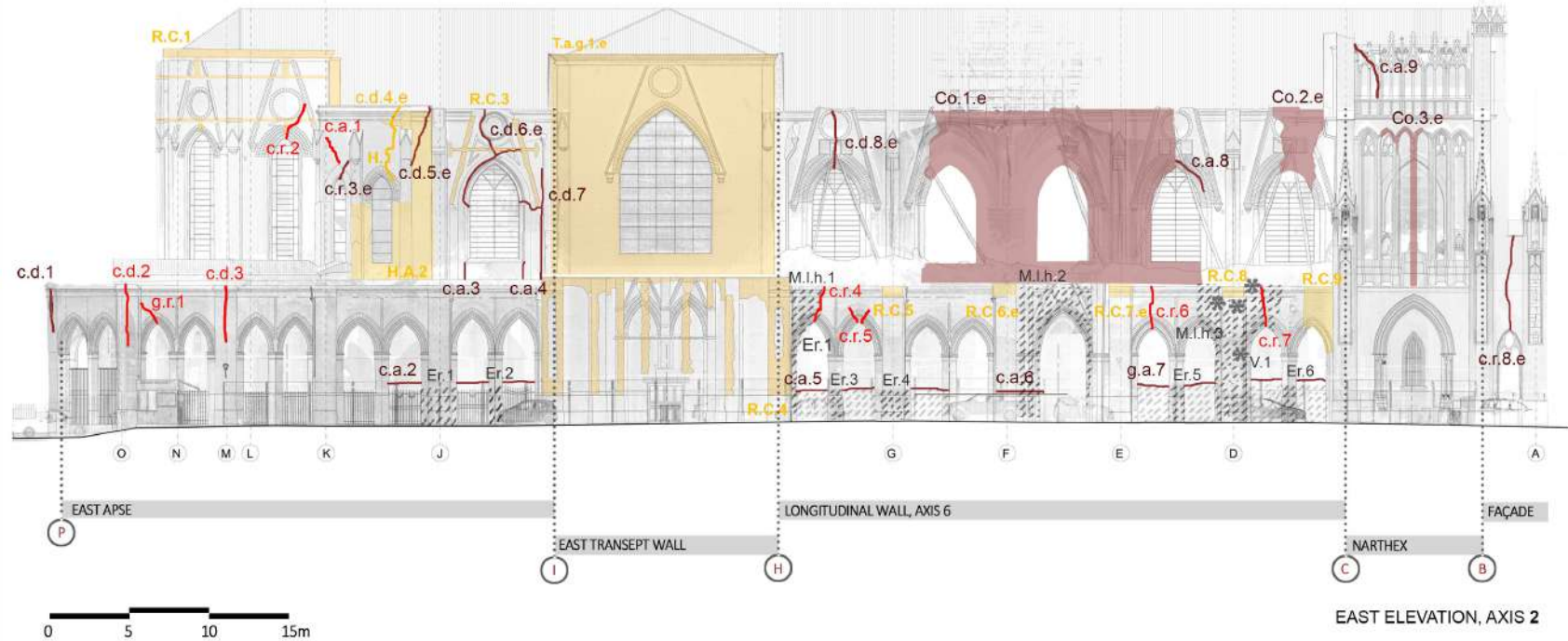
### DEGRADATION PHENOMENA THAT REDUCES STRUCTURAL EFFICIENCY

**—** Degradation of the masonry  
Erosion, Er.i, and Mosses lichens and fungi, M.I.h.i

**\*** Presence of vegetation, Vi

**—** Structural discontinuities  
Heterogeneous materiality (Reinforced Concrete, R.C., Concrete C., Steel, S., Tabique, T.a.g.i, Masonry type1-2-3, M01-2-3, and Incannucciato, I.i)

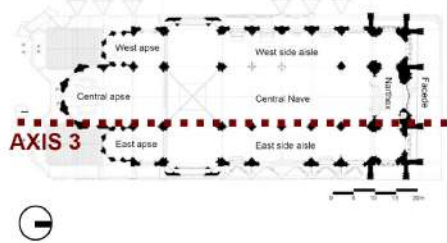
## CRACK PATTERN OF BASILICA DEL SALVADOR\_BS07



WEST ELEVATION, AXIS 2

## INDIVIDUATION AND LOCATION ANALYZED AXIS:

### AXIS 3 EAST AND WEST



### CRACK PATTERN

**c.a.i** Capillar crack, Initial, c.i.i, and Advanced, c.a.i  
In the first phase of an initial capillary crack, it is not possible to directly determine the corresponding points of the edge, but only the shape of crack, while in the advanced step it is possible to identify both elements of analysis.

**P.H.** Crack corresponding to plastic hinge, P.H.  
A macro-element undergoes a rigid rotation around a plastic hinge, P.H., generally corresponding to horizontal or diagonal crack.

**c.r.i** Rotating crack, c.r.i  
The block during cracking undergoes a rigid rotation by which the two edges of the crack move away.

**c.d.i** Detachment crack, c.d.i  
The block is completely separated from the rest of the building.

**co.i** Partial collapse or loss of material  
**Co.i** Total collapse, localized decomposition of wall pieces

**D.b.i** Detachment of beam or metal tie  
Detachment of beam or tie-rod and loss of operability or, and / or severe deformation of a key

— Crack pattern after 2010 Maule earthquake

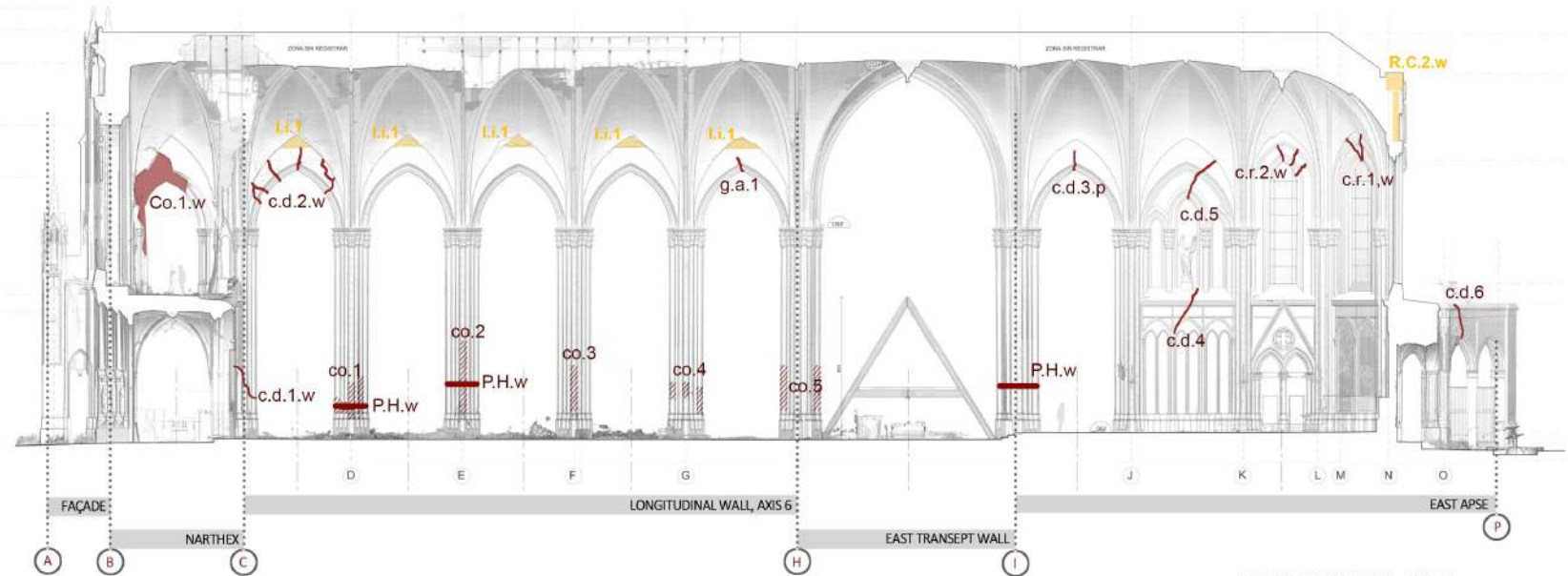
### DEGRADATION PHENOMENA THAT REDUCES STRUCTURAL EFFICIENCY

**Erosion, Er.i, and Mosses lichens and fungi, M.I.h.i**

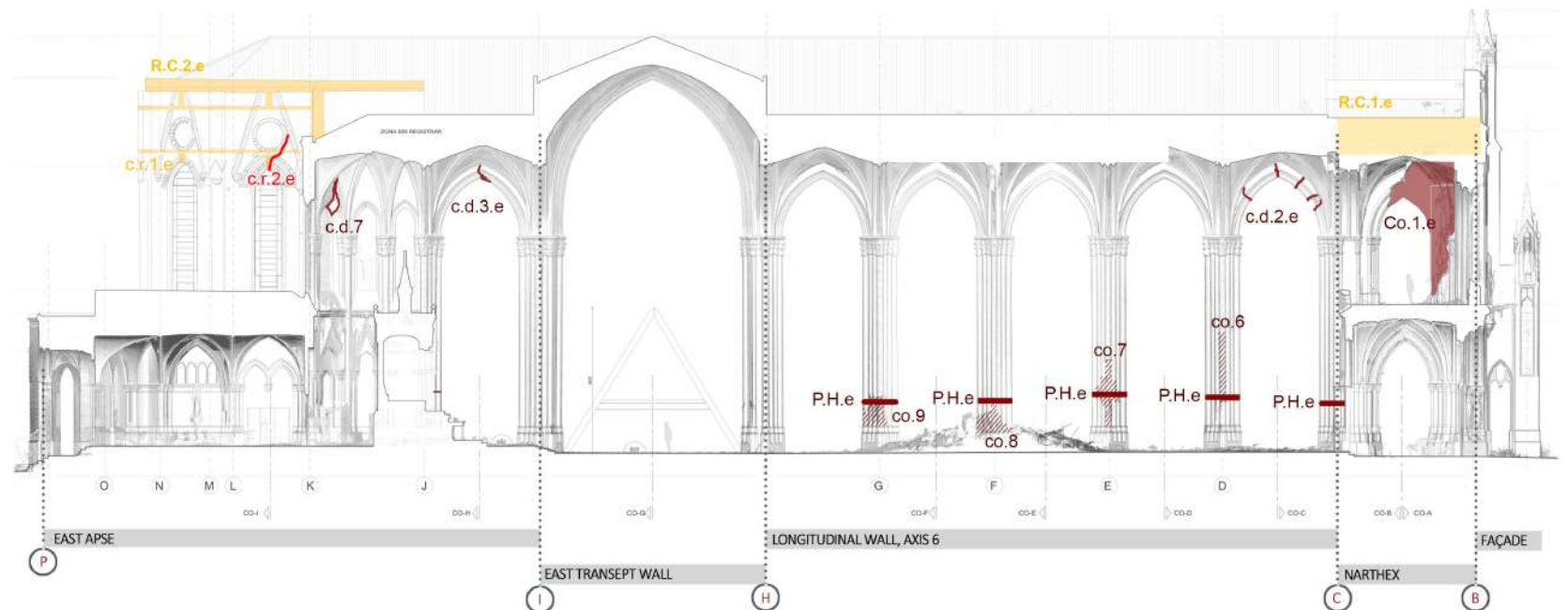
**Presence of vegetation, Vi**

**Structural discontinuities**  
Heterogeneous materiality (Reinforced Concrete, R.C., Concrete C., Steel, S., Tabique, T.a.g.i, Masonry type1-2-3, M01-2-3, and Incannucciato, I.i)

## CRACK PATTERN OF BASILICA DEL SALVADOR\_BS08



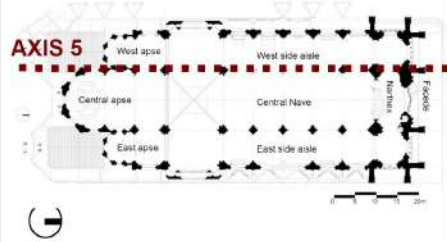
WEST ELEVATION, AXIS 3



EAST ELEVATION, AXIS 3

## INDIVIDUATION AND LOCATION ANALYZED AXIS:

### AXIS 5 EAST AND WEST



## CRACK PATTERN

**c.a.i** Capillar crack, Initial, c.i.i, and Advanced, c.a.i  
In the first phase of an initial capillar crack, it is not possible to directly determine the corresponding points of the edge, but only the shape of crack, while in the advanced step it is possible to identify both elements of analysis.

**P.H.** Crack corresponding to plastic hinge, P.H.  
A macro-element undergoes a rigid rotation around a plastic hinge, P.H., generally corresponding to horizontal or diagonal crack.

**c.r.i** Rotating crack, c.r.i  
The block during cracking undergoes a rigid rotation by which the two edges of the crack move away.

**c.d.i** Detachment crack, c.d.i  
The block is completely separated from the rest of the building.

**co.i** Partial collapse or loss of material  
**Co.i** Total collapse, localized decomposition of wall pieces

**D.b.i** Detachment of beam or metal tie  
Detachment of beam or tie-rod and loss of operability or, and / or severe deformation of a key

Crack pattern after 2010 Maule earthquake

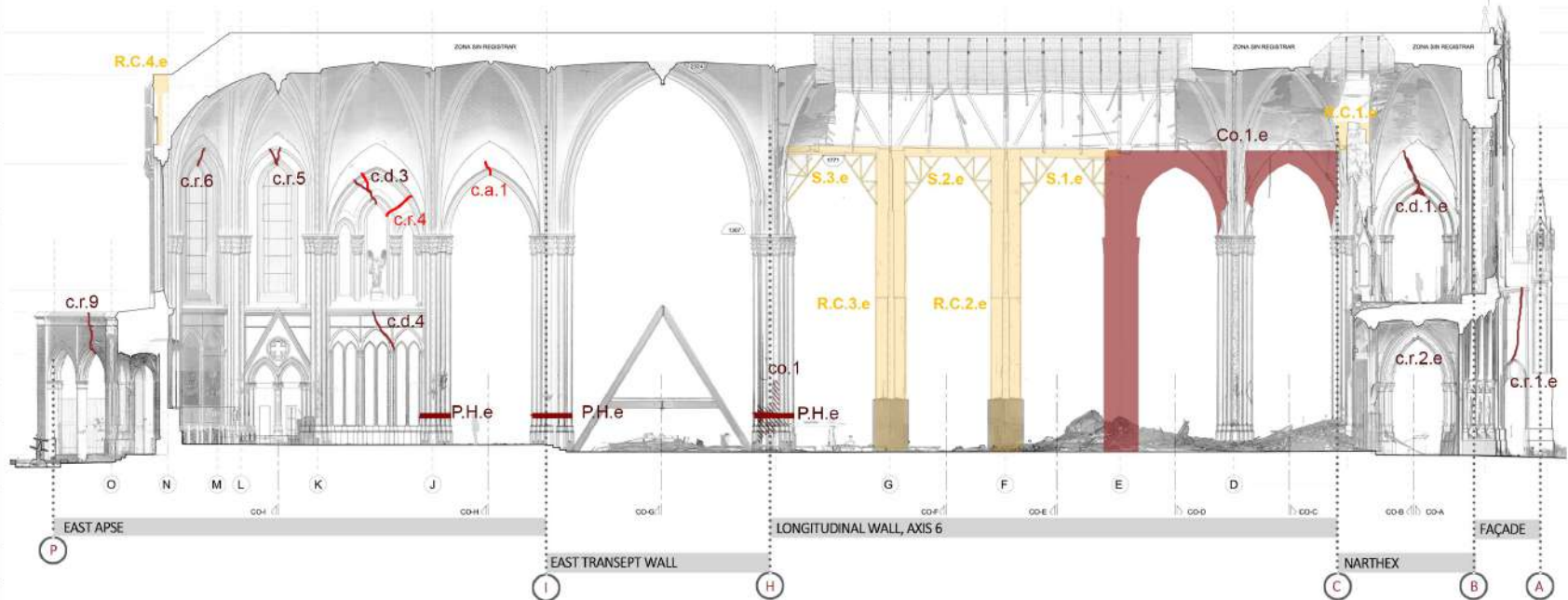
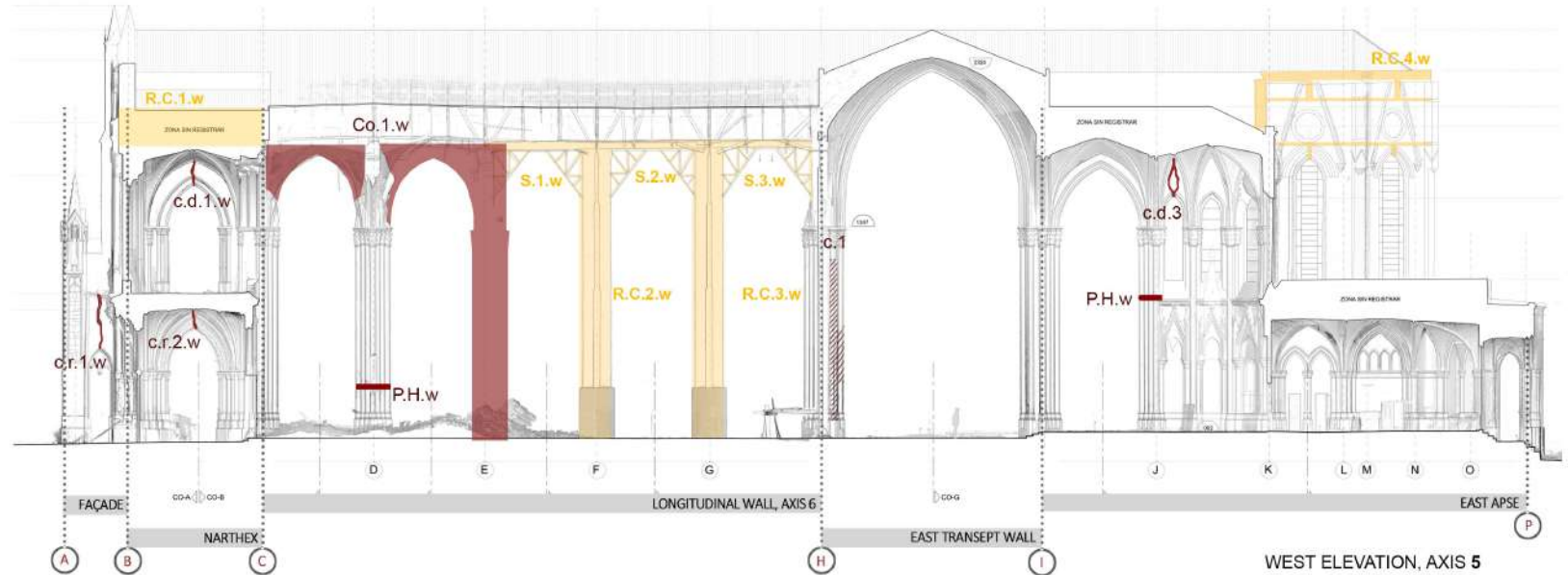
## DEGRADATION PHENOMENA THAT REDUCES STRUCTURAL EFFICIENCY

**Erosion, Er.i, and Mosses lichens and fungi, M.I.h.i**

**Presence of vegetation, Vi**

**Structural discontinuities**  
Heterogeneous materiality (Reinforced Concrete, R.C., Concrete C., Steel, S., Tabique, T.a.g.i, Masonry type1-2-3, M01-2-3, and Incannucciato, I.i)

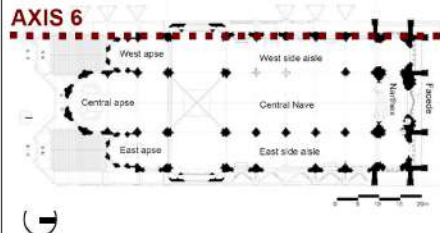
## CRACK PATTERN OF BASILICA DEL SALVADOR\_BS09



EAST ELEVATION, AXIS 5

## INDIVIDUATION AND LOCATION ANALYZED AXIS:

### AXIS 6 EAST AND WEST



### CRACK PATTERN



Capillary crack, Initial, c.i.i. and Advanced, c.a.i.

In the first phase of an initial capillary crack, it is not possible to directly determine the corresponding points of the edge, but only the shape of crack, while in the advanced step it is possible to identify both elements of analysis.



Crack corresponding to plastic hinge, P.H.

A macro-element undergoes a rigid rotation around a plastic hinge, P.H., generally corresponding to horizontal or diagonal crack.



Rotating crack, c.r.i.

The block during cracking undergoes a rigid rotation by which the two edges of the crack move away.



Detachment crack, c.d.i.

The block is completely separated from the rest of the building.



Partial collapse or loss of material



Total collapse, localized decomposition of wall pieces



Detachment of beam or metal tie

Detachment of beam or tie-rod and loss of operability or, and / or severe deformation of a key



Crack pattern after 2010 Maule earthquake

### DEGRADATION PHENOMENA THAT REDUCES STRUCTURAL EFFICIENCY



Degradation of the masonry  
Erosion, Er.i, and Mosses lichens and fungi, M.I.h.i.



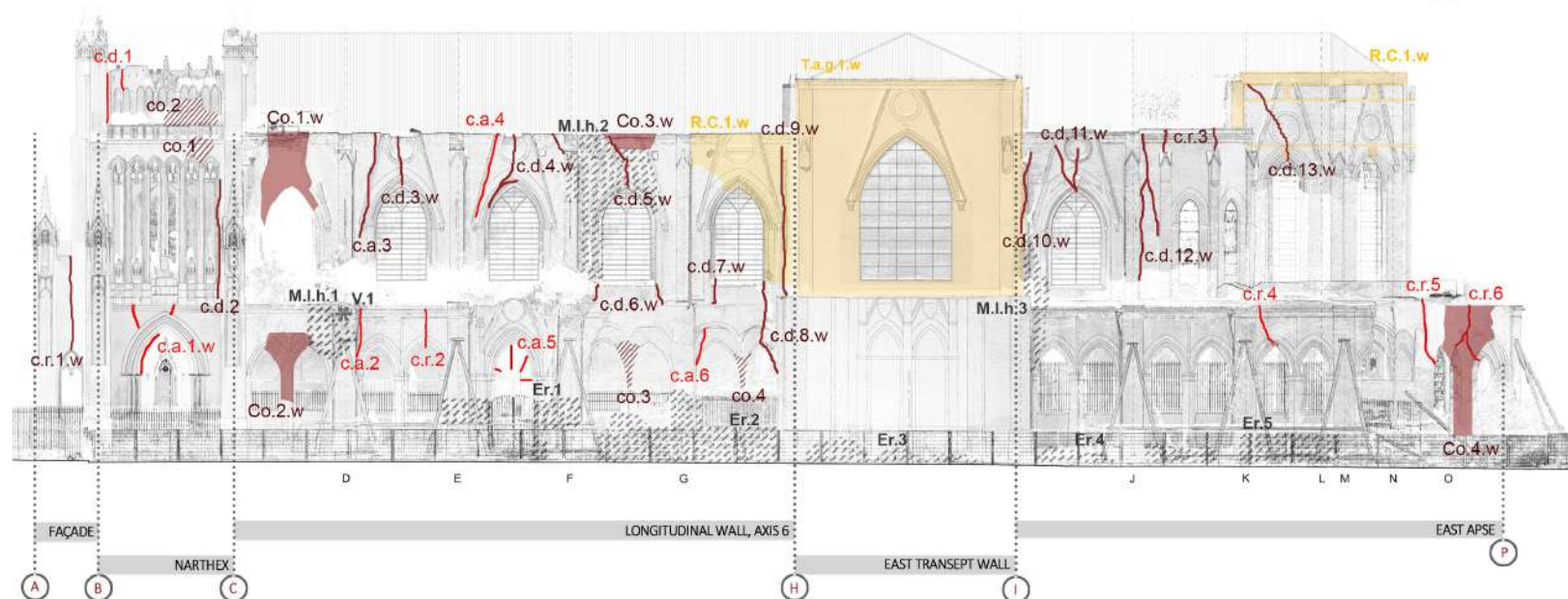
Presence of vegetation, Vi



Structural discontinuities

Heterogeneous materiality (Reinforced Concrete, R.C., Concrete, C., Steel, S., Tabique, T.a.g.i., Masonry type 1-2-3, M01-2-3, and Incannucciato, I.i.)

## CRACK PATTERN OF BASILICA DEL SALVADOR\_BS10



SIDE WEST ELEVATION, AXIS 6

